11 January 2008 | S10

Science

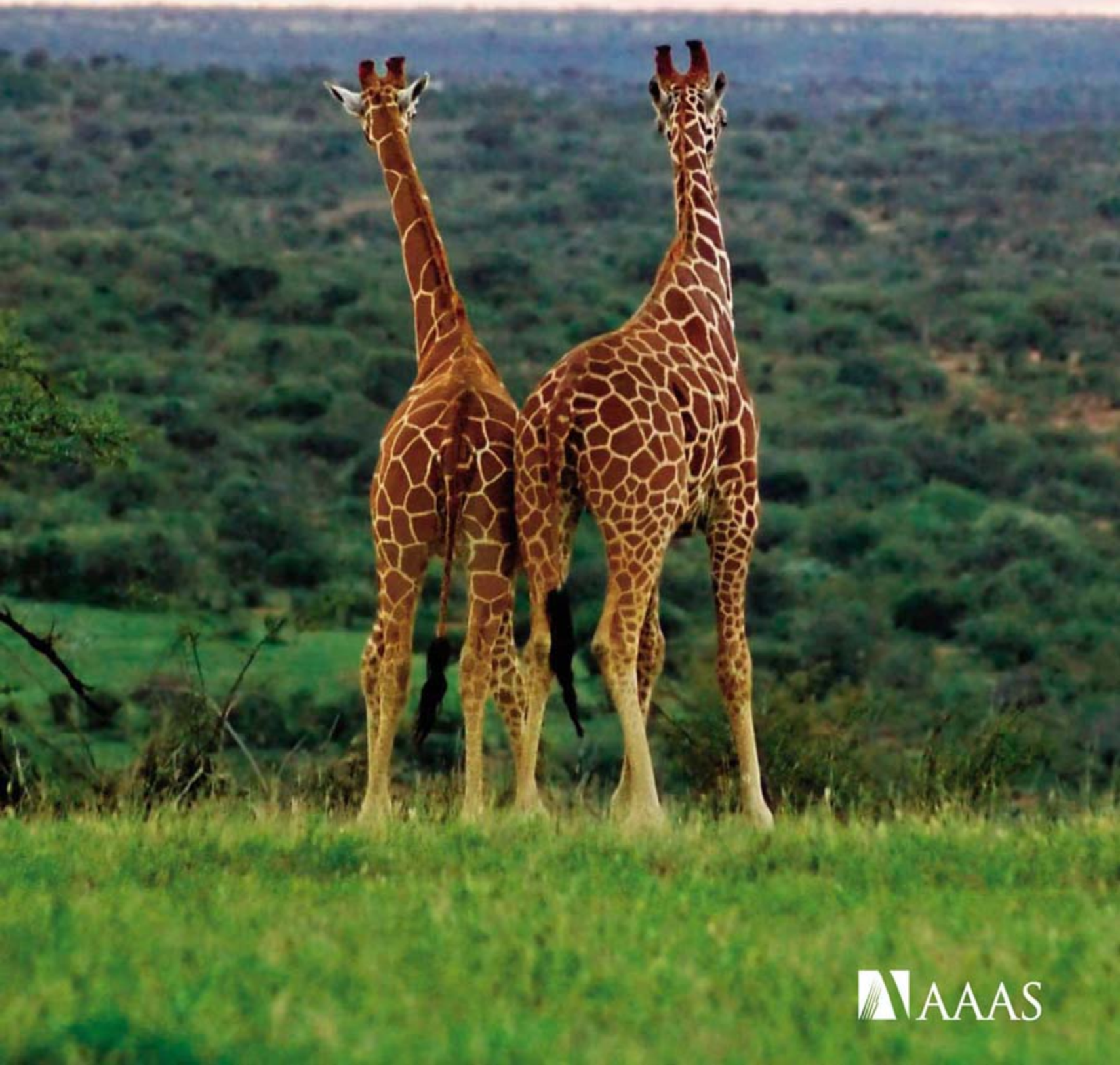

AAAS

Volume 319, Issue 5860

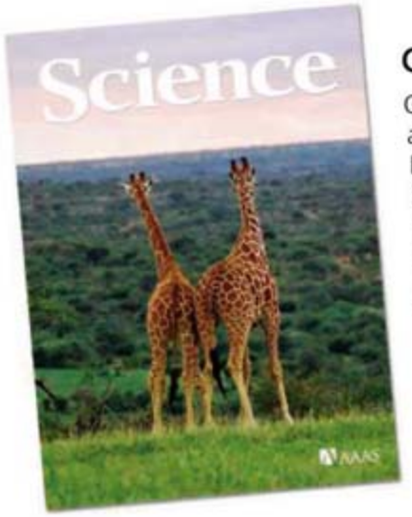

COVER

Giraffes eye a smorgasbord of *Acacia* at the Mpala Research Centre in Kenya. Large herbivores such as giraffes are key to maintaining a mutually beneficial relationship between ants and *Acacia* in an East African ecosystem. See page 192.

Photo: Amy Wolf

DEPARTMENTS

EDITORIAL

NEWS OF THE WEEK

NEWS FOCUS

LETTERS

BOOKS *ET AL.*

POLICY FORUM

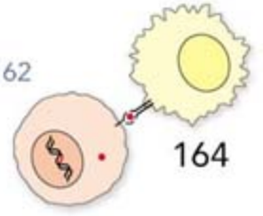

PERSPECTIVES

CONTENTS continued >>

SCIENCE EXPRESS

www.sciencexpress.org

VIROLOGY

Identification of Host Proteins Required for HIV Infection Through a Functional Genomic Screen
A. L. Brass et al.
An RNAi screen identified 237 new and 38 known human proteins required for HIV infection, including ones used in Golgi transport and in viral integration and transcription. *>> News story p. 143*
10.1126/science.1152725

GENETICS

Widespread Genetic Incompatibility in *C. elegans* Maintained by Balancing Selection
H. S. Seidel, M. V. Rockman, L. Kruglyak
Strong natural selection is maintaining multiple alleles of a gene in wild populations of the nematode *C. elegans*, despite their negative effect on fitness.
10.1126/science.1151107

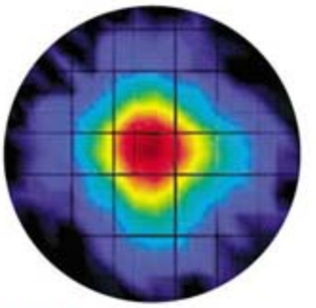

PHYSICS

Electronic Liquid Crystal State in the High-Temperature Superconductor $YBa_2Cu_3O_{6.45}$
V. Hinkov et al.
Neutron scattering measurements suggest that ordering of fluctuating electron spins explains the liquid crystal phases recently seen in some correlated electron systems.
10.1126/science.1152309

PHYSICS

Observation of the Spin Hall Effect of Light via Weak Measurements
O. Hosten and P. Kwiat
Displacement of light at an air-glass interface depends on its polarization, showing that photons have a spin Hall effect comparable to that seen for electrons.
10.1126/science.1152697

TECHNICAL COMMENT ABSTRACTS

OCEANS

REVIEW

ECOLOGY

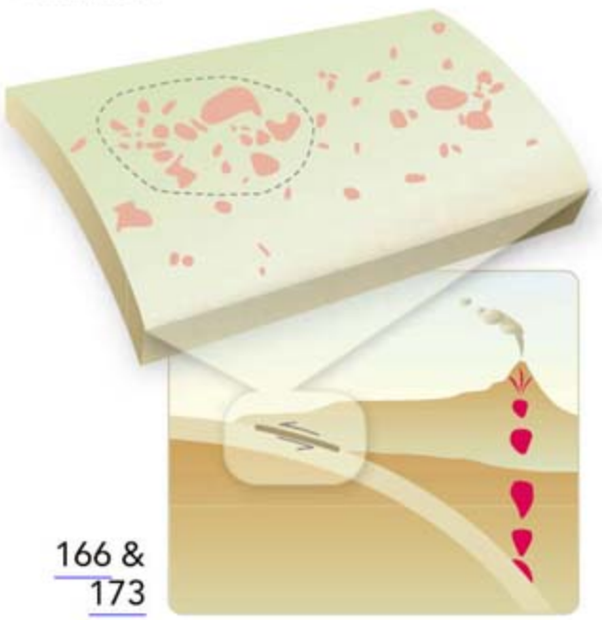

166 & 173

BREVIA

GEOPHYSICS

REPORTS

ASTRONOMY

PHYSICS

CHEMISTRY

CONTENTS continued >>

REPORTS *CONTINUED...*

165 & 206

AAAS
ADVANCING SCIENCE, SERVING SOCIETY

SCIENCE (ISSN 0036-8075) is published weekly on Friday, except the last week in December, by the American Association for the Advancement of Science, 1200 New York Avenue, NW, Washington, DC 20005. Periodicals Mail postage (publication No. 484460) paid at Washington, DC, and additional mailing offices.

Copyright © 2008 by the American Association for the Advancement of Science. The title SCIENCE is a registered trademark of the AAAS.
Domestic individual membership and subscription (51 issues): $144 ($74 allocated to subscription). Domestic institutional subscription (51 issues): $770; Foreign postage extra: Mexico, Caribbean (surface mail) $55; other countries (air assist delivery) $85. First class, airmail, student, and emeritus rates on request. Canadian rates with GST available upon request, GST #1254 88122. Publications Mail Agreement Number 1069624. SCIENCE is printed on 30 percent post-consumer recycled paper. **Printed in the U.S.A.**

Change of address: Allow 4 weeks, giving old and new addresses and 8-digit account number. **Postmaster:** Send change of address to AAAS, P.O. Box 96178, Washington, DC 20090–6178. **Single-copy sales:** $10.00 current issue, $15.00 back issue prepaid includes surface postage; bulk rates on request. **Authorization to photocopy** material for internal or personal use under circumstances not falling within the fair use provisions of the Copyright Act is granted by AAAS to libraries and other users registered with the Copyright Clearance Center (CCC) Transactional Reporting Service, provided that $20.00 per article is paid directly to CCC, 222 Rosewood Drive, Danvers, MA 01923. The identification code for *Science* is 0036-8075. *Science* is indexed in the *Reader's Guide to Periodical Literature* and in several specialized indexes.

CONTENTS continued >>

Future fuel?

SCIENCE**NOW**

www.sciencenow.org DAILY NEWS COVERAGE

Biofuels on a Big Scale
Switchgrass produces five times as much energy as required to make it into a crop-based fuel.

Evolution: Read All About It!
New booklet aims to bring Darwin's theory to the masses.

Third Gene Copy Is a Charm
A gene triplicated in Down syndrome may provide cancer protection.

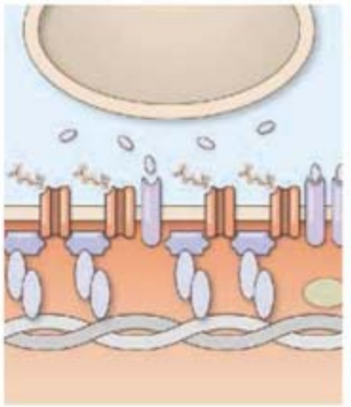

Receptor clustering at the neuromuscular junction.

SCIENCE **SIGNALING**

www.stke.org THE SIGNAL TRANSDUCTION KNOWLEDGE ENVIRONMENT

PERSPECTIVE: Notch and Integrin Affinity—A Sticky Situation
A. Karsan
Notch-dependent activation of R-Ras reverses H-Ras–mediated suppression of integrin activity.

PERSPECTIVE: An Emerging Picture of Synapse Formation—A Balance of Two Opposing Pathways
F. Ono
A dispersing and a clustering pathway for acetylcholine receptors converge on the postsynaptic protein rapsyn in skeletal muscle.

Following childhood dreams to a career.

SCIENCE **CAREERS**

www.sciencecareers.org CAREER RESOURCES FOR SCIENTISTS

Special Feature: Changing Careers, Following Dreams
K. Travis
Moving forward can mean looking back at childhood fascinations or what first engaged your love for science.

Finding the Way Back to a First (Career) Love
S. Webb
Like rekindling an old romance, the pursuit of an old interest can be exciting and rewarding.

The Accidental Paleontologist
E. Quill
Mike Taylor's fascination with sauropods led him to do a Ph.D.

In Person: A Career Home Run
K. Woolner
A software developer's hobby in baseball statistics landed him a job with a major league baseball team.

SCIENCE**PODCAST**

Download the 11 January *Science* Podcast to hear about newly identified host proteins involved in HIV infection, cancer immunotherapy, glaciation during the Cretaceous, and more.
www.sciencemag.org/about/podcast.dtl

CREDITS: (*SCIENCE NOW*) COURTESY OF USDA-ARS; (*SCIENCE CAREERS*) COURTESY MIKE TAYLOR

Separate individual or institutional subscriptions to these products may be required for full-text access.

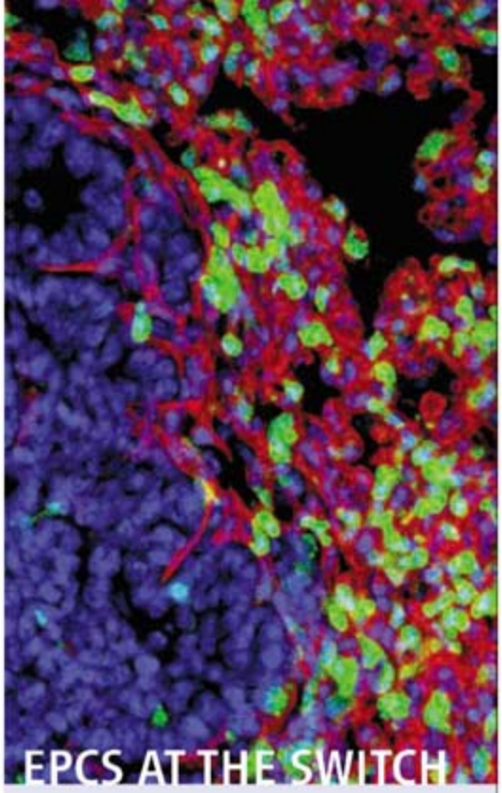

EPCS AT THE SWITCH

To ensure a steady supply of oxygen and nutrients, tumors send signals that stimulate the growth of new blood vessels. Bone marrow–derived cells called endothelial progenitor cells (EPCs) are known to be recruited to the tumor-associated growing vessels, but the presence of these cells at only very low levels in the tumor vasculature has made it difficult to assess their functional contribution. Studying mouse models of lung metastasis, **Gao *et al.*** (p. 195; see the Perspective by Rafii and Lyden) show that EPCs are critical regulators of the "angiogenic switch" that helps drive the progression of dormant micrometastases to lethal metastases. Genetic manipulations that blocked EPC mobilization in tumor-bearing mice inhibited angiogenesis, impaired formation of lung metastases, and increased survival time.

Exotic Superconductors in Magnetic Field

When a magnetic field is applied to a superconductor, a regular lattice of vortices usually forms in which each vortex is threaded by a single quantum of magnetic flux. This process is often described by the phenomenological Ginzburg-Landau theory in terms of two length scales for the magnetic field, a coherence length and a penetration depth. **Bianchi *et al.*** (p. 177) now report neutron-scattering results on the heavy fermion compound $CeCoIn_5$ that show a complete departure from this model. The authors suggest that the response is caused by spin polarization of the quasiparticles within the normal state vortex core that arises from the superconducting state being near a quantum critical point.

Chemical Ins and Outs

In bimolecular nucleophilic substitution (the S_N2 reaction), an attacking group, usually an anion, binds to a carbon center and simultaneously ejects a leaving group on the opposite side. This reaction has been understood in broad terms for many decades, but many details have been obscured by medium effects and the low-energy discrimination attainable in gas-phase studies. **Mikosch *et al.*** (p. 183; see the Perspective by Brauman) have achieved precise control over the gas phase collision energies of Cl^- and CH_3I and mapped out the quantum mechanical dynamics that lead to CH_3Cl and I^-. Analysis in concert with theoretical simulations reveals a progression with increasing energy from a mechanism involving a pre-reaction complex to a more direct displacement.

Cold Cretaceous Pockets

Although the Cretaceous was a period of exceptionally warm sea surface temperatures and high sea levels, geological and isotopic evidence (such as sea-level changes and $\delta^{18}O$ excursions) suggests that glaciation occurred during that period. **Bornemann *et al.*** (p. 189; see the news story by Kerr) now show significant glaciation occurred during the peak of the Creatceous warmth, around 91 million years ago. By combining measurements of the $\delta^{18}O$ of foraminifera, which is a function of ocean temperature and ice volume, and a membrane lipid index that solely reflects temperature changes, the authors show that there was a 200,000-year interval of glaciation, possibly as an ice sheet in Antarctica about half the size of the current ice cap.

Dwarf Galaxy Puzzles

The stars and dark matter of dwarf galaxies are less concentrated than theories predict. **Mashchenko *et al.*** (p. 174, published online 29 November) used computer simulations to model the effects of expelled material from supernovae and stellar winds on the overall properties of dwarf galaxies. Such stellar feedback of material drives large-scale bulk motions of interstellar gas that change the gravitational potential such that the central matter density of the galaxy is reduced. This effect helps explain many puzzling properties of dwarf galaxies, such as their large dark matter cores, globular cluster distributions, and stellar population gradients.

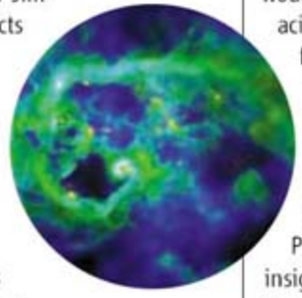

Where the Action Is

An immune response to infection begins within the secondary lymphoid tissues, where foreign antigen is presented to T cells by dendritic cells. Activated T cells then migrate to the infected peripheral tissues. **Wakim *et al.*** (p. 198) present evidence that may revise the view that peripheral sites are simply arenas for the end stages of combat. A pathogen (herpes simplex virus) was experimentally reactivated in transplanted nervous tissue in combination with adoptively transferred T cells. Fresh T cell activation was detected at these sites, and as happens in lymph nodes, this process required dendritic cells and the help of $CD4^+$ T cells.

Expressing Estrogen-Responsive Genes

Estrogens, upon recruitment of their cognate receptors, govern the expression of target genes. **Perillo *et al.*** (p. 202) show that transcription of estrogen-responsive genes is driven by hormone-dependent demethylation of a critical lysine in histone H3 to induce a local oxidative burst that modifies the surrounding DNA by guanine oxidation, which is subsequently removed by specific glycosylases. 8-oxo-guanine–DNA glycosylase 1 and the topoisomerase IIβ enzyme are recruited to these loci and bend the intervening DNA-chromatin region to mark the site where transcription begins and drive expression of estrogen-responsive genes.

Find Your Partner

The interactions of proteins with each other and of protein subunits within a complex are, as one would expect, primarily dictated by the amino acid side chains located at the contact interfaces. Interfacial residues can be hotspots of evolutionary change, and cross-species comparisons of changes often provide insights into the link between oligomeric structure and catalytic-regulatory functions. **Grueninger *et al.*** (p. 206; see the Perspective by Janin) have applied these insights in a project to alter, in a rational fashion, the oligomeric state of five enzymes. The authors conclude that symmetry elements are key to achieving success in the redesign of natural protein-protein interactions.

CREDITS (TOP TO BOTTOM): GAO *ET AL.*; ©MASHCHENKO, WADSLEY, AND COUCHMAN

A Case for New Institutions

Kamaljit S. Bawa is a Distinguished Professor of Biology at the University of Massachusetts, Boston, and president of the Ashoka Trust for Research in Ecology and the Environment, Bangalore, India.

Ganesan Balachander is Representative of the Ford Foundation for South Asia, Delhi, India.

Peter Raven is president of the Missouri Botanical Garden, St. Louis, MO, USA.

THE ENVIRONMENT IN MOST COUNTRIES IS BEING DEGRADED, POVERTY WORLDWIDE IS increasing, and the gaps between rich and poor individuals and nations are widening. One half of the world's human population still survives on less than $2 per day. These people face the prospect of environmental degradation of their ecosystems that is likely to be exacerbated by climate change. Yet these local ecosystems contain much of our planet's biodiversity and are also the sources of livelihoods and ecosystem services for the rural poor and indirectly for the global community. A key to halt, and then reverse, these environmental and economic trends may lie in new and imaginatively conceived institutions of knowledge in developing countries.

Increased knowledge has always provided the basis for human advance. In recent times, wealth has been generated mainly by technical innovation and entrepreneurship, whereas gains on social and environmental fronts have been driven by a broader intellectual tradition. In developed countries, these traditions have been organized into knowledge institutions such as universities. In developing countries, modern universities have, unfortunately, lacked the historical, social, economic, and political contexts that shaped those in the developed world. As a result, these institutions have largely failed to address contemporary economic and environmental problems.

Moreover, knowledge institutions in the developing world face unique challenges. Current problems associated with hunger, inequities, and environmental degradation are complex and require considerable human resources and new knowledge. And institutions that can translate knowledge into action, such as nongovernmental organizations, extension arms of universities, and community user groups, are very few and have a weak capacity to meet contemporary needs. Universities in the developing world, generating knowledge for knowledge's sake or, more often, duplicating knowledge, are not moving fast enough to develop programs to meet new challenges.

Innovative knowledge institutions and partnerships are needed, and they must be guided by certain principles. Highly varied local situations and the uncertainty of complex social and ecological systems call for flexible, experimental, and adaptive learning-based approaches. The new institutions must also be problem-driven. The alleviation of poverty and environmental sustainability should be explicit goals for which knowledge must be generated. Institutions must transcend traditional disciplinary boundaries to generate new ideas and technologies and link science with policy and governance to frame questions and foster social change. Two examples of such new institutions in the developing world meet only some of these criteria: the Ashoka Trust for Research in Ecology and the Environment (ATREE) in India and the EARTH University in Costa Rica. Considering the magnitude of the problems, many more are required.

Our experience with ATREE suggests that new knowledge institutions function best by having partnerships with nongovernment and government agencies, as well as with community organizations. Flexible mandates, freedom from bureaucratic control, and a focus on specific problems, such as the harmonization of rural livelihoods and conservation at specific sites (for example, in the Western Ghats and Eastern Himalaya biodiversity hot spots), have been critical for forging frameworks to implement work that is relevant to the identified societal needs. Collaboration with appropriate institutions in the developed world that entails integration of different knowledge systems, mutual respect, and symmetrical partnerships adds a global perspective that is important for sharing knowledge and resolving global problems.

Several supportive actions are necessary for new institutions to emerge and flourish. China, India, and other countries are making huge investments in knowledge institutions and could easily channel resources into new institutions or into existing institutions that adopt broad public mandates. The new class of wealthy social entrepreneurs emerging in the fast-growing economies of Asia and Latin America, committed to philanthropy, could be convinced that support for these new institutions will provide stable long-term solutions, even when immediate results from social welfare programs may seem more attractive. Finally, the reallocation of resources by bilateral donor agencies and foundations from short-term projects to new institutions that genuinely address long-term capacity-building could also reverse the present economic and environmental trends.

– Kamaljit S. Bawa, Ganesan Balachander, Peter Raven

10.1126/science.1151835

CREDIT: JONATHAN EVANS/GETTY IMAGES

DEVELOPMENT

A Need for Glia

The mammalian cerebral cortex, the seat of higher thought, develops from the inside out, as younger neurons born in the ventricular zone migrate past older neurons to form ever more superficial layers. Radial glial cells serve as guide wires along which the migrating neurons travel, and these same radial glial cells also serve to produce new neurons. As migrating neurons navigate through the glial cell scaffold, they move stepwise by means of transient adhesive contacts mediated by gap junction proteins. Integrins are αβ subunit receptors located in the plasma membrane and link the extracellular matrix to the intracellular cytoskeleton. Belvindrah *et al.* have taken a closer look at how β1 integrin contributes to the organization of these cortical cell migrations. They used an existing mouse line, in which both radial glia and migrating neurons were deficient in β1 integrin, and compared it with a mouse line they developed for this analysis, with β1 integrin knocked out only in the migrating neurons. When the radial glia lacked β1 integrin, they seemed disorganized in their anchor points, and the cortex developed abnormally, whereas when only the neurons lacked β1 integrin, migration proceeded normally. Tissue culture analysis showed that the normal formation of neurite extensions depended on the expression of β1 integrin in the glia, but not in the neurons. It seems that what matters for how β1 integrin affects the layering of the developing cortex is not its expression in neurons but rather its expression in glial cells. — PJH

J. Neurosci. **27**, 13854 (2007).

CREDITS (TOP TO BOTTOM): BELVINDRAH *ET AL.*, *J. NEUROSCI.* **27**, 13854 (2007); LEE AND KIM, *LANGMUIR* **24**, 142 (2008)

VIROLOGY

Aided by Amyloid

The role played by semen in the sexual transmission of HIV may be more than simply as an innocuous carrier. Münch *et al.* show that semen contains factors that can actually amplify the infectious potential of HIV by helping to promote the binding of the virus to target cells. Within semen, the enzyme prostatic acidic phosphatase can break down and form fragments that can, in turn, coalesce into amyloid-like fibrils. These fibrils can bind to HIV virions and enhance their binding to target cells—effectively amplifying the chance of successful viral infection by several orders of magnitude. Addition of the fibrils at physiological concentrations increased HIV infection in susceptible cell cultures, cultures of human tonsils, and in transgenic rats. It remains to be confirmed to what extent this mechanism is effective during human-to-human sexual transmission, but if it is an important factor, it may represent a valuable target in efforts to prevent transmission. — SMH

Cell **131**, 1059 (2007).

MATERIALS SCIENCE

How to Walk on Water

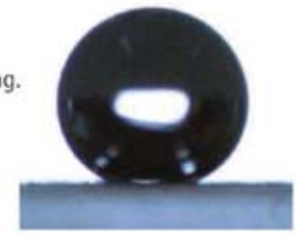

Water striders can skate and jump on water without drowning. The legs of these insects have a hierarchical structure of hydrophobic hairs; the resulting highly water-repellent surface is thought to help the insects move on water, because small hydrophobic objects can float, or sink with a delay, even when their density is higher than that of water. Floating is one thing though—jumping onto and off of a liquid water surface quite another. How do the impact conditions affect the response of the water surface? To investigate this question, Lee and Kim studied the impact behavior of small superhydrophobic spheres. They found that at low impact velocity, the spheres oscillate on the surface while afloat. As the impact velocity increases, they bounce off the water surface. At even higher velocity, the spheres penetrate the water surface and sink. Whether the spheres bounce off depends on the viscosity of the liquid and the hydrophobicity of the sphere. Thus, the superhydrophobic legs are crucial to the water striders' ability to jump on water and avoid drowning. Future robots may mimic such behavior. — JFU

Langmuir **24**, 142 (2008).

CHEMISTRY

Aromatic Surprise

Unsaturated hydrocarbon rings are constructively classed by their number of electrons available for pi-bonding: A multiple of four confers instability in a planar configuration (as in cyclobutadiene), whereas even nonmultiples of four (as in benzene and naphthalene) confer exceptional stability, termed aromaticity. Cyclic analogs in which the carbons are replaced by heavier atoms can be subject to greater degrees of spin-orbit coupling, and it is thus unclear how straightforwardly the aromaticity picture extrapolates.

Ugrinov *et al.* explored this question in analyzing an unusual compound they prepared and crystallographically characterized—a dianionic parallelogram with arsenic (As) and tellurium (TE) centers at opposite corners and charge-balancing potassium cations sequestered by crown ethers above and below the plane. A simplistic analysis would suggest that four lone pairs (one each per As and Te center) should sum to an anti-aromatic configuration. However, calculations using density functional theory suggest that the experimental geometry is consistent with a spin triplet ground state and that the net electronic configuration is in fact closer to an aromatic system. — JSY

J. Am. Chem. Soc. 10.1021/ja075513l (2007).

The Wine Divide

Environmentally conscious enophiles in the eastern third of the United States may be in for a surprise. A recent analysis of carbon emissions suggests that they will contribute less to global warming if they drink French rather than California wines.

Tyler Colman, a wine blogger (www.drvino.com) and instructor at New York University, teamed up with Pablo Päster, a sustainability engineer at URS Corp. in Oakland, California, to do a carbon life-cycle analysis. Their conclusion: Transportation outweighs all aspects of production. Shipping a 750-milliliter bottle from Bordeaux to New York City emits 1.8 kilograms of carbon, whereas trucking one from the Napa Valley emits 2.6 kg.

The Napa-Bordeaux line.

Other wine tips the authors report in a working paper posted at www.wine-economics.org: Because most of the weight is in the glass, bigger bottles are better. Boxed wine is a good alternative, but local wine is the greenest of all.

Genes R Us

Personal genomics revved into high gear last year thanks to DNA chips that make it possible to cheaply scan the entire genome (*Science*, 21 December 2007, p. 1842). You can track the flood of new discoveries at SNPedia (www.snpedia.com), a Web site run by two biotech veterans in Bethesda, Maryland, that catalogs SNPs culled from the literature.

SNPs are single-nucleotide polymorphisms: single-base variations in DNA that researchers are tying to traits and disease risks. Browse by medical conditions (77 so far) and discover, for example, that carrying two copies of the T version of a SNP called rs2273535 raises your risk of colon cancer by 50%; another SNP, rs6152, is associated with baldness. Visitors can also search by genetically influenced drug reactions (48) and genes (128). There are links to relevant papers and sites (including James Watson's and J. Craig Venter's respective genomes) and to blogs by people who are sending their DNA to a lab to be "SNP chipped." The site is also a wiki, which means anyone can contribute.

The site "could be a very valuable research tool," says computational biologist Mark Daly of the Broad Institute in Cambridge, Massachusetts. "It will be great to see how this develops."

Man With a One-Wheel Mind

A retired unicycling dermatologist has gotten press, and a few laughs, by claiming a link between testosterone and humor.

Sam Shuster of Newcastle upon Tyne, U.K., rode around town on his unicycle for a year, recording the reactions of 400 passersby. Reporting in the 22 December 2007 issue of the *British Medical Journal*, Shuster relates that about 75% of male reactions were "attempts at comedy," whereas 95% of the females "praised, encouraged, or expressed concern." The most aggressive reactions came from youthful males, who shouted things such as "Fall off, granddad" and kicked soccer balls at him. Responses mellowed with time, Shuster observed, with older men joking about his having lost a wheel or his handlebars. Elderly men tended to comment on the difficulty, saying things such as "It's quicker to walk." Shuster's interpretation is that as men age, "aggression is concealed by wit." He speculates that humor eventually takes on a life of its own, persisting beyond high testosterone levels.

Sociologist Alan Booth of Pennsylvania State University in State College is skeptical of a testosterone-humor connection—except "to the extent humor means demeaning someone." Aggression is "probably just one aspect" of humor, suggests psychologist Roy Baumeister of Florida State University in Tallahassee. He says that in his experience, men are often more likely than women to use self-deprecating humor, hardly an expression of aggression.

Hang Up and Get Moving

Research has shown that talking on a cell phone makes a driver about five times as likely to have an accident. Now it turns out that cell phones also cause traffic congestion and delays.

Researchers led by David Strayer, a psychologist at the University of Utah, Salt Lake City, put 36 undergraduates into a driving simulator and had each drive about 15 kilometers of freeway with various amounts of traffic. If they were talking on a hands-free cell phone, they drove 3.2 kilometers per hour more slowly and were 21% less likely to pass a slow-moving vehicle on a crowded freeway.

That means for a typical commuter, talking could lengthen the drive time by 5% to 10%, the group estimates in a paper prepared for this month's meeting of the National Academies' Transportation Research Board in Washington, D.C. "As you increase traffic density, the impact of distracted drivers becomes more pronounced," says Strayer. The team is now using traffic models to figure out the exact toll on other drivers. It could be big: In 2005, the U.S. Department of Transportation found that 6% of drivers were using cell phones at any given daytime moment.

CREDITS (TOP TO BOTTOM): BOBBIE SHUSTER; COLMAN AND PÄSTER; IVANA VLADISAVLJEVIC

<< Two Cultures

HEADBANGERS. The Amygdaloids, a rock band formed by researchers at New York University, has played only 10 shows in its first year of existence. But the band's songs about brain science, fear, and love now grace a new CD, *Heavy Mental*, and last week the band gave a free performance at the Kennedy Center in Washington, D.C. Here's who they are:

Band Member (l to r)	Music Idol	Science Idol	Favorite Lyric
Joseph LeDoux, Neuroscientist/Rhythm guitarist	Guitarist Pete Kennedy	Darwin	"My body wants you but my mind says no."
Nina Galbraith Curley Grad student/Bass guitarist	Bassist, James Jamerson	Marie Curie	"You left a trace in my memory / A permanent place in my synaptic sea."
Daniela Schiller, Postdoc/Drums	Singer/songwriter Tom Waits	Albert Einstein	"You can't see inside of me / That's a place only I can be."
Tyler Volk, Biologist/Lead guitarist	Guitarist Jimi Hendrix	Galileo	"Don't go looking too hard / it's all a nut in your brain."

MOVERS

QUALIFIED. Merit triumphed over politics in Italy's choice of a new research chief, according to scientists who hope that big changes will follow. Theoretical physicist Luciano Maiani was named head of the $1.5 billion National Research Council (CNR) in December and is expected to be confirmed soon to the 4-year post. Maiani, best known for jointly predicting the charm quark with two other scientists, served as director general of CERN from 1999 to 2003 and previously ran Italy's National Institute of Nuclear Physics.

CNR has been without a director since the resignation of former chief Fabio Pistella last summer. Critics claimed that Pistella was a political favorite and publicly challenged his qualifications to run the agency. Last year, to cut political interference, the Italian government adopted a new system for selecting research heads, in which an international selection committee sifts applications and proposes three names to the government to choose from. Maiani was picked from about 50 applicants.

Maiani says he wants to restore CNR's role as the primary driver of Italian research. He intends to ramp up the agency's programs in particle physics, astronomy, and areas of medicine and biology. Luciano Pietronero, head of CNR's Institute of Complex Systems in Rome, says Maiani's experience makes him "perfectly suited for the challenge of revitalizing the agency."

IN THE COURTS

CLEARED. A French court has removed the taint of espionage from chemist Luu Bang. But Luu is still looking to his employer, the National Centre for Scientific Research (CNRS), to restore his honor.

Luu, 67, was arrested at the Strasbourg airport on 8 April 2006 while on his way to Guangdong, China, to attend a seminar on Sino-French collaboration. Border police found four vials containing a white powder in his suitcase. Luu said they were chemicals for prospective scientific partners in China, but CNRS filed a theft report and suspended Luu as emeritus researcher (*Science*, 28 April 2006, p. 512).

The French government eventually charged him with "breach of trust" for trying to take the samples abroad without proper consent. But last month, an appeals court in Colmar in eastern France said that CNRS did not have internal rules governing such shipments and that Luu had notified the French consulate in Guangzhou of his plan. The government did not use the 5 days it had to appeal the verdict. CNRS did not respond to requests for comment.

Got a tip for this page? E-mail people@aaas.org

Deaths

FIRST IN CLIMATE. The founding chair of the Nobel Prize–winning Intergovernmental Panel on Climate Change (IPCC), Bert Bolin, 82, died 30 December 2007 in Stockholm, Sweden, of stomach cancer.

"A lot of credit [for the Nobel] has to go to Bert," says Robert Watson of the University of East Anglia, U.K., Bolin's successor at IPCC. "If he had not done the superb job that he did, it wouldn't have happened." IPCC's current chair, Rajendra Pachauri, and Al Gore accepted the prize at the Nobel ceremony last month.

Beginning in the 1950s, Bolin's work at Stockholm University on the cycling of carbon through land, ocean, and atmosphere drew attention to the carbon cycle's vital role in climate change. In 1988, he became IPCC's first chair and set the organization's direction through its first two major climate assessments involving thousands of climate scientists. After the Nobel Peace Prize was announced, he told *Science* that their hard work helped "to unite the scientific community around the part of climate knowledge that is really robust without going beyond that to speculation."

CREDITS (TOP TO BOTTOM): NYU; CNR; STOCKHOLM UNIVERSITY

Ants, plants, and herbivores 146

Protecting whales from the Navy's sonar 147

PARTICLE PHYSICS

Budget Cuts Mean Layoffs at Two DOE Labs, End for SLAC Collider

An unexpectedly tight science budget this year at the U.S. Department of Energy (DOE) will shut down a particle collider in California and curtail activities at another accelerator lab in Illinois. In addition, up to 325 scientists, technicians, and workers are facing layoffs after Congress last month turned a planned 4% increase in the particle physics budget into an 8.5% reduction.

The 2008 budget, signed into law the day after Christmas, hit DOE's particle physics program especially hard (*Science*, 4 January, p. 18). Physicists at the Fermi National Accelerator Laboratory (Fermilab) in Batavia, Illinois, fretted that their Tevatron collider would have to shut down for a month. Instead, DOE officials have decided to pull the plug on the PEP-II collider at the Stanford Linear Accelerator Center (SLAC) in Menlo Park, California, at the beginning of March, 7 months ahead of schedule, SLAC Director Persis Drell announced on 7 January.

"This came as a total surprise," says Hassan Jawahery, a physicist at the University of Maryland, College Park, who leads the 600-member international collaboration working with BaBar, the particle detector fed by PEP-II. "We had a full program ahead of us."

SLAC will also lay off 125 of its 1600 employees. "While I cannot reduce the magnitude or the impact of the coming layoff, I can acknowledge how painful this will be," Drell told the lab staff. SLAC administrators had already planned to replace 100 employees as researchers complete an x-ray laser and pursue studies in materials science.

Like a bystander hit by an errant bullet, PEP-II is a victim of cuts aimed at other projects. Federal legislators slashed by three-quarters DOE's requested $60 million for research and development for the proposed International Linear Collider (ILC), a 30-kilometer-long, multibillion-dollar particle smasher that many physicists say is key to the field's future. U.S. researchers hope the machine will be built at Fermilab, but the 2008 cuts cast a dark cloud over the entire project. Research on superconducting accelerator technology, known as SRF, wound up with $5 million rather than the $23 million requested. For Fermilab, an expected $47 million turned into $15 million. SLAC got $4 million for ILC instead of $20 million.

Shared pain. SLAC's new director, Persis Drell, laments layoffs.

Those numbers jolted both labs, which had already spent all the money they will receive this year for those projects. The day after the budget passed, Fermilab Director Pier Oddone announced that 200 of the lab's 1900 employees would be laid off. But because the labs must give 60 days' notice, the ILC and SRF projects will effectively consume millions of dollars more. Oddone now says a healthy budget request for 2009, due out next month, could mean fewer layoffs.

That money must come out of other projects. At first, Fermilab officials worried that they would have to shut down the Tevatron, even as researchers strain to spot the Higgs boson before it is snagged by the higher-energy Large Hadron Collider (LHC), which will power up this summer at the European lab, CERN, near Geneva, Switzerland. "It's a critical time for the Tevatron," Oddone says. But he says a "rolling furlough," in which all employees take 2 or 3 days a month of unpaid leave, will keep the machine going.

PEP-II won't be so lucky. DOE cannot afford to run both colliders, so officials opted to scuttle PEP-II ahead of its scheduled shutdown on 30 September. "Based on the guidance we have received from the scientific community, … the operation of the Tevatron in 2008 has a higher scientific priority," says Dennis Kovar of DOE's Office of Science.

Both machines are looking for signs of massive new particles, but in very different ways. Fermilab's Tevatron aims to create the Higgs and other new particles by smashing protons into antiprotons at the highest energies. By colliding electrons and antielectrons at lower energy, SLAC's PEP-II produces copious quantities of particles called B mesons, whose properties depend on particles popping in and out of "virtual" existence around them. Studies of B mesons have already set limits on what the Tevatron and the LHC might see directly.

PEP-II has produced about 500 million B meson/anti–B meson pairs since 1999 and would have produced 250 million this year alone. The extra data could have revealed rare decays, Jawahery says, and would have helped BaBar compete with the Belle experiment at KEK, the Japanese lab at Tsukuba, which is fed by the KEKB collider.

Overall, the DOE particle physics budget fell to $688 million from a requested $782 million; it received $752 million in 2007. Few expect the budget to rebound next year. "We've had 2 years in which increases for the physical sciences were eliminated at the last minute," says Burton Richter, former director of SLAC. "Are we going to be in the same sort of budget stalemate in 2009?"

Meanwhile, particle physics proceeds apace in Japan. Last week, KEK officials announced that they intend to build a "super B factory" to crank out even more B mesons once KEKB finishes its work in 2009.

–ADRIAN CHO

Lab	Projects to be halted	Workers now on project	2008 budget request	2008 funding allocated
Fermilab	ILC	170	$24 million	$10 million
	SRF		$23 million	$5 million
	NOvA (neutrinos)	70	$36 million	none
SLAC	ILC	73	$20 million	$4 million
	Running PEP-II	NA	$22 million	$15 million

Down and out. SLAC will shut down PEP-II in March, and hundreds of people will be laid off at the two labs, to cope with a disappointing 2008 budget.

CREDITS (TOP TO BOTTOM): IMAGE COURTESY OF DIANA ROGERS/SLAC; SOURCE: FERMILAB AND SLAC

Upgrading China's universities
148

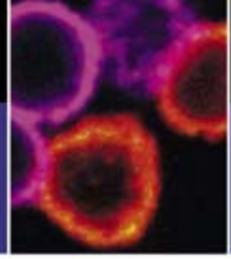

How tumors sabotage immunotherapies?
154

VIROLOGY

HIV Gets By With a Lot of Help From Human Host

HIV is ridiculously simple yet astonishingly complex. The virus contains a mere 9000 bases of RNA—one-millionth the amount of genetic material in a human cell—and a paltry suite of nine genes that code for a measly 15 proteins. Yet this virus can relentlessly nibble at immune cells until the entire system collapses, opening the door for a vast array of illnesses and, ultimately, death. For HIV to do its damage, however, it must repeatedly infect new cells and copy itself, a feat that requires help from its human host. And as a startling paper published online (www.sciencemag.org/cgi/content/abstract/1152725) by *Science* this week explains, that's where HIV's complexity becomes abundantly apparent. The findings also spotlight intriguing, novel drug targets. "This is destined to be one of the key HIV papers of this decade, if not longer," says Robert Gallo, who heads the Institute of Human Virology in Baltimore, Maryland, and did landmark studies that tied HIV to AIDS.

Using cutting-edge molecular techniques, a team led by geneticist Stephen Elledge at Brigham and Women's Hospital in Boston found that the virus relies on 273 human proteins to do its dirty work. These so-called HIV dependency factors (HDFs)—only 36 of which researchers had previously identified—enable the virus to attach to immune cells, wiggle in, shed the protein coat that surrounds its RNA, convert that to DNA, shuttle the genetic material into the nucleus, transcribe genes into amino acids, and then assemble proteins, sprinkle them with sugars, and help newly minted HIVs bud through the surface, where they then go on to find their own cellular prey. "Some viruses carry their houses on their backs, and other viruses invade other people's houses and take over," says Elledge, who had never done an HIV study before but was attracted by the virus's small size. "HIV is more of the latter, and it requires lots and lots of different host functions."

Elledge, postdoc Abraham Brass, and co-workers—including Judy Lieberman, director of the Division of AIDS at Harvard Medical School in Boston—found these HDFs by using libraries of recently discovered small interfering RNAs (siRNAs), which can disrupt transcription and thereby prevent genes from making their products. Specifically, they took human cells and effectively short-circuited every known gene, one at a time, and then tested whether HIV could establish an infection and copy itself. In all, their genomewide RNA interference screen disrupted more than 21,000 human genes, and by a process of elimination, they isolated the ones that HIV hijacks. "This is an excellent example of siRNA screening," says retrovirologist Warner Greene, who heads the Gladstone Institute of Virology and Immunology at the University of California, San Francisco. "This single paper could guide several interesting graduate student theses in the future."

Gallo says the findings have already led to many new insights, and he shares the study investigators' enthusiasm that these HDFs may make excellent targets for drugs. Elledge compares the strategy to that of much-ballyhooed cancer drugs known as angiogenesis inhibitors, which strangle the blood supply to tumors rather than attack the tumors themselves.

More than two dozen current drugs disable key HIV enzymes. (The U.S. Food and Drug Administration in August for the first time approved an HDF inhibitor, which blocks a receptor the virus docks onto for cell entry called CCR5, but its use is limited to people who have failed to respond to several other drugs.) Although drugs that cripple HIV work powerfully when combined into cocktails, the virus can mutate around each of them, preventing them from binding to their viral targets, eventually leading to drug resistance. Elledge and co-workers contend that HIV would have more difficulty escaping drugs that interfere with HDFs. True, HIV could evolve the capacity to copy itself without one of these factors, but that's a much more difficult task for the virus than mutating to prevent a drug from binding to a viral enzyme. On the flip side, human proteins don't mutate with anywhere near the ease of viruses, which makes it less likely that an HDF would develop drug resistance.

Greene and others caution that targeting host proteins could lead to serious ▶

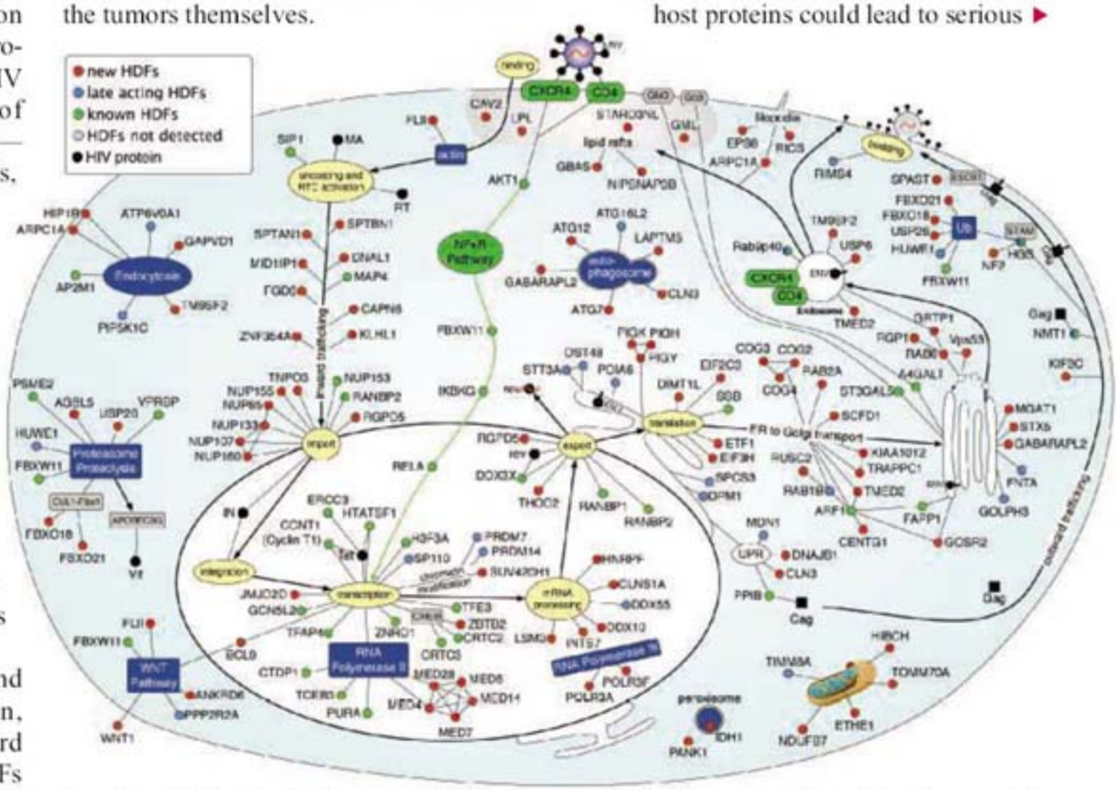

CREDIT: A. L. BRASS *ET AL.*, *SCIENCE*

Complex relationship. HIV (*top*, purple) relies on more than 200 human proteins to infect immune cells, enter the nucleus, integrate itself into the chromosomes, and then make copies of itself.

side effects—after all, these HDFs presumably exist to help humans, not the virus. It's also a tall order to discover effective inhibitors against HDFs, says Deborah Nguyen, who with colleagues at the Genomics Institute of the Novartis Research Foundation in San Diego, California, recently published a more limited siRNA study to identify new HIV treatment strategies. "Unfortunately, I think this barrier won't be crossed for a while," predicts Nguyen, who says industry's interest in anti-HIV drug R&D is also waning.

Elledge acknowledges the hurdles but counters that many marketed drugs against other diseases target human proteins and provide more benefit than harm. And the hundreds of HDFs his group has identified may play limited roles in human health and development. "Perturbing one may not have a profound effect on a cell, but it may on HIV," he says. Yet he agrees that this flood of new data is confusing: "It takes some hard thinking about where to go next."

Greene says the most immediate challenge is to elucidate the molecular details of how these 273 HDFs interact with HIV. "Currently, the authors can only suggest possible connections," he says. "But what a great starting point." **–JON COHEN**

GEOPHYSICS

Daggers Are Drawn Over Revived Cosmic Ray–Climate Link

Last year, climate change scientists thought they had driven a silver stake through the idea that fluctuations in solar activity were behind global warming in the last century. Now, a high-profile team led by geophysicist Vincent Courtillot, director of the Institut de Physique du Globe in Paris, has sought to raise the dead in a paper linking changes in Earth's magnetic field to temperature variations in recent millennia.

The paper, which appeared last year in *Earth and Planetary Science Letters*, has drawn fierce criticism, including a rebuttal in the 15 January issue of *EPSL*, and sparked a rancorous debate on a climate blog. "There is nothing new nor valuable in Courtillot's paper," asserts Gilles Delaygue, a geochemist at the University Paul Cézanne Aix-Marseille 3. Not so, says Courtillot. "If we are proven to be right, this will seriously backlash on scientists' credibility," he says.

To illustrate how the sun and Earth's magnetic field influence climate, Courtillot's team presented a graph depicting how fluctuations in solar brightness and the strength and orientation of the geomagnetic field shifted up and down in unison with global temperatures during the past century. This was particularly apparent, they claim, from 1940 to 1970, when a decrease in solar brightness and subsequent weakening of the geomagnetic field was followed by a 0.2°C decline in average annual global temperatures. On centurial scales, Courtillot's team speculates that a higher flux of cosmic rays seeds cloud formation; more clouds would result in lower temperatures. On a millennial scale, they argue, changes in Earth's inner dynamo lead to rapid shifts of our planet's magnetic dipole. Currently, the magnetic north and south poles are located near the geographic poles, funneling cosmic rays into a bone-dry lower atmosphere. According to the team, when the dipole wanders toward more humid latitudes, more cosmic rays may interact with water vapor in the lower atmosphere, influencing cloud formation.

Their study challenges reports last year from the United Nations Intergovernmental Panel on Climate Change (IPCC), which hold that the primary driver of global warming in the past century is rising atmospheric concentrations of carbon dioxide and other greenhouse gases, largely from industrial and auto emissions. Courtillot is one of a handful of credible scientists who reject IPCC's bottom line. "Magnetic field fluctuations and sun pulses fit with global temperature change better than carbon dioxide does," he asserts, reviving a hypothesis that many scientists believe the IPCC reports had discredited. Knowing they are touching a sore spot, Courtillot cautions: "We are not yet drawing conclusions nor giving definitive explanations. We are providing new evidences from observations." He and his team acknowledge that "anomalous warming" in the past 2 decades apparently cannot be linked to solar or geomagnetic activity, although they decline to ascribe it to greenhouse gases.

More than a coincidence? In this controversial figure, Vincent Cortillot and colleagues argue that variations in Earth's geomagnetic field (ESK and SIT) and solar irradiance are linked to global temperatures in the 20th century, until the advent 2 decades ago of what they call an "anomalous warming."

Climate change researchers have set out to strangle the hypothesized climate-geomagnetism connection in its crib. In a comment in *EPSL*, Delaygue and climatologist Edouard Bard of the Collège de France point to flawed analyses of temperature records and other data that they claim undermine the study. Above all, they dismiss the proposed link between solar brightness and cooling in the middle of the 20th century. That cooling, Bard says, is known to be linked to sulfate aerosols, mainly from industrial emissions. "This was an obfuscation of a well-understood phenomenon," geophysicist Raymond Pierrehumbert of the University of Chicago in Illinois commented on RealClimate.org, a Web site run by climate scientists. Climatologist Phil Jones of the University of East Anglia in Norwich, U.K., adds that there is no need to invoke geomagnetism to explain the temperature record.

This is unlikely to be the last word in the saga. "Many mechanisms that have been debunked have not been debunked at all," claims Courtillot, who says that he will soon publish two studies arguing that methods used to measure global temperature need to be revised. Delaygue and many others, however, say that Courtillot's group is doing more harm than good by downplaying the carbon dioxide–climate change link. **–JACOPO PASOTTI**

Jacopo Pasotti is a writer in Basel, Switzerland.

CREDIT: LE MOUËL *ET AL.*, *EPSL* 232, 273 (2006), ELSEVIER

PALEOCLIMATE

More Climate Wackiness in the Cretaceous Supergreenhouse?

Climate modelers already had their hands full explaining what warmth-loving crocodiles were doing in the high Arctic 90 million years ago in the Cretaceous period. They just couldn't make their models get that warm in any polar region—north or south—without some serious cheating. Then, some researchers claimed they had evidence of a great sheet of glacial ice sitting on Antarctica at the height of this Cretaceous hothouse.

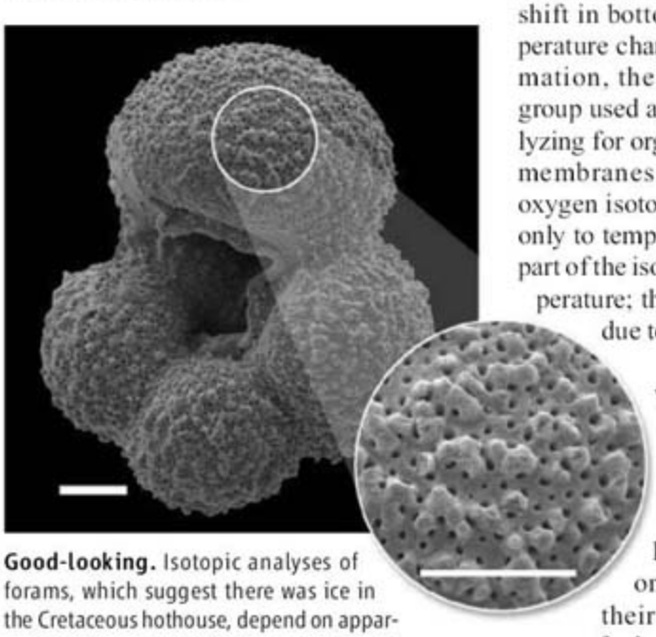

Good-looking. Isotopic analyses of forams, which suggest there was ice in the Cretaceous hothouse, depend on apparently unaltered shells (scale bars = 50 μm).

CREDIT: A. BORNEMANN

Now, on page 189, paleoceanographers present new data that make a case for ice. "They've done it exactly right," says paleoceanographer Timothy Bralower of Pennsylvania State University in State College. "This is a provocative paper. It's going to stir it up again."

The new work draws on a classic analysis of microfossils boosted by a newer innovation. Paleoceanographer André Bornemann of Leipzig University in Germany and his colleagues analyzed apparently unaltered Foraminifera picked from a sediment core drilled from Demerara Rise beneath the western equatorial Atlantic. Following a classic technique, the researchers measured oxygen isotopes in the forams' shells. They found a sharp shift toward the heavier oxygen-18 isotope in both surface- and bottom-dwelling forams from 91.2 million years ago.

Bornemann and his colleagues take the 200,000-year-long isotopic spike as a sign that an ice sheet existed then with at least half the volume of the modern Antarctic ice sheet. Whenever water leaves the ocean to fall as snow, which feeds ice growth, water molecules containing the lighter oxygen-16 isotope evaporate more readily, leaving more of the heavier oxygen-18 behind in seawater for forams to take up. Changing seawater temperature can also shift the isotopic composition of forams, but seeing the shift in bottom-dwellers—for whom temperature changes little—argues for ice formation, the group says. As a check, the group used a relatively new technique: analyzing for organic compounds unique to the membranes of certain microbes. Unlike oxygen isotopes, this technique is sensitive only to temperature. It confirmed that only part of the isotopic shift could be due to temperature; the rest, the group concludes, is due to ice formation.

"I've been a doubter of this whole business [of Cretaceous ice] for a long time," says paleoceanographer Richard Norris of Scripps Institution of Oceanography in San Diego, California, who is second author on the paper. But as their data came in, "I began to be more of a believer. Still, I'm not prepared to say we've nailed it." For one thing, in July 2007, paleoceanographer Kazuyoshi Moriya of Kanazawa University in Japan and colleagues published an oxygen isotopic study of another claimed interval of Cretaceous ice 95 million years ago. They found no isotopic variation in surface-dwelling forams.

For another, despite a half-century of experience with a growing selection of paleoceanographic techniques, "we're right at the limit of what our proxies tell us, or a bit beyond," says Bralower. And then there's the searing Cretaceous climate. Karen Bice of Woods Hole Oceanographic Institution in Massachusetts studies hot paleoclimates through both models and proxy data. To her, lots of ice chock-a-block in time with Arctic crocs and hot-tub tropical oceans "is a difficult picture to buy." Analyses of more forams, researchers say, from more places in the world are in order.

–RICHARD A. KERR

Public-Access Backlash

Opponents of a new congressional rule that orders the U.S. National Institutes of Health (NIH) to post online copies of papers it funds are questioning the legality of the order. Buried in a spending bill (*Science*, 4 January, p. 18), the directive asks NIH to make mandatory an existing policy, mostly ignored, that asks grantees to submit copies of their peer-reviewed, accepted manuscripts to NIH for release within 12 months after publication. Last week, the Association of American Publishers (AAP) complained that the new policy "undermines" publisher copyright and is "inconsistent" with U.S. intellectual property laws. Open-access advocates support the new law because it gives taxpayers access to government-funded research.

AAP's Allan Adler says he's waiting to see how NIH will implement the law. But at minimum, AAP wants NIH to get public input in a formal rulemaking. In a statement, NIH said that "the law regarding a mandatory policy and copyright is clear." The agency is expected to announce its plan as soon as next week.

–JOCELYN KAISER

Coming to America

The number of new foreign students entering graduate programs in the United States has rebounded to nearly the levels predating the terrorist attacks of 2001. The U.S. National Science Foundation's latest *Survey of Graduate Students and Postdoctorates in Science and Engineering* shows that first-time foreign student enrollment in graduate science and engineering programs rose by 16% from 2005 to 2006, to 33,435, after dipping to 27,712 in 2004. The latest number is just shy of the 34,204 enrollments in the fall of 2001.

The increase is calming fears that visa restrictions put in place after the terrorist strikes are driving foreign talent to competing nations such as Canada and Australia. The uptick "suggests that the proactive steps by U.S. universities and by the U.S. government have been paying off and that America remains the destination of choice for graduate students, especially in the STEM [science, technology, engineering, and mathematics] fields," says Peggy Blumenthal of the Institute of International Education in New York City. But, she says, the numbers of students from some countries such as Pakistan and Egypt are still well below pre-9/11 levels, and competition for the best young talent remains fierce. "So we cannot afford to be complacent about the turnaround," she says.

–YUDHIJIT BHATTACHARJEE

REGULATORY POLICY

Panel: EPA Proposal for Air Pollution Short on Science

Time for review. EPA may revise its air standard for lead, which comes in large part from smelters like this one in Missouri.

A major attempt to streamline—or, critics claim, politicize—the revision of important air-quality standards has run into trouble. One year ago, the U.S. Environmental Protection Agency (EPA) overhauled its lengthy process of updating the National Ambient Air Quality Standards (NAAQS), which have far-reaching impacts on many regulations. Some critics feared the move would allow politics to trump science by giving agency appointees more say and sidelining external scientific review (*Science*, 15 December 2006, p. 1672). Now, some members of the agency's Clean Air Scientific Advisory Committee (CASAC) suspect that has happened in the first "policy assessment" created under the new process.

"It was just a disaster," says CASAC chair Rogene Henderson of the Lovelace Respiratory Research Institute in Albuquerque, New Mexico. The document, which requests public comment on possible changes to the standard for airborne lead, lacked adequate scientific analyses, Henderson says. It also included controversial ideas favored by industry, such as no longer regulating air emissions of lead under NAAQS, that CASAC had already nixed. As *Science* went to press, Henderson and other committee members were conferring about the document and how to improve the process. EPA's deputy administrator acknowledges shortcomings but says they reflect growing pains.

The Clean Air Act mandates that EPA set the ambient air quality standards according to the best available science and review them every 5 years. Lead is the first of the six pollutants covered under NAAQS to go through the new procedure. The review began in 2005, after the Missouri Coalition for the Environment sued EPA for having missed its statutory deadline to review the lead standard. Many of the new steps went well, according to EPA and CASAC.

A snag emerged with the policy assessment, formally known as an Advance Notice of Proposed Rulemaking. The notice is a shorter version of a document, prepared in previous NAAQS reviews, called the staff paper, which analyzed the scientific evidence for various changes to the standard and their impact on health. When CASAC was given the notice for comment on 17 December, however, some members were frustrated. "The lack of science is really a major problem," Henderson says. "We can't do our job without the analysis of the data." Marcus Peacock, EPA's deputy administrator and an architect of the new process, says the agency was under court order to create a staff paper for lead, and it had little time to produce the notice as well. More time will be spent on the notice for the next pollutant, he says, because the staff paper will be eliminated.

More discouraging to CASAC was the inclusion of the option of removing lead from the list of NAAQS pollutants, which the agency had previously floated (*Science*, 15 December 2006, p. 1671). Although both CASAC and EPA scientists have cautioned against this option, the notice offers it again for comment with no scientific rationale. "We were quite upset," says committee member Joel Schwartz, an epidemiologist at Harvard School of Public Health in Boston. "It seems like there were people that wanted policy options that did not have scientific support."

Peacock says that the agency wants to keep all options open—even removing the lead standard—in case new data or interpretations come in. "Frankly, I think that's unlikely," he admits, "but in a rulemaking process, you have to remain open." Comments on the proposed options are due 16 January. Under the court order, EPA must decide whether to revise the standard by 1 May and finalize any change by 1 September. **–ERIK STOKSTAD**

ECOLOGY

The Importance of Being Eaten

Like any close relationship, the partnership between acacia trees and the helper ants that fend off intruders for them can turn nasty. As ecologist Todd Palmer of the University of Florida, Gainesville, and colleagues reveal on page 192, ants and acacias in East Africa fall out when large herbivores such as giraffes, elephants, and antelopes are absent. Loss of these plant-eaters across Africa, the authors suggest, might therefore unleash unexpected ecological changes.

Conservationists often assume that safeguarding large animals such as elephants—the megafauna—will bring other preservation payoffs, says ecologist Douglas Yu of the University of East Anglia in Norwich, U.K. This research shows "that there's a link between saving megafauna and saving the little things that run the world."

The close interaction between acacia trees and their ants is one of the best-known examples of mutualism, an ecological relationship in which both parties gain. Brush up against an acacia growing in the highlands of central Kenya, for instance, and you might meet its fierce guardian, *Crematogaster mimosae*, whose swarming attacks can chase off mammalian herbivores that try to munch on the tree. The plant feeds and houses these defenders by exuding sweet nectar and growing large, hollow thorns where the ants shelter their young. Three other ant species that provide varying amounts of protection can inhabit the trees, and the four rivals battle to the death for control of individual acacias. But *C. mimosae* is the dominant species.

Palmer's curiosity about this mutualism was piqued several years ago when he noticed something unusual about plots of land that, as part of a different project, had been enclosed by herbivore-deterring electric fences. Even though the trees outside the wire were getting eaten—the ants aren't perfect protectors—they still seemed healthier than the trees inside.

After comparing plots of acacia trees that had been open or enclosed for a decade, the researchers can now offer an explanation for this seeming paradox: Without herbivores, the intricate relationship between the trees and *C. mimosae* unravels. With their leaves out of

CREDIT: JAMES A. FINLEY/AP PHOTO

ENVIRONMENT

Marine Mammals Still Imperiled After Sonar Ruling

LOS ANGELES, CALIFORNIA—Marine mammals won some protection last week from the U.S. Navy's submarine-chasing sonar technology. A federal judge imposed significant restrictions on use of the technology, known as mid-frequency active (MFA) sonar, in training exercises taking place off the southern California coast through January 2009. Environmental groups that brought the suit hailed the ruling. But researchers say it still leaves the most vulnerable species with little added protection.

MFA sonar detects ultraquiet submarines by bouncing powerful sound waves off their hulls. For more than 10 years, mass strandings of beaked whales and other marine mammals have been linked to its use, although the mechanism is not clear. Ruling on 3 January that the sonar posed a risk to species in the waters off southern California, Judge Florence-Marie Cooper of the U.S. District Court for the Central District of California ordered the Navy not to use it within 22 kilometers of the coast. She also told the Navy to use shipboard observers, aircraft, and hydrophones to monitor for marine mammals before and during the exercises and to turn off an MFA system if a marine mammal was detected within a 2000-meter "safe zone."

The Navy had sought less stringent restrictions. But Cooper called one such proposal—a safe zone of 180 meters—"grossly inadequate to protect marine mammals from debilitating levels of sonar exposure." At the same time, Cooper said that granting the 45-kilometer exclusion zone sought by plaintiffs, led by the Natural Resources Defense Council (NRDC), a New York City–based nonprofit, would "prevent the Navy from training to detect submarines in the very bathymetry [deep submarine canyons] in which submarines are most likely to hide."

Those canyons are also a popular foraging spot for beaked whales, the group most susceptible to MFA sonar. Robin Baird, a marine mammalogist with the Cascadia Research Collective in Olympia, Washington, who gave expert testimony in the case, says the zone will protect porpoises and migrating whales, but it does little for beaked whales. Likewise, a 2000-meter safe zone around sonar sources won't necessarily protect beaked whales, who Baird says are "more or less invisible" even at 300 meters.

Baird says that sea-floor hydrophone arrays, such as the Navy operates off San Clemente Island, can detect the whales' clicks and warn vessels of their presence. In other areas of the exercise zone, however, the downward directionality of the whales' clicks, coupled with the high speed of Navy vessels, makes ship-mounted hydrophones "fairly ineffective," according to Baird.

Necroscopies of stranded individuals point to decompression sickness—bubbles in the blood formed by rapid changes in pressure—as the cause of death. However, says Baird, "there's still a lot of uncertainty about what could lead to those symptoms." One possible reason that MFA sonar is particularly problematic for beaked whales is that its pings mimic the calls of killer whales, their primary predators. In a recent study, Peter Tyack of the Woods Hole Oceanographic Institution in Massachusetts speculates that the false calls might prompt the whales to leave the area rapidly by making a series of short, shallow dives that promote bubble growth.

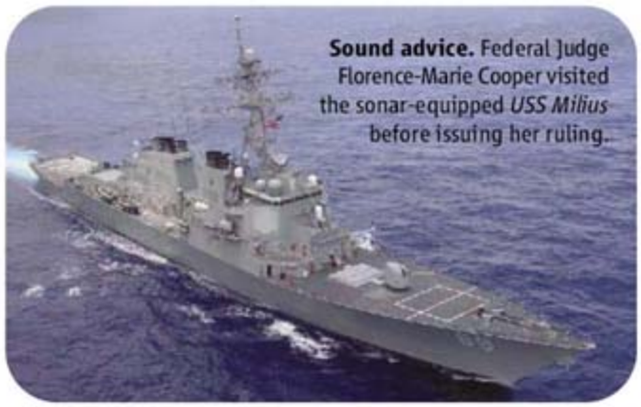

Sound advice. Federal Judge Florence-Marie Cooper visited the sonar-equipped *USS Milius* before issuing her ruling.

Cooper ordered a more sweeping ban in an initial ruling last August, but an appellate court in November told her to narrow the ruling. The Navy isn't satisfied. "We do not believe [the ruling] struck the right balance between national security and environmental concerns," says Commander Jeff Davis, a Navy spokesperson. The government is expected to appeal the ruling.

–BENJAMIN LESTER

Benjamin Lester, a former *Science* intern, is a freelance writer in Washington, D.C.

danger, acacias cut back on hollow thorns and nectar-producing glands. Meanwhile, the ants became less vigilant and were more likely to raise herds of sap-sucking scale insects, which provide the ants with food much the way dairy cattle provide milk. Besides pilfering a tree's liquid—a scarce resource in this dry habitat—the scale insects might spread plant disease, Palmer says.

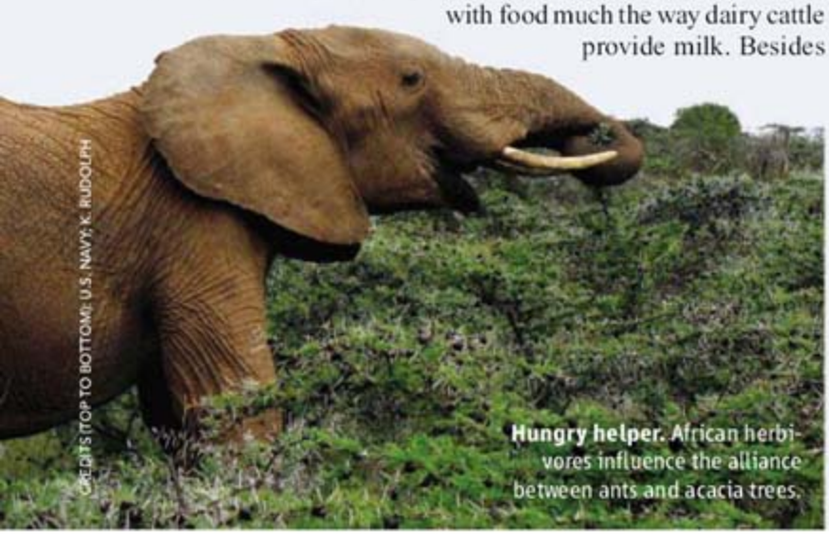

CREDITS (TOP TO BOTTOM): U.S. NAVY; K. RUDOLPH

Hungry helper. African herbivores influence the alliance between ants and acacia trees.

A related ant species, *C. sjostedti*, also took over the enclosed trees. A lackadaisical guardian, it somehow encourages colonization by wood-boring beetles that *C. mimosae* typically fends off. *C. sjostedti* nests in the holes the beetle drills instead of in the acacia's hollow thorns. The researchers determined that an acacia inhabited by *C. sjostedti* grows more slowly and is twice as likely to die as trees inhabited by the other ant species. "Big African mammals are important for maintaining cooperation between ants and plants," Palmer says, and this reciprocity "falls apart within a decade of herbivore removal."

Researchers often describe changes "rippling" through interlinked ecosystems, says evolutionary ecologist Anurag Agrawal of Cornell University. "This work illustrates rippling and puts mutualism into that context," he says. Competition and predation dominate studies of how interactions between species mold ecosystems, says evolutionary ecologist Judith Bronstein of the University of Arizona, Tucson. But scientists are now "getting a glimmer of how mutualisms are important in structuring communities."

–MITCH LESLIE

Gunning for the Ivy League

As they strive to become world-class educational institutions, China's universities must overcome a host of impediments, from antiquated curricula to mounting debt

TIANJIN, CHINA—When Rao Zihe became president of Nankai University in May 2006, he hatched a plan to restore glory to a faltering institution. To shake up the system, Rao set out to hire new deans for 15 of the 21 colleges. Applications flooded in. After interviewing six or eight candidates for each post en masse at Nankai's leafy campus here in Tianjin, a port city 120 kilometers east of Beijing, Rao chose his deans. Then he pulled a switcheroo: He offered faculty positions to all the runners-up—several dozen scientists—and most accepted.

Like a baseball executive building his team, Rao aimed for up-and-comers, mostly assistant and associate professors from top-tier institutions, including Yale University, Cornell University, and the University of Oxford. He brought aboard part-time senior academics and retired government officials to provide experience. All told, Rao hired more than 200 new faculty members—more than 10% of the academic staff—in the first 18 months of his term. Renewing the faculty one professor at a time "wouldn't achieve my objectives" of overhauling curricula and teaching methods and setting higher standards, he says: "We need a critical mass [to change] the environment."

Nankai's makeover is part of a broad push by Chinese authorities to create a tertiary education system that matches the country's aspirations. And like everything in China these days, it's being done in a hurry. In a remarkably short time, China has moved from universities for an elite few to mass higher education. University enrollment soared from 3.6 million in 1998 to 25 million in 2006. Nearly a quarter of college-age youth now receive tertiary education, surpassing the country's goal of 15% by 2010.

The quality of education has largely been an afterthought—until now. According to today's mantra, a vigorous higher education system will promote homegrown innovation. Aiming for the stars, Chinese educators and leaders want their top universities to join the ranks of the world's best.

They have a long way to go. "There's a huge gap between China's universities and world-class universities," says economist Yingyi Qian of the University of California, Berkeley, now on leave while heading the School of Economics and Management at Tsinghua (Qinghua) University in Beijing. Undergraduates at China's top universities are on a par with those at top U.S. schools, says Qian, who has studied how China's education revolution compares to the shift from elite to mass education in the United States in the late 19th century. As China expands the system, it needs to add quality to quantity, Qian and others say, by employing far more world-class professors. He predicts that will take decades.

One big handicap is insufficient funding: Government support has not kept pace with rising enrollments or China's soaring gross domestic product. Many universities borrowed heavily to finance expansions and overhauls and are now saddled with debt. "If the government does not increase the investment [in higher education], then there will really be a problem here," says Ma Wanhua, an education professor at Peking (Beijing) University.

Another key ingredient in short supply is academic freedom. The central government appoints national university presidents, approves curricula, decides evaluation criteria, and sets admission standards through the Ministry of Education's entrance exam, a matriculation requirement for all national universities. "If a university does not have academic freedom as its core

Higher Education in China

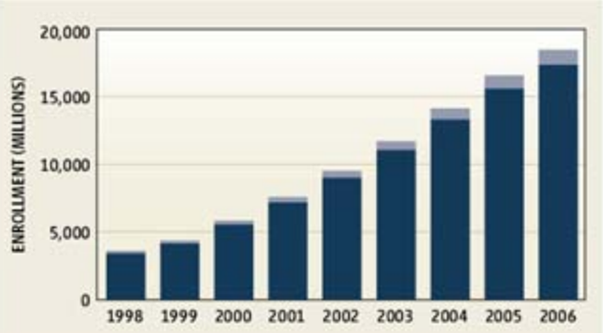

Rising fast. Enrollment at 4-year universities (blue) and graduate schools (light blue) in China has taken off since 1998.

SOURCE: CHINESE MINISTRY OF EDUCATION; CREDIT: NANKAI UNIVERSITY

More than a face-lift? Nankai University hopes that dozens of new professors and deans will reinvigorate its educational programs and rehabilitate its reputation.

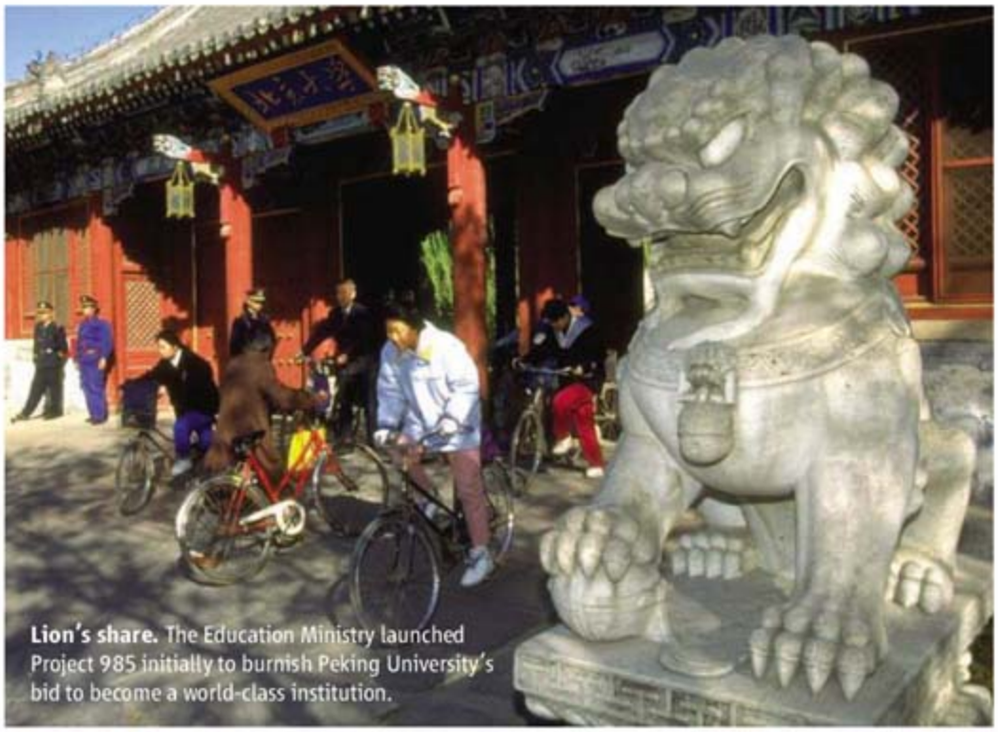

Lion's share. The Education Ministry launched Project 985 initially to burnish Peking University's bid to become a world-class institution.

value, no matter how grand its buildings, how beautiful its campus, and how luxurious its facilities, it's useless to talk about world-class," Yang Dongping, an education scholar at the Beijing Institute of Technology, warned recently in the newspaper *Nanfang Zhoumo* (*Southern Weekend*).

Great Leap Forward?

Before the People's Republic of China was founded in 1949, the country had scores of comprehensive universities. In the 1950s, China adopted the Soviet model of specialized higher education. For example, to remake Tsinghua in the likeness of the Moscow Power Engineering Institute, nonengineering departments were moved to other universities. All universities were ordered to focus on education and leave research to institutes of the Chinese Academy of Sciences. These moves "completely destroyed" the previous education system, Qian says. Colleges founded in the 1950s concentrated on a single specialty: textiles, railways, metallurgy, and so on. Then in the 1960s, the Cultural Revolution shut down universities altogether. They resumed operations in the late 1970s but only admitted a tiny number of elite students.

Enrollments rose steadily, but by 1998, only one in 10 college-age youth were educated beyond high school. The next year, campus gates swung wide open, when Tang Min, an economist with the Asian Development Bank, suggested that China counter an economic slump by expanding university enrollment to boost domestic spending. The suggestion appealed to China's leadership, which realized that economic development required more homegrown engineers and scientists. Admissions have since risen fivefold.

As early as 1995, the education ministry launched a plan to prepare 100 universities for the 21st century. Project 211 put $2.3 billion on the table, mainly for infrastructure and curriculum development. In 1998, after then-President Jiang Zemin proclaimed that "China must have a number of first-rate universities of international advanced level," the ministry hatched Project 985, which aims to help universities fortify existing strengths and develop new research areas. Originally intended for Peking University (Beida) and Tsinghua University—widely considered China's two best—the program has since been expanded to three dozen universities. Most of the money has gone to building capacity. For example, Beida used a portion of its $225 million 985-phase-1 allocation to establish the Institute of Molecular Medicine, focusing on translational research for cardiovascular diseases.

Despite this largess, the central government's overall university budget allocation has declined from an average of $847 per student in 1998 to $672 per student in 2005, according to former education minister Chen Zhili. Compounding the decline, many local governments have failed to honor pledges to match central-government funding.

Since 1998, the funding shortfall has forced universities to borrow an estimated $25 billion from banks, mainly to finance expansions. An extreme case is the new Jilin University (Jida) in Changchun, created in 2000 from the merger of five local institutions. (The government was then urging such mergers as a way of creating comprehensive universities that would be globally competitive.) Jida borrowed $400 million over 5 years, largely for bricks and mortar. Its precarious finances were further undermined when the Jilin provincial government failed to deliver promised support. Now the university is saddled with interest payments of about $20 million annually, which is contributing to a budget shortfall of $70 million. The financial mess came to light when an internal memo calling on faculty and students to brainstorm solutions got posted on the Internet in March. Jida's president has since publicly acknowledged the problem.

Jida is hardly alone. A team led by Beida education scholar Bao Wei reported to the nation's legislators last March that 72 major national universities have $4.5 billion in outstanding loans—an average of $62.5 million per university.

Universities have tried to balance their books by increasing tuition, which rose 25-fold over 2 decades to an average of $625 per year in 2005, according to the 2006 *Blue Book on Education* in China. In comparison, average per capita income in rural China was $376 that year. Although tuition is a huge burden for many families, Beida President Xu Zhihong says it covers a minuscule fraction of costs. Public universities cannot increase tuition without approval from the education ministry, which in 2006 ordered a 5-year freeze on tuition and fees.

"We needed new people, new fields, new subjects."

—RAO ZIHE, NANKAI UNIVERSITY

So universities resorted to setting up affiliated "independent" colleges that cater to students who fail to pass the entrance exams for public universities but are able to pay higher tuition. About 300 such colleges are enrolling students. "We don't know what the standards of these newly established universities are," says Ma. Although the ministry barred public

CREDITS (TOP TO BOTTOM): FORREST ANDERSON/TIME LIFE PICTURES/GETTY IMAGES; D. NORMILE/SCIENCE

universities from opening more affiliates and ordered them to disassociate themselves from existing ones, those already established will be allowed to continue on their own. In another tap on the brakes, the ministry has limited the annual growth rate of admissions to no more than 5% for the foreseeable future.

At a press conference last autumn, Education Minister Zhou Ji played down the debt crisis as a "special situation in a historic process and not as bad as some have imagined." Zhou said that the central and local governments would increase allocations to universities. Observers expect that any ramping up will be gradual.

It's the faculty

Financial ills are likely to be cured sooner than ailing faculties. At most Chinese universities, senior faculty members entered their university as undergrads and joined the faculty while working on Ph.D. degrees. Such inbreeding, Rao and others say, results in outmoded courses, antiquated teaching methods, and a lack of fresh ideas for research. When Rao arrived at Nankai, the university's life sciences courses focused on traditional disciplines such as entomology and botany and ignored emerging fields; curricula and teaching methods were little changed from the half-century-old Soviet-style model; and there was little interaction among departments. "We needed new people, new fields, new subjects," Rao says. Meanwhile, throughout the 1980s and 1990s, many of China's best and brightest scholars established careers overseas.

Brainstorming. Jilin University's president implored everyone on campus to think of ways to solve the school's debt problem.

The need to infuse new blood into universities was recognized in the 1990s, when the government set up incentive programs to tap the expertise of expatriate Chinese. Many programs offered lucrative incentives for overseas scholars to return. The programs have had mixed results: Some of these "sea turtles"—as the returnees are nicknamed in Chinese—were looking for easy moonlighting gigs. Indeed, some star part-timers offer their host institutions little more than high-profile names that are good for public relations (*Science*, 22 September 2006, p. 1721). "We call them 'seaweed,' "

ENGINEERS AIM FOR A QUALITY BOOST

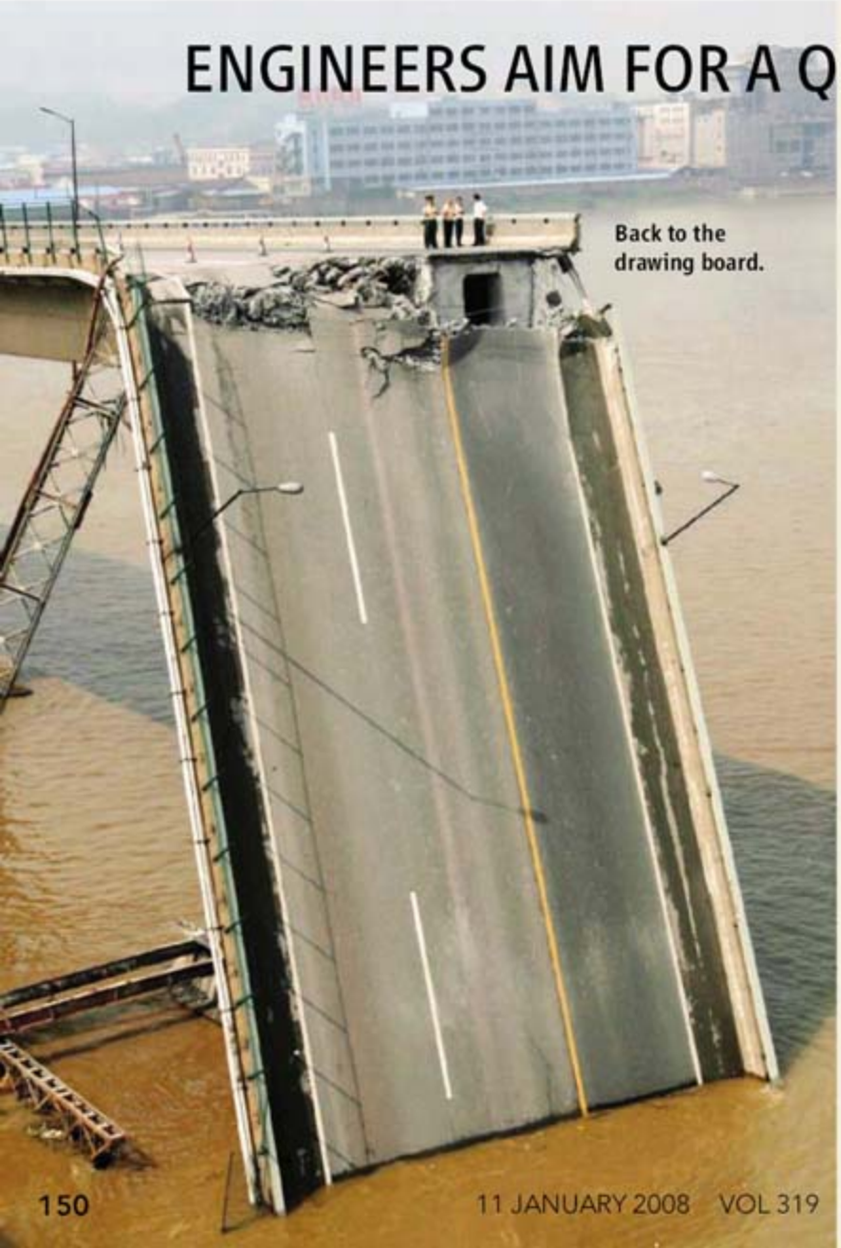

Back to the drawing board.

The phenomenal numbers of scientists and engineers churned out by China's universities has prompted much hand-wringing in the West. Three years ago, for example, when the U.S. National Academies called for a broad federal effort "to create new, high-quality jobs for all Americans," a draft report echoed some widely used, scary numbers: In 2004, the United States produced roughly 70,000 bachelor's-trained engineers versus China's 600,000 and India's 350,000.

Such statistics are misleading, claims a team led by Gary Gereffi and Vivek Wadhwa, both of Duke University in Durham, North Carolina. Each country, they note, uses differing methodologies and different definitions of "engineer." China's figures include graduates from 2- and 3-year programs and vocational fields such as car repair. U.S. numbers, in contrast, exclude computer science and information technology majors, which Gereffi and Wadhwa argue should fall under a broad definition of engineering. Their reanalysis of the 2004 numbers found that 137,000 students graduated from rigorous 4-year engineering programs in the United States compared with 351,000 in China and 112,000 in India.

> *"The Chinese increased quantity at the cost of quality."*
>
> —VIVEK WADHWA, DUKE UNIVERSITY

Just how talented are the droves of overseas engineers? "The bottom line is that the Chinese increased quantity at the cost of quality," says Wadhwa, whose team examined this topic in the January 2008 issue of the *Journal of Engineering Education*. Interviews with companies in China indicate that although top Chinese universities produce solid engineers, the quality of graduates of most universities is poor, Wadhwa says.

The Chinese government has recognized the quality gap. Last September, it launched a pilot program on engineering education reform to raise quality at 10 top Chinese universities, including Tsinghua. For Tsinghua and the handful of other institutions that attract the best students, says Yingyi Qian, who heads Tsinghua's School of Economics and Management, "if I cannot turn them out to be competitive on the global stage, that's a failure."

–D.N. AND H.X.

CREDITS (TOP TO BOTTOM): CHINA PHOTOS/GETTY IMAGES; AP

says Bo Li, an ecologist at Fudan University in Shanghai.

Other part-timers offer genuine added value to a host institution. One example is forest ecologist Chen Jiquan of the University of Toledo, Ohio, who for the past four summers has organized an ecology lecture series at Fudan. Last year, Chen flew in leading lights, including Jerry Franklin of the University of Washington, Seattle, to lecture to several dozen graduate students who competed for a position in the seminar. "This way the students are exposed to the frontiers of science," Chen says. For the short term, a reliance on part-timers is "beneficial" in exposing professors and students to new ideas and global trends, Qian says. But building world-class institutions, he notes, is a full-time job.

The tide may be turning. More and more highly qualified Chinese-born academics are forsaking overseas posts to devote all their energies to building China's education system. Although they earn less in China, they have other motivations. Yi Rao said that for him it was a "sense of belonging." He gave up an endowed professorship at Northwestern University's Feinberg School of Medicine in Chicago, Illinois, to become the dean of Beida's College of Life Sciences in September. Rao was the first endowed professor in life sciences to return to China full-time. Another senior returnee is structural biologist Yigong Shi, currently a professor in the Department of Molecular Biology at Princeton University. He has been advising Tsinghua University since 2003 and plans to soon take up a full-time position there to lead its School of Biological Sciences and Biotechnology.

Nankai's Rao went a step further, recruiting entire teams. Immunologist Yin Zhinan, who gave up a tenure-track position at Yale University to become dean of Nankai's College of Life Sciences, says that he would have worried about being ineffectual if he were one of only a few coming back. "For modern biomedical science, you really need collaboration and interaction. If you are the only one, there aren't enough resources or enough interaction," he says. With 55 new faculty members in life sciences, medicine, and pharmacology, Yin says, "we should be able to build a unique biomedical program."

Rao's team-building is a work in progress, in that some recruits are at Nankai only part-time. Romano Rupp, a physicist at the University of Vienna in Austria, is dean of Nankai's Teda Applied Physics School—but is only in Tianjin when his class schedule in Vienna permits. One of Nankai's new deans asked not to be identified in *Science* because he has yet to negotiate the terms of his departure from his current institution. He will be working at Nankai part-time for at least 2 years. Other new recruits say that a challenge for Nankai is bringing facilities, students, and logistical support up to levels they grew accustomed to overseas. If support fails to match expectations, they say, the best may leave. For this reason, "it is too early to tell" whether the overseas hires will have an impact at Nankai, says Ge Molin, a mathematician who has spent his entire career at the university.

One priority. In Beijing's smoldering summer, a worker keeps Tsinghua's lawn in front of its Soviet-style building at Harvard standards.

CREDIT: HAO XIN

Nankai is getting some funding from the Tianjin government. "To be honest, we don't know" how long the support will continue, Yin says. Rao admits that he agreed to less than a full commitment—a "soft landing," he calls it—for many recruits so that they could wrap up affairs at the institutions they are leaving. But in the long run, he says, "I cannot tolerate any deans being part-time."

The Chinese government hopes to tackle the dearth of qualified faculty members by redoubling efforts to send graduate students overseas. Last year, the government promised to give the China Scholarship Council $1.3 billion over 5 years to pay for 5000 scholarships a year for students who have been accepted by Western institutions. The rationale is that foreign-trained Ph.D.s will boost faculty quality when they return home, as required by award contracts. The program has been criticized, however, for shortchanging domestic graduate programs and grad students, who receive stipends of less than $100 per month.

Fresh blood among faculties won't, by itself, reform all the entrenched practices and petty regulations that conspire to keep Chinese universities out of the higher echelons. Education ministry requirements are so detailed that, for example, they specify that only full professors can supervise Ph.D. students. "In the U.S., who supervises graduate students and Ph.D. students? All professors, including assistant professors!" Qian says. "The assistant and associate professors are on the frontier." Qian hopes that an awareness of practices at top foreign universities will prompt reforms in China. "Just having this goal [of seeking world-class status] will be enormously helpful," he says.

These issues will not be resolved in a hurry. Yin worries that Chinese impatience is leading to unrealistic expectations about how quickly educational quality can be improved. "We really need to calm down. You cannot expect a big outcome in 2 or 3 years," he says. Beijing's Rao agrees and claims that China's best universities—even Beida and Tsinghua—are still third-rate. "It is premature, if not counterproductive, to raise expectations about Chinese universities becoming world-class soon," he says. "Let's be realistic and first take steps to make them second-rate before we go further."

–HAO XIN AND DENNIS NORMILE

With reporting by Gong Yidong of *China Features* in Beijing and Richard Stone in Shanghai.

VALÉRIE PÉCRESSE INTERVIEW

After Initial Reforms, French Minister Promises More Changes

Despite fierce protests, France's new higher education and research minister pushed through a major university reform bill. I'm only getting started, she says

PARIS—French Higher Education and Research minister Valérie Pécresse has survived her first big political test. In November and December, students organized occupations and strikes at almost half of France's universities to demand the repeal of the "Pécresse Law." Designed to give universities more autonomy and part of French President Nicolas Sarkozy's plan to revamp the nation's research, the law had been presented in June and was approved by France's Parliament in August.

The protests, fueled by broader discontent about pension changes and salaries, eventually died down. And Pécresse has already announced other reforms, including a plan to reduce the 50% failure rate among first-year university students. Although some say further shakeups in France's education system are long overdue, left-leaning researchers' groups are wary of the minister's plans to boost project-based funding and private research.

Pécresse, 40, arrived with little previous experience in research or higher education. A graduate of the elite École Nationale d'Administration in Paris—the training ground for many French politicians—she had a series of jobs in the government of former president Jacques Chirac. In 2002, she was elected to the National Assembly, where she has focused on family issues.

–MARTIN ENSERINK

Q: Were you impressed by the intensity of the student protests last fall?

V.P.: If you're a minister for higher education in France and you want to change things, then you have to be prepared for demonstrations, strikes, and violent uproar. So I knew it was coming. Of course, there was real opposition, but many of the students simply had unfounded fears about the new law. I gave them reassurances, but also I told them: "This is the law of the Republic. It's being implemented. I cannot repeal it."

Q: How much will this reform really change the university landscape?

V.P.: It may not look like a big deal through an Anglo-Saxon prism, but for France, it's completely revolutionary. Our universities are still very bureaucratic. They have huge elected councils. Presidents are elected by 140 people. It takes 12 to 18 months to recruit one researcher. The law gives universities the ability to handle their own budgets, their own human resources. They can develop their own research and education strategies—and they will bear responsibility for the success or failures of their labs and students. They can start foundations to raise private money. That's revolutionary, too.

I think all of this will also lead to a change in culture. In France, there's almost no spirit of belonging to a university. Students come in, they study, and they leave. Even professors don't feel very attached to the institute. I think people will start taking more pride in their universities.

Q: The universities did not get the right to select their own students—they have to accept anybody who has passed the state-run baccalauréat exam—or set tuition fees. Why not?

V.P.: The baccalauréat is our selection procedure. That costs millions of euros, and it takes a full month. So why would we introduce another form of selection at the entrance of the university? As to tuition fees, my priority is for universities to raise new money through partnerships with the private sector and by offering "lifelong learning" programs, to be paid for by employers. I want them to try that first. I'm not sure that the French people could accept a decision to let universities determine their tuition fees.

Q: Some scientists have expressed concern that your plans will undermine the role of big government institutes like the National Centre for Scientific Research (CNRS) and the National Institute for Health and Medical Research (INSERM). Some fear they might even be turned into funding agencies.

V.P.: They won't become funding agencies, but their organization will need to change. About 80% of our research is done in so-called mixed units, made up of researchers from universities and CNRS or INSERM. At the moment, they often have four or five forms of supervision, four or five accounting systems. … That's too complex; there's too much red tape. I have created a commission presided over by my predecessor, François d'Aubert, to look at this.

Apart from that, I do want to increase the emphasis on project-funded science, which is something completely new as well. Our National Research Agency (ANR) is only 2 years old, and its budget will increase by 25% until 2012.

Q: Yet many French researchers appear wary of project-based funding. They say it's an Anglo-Saxon model …

V.P.: They must never have visited Germany.

Q: … that creates a rat race and stifles researchers' freedom and creativity.

V.P.: Well, science is at the service of society. It's paid for with public money that must be invested very efficiently and on the basis of excellence. Project-based funding is part of that strategy. In addition, we can use it to address new research priorities that would otherwise be neglected. And it's not true that it stifles creativity. The ANR is also a way to help young, very creative researchers who would not find their way in the current, bureaucratic system.

CREDIT: JOEL SAGET/AFP/GETTY IMAGES

Getting a Quick Read on the Biggest Tsunami Earthquakes

As a huge tsunami raced unnoted across the Bay of Bengal toward India in December 2004, seismologists feverishly sized up the earthquake that had generated it. In those first minutes, the signals pouring in from seismometers suggested its magnitude was 8.5, only marginally large enough to threaten India with a tsunami. Wrong. It turned out to be a great magnitude-9.1 quake capable of generating a far-traveling destructive tsunami (*Science*, 14 January 2005, p. 201). The magnitude based on conventional early-arriving seismic waves—then seismologists' only means of rapidly determining the tsunami threat—vastly underestimated the power of the great quake.

A warning, please. New seismic techniques will greatly improve tsunami alerts.

CREDIT: JOHN STANMEYER/AP

At the meeting, two groups reported new techniques for accurately determining the tsunami threat in 10 to 20 minutes rather than waiting hours for reliable data. Seismologists Hiroo Kanamori of the California Institute of Technology in Pasadena and Luis Rivera of Louis Pasteur University in Strasbourg, France, proposed using so-called W phases, low-frequency seismic waves with periods of 100 seconds to 1000 seconds. After a 1992 Nicaraguan quake produced a surprisingly large tsunami, Kanamori recognized that early-arriving W phases accurately reflect a quake's tsunami-generating power.

But W phases were too difficult to extract from the seismic record. Kanamori and Rivera have now modified an existing technique so that it quickly picks W phases out of records and extracts the needed information. Applied to a half-dozen quakes, the technique provided the same magnitude estimates as waves arriving hours later at the same stations. Kanamori believes W phases can be used to determine an accurate magnitude of great quakes within 15 to 20 minutes of their start, maybe 10 minutes if there are enough seismometers nearby.

Seismologists Andrew Newman and Jaime Convers, both of the Georgia Institute of Technology in Atlanta, took a more empirical approach. Noting that "tsunami earthquakes" like the 1992 Nicaraguan quake produce weak but long-lasting shaking, they simply plotted 40 large earthquakes by the amount of high-frequency energy they released—their shaking—against their duration. The tsunami-generating quakes clearly stood apart without any false alarms. And they could be identified within 10 minutes of the quake, Newman said.

Both of the new techniques "are hot for us," says seismologist Barry Hirshorn of the Pacific Tsunami Warning Center in Ewa Beach, Hawaii, and will be made operational as quickly as possible. **–RICHARD A. KERR**

CLIMATE TIPPING POINTS COME IN FROM THE COLD

Tipping points, once considered too alarmist for proper scientific circles, have entered the climate change mainstream. At the meeting, a nearly packed half-day session considered the prospects for a climate system that is still creeping through change but might soon cross a threshold into an entirely new way of operating. The new climate regime may have no sea ice in Arctic summers, a much smaller ice sheet on West Antarctica and higher sea levels, or wildly redirected storm tracks. Current understanding of climate allows that such drastic transitions can happen, the speakers agreed. Earth may even be in the midst of one now.

As evidence, glaciologist Richard Alley of Pennsylvania State University in State College cited Earth's response to the warming that has occurred over the past 3 decades. Compared with the soaring global temperatures that the strengthening greenhouse could drive through the rest of this century, that warming has been rather small, Alley said. Yet it is having immediate and often unexpected effects, he observed.

> *"The tipping point for perennial sea ice has likely already been reached."*
>
> —JOSEFINO COMISO, GODDARD SPACE FLIGHT CENTER

Since the 1960s, mountain glaciers around the world have begun to shrink and are dwindling rapidly. Arctic summer sea ice took a severe hit last year after decades of slow losses. And the Greenland ice sheet is now clearly shrinking under some unexpected attacks. Warming seas are weakening glaciers' surprisingly fragile ice tongues, which help slow glaciers' rush to the sea. And meltwater on the surfaces of glaciers is plunging down giant cracks to glacier beds, where it's lubricating the glaciers' seaward slip-sliding. "If a very small warming makes such a difference," Alley said, "it raises the question of what happens when more warming occurs."

Sea ice specialist Josefino Comiso of NASA's Goddard Space Flight Center in Greenbelt, Maryland, said at the meeting that in the Arctic, "the tipping point for perennial sea ice has likely already been reached." Ice persisting from year to year has not been steadily shrinking in area, he said. The decline of summer sea ice accelerated in the mid-1990s; since then, summer ice has been disappearing more than three times faster than before. And the feedback between solar warming of newly ice-free Arctic waters and the loss of still more ice has become more and more obvious. Only colder summers and colder winters can save summer sea ice from oblivion, he said, an unlikely development at this point.

Other speakers presented possible tipping points that have gotten less attention: an eventual sudden shift in jet streams that would bring rapid climate change to North America and Europe and the abrupt collapse of the Amazon tropical forest, among others. Clearly, the possibilities are proliferating faster than researchers can confirm or deny them. **–R.A.K.**

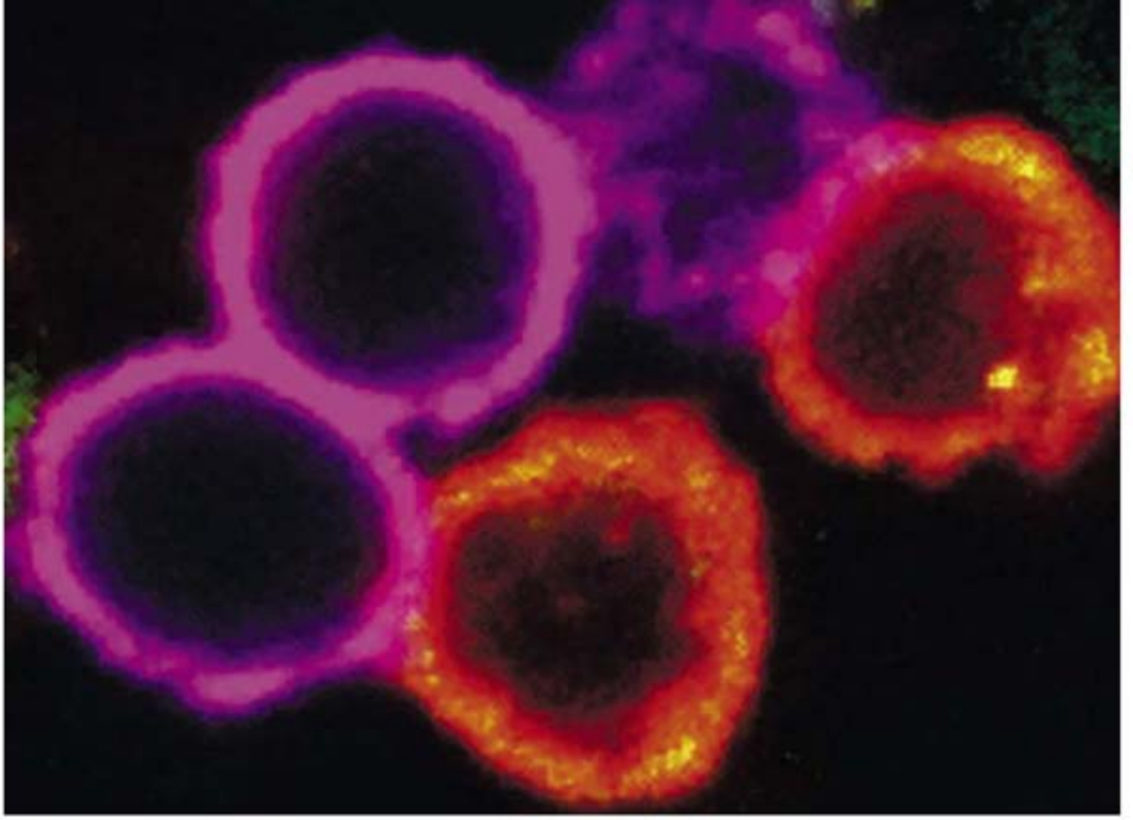

Close contact. MDSCs (red) are shown here interacting with CD8+ T cells (magenta).

CANCER IMMUNOLOGY

Cancer's Bulwark Against Immune Attack: MDS Cells

First noticed in the 1970s, myeloid-derived suppressor cells appear to play a key role in sustaining tumors; new methods of overcoming them are being tested

For decades, researchers have been engaged in a frustrating effort to harness the power of the immune system to fight cancer. The approach works well enough in test tubes and experimental animals. Many types of cancer cells are studded with antigens that distinguish them from normal cells, and activated immune cells can seek out these targets and kill the cells that carry them. Yet attempts to destroy tumors by sparking similar responses in human patients, using so-called cancer vaccines and other immunotherapies, have largely ended in failure. Now, researchers may have an answer to this puzzle: A recently identified class of immune cells may help sabotage these efforts.

Within the past few years, researchers have found that production of cells known as myeloid-derived suppressor cells (MDSCs) is markedly increased in cancer patients. As their name suggests, MDSCs are potent suppressors of several facets of the immune system. By damping down antitumor responses, MDSCs might contribute both to the original growth of the cancers and to the failure of immunotherapies.

MDSCs might help explain another aspect of cancer biology as well: the apparent link between tumor growth and chronic inflammation (*Science*, 5 November 2004, p. 966). Regulatory molecules, or cytokines, produced either by the cancer cells themselves or by other cells in the tumor environment, help trigger MDSC accumulation. And many of these cytokines also promote inflammation, suggesting that MDSCs may be at least partly responsible for inflammation's carcinogenic effects.

Some clinical implications of these findings are already beginning to emerge. As cancer immunologists learn what makes MDSCs tick, they are using that information to design strategies to counteract them in the hope that this will make anticancer vaccines and other immunotherapies more effective. Indeed, researchers have already identified drugs that inhibit MDSCs and have begun preliminary clinical trials. If what the field has learned so far is correct, "using different drugs [to block MDSC action] could drastically improve responses to cancer vaccines," predicts Dmitry Gabrilovich of the H. Lee Moffitt Cancer Center and the University of South Florida in Tampa.

MDSC pioneers. Vincenzo Bronte (*left*) and Dmitry Gabrilovich (*right*) were instrumental in linking MDSCs to cancer growth.

Early sightings

Although MDSC-like cells have been known since the 1970s, "the association with cancer is recent," says Vincenzo Bronte of the Istituto Oncologico Veneto in Padua, Italy. It can be traced partly to researchers' efforts to find out why cancer vaccines weren't working.

About 10 years ago, for example, Bronte, then working with cancer immunologist Steven Rosenberg at the U.S. National Cancer Institute in Bethesda, Maryland, got a surprising result when he immunized mice with a tumor antigen and then gave a booster shot of the same antigen 6 days later. The animals' immune response was not enhanced as expected. It was suppressed instead. Bronte and his colleagues traced the problem to an unusual group of immune cells—later called MDSCs—that were somehow taking out the $CD8^+$ T cells that would normally respond to the antigen in the vaccine.

Analysis revealed that these suppressors were immature cells from the myeloid line that produces macrophages and the dendritic cells that are needed to trigger immune responses. Their normal function, the researchers proposed, is to help put the brakes on immune responses so that they don't run out of control.

CREDITS (TOP TO BOTTOM): SRINIVAS NAGARAJ; COURTESY OF VINCENZO BRONTE; COURTESY OF DMITRY GABRILOVICH

In cancer patients, though, their long-term persistence is a problem. "There's nothing special about these cells; they're normal immature myeloid cells," Gabrilovich says. But, he adds, they "are supposed to differentiate normally and not get activated and hang around in this state."

As researchers soon learned, cancer leads to increased myeloid suppressor cells even without vaccination. In the late 1990s, Gabrilovich, in collaboration with M. Rita Young at Loyola University Chicago in Illinois, was also trying to find out why cancer vaccines are so ineffective. "We started looking at mice with tumors," he recalls, and found that as much as 40% of the cells in the animals' spleens—an organ that produces and stores various immune cells until they're needed—were myeloid-derived suppressor cells. Human cancer patients, too, had three to five times more of the cells than did healthy controls. Meanwhile, the numbers of dendritic cells were decreased.

These cellular changes get more pronounced as tumors grow. As a result, patients with advanced tumors—precisely the ones who have been in most clinical vaccine trials—have large numbers of suppressor cells that could interfere with their treatment. "There's no question about it; we're going to have to deal with these cells to do immunotherapy," says Suzanne Ostrand-Rosenberg of the University of Maryland, Baltimore County.

Researchers are beginning to explore several ways of dealing with MDSCs. One approach exploits the fact that they are developmentally immature. To promote the differentiation of the cells, Gabrilovich and his colleagues have turned to all-trans retinoic acid (ATRA), which is already used clinically to treat people with promyelocytic leukemia.

In a pilot study, the researchers gave the drug to 18 kidney cancer patients, all of whom had elevated MDSC levels. The short-term study was not designed to look for clinical improvements such as tumor shrinkage. But the immune status of the drug recipients improved; they had fewer MDSCs, more dendritic cells, and better immune responses. The Moffitt team is now beginning a more extensive trial that will test a combination of ATRA with a cancer vaccine. "Simply eliminating these cells won't do," Gabrilovich says. "You have to combine that with active immunotherapy."

Versatile actors

MDSCs turn out to have many ways of blocking immune responses. They can hit both the so-called innate and adaptive branches of immunity. On the adaptive side, they suppress antibody-producing B cells and $CD4^+$ (helper) T cells in addition to $CD8^+$ (killer) T cells.

One way they inhibit T cells is by blocking an essential activation step: the binding of antigen to the T cell receptor. About 4 years ago, Gabrilovich and his colleagues found that MDSCs release highly reactive molecules, including certain forms of oxygen and peroxynitrite. Findings from Bronte's group also pointed to an important role for peroxynitrite in immune suppression mediated by MDSCs. In a study published in the July 2007 issue of *Nature Medicine*, the Gabrilovich team further showed that peroxynitrite causes nitrate addition to T-cell receptors, rendering them incapable of binding antigens they would otherwise recognize.

Other researchers are focusing on a key regulator of T cells: the amino acid arginine. Its importance originally emerged in studies of patients who experienced serious trauma, including surgery. These individuals have low T-cell counts, making them very susceptible to infections, which can be fatal, particularly if they lead to a condition called sepsis.

Researchers, including a team led by brothers Juan Ochoa, a surgeon at the University of Pittsburgh Medical Center in Pennsylvania, and Augusto Ochoa, an immunologist at Louisiana State University (LSU) Health Sciences Center in New Orleans, have linked this immunosuppression to low levels of arginine in the patients. They found, for example, that in lab cultures, the amino acid is needed both for normal T-cell replication and for production of the zeta chain of the T-cell receptor. "The next question," Juan Ochoa says, "is what was destroying arginine."

Further work showed that it was none other than MDSCs. These cells are loaded with the enzyme arginase, which degrades the amino acid. About 2 years ago, Juan Ochoa and his colleagues showed that mice subjected to surgical stress produce large numbers of the cells, which proved to be potent inhibitors of T-cell activation. The researchers have also found high arginase production in cells from human trauma patients but haven't yet pinned down the exact nature of those cells.

Meanwhile, studies of both animal models and human patients have pointed to a similar immunosuppressive role of MDSC-produced arginase in cancer. In one study about 3 years ago, the Ochoas, with LSU's Paulo Rodriguez and colleagues, showed that arginase produced by MDSCs associated with lung cancers growing in mice impairs T-cell function in the animals by decreasing expression of the receptor zeta chain. MDSCs "interfere with the T-cell antigen receptor so that there is no signal" to activate the cells, Augusto Ochoa says.

The researchers also showed that treatment with an arginase inhibitor significantly slowed the growth of lung tumors in mice. Since then, the Ochoas and others have found that MDSCs from human cancer patients produce large amounts of arginase and nitric oxide synthase (NOS), another enzyme that degrades arginine.

These findings suggest that treatments that raise arginine levels in T cells can alleviate the

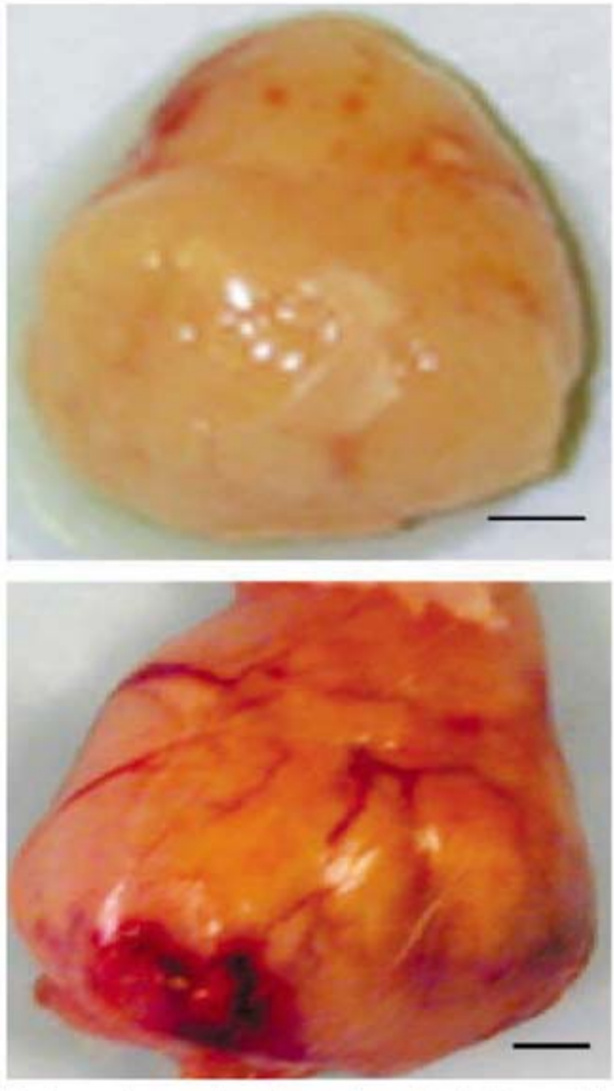

Angiogenesis promoters. A mouse tumor (*bottom*) exposed to VEGF-producing MDSCs has more blood vessels and grows larger than a control tumor (*top*) not exposed to the cells.

CREDIT: L. YANG ET AL., CANCER CELL 6, 409 (2004)

immunosuppression occurring in trauma and cancer patients. Indeed, dietary arginine supplements have already proved useful in combating infections in trauma patients, and preclinical work indicates that drugs that interfere with the synthesis or function of arginase and NOS might counteract the immunosuppressive effects of MDSCs. Ivan Borrello and Paolo Serafini at Johns Hopkins University School of Medicine in Baltimore, Maryland, working with Padua's Bronte, have looked at three such drugs—sildenafil (Viagra), tadalafil (Cialis), and vardenafil (Levitra)—that are much better known for their role in treating erectile dysfunction.

As Borrello and his colleagues reported a little more than a year ago in *The Journal of Experimental Medicine*, sildenafil in particular can decrease production of arginase and NOS by MDSCs, thereby boosting T-cell responses. In mice with colon or mammary tumors, treatment with both the drug and the T cells primed to recognize the appropriate cancer produced much greater inhibition of tumor growth than treatment with the T cells alone. Bronte and his colleagues have found similar effects in a mouse-tumor model with an aspirin derivative called NO-aspirin.

The inflammation connection

Much evidence throughout the past several years has supported the idea that inflammation promotes tumor growth. Exactly how it does that isn't clear, but recent evidence implicates MDSCs. Researchers have found that cancer cells produce a variety of proteins that either are directly inflammatory or can trigger the production of inflammatory cytokines in the tumor environment. Some foster MDSC accumulation, and, to make matters worse, MDSCs themselves have pro-inflammatory effects, thereby creating a vicious cycle that may perpetuate their own maintenance as well as tumor growth.

One early sign of an inflammatory link came from Gabrilovich and colleagues in 1996. They found that a protein called vascular endothelial growth factor (VEGF), which is released by tumor cells, promotes the accumulation of MDSCs by blocking dendritic cell maturation. VEGF helps tumors grow by stimulating angiogenesis, the formation of the new blood vessels they need. Angiogenesis is also a component of inflammation. And about 4 years ago, two independent teams, one led by Mario Colombo and Cecilia Melani of the Istituto Nazionale per lo Studio e la Cura dei Tumori in Milan, Italy, and the other by P. Charles Lin of Vanderbilt University School of Medicine in Nashville, Tennessee, showed that MDSCs also produce VEGF, thereby further promoting tumor growth and their own formation.

More recent work suggests that it may be possible to break this vicious cycle. Lin and others have found that VEGF secretion by MDSCs requires the activity of an enzyme called metalloproteinase-9. And the Colombo team now reports that a drug that inhibits this enzyme can reduce VEGF concentrations and the number of circulating MDSCs in mice that have mammary tumors. The drug also boosted responses to a vaccine directed against the tumor. (The results appeared in the December 2007 issue of *Cancer Research*.)

As shown by Ostrand-Rosenberg and her colleagues, the pro-inflammatory cytokine interleukin (IL)-1β also stimulates MDSC production, making it another target for drugs aimed at overcoming immune suppression in cancer patients. Evidence to support this idea comes from experiments on mice lacking the receptor through which IL-1β exerts its effects. As the Maryland team reported in the October issue of *Cancer Research*, mammary tumors implanted in the animals show reduced growth and metastases. "This led us to hypothesize that [MDSCs] are one of the connections between chronic inflammation and cancer," Ostrand-Rosenberg says.

Tumor cells also produce COX-2, a key enzyme in the pathway that makes inflammatory molecules such as prostaglandin E2 (PGE2). Ostrand-Rosenberg's team has found that MDSCs have receptors for the prostaglandin and that drugs that mimic its effects increase their formation while PGE2 inhibitors block it. In addition, the Ochoas and their colleagues have found that PGE2 stimulates arginase production by the cells. And both teams have shown in mouse models that COX-2 inhibitors can slow tumor growth. That may help explain why individuals who take COX-2 inhibitors, which have been widely used for treating arthritis and other inflammatory conditions, seem less prone to developing cancer than people who don't take the drugs.

Not only are MDSCs induced by inflammatory molecules, but in a situation similar to that seen with VEGF, they themselves can promote inflammation. Macrophages, which are part of the innate immune system, come in two types; M1 macrophages promote activity of killer T cells through their production of IL-12 and are thus antitumor, whereas M2 macrophages promote inflammatory responses through their production of IL-10.

In work reported earlier last year in The *Journal of Immunology*, Ostrand-Rosenberg's team found that MDSCs enhance the growth of mammary tumors in mice by interacting with M1 macrophages and converting them to the M2 type. "This sets up a strong feedback," she says, to further enhance MDSC activity. The results also indicate that the drug gemcitabine, which is already used to treat some cancers, exerts some of its effects by restoring IL-12 production by macrophages.

All in all, researchers are finding that MDSCs are extremely versatile immune suppressors and clearly a force to be reckoned with if immunotherapy is to succeed.

–JEAN MARX

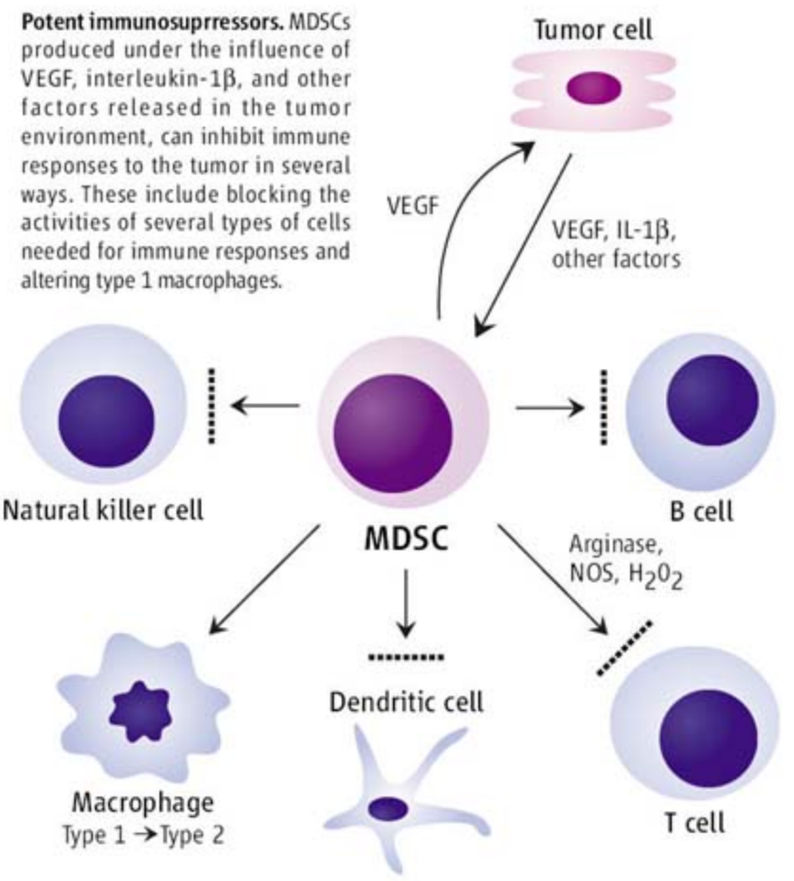

Potent immunosuprressors. MDSCs produced under the influence of VEGF, interleukin-1β, and other factors released in the tumor environment, can inhibit immune responses to the tumor in several ways. These include blocking the activities of several types of cells needed for immune responses and altering type 1 macrophages.

CREDIT: J. NEWFIELD/SCIENCE

LETTERS

edited by Jennifer Sills

Fighting Algae in Kaneohe Bay

"CALL THE HOSE BRIGADE!" (RANDOM SAMPLES, 10 AUGUST 2007, P. 729) DESCRIBES AN EFFORT to remove a massive nuisance algae bloom killing corals in Kaneohe Bay, Hawaii, by sucking it up with huge barge-mounted vacuum cleaners. Unfortunately, this will give only temporary results and will fail in the long run unless the nutrient excess that fuels the rapid growth is removed. Kaneohe Bay is a classic example of coral reef eutrophication: Benthic algal blooms caused by point discharges of sewage killed the reef in the 1970s, but died when the outfall was removed, allowing the reef to gradually recover (*1*). With continued suburbanization of the watershed, uncontrolled nutrients that discharge to the bay from golf courses, lawn fertilizers, and road runoff have again raised the nutrient concentrations (*2*, *3*) above the thresholds for nuisance algae (*4*–*6*). Aside from the temporary success in Kaneohe Bay, there are very few examples of algae being successfully removed. In one bay in Jamaica where all the land-based nutrients were diverted, nuisance algae that were choking the reef began to die in weeks, and only a few dying clumps of weedy algae remained 2 months later (*7*). If algae are starved of nutrients, they die very quickly, and will not return unless nutrient thresholds are again exceeded. But no amount of sucking them off will work when they grow right back because they are overfertilized. It is the suckers paying for this well-intentioned, but ultimately futile, effort who will be hosed unless the underlying causes of eutrophication are removed.

THOMAS J. GOREAU

Global Coral Reef Alliance, 37 Pleasant Street, Cambridge, MA 02139, USA. E-mail: goreau@bestweb.net

References

1. A. Banner, *Proc. 2nd Int. Coral Reef Symp.* **2**, 685 (1974).
2. E. Laws, C. Allen, *Pac. Sci.* **50**, 194 (1996).
3. S. Larned, J. Stimson, *Mar. Ecol. Prog. Ser.* **145**, 95 (1996).
4. P. Bell, *Water Res.* **26**, 553 (1992).
5. B. Lapointe, N. Littler, D. Littler, *Proc. 7th Int. Coral Reef Symp.* **1**, 323 (1992).
6. T. Goreau, K. Thacker, *Proc. Caribb. Water Wastewater Assoc.* **3**, 98 (1994).
7. T. Goreau, paper presented at the *UN Expert Meeting on Waste Management in Small Island Developing States*, Havana, Cuba, 27 October to 1 November 2003.

Response

T. J. GOREAU FEELS STRONGLY THAT THE PRIMARY cause of algal overgrowth of the coral reefs in Kaneohe Bay is eutrophication. We think he may have missed the point. While we agree that nutrient enrichment and overfishing are both important in causing algal blooms and coral-algal phase shifts on reefs around the world (*1*–*6*), including Kaneohe Bay in the 1970s (*7*), the story today is much more complicated (*8*–*12*).

First, the species of algae targeted for removal by the Super Sucker are non-native or alien species introduced to Kaneohe Bay for aquaculture research in the 1970s and have been growing unchecked since that time. These species are native to the western tropical Pacific and are cultivated for the carrageenan and agar industries in numerous areas covering thousands of hectares where eutrophication is not a problem (*13*).

Second, exotic species are considered one of the largest threats to global biodiversity where they alter ecosystem structure and function and cause substantial economic losses (*14*). The methods to remove alien algae from reefs in Kaneohe Bay were developed as a means to prevent or reduce negative effects of an invading species, while buying time for the development of biological control methods with the native sea urchin *Tripneustes gratilla* (*15*). Preliminary data (*8*) are encouraging, as areas that have been cleared by the Super Sucker remain clear of alien algae and have increased coral recruitment after just 2 years.

***Gracilaria salicornia* in Kaneohe Bay, Hawaii.** This exotic red alga, shown here overgrowing reef-building corals, is one of the species targeted for removal using the underwater vacuum cleaner known as the Super Sucker.

CREDIT: JENNIFER SMITH

Third, some introduced species are successful in new environments because they are competitively superior and because they have no natural predators. While nutrient enrichment can increase algal growth rates, more recently published nutrient concentrations from across Kaneohe Bay (*16*) have consistently reported values below Lapointe's "threshold values." Other factors such as reduced herbivory are also clearly important, but our data show that these algae are not preferred food sources for herbivorous fishes in Hawaii (*9*). Because these alien algae are able to grow in low-nutrient environments and are not readily consumed by herbivorous fishes, they may be able to spread to Hawaii's most pristine reefs. Given this, we believe that it is our responsibility as scientists and conservation biologists to take action and help to prevent the death of yet another coral reef.

JENNIFER E. SMITH,[1]* ERIC J. CONKLIN,[2] CELIA M. SMITH,[3] CYNTHIA L. HUNTER[4]

[1]National Center for Ecological Analysis and Synthesis, University of California, Santa Barbara, CA 93101, USA. [2]The Nature Conservancy, Honolulu, HI 96817, USA.

[3]Department of Botany, University of Hawaii Manoa, Honolulu, HI 96822, USA. [4]Biology Program, University of Hawaii Manoa, Honolulu, HI 96815, USA.

*To whom correspondence should be addressed. E-mail: jsmith@nceas.ucsb.edu

References

1. D. R. Bellwood *et al.*, *Nature* **429**, 827 (2004).
2. T. Hughes *et al.*, *Limnol. Oceanogr.* **44**, 1583 (1999).
3. T. P. Hughes, *Science* **265**, 1547 (1994).
4. B. E. Lapointe, *Limnol. Oceanogr.* **42**, 1119 (1997).
5. B. E. Lapointe, *Limnol. Oceanogr.* **44**, 1586 (1999).
6. J. E. Smith *et al.*, *Coral Reefs* **19**, 332 (2001).
7. S. V. Smith *et al.*, *Pac. Sci.* **35**, 279 (1981).
8. E. J. Conklin, Ph.D. dissertation, University of Hawaii (2007).
9. E. J. Conklin, J. E. Smith, *Biol. Invasions* **7**, 1029 (2005).
10. C. L. Hunter, C. W. Evans, *Bull. Mar. Sci.* **57**, 501 (1995).
11. J. E. Smith *et al.*, *Pac. Sci.* **56**, 299 (2002).
12. J. Stimson *et al.*, *Coral Reefs* **19**, 343 (2001).
13. W. L. Zemke-White, M. Ohno, *J. Appl. Phycol.* **11**, 369 (1999).
14. P. M. Vitousek *et al.*, *Science* **277**, 494 (1997).
15. J. Stimson *et al.*, *Mar. Biol.* **151**, 1761 (2007).
16. E. F. Cox *et al.*, *Mar. Ecol. Prog. Ser.* **324**, 19 (2006).

Taihu Lake Not to Blame for Wuxi's Woes

THE ALGAL BLOOM OBSERVED IN TAIHU LAKE IN the summer of 2007 and sensationalized in a News Focus story ("Doing battle with the green monster of Taihu Lake," 31 August 2007, p. 1166) is certainly a serious environmental and ecological problem. However, the issue that drew public attention to Taihu Lake and the very visible bloom was actually a separate incident that affected the aesthetic quality of water in the city of Wuxi.

Environmental monitoring indicated that the first wave of algal bloom occurred in Taihu Lake in late April 2007. However, the offensive taste and odor in the drinking water of Wuxi City occurred from the end of May to early June. It has since become clear that the taste and odor were not caused directly by algal bloom in Taihu Lake, but were instead the result of an intrusion into the main water intake of Wuxi City by a distinct black water "agglomerate" of unknown origin; the duration of this agglomerate can be tied to ammonium levels, which increased suddenly—from an average value of about 0.23 to 0.97 mg/liter—on 28 May and began to decrease gradually after peaking at 4.0 mg/liter on 31 May. The unusually high concentrations of ammonium observed during this time are not normally associated with the processes in algal blooms. Samples were collected on 4 June 2007 from both the drinking-water intake and the water agglomerate. Analysis of the samples, which had strong septic and marshy odors (*1*, *2*), detected dimethyl trisulfide (*3*, *4*) at concentrations of 11,399 and 1768 ng/liter in the two samples, respectively—high enough to account for the odors (*5*, *6*). Dimethyl trisulfide and related alkyl sulfide compounds are produced by many bacteria (e.g., *Pseudomonas* sp.) that break down the amino acids methionine and cysteine into hydrogen sulfide, methylmercaptan, and dimethylpolysulfides (*7*–*11*). The sample analysis also detected two typical algal metabolites—2-methyl-iso-borneol and geosmin (*12*–*14*)—that give earthy or musty odor to water, but these concentrations were much lower than the dimethyl trisulfide. It is clear from these findings that dimethyl trisulfide and related alkyl sulfide compounds, not 2-methyl-iso-borneol and geosmin, were the main odor-causing compounds in Wuxi's water supply. Although it is not clear where the black-water agglomerate and the alkyl sulfide compounds came from, it is unlikely that these compounds are the direct metabolites of algae. Of course, degradation of cyanobacteria might also produce such compounds.

It is well known that some cyanobacteria—such as *Microcystis aeruginosa*, the main visible culprit in Taihu Lake—do produce a range of toxins that can be harmful to human health. Further systematic monitoring data of raw water samples from the same water intake in Wuxi were collected on 4 and 8 June 2007 for the analysis of dissolved microcystins. The analytical results show that microcystin-Leu-Arg (MC-LR) and microcystin-Arg-Arg (MC-RR), some of the most frequently recorded microcystins associated with algal blooms worldwide (*15*, *16*), were undetectable for the sample of 4 June and were present only in small amounts (64 and 72 ng/liter, respectively) in the sample of 8 June. The level of microcystins detected did not exceed the WHO Drinking Water Guidelines maximum of 1 μg/liter.

The algal bloom in Taihu Lake in 2007 was in fact not much different from those in previous years. According to the local monitoring data, algal density near the water intake during the odor event period (end of May 2007) was much lower than the highest value recorded in August 2003. The trigger for public concern about the water supply was in reality a complex chemical event of biological origin, which has not previously been associated with blooms of *Microcystis aeruginosa* in Taihu Lake.

MIN YANG,[1] JIANWEI YU,[1] ZONGLAI LI,[1] ZHAOHAI GUO,[1] MICHAEL BURCH,[2] TSAIR-FUH LIN[3]

[1]State Key Laboratory of Environmental Aquatic Chemistry Research Center for Eco-Environmental Sciences, Chinese Academy of Sciences, Post Office Box 2871, Beijing, 100085, China. [2]Australian Water Quality Centre, Private Mail Bag 3, Salisbury SA 5108, Australia. [3]Department of Environmental Engineering, National Cheng Kung University, University Road, Tainan City, 70101, Taiwan.

References and Notes

1. J. H. M. Bartels *et al.*, *J. Am. Water Works Assoc.* **78**, 50 (1986).
2. A. M. Dietrich *et al.*, *Water Sci. Technol.* **40**, 45 (1999).
3. D. Khiari *et al.*, *Water Sci. Technol.* **25**, 97 (1992).
4. D. Khiari *et al.*, *J. Am. Water Works Assoc.* **89**, 150 (1997).
5. J. E. Wajon, A. Heitz, *Chemosphere* **14**, 85 (1985).
6. J. Mallevialle, I. H. M. Suffet, *Identification and Treatment of Tastes and Odors in Drinking Water* (American Water Works Research Foundation, Denver, CO, 1987).
7. J. N. Labows *et al.*, *J. Clin. Microbiol.* **12**, 521 (1980).
8. H. Kadota, Y. Ishida, *Annu. Rev. Microbiol.* **26**, 127 (1972).
9. S. Ito *et al.*, *J. Biochem. (Tokyo)* **78**, 1105 (1975).
10. C. Scholler *et al.*, *Chemosphere* **35**, 1487 (1997).
11. J. E. Wajon, A. Heitz, *Water Sci. Technol.* **31**, 87 (1995).
12. G. Izaguirre *et al.*, *Appl. Environ. Microbiol.* **43**, 708 (1982).
13. I. H. M. Suffet *et al.*, *J. Am. Water Works Assoc.* **88**, 168 (1996).
14. I. H. M. Suffet *et al.*, *Water Sci. Technol.* **40**, 1 (1999).
15. M. E. van Apeldoorn *et al.*, *Mol. Nutr. Food Res.* **51**, 7 (2007).
16. K. Harada, *Chem. Pharm. Bull.* **52**, 889 (2004).
17. This work was supported by the National Natural Science Foundation of China (50525824 and 50621804).

Correcting the Record on the Data Quality Act

AFTER DONALD KENNEDY INDICATED IN HIS Editorial on medical marijuana ("Turning the tables with Mary Jane," 4 May 2007, p. 661) that the Data Quality Act (DQA) (*1*) could be useful for public interest groups as well as industry, Schick *et al.* ("The tobacco industry and the Data Quality Act," Letters, 17 August, p. 898) complained that the Editorial failed to mention the documented leadership role that Phillip Morris played in the genesis of the DQA. However, the Schick *et al.* Letter confused the Data Access Act with the DQA. The DQA implemented provisions of the Paperwork Reduction Act (PRA) of 1995 (*2*) that required the Office of Management and Budget to issue guidance on federal information dissemination; it has nothing to do with access to raw data.

Neither Phillip Morris (a multiproduct company) nor any other tobacco company (or nontobacco company for that matter) played a leadership role in the genesis of the DQA. While working with the Center for

Letters to the Editor

Letters (~300 words) discuss material published in *Science* in the previous 3 months or issues of general interest. They can be submitted through the Web (www.submit2science.org) or by regular mail (1200 New York Ave., NW, Washington, DC 20005, USA). Letters are not acknowledged upon receipt, nor are authors generally consulted before publication. Whether published in full or in part, letters are subject to editing for clarity and space.

Regulatory Effectiveness in Washington, DC, I was personally involved with the development of the DQA, and no industry entity contributed to its formulation. Moreover, as is evident from its plain wording, the genesis of the DQA lay in the information dissemination provisions of the 1995 PRA, and hearings and debate on those provisions began at least as early as 1989.

The DQA provisions underwent public consideration by Congress starting in 1998, and discussions proceeded almost continuously until its enactment in 2000 [e.g., (*3*–*5*)]. Entire commentary articles have been based on the false premise that it was enacted covertly [e.g., (*6*)].

Finally, it should be noted that the DQA has been used extensively by public interest groups, private citizens, and other non-industry petitioners challenging government information on subjects other than medical marijuana (*7*).

WILLIAM G. KELLY JR.

Center for Regulatory Effectiveness, Driggs, ID 83422, USA.

References and Notes

1. 44 U.S.C. § 3516, note, Pub. L. 106554, Sec. 1(a)(3) [title V, Sec. 515], Dec. 21, 2000. The Act does not have an official title, and it is also frequently referred to as the Information Quality Act.
2. 44 U.S.C. §§ 3501 *et seq*.
3. H.R. Rep. No. 105–592 at 49–50 (22 June 1998).
4. Hearings Before the Subcommittee on Treasury, Postal Service, and General Government Appropriations of the House Committee on Appropriations, 28 March 2000, Part 3, at 477–79, 509–17, 558.
5. H.R. Rep. No. 106756 at 54–55, 83 (18 July 2000).
6. L. Rosenstock, *JAMA* 295, 2407 (2006).
7. All federal agencies maintain a Web site that lists and describes DQA petitions submitted to them and their responses.

TECHNICAL COMMENT ABSTRACTS

COMMENT ON "The Southern Ocean Biological Response to Aeolian Iron Deposition"

Philip W. Boyd and Douglas Mackie

Cassar *et al.* (Reports, 24 August 2007, p. 1067) proposed that aerosol-iron input enhances Southern Ocean export production. Their conclusion critically depends on aerosol-iron modeling simulations not validated with iron-deposition data and dust dissolution rates based on Northern Hemisphere atmospheric chemical conditions (low pH). This diminishes the relevance of their findings and demonstrates that applying such models to this region is premature.

Full text at www.sciencemag.org/cgi/content/full/319/5860/159a

RESPONSE TO COMMENT ON "The Southern Ocean Biological Response to Aeolian Iron Deposition"

Nicolas Cassar, Michael L. Bender, Bruce A. Barnett, Songmiao Fan, Walter J. Moxim, Hiram Levy II, Bronte Tilbrook

Net community production in the Southern Ocean is correlated with simulated local dust deposition, and more so with modeled deposition of soluble iron. Model simulations of the latter two properties are consistent with observations in both hemispheres. These results provide strong evidence that aerosol iron deposition is a first-order control on net community production and export production over large areas of the Southern Ocean.

Full text at www.sciencemag.org/cgi/content/full/319/5860/159b

CORRECTIONS AND CLARIFICATIONS

News Focus: "In the HIV era, an old TB vaccine causes new problems" by M. Enserink (16 November, p. 1059). The story stated that the live TB vaccine Bacille Calmette-Guérin (BCG) was developed by researchers at the Pasteur Institute in Paris. In fact, Albert Calmette and Camille Guérin did most of their work at the Pasteur Institute in Lille, beginning in 1897 and persevering under extremely difficult circumstances during World War I. In 1919, Calmette joined the Pasteur Institute in Paris, by which time the vaccine development was essentially complete. BCG was first used in Paris in 1921.

Make a Gift to AAAS

Through philanthropic support, you can make a strong statement about your commitment to AAAS's mission.

Contributions from our members and friends are used in their entirety to support the AAAS Fund for Excellence which enables us to promote science in all forms.

We are pleased to offer multiple, convenient methods for contributing to our programs and activities. If you would like to learn more about AAAS or ways of giving, please visit our Web site at **www.aaas.org** and select **"Make a Gift"** in the left-hand tower.

Thank you for your support.

The AAAS Development Team is available to help you in any way.
Phone: (202) 326–6636 or e-mail: development@aaas.org.

AAAS
ADVANCING SCIENCE, SERVING SOCIETY

HISTORY OF SCIENCE

Delicious Tales of Guinea Pigs, Etc.

Vassiliki Betty Smocovitis

Rumor has it that the great mathematical population geneticist Sewall Wright could be so absent-minded that, needing room for his equations on the blackboard one day, he made an ersatz eraser out of a fractious guinea pig he had brought to class. The story happens to be untrue [as William Provine's careful research showed (*1*)], but it can spice up an otherwise bland historical stew for nonspecialists. Along with other fun anecdotes, interesting asides, and startling connections, it appears in Jim Endersby's charming *A Guinea Pig's History of Biology*.

The book isn't all fun and games, however. It is part of a growing trend among historians of biology to concentrate on "the organism," variously used as model, experimental system, or just plain object of study. In one guise, the movement merely seeks to explore the varied ways in which biologists' organisms have shaped the development of biology. In another, it has a more ambitious project: to give "voice" or perhaps even agency to nonhumans (though the latter has been the subject of much debate). So, silly as it seems, the book's title isn't just a cute way to entice readers' interests; it is also a kind of word play on a body of literature that has made "historical actors" of things like microbes and sea scallops (*2*, *3*).

Blessedly, discussion of such challenges to traditional understanding of science is brief and included mostly in the preface and acknowledgments. The remaining 12 chapters are devoted to the subject at hand, which is not so much the history of biology as the history of genetics and evolution retold (with occasional additions of microbiology, physiology, and cell biology) through some of the many prominent organisms studied. Each chapter is actually an independent essay that can be read alone; each is framed by an organism that has played some interesting historical role and arranged around some key event. Some are instantly recognizable "celebrity" organisms (e.g., the fruit fly *Drosophila melanogaster* and maize, *Zea mays*), others are more obscure and now extinct (e.g., quagga, *Equus quagga*) or largely forgotten (e.g., Gregor Mendel's pale hawkweed, *Hieracium auricula*, and Hugo de Vries's evening primrose, *Oenothera lamarckiana*), while still others are actively used by researchers (e.g., the cress *Arabidopsis thaliana* and zebrafish, *Danio rerio*). One chapter is devoted to a genetically engineered organism (the famously trademarked OncoMouse).

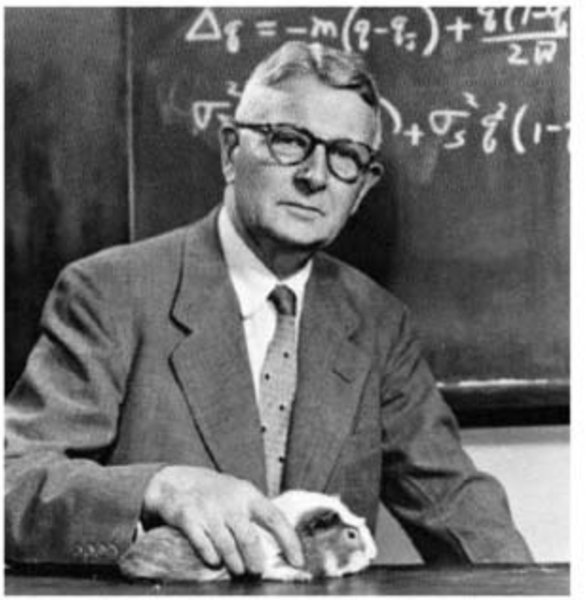

Sewall Wright and one of his guinea pigs.

What emerges is a lighthearted retelling of a familiar story that will appeal to a wide audience. As we learn about the breeding patterns in horses and zebras, we also learn about the leisurely interests of Victorian aristocrats, radical political movements, and the challenges of gardening in an increasingly industrial context. While gaining an understanding of Victorian attempts to study inheritance in humans, we learn about the growing concern with London's sanitation, the famous Health Exhibition, and the development and use of industrial ceramics as toilet bowls and sewer pipes by Doulton and Company (now known as Royal Doulton, the maker of fine dinnerware). As we learn much about the guinea pig as model organism for geneticists, we gain an appreciation of its culinary merits.

A Guinea Pig's History of Biology
The Plants and Animals Who Taught Us the Facts of Life

by Jim Endersby

Heinemann (Random House), London, 2007. 511 pp. £20. ISBN 9780434012596. Harvard University Press, Cambridge, MA. $27.95. ISBN 9780674027138.

The reviewer is at the Department of Zoology and the Department of History, University of Florida, Gainesville, FL 32611, USA. E-mail: bsmocovi@ufl.edu

Although enjoyable, this approach has some drawbacks. Throughout the book, necessary historical details or critical developments are missing or "off," while irrelevant digressions and asides include far more detail than needed. For example, the chapter framed by the guinea pig, *Cavia porcellus*, (really the chapter on the "modern" synthesis of evolution) provides a fascinating discussion of historical and ethnographic uses of the experimental cavy (along with descriptions of recipes) but a misleading picture of the historical event it is supposed to cover. That synthesis wasn't all due to the use of guinea pigs and *Drosophila*, the insights of theoretical population geneticists like Wright, or the field work and experiments of Theodosius Dobzhansky. It is almost as though Ernst Mayr, Julian Huxley, George Gaylord Simpson, and G. Ledyard Stebbins Jr. (among many others) and their critical contributions didn't exist. Given the book's many plant examples, Stebbins, whose classic book (*4*) brought botany into the synthesis, would have been a much more appropriate end point for the chapter than his friend Dobzhansky. One must also wonder what kind of historical account of evolution can be told without fossils. And although the book is to be lauded for including so much from the botanical side, the actual historical analysis is disappointing. It's great to feature *Oenothera* for the section on the "eclipse of Darwin" (the interval of time around 1900), but to give it a central place in understanding the phenomenon of polyploidy isn't fair. That part properly belongs to the Kew primrose, *Primula kewensis*, and the histories of polyploidy, apomixis, and hybridization are vastly more complicated than portrayed here.

In short, the book offers lay readers an engaging and lively introduction to the history of biology. But I'm not sure that it actually enriches historical understanding of the field.

References

1. W. B. Provine, *Sewall Wright and Evolutionary Biology* (Univ. of Chicago Press, Chicago, 1986).
2. B. Latour, *Pasteurization of France* (Harvard Univ. Press, Cambridge, MA, 1988).
3. M. Callon, in *Power, Action and Belief: A New Sociology of Knowledge*, J. Law, Ed. (Routledge and Kegan Paul, London, 1985), pp. 196–229.
4. G. L. Stebbins, *Variation and Evolution in Plants* (Columbia Univ. Press, New York, 1950).

10.1126/science.1152226

CREDIT: COURTESY WILLIAM PROVINE/CORNELL UNIVERSITY

PHYSICAL CHEMISTRY

Keeping Time

Stephen Gray

Books on quantum mechanics are often organized more in terms of what is easy to understand and calculate than in terms of what actually applies to the world at large. They typically contain much discussion from the perspective of the time-independent Schrödinger equation (TISE), $H\Psi(x) = E\Psi(x)$. This equation determines the allowed stationary states of a system (defined by its Hamiltonian operator, H), which could be anything from a particle such as an electron to a complex molecule containing many atoms. Depending on the problem details, the stationary state energies (E) take on only certain discrete values (as in the well-known hydrogen atom problem) or take on a continuous range of values (as in problems involving collisions). Associated with each allowed energy, E, is a wavefunction, $\Psi(x)$, where x denotes the system's coordinates. The absolute square, $|\Psi(x)|^2$, is related to the likelihood of finding the system in a specific region of space.

Introduction to Quantum Mechanics
A Time-Dependent Perspective
by David J. Tannor
University Science, Sausalito, CA, 2007. 686 pp. $84.50. ISBN 9781891389238.

But for the most part, the universe isn't stationary: the positions of things change with time (t). For matters concerning time, one turns to another equation, the time-dependent Schrödinger equation (TDSE). This equation determines the time-evolving wavepacket, $\Psi(x,t)$, and is written

$$i\hbar\frac{\partial}{\partial t}\Psi(x,t) = H\Psi(x,t)$$

where $i = \sqrt{-1}$ and $\hbar$ is Planck's constant divided by 2π. The TDSE may appear briefly in the early parts of quantum mechanics books and also later on, when spectroscopic transition rates are discussed. However, one must be lucky to find a full chapter on the TDSE, although it is the more general equation because it describes the system's evolution through time—and thus compares in importance to Newton's equations in the world of classical mechanics.

What we have in David Tannor's *Introduction to Quantum Mechanics* is an advanced textbook in which the TDSE occupies center stage. It reflects how the time-dependent quantum mechanical picture has grown more important in the research literature over the past 30 years. This has been especially true in the discipline of physical chemistry (or chemical physics), where a number of major advances in time-domain theory and experiment have arisen.

The pioneering ideas and approaches developed by Eric Heller and his collaborators starting in the mid-1970s led to a new way of viewing molecular spectroscopy and reaction dynamics. For example, a molecular absorption spectrum is viewed as resulting from placing an appropriate initial wavepacket, $\Psi(x,t = 0)$, on an excited state potential energy surface and then seeing how it evolves according to the TDSE. The Fourier transform of a certain correlation function inferred from $\Psi(x,t)$ is proportionate to the absorption spectrum. Although to the general reader this description may sound a little obtuse, to many researchers—theoreticians and experimentalists alike—this is a tremendous conceptual insight compared to the banal time-independent picture of calculating certain matrix elements (or integrals) involving stationary state wavefunctions.

Also crucial were advances in laser technology that have allowed experimental research on time-domain quantum dynamics to bloom. For example, Ahmed Zewail received the 1999 Nobel Prize in Chemistry for his experimental work that studied chemical reactions in real time with femtosecond (10^{-15} s) spectroscopy. In addition, the combination of substantial methodological advances due to Ronnie Kosloff and others starting in the 1980s and the steady growth in computing power now make the task of actually solving the TDSE easier than it has ever been.

The book offers a thorough, erudite treatment of time-dependent quantum mechanics with an emphasis on the spectroscopy and dynamics of atomic and molecular systems. Throughout, readers are challenged to understand the mathematical structure behind the pictures and concepts. The extensive reference lists and occasional historical notes will help them do so.

One recurring theme is the correspondence between quantum and classical mechanics: how quantum motion is intimately connected with the behavior of a corresponding classical system. Part of the appeal of wavepackets (going back to Schrödinger's original exposition of coherent state wavepackets) is that they provide a direct and intuitive quantum analog of classical motion. Tannor (a professor at the Weizmann Institute of Science, Israel) lucidly brings out this correspondence through numerous examples and, at a more rigorous mathematical level, a chapter on path integrals and semiclassical theory.

Tannor provides a rigorous, self-contained development of modern time-dependent quantum mechanics and discusses numerous applications in molecular spectroscopy and reaction dynamics. With its fresh and conceptually appealing perspective, *Introduction to Quantum Mechanics* could change how quantum mechanics is perceived and taught.

10.1126/science.1151473

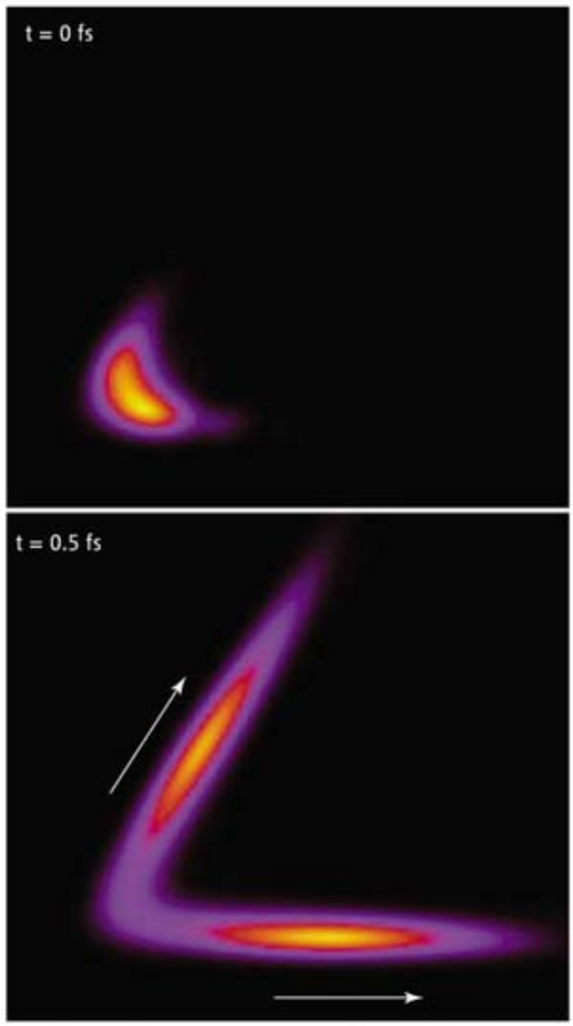

Visual appeal. An initial wavepacket "launched" at the transition state for a chemical reaction involving atoms A, B, and C (top) subsequently (bottom) bifurcates, leading to different product arrangements (AB + C and A + BC).

CREDIT: STEPHEN GRAY

The reviewer is at the Chemical Sciences and Engineering Division, Argonne National Laboratory, 9700 South Cass Avenue, Argonne, IL 60439, USA. E-mail: gray@tcg.anl.gov

ENVIRONMENT

Ocean Iron Fertilization—Moving Forward in a Sea of Uncertainty

It is premature to sell carbon offsets from ocean iron fertilization unless research provides the scientific foundation to evaluate risks and benefits.

Ken O. Buesseler,[1]* Scott C. Doney,[1] David M. Karl,[2] Philip W. Boyd,[3] Ken Caldeira,[4] Fei Chai,[5] Kenneth H. Coale,[6] Hein J. W. de Baar,[7] Paul G. Falkowski,[8] Kenneth S. Johnson,[9] Richard S. Lampitt,[10] Anthony F. Michaels,[11] S. W. A. Naqvi,[12] Victor Smetacek,[13] Shigenobu Takeda,[14] Andrew J. Watson[15]

The consequences of global climate change are profound, and the scientific community has an obligation to assess the ramifications of policy options for reducing greenhouse gas emissions and enhancing CO_2 sinks in reservoirs other than the atmosphere (*1*, *2*).

Ocean iron fertilization (OIF), one of several ocean methods proposed for mitigating rising atmospheric CO_2, involves stimulating net phytoplankton growth by releasing iron to certain parts of the surface ocean. The international oceanographic community has studied OIF, including 12 major field programs with small-scale, purposeful releases of iron since 1993 (*3*, *4*). Although these experiments greatly improved our understanding of the role of iron in regulating ocean ecosystems and carbon dynamics, they were not designed to characterize OIF as a carbon mitigation strategy. The efficacy by which OIF sequesters atmospheric CO_2 to the deep sea remains poorly constrained, and we do not understand the intended and unintended biogeochemical and ecological impacts. Environmental perturbations from OIF are nonlocal and are spread over a large area by ocean circulation, which makes long-term verification and assessment very difficult. Modeling studies have addressed sequestration more directly and have suggested that OIF in areas of persistent high nutrients (so-called high-nutrient, low-chlorophyll areas) would be unlikely to sequester more than several hundred million tons of carbon per year. Thus, OIF could make only a partial contribution to mitigation of global CO_2 increases.

Despite these uncertainties in the science, private organizations are making plans to conduct larger-scale iron releases to generate carbon offsets. We are convinced that, as yet, there is no scientific basis for issuing such carbon credits for OIF. Adequate scientific information to enable a decision regarding whether credits should be issued could emerge from reducing uncertainties; this will only come through targeted research programs with the following specific attributes:

- Field studies on larger spatial and longer time scales, because ecological impacts and CO_2 mitigation are scale-dependent.
- Consideration of OIF in high- and low-nutrient regions to understand a wider range of processes that are affected by iron, such as nitrogen fixation and elemental stoichiometry.
- Detailed measurements in the subsurface ocean to verify the fate of fixed carbon, including remineralization length scales of carbon, iron, and associated elements.
- Broad assessment of ecological impacts from bacteria and biogeochemistry to fish, seabirds, and marine mammals.
- Characterization of changes to oxygen distributions, biophysical climate feedbacks, and cycling of non-CO_2 greenhouse gases, such as methane, nitrous oxide, and dimethylsulfide.
- Long-term monitoring and use of models to assess downstream effects beyond the study area and observation period.
- Improved modeling studies of the results and consequences of OIF, including higher spatial resolution, better ecosystem parameterization, inclusion of other greenhouse gases, and improved iron biogeochemistry.
- Analysis of the costs, benefits, and impacts of OIF relative to other climate and carbon mitigation schemes and to the impacts of global change if we take no action.

The organization of such experiments is as critical as the scientific design. The scope of the problem will require individual sponsors and partnerships of national science agencies, philanthropies, and commercial entities. Academic scientists need to be involved but must maintain independence. This can be accomplished by regulating experiments in a uniform manner under such international agreements as the London Convention, widely distributing science plans and results via open meetings and peer-reviewed journals, and requiring clear and explicit statements of conflicts of interest.

This group feels it is premature to sell carbon offsets from the first generation of commercial-scale OIF experiments unless there is better demonstration that OIF effectively removes CO_2, retains that carbon in the ocean for a quantifiable amount of time, and has acceptable and predictable environmental impacts. As with any human manipulation of the environment, OIF carries potential risks, as well as potential benefits; moving forward on OIF should only be done if society is willing to acknowledge explicitly that it will result in alteration of ocean ecosystems and that some of the consequences may be unforeseen. We are currently facing decisions on climate regulations, such as the post-Kyoto framework discussed in Bali, carbon cap-and-trade bills in the U.S. Congress, and consideration of OIF by the parties to the London Convention, and we feel that ocean biogeochemical research will help inform these important policy decisions.

[1]Department of Marine Chemistry and Geochemistry, Woods Hole Oceanographic Institution, Woods Hole, MA 02543, USA. [2]School of Ocean and Earth Science and Technology, University of Hawaii, Honolulu, HI, USA. [3]National Institute of Water and Atmospheric Research, Centre for Chemical and Physical Oceanography, Department of Chemistry, University of Otago, Dunedin, New Zealand. [4]Department of Global Ecology, Carnegie Institution, Stanford, CA, USA. [5]School of Marine Sciences, University of Maine, Orono, ME, USA. [6]Moss Landing Marine Laboratories, Moss Landing, CA, USA. [7]Royal Netherlands Institute for Research, Isle of Texel, The Netherlands. [8]Institute of Marine and Coastal Sciences, Rutgers University, New Brunswick, NJ, USA. [9]Monterey Bay Aquarium Research Institute, Moss Landing, CA, USA. [10]National Oceanography Centre, Southampton, UK. [11]Wrigley Institute for Environmental Studies, University of Southern California, Los Angeles, CA, USA. [12]National Institute of Oceanography, Goa, India. [13]Alfred Wegener Institute for Polar and Marine Research, Bremerhaven, Germany. [14]Department of Aquatic Bioscience, University of Tokyo, Tokyo, Japan. [15]School of Environmental Sciences, University of East Anglia, Norwich, UK.

*Author for correspondence. E-mail: kbuesseler@whoi.edu

References

1. L. Dilling *et al.*, *Annu. Rev. Environ. Resour.* **28**, 521 (2003).
2. S. Pacala, R. Socolow, *Science* **305**, 968 (2004).
3. H. J. W. de Baar, *J. Geophys. Res.* **110**, C09S16 (2005).
4. P. W. Boyd *et al.*, *Science* **315**, 612 (2007).

10.1126/science.1154305

CANCER

A Few to Flip the Angiogenic Switch

A relatively small number of endothelial progenitor cells have a profound effect on tumor growth and metastasis.

Shahin Rafii and David Lyden

The rapid formation of blood vessels, a process known as the angiogenic switch, is required for progression of dormant or micrometastatic tumors to macrometastatic invasive tumors. New blood vessels may either sprout from preexisting mature ones or form de novo by recruiting circulating endothelial progenitor cells derived from the bone marrow (*1*–*3*). Although these progenitors can incorporate into human tumors and transplanted tissue (*4*, *5*), they do so in small numbers, raising doubt about their physiological contribution to neo-angiogenic processes. On page 195 of this issue, Gao *et al.* cast any doubt aside by showing that notwithstanding their low numbers, recruitment of these endothelial progenitor cells is pivotal for the progression of avascular micrometastatic tumors to lethal macrometastatic ones (*6*).

Why has there been so much confusion? It may be that only certain types of tumors (*7*), producing distinct proangiogenic chemokines (*1*, *8*–*11*), demand bone marrow-derived endothelial progenitor cells to initiate (*12*) and possibly maintain nascent vessels within specific primary and metastatic lesions (*13*). Indeed, the extent of progenitor cell incorporation is maximal in relapsing tumors (*9*) and in certain aggressive carcinomas (*14*). But the main reason for inconsistent results is probably the phenotypic similarities between hematopoietic cells and true endothelial progenitor cells (those with bone marrow repopulating potential) (*2*, *3*), and the technical hurdles involved in distinguishing and localizing them in the lumen of functional blood vessels. In some mouse studies, the majority of the bone marrow–derived cells in tumors was not endothelial, but of hematopoietic lineage, and were positioned perivascularly rather than incorporated into the vessel lumen (*15*, *16*). However, in these reports, it was unclear whether true endothelial progenitors were transplanted into recipient bone marrow.

To circumvent these problems, Gao *et al.* tracked endothelial progenitor cells by labeling with green fluorescent protein and by assessing the expression of vascular-specific molecular markers, including the cell adhesion molecules VE-cadherin and CD31, VEGFR2 (a receptor for vascular endothelial growth factor), and Id1, a transcription factor that promotes angiogenesis. Using mouse models of lung (metastatic mouse Lewis Lung carcinoma) and breast (spontaneous MMTV-PyMT) cancer models, the authors demonstrate that about 12% of the endothelial cells within macrometastases were derived from bone marrow. Remarkably, when the expression of Id1 was reduced in these small number of progenitors, their mobilization from bone marrow decreased by 96%, angiogenesis was blocked, tumor formation decreased, and the animal's survival improved.

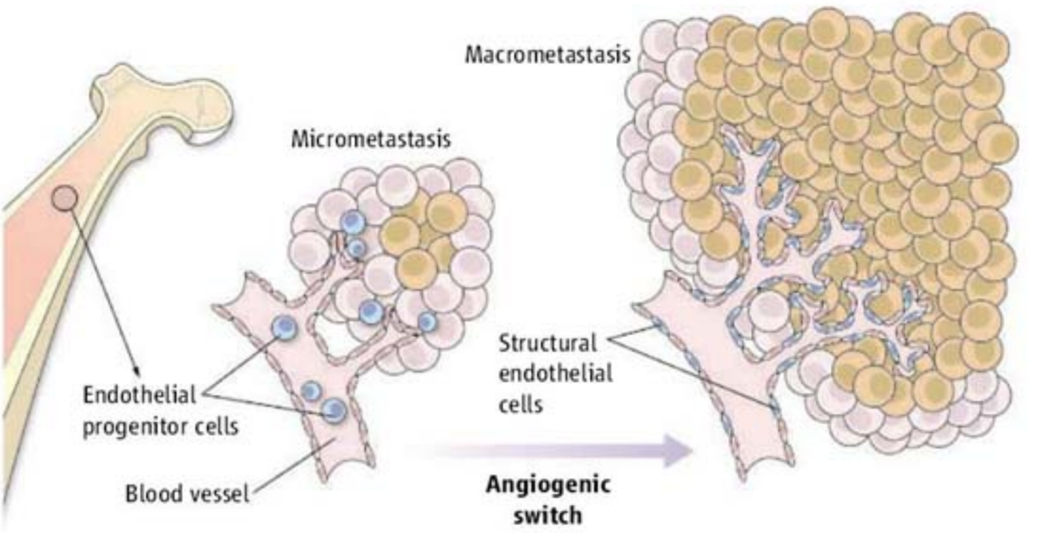

Few but mighty. Bone marrow–derived endothelial progenitor cells contribute instructively to micrometastasis and structurally to the emergence of macrometastatic tumor nodules.

The inhibition of Id1 did not affect tumor cell dissemination or the initial colonization of organs by malignant cells, but rather, shut off the mobilization and recruitment of particular endothelial progenitor cells (those expressing Id1, VE-cadherin, and low amounts of CD31). These specific progenitor cells infiltrated micrometastatic lesions and produced proangiogenic growth factors before the initiation of macrometastases. Ultimately, subsets of these progenitor cells differentiated (to express VE-cadherin and increased amounts of CD31) and integrated into the lumen of tumor neovessels. These data suggest that bone marrow–derived endothelial progenitors are unique in providing both instructive (paracrine) and structural (vessel incorporation) roles to promote tumor macrometastasis (see the figure). They also extend previous studies demonstrating that hematopoietic progenitor cells initiate metastatic colonization (*10*), whereas endothelial progenitor cells promote progression of the metastatic lesion.

How can bone marrow–derived endothelial progenitor cells be distinguished from preexisting tumor endothelium or hematopoietic cells (*17*)? A phenotypic definition by specific molecules (including the presence of Id1, VE-cadherin, VEGFR2, CD31, CD13, and the growth factor receptor c-Kit, but absence of the cell adhesion molecule CD11b and the phosphatase CD45) have been used previously to mark endothelial progenitor cells incorporated in the lumen of tumor vasculature (*12*). However, some of these markers are expressed by subsets of hematopoietic lineages, and therefore phenotyping must be carefully performed (*2*, *3*). Another complicating factor is the potential contribution of recently discovered cells similar to endothelial progenitor cells resident within organs other than the bone marrow (*18*). Lack of functional standardized bioassays to quantify the scarce populations of true endothelial progenitor cells is a major hurdle in assessing whether bone marrow transplantations performed in different laboratories (*2*, *3*, *15*, *16*) results in engraftment of sufficient numbers of progenitor cells to interrogate their contribution to tumor neo-angiogenesis. Therefore, establishing standardized in vivo functional assays to detect and quantify

The authors are at Howard Hughes Medical Institute, Weill Cornell Medical College, New York, NY 10065, USA. E-mail: dcl2001@med.cornell.edu; srafii@med.cornell.edu

CREDIT: C. BICKEL/SCIENCE

repopulating progenitors is urgently needed.

Major issues still need to be resolved. It is unclear why endothelial progenitor cells are recruited only by certain tumors. And the role of proangiogenic factors elaborated by (or specific to) endothelial progenitor cells needs further investigation. Whether their continuous recruitment contributes to maintaining stabilized tumor vessels also has yet to be determined.

References

1. D. Lyden *et al.*, *Nat. Med.* **7**, 1194 (2001).
2. S. Rafii, D. Lyden, R. Benezra, K. Hattori, B. Heissig, *Nat. Rev. Cancer* **2**, 826 (2002).
3. F. Bertolini, Y. Shaked, P. Mancuso, R. S. Kerbel, *Nat. Rev. Cancer* **6**, 835 (2006).
4. B. A. Peters *et al.*, *Nat. Med.* **11**, 261 (2005).
5. E. Minami, M. A. Laflamme, J. E. Saffitz, C. E. Murry, *Circulation* **112**, 2951 (2005).
6. D. Gao *et al.*, *Science* **319**, 195 (2008).
7. M. B. Ruzinova *et al.*, *Cancer Cell* **4**, 277 (2003).
8. Y. Shaked *et al.*, *Cancer Cell* **7**, 101 (2005).
9. Y. Shaked *et al.*, *Science* **313**, 1785 (2006).
10. R. N. Kaplan *et al.*, *Nature* **438**, 820 (2005).
11. I. Petit, D. Jin, S. Rafii, *Trends Immunol.* **28**, 299 (2007).
12. D. J. Nolan *et al.*, *Genes Dev.* **21**, 1546 (2007).
13. D. G. Duda *et al.*, *Blood* **107**, 2774 (2005).
14. H. Spring, T. Schuler, B. Arnold, G. J. Hammerling, R. Ganss, *Proc. Natl. Acad. Sci. U.S.A.* **102**, 18111 (2005).
15. M. De Palma *et al.*, *Cancer Cell* **8**, 211 (2005).
16. J. R. Gothert et al., *Blood* **104**, 1769 (2004).
17. M. C. Yoder et al., *Blood* **109**, 1801 (2007).
18. A. Aicher *et al.*, *Circ. Res.* **100**, 581 (2007).

10.1126/science.1153615

CANCER

Quo Vadis, Specificity?

Hans Schreiber and Donald A. Rowley

Mutations in cancer cells can give rise to tumor-specific antigens, but abnormal processing of normal molecules in these cells can also elicit an immune response.

Finding molecules exclusively expressed by tumor cells is one of the great hopes in the fight against cancer, because therapeutically targeting such molecules, or antigens, should eradicate cancer without harming normal tissue. The extremely large repertoire of T cells bearing distinct receptors allows the immune system to recognize a multitude of antigens with great specificity and selectivity. On page 215 of this issue, Savage *et al.* (*1*) report that T cells recognize a fragment of a ubiquitous nuclear protein, histone H4, yet somehow bypass recognizing normal cells, infiltrating prostate cancer instead.

The authors are in the Department of Pathology, University of Chicago, Chicago, IL 60637, USA. E-mail: hszz@midway.uchicago.edu

Cancer is caused by somatic mutations and/or the introduction of genes from cancer-causing viruses, which leads to the expression of cancer-specific proteins and potential antigens (see the figure). This has led to the controversial idea of the evolution of adaptive immunity to prevent the development of cancers. All cancers in man (and mouse) that have been analyzed express bona fide tumor-specific antigens that could be targeted by T cells. In some cases, the same tumor types share mutations and antigens (*2*, *3*). But each patient's cancer seems to have a unique set of mutations (*4*, *5*) that can provoke a powerful immune response (*6*). When it was shown that cancer in mice could be eradicated if the animals were immunized with their own, autochthonous cancer cells, it meant that the immune system could be primed for subsequent challenge by the same tumor, bearing unique, immune-reactive antigens (*7*). However, unique antigens have remained unexploited clinically, because highly personalized therapy would be required.

The mice with primary prostate cancers studied by Savage *et al.* mounted an immune response to a nonmutated peptide derived from histone H4, a nuclear protein. At first, this may not seem so surprising, because immune responses of cancer patients often recognize molecules expressed by both cancer cells and some normal cells, so-called self-antigens. What is remarkable and unexplained is that histone H4 is expressed not only by prostate cancer cells but also by all normal somatic cells, yet was recognized only in cancerous tissue by the immune system. Perhaps the histone H4 antigen is processed and "presented" at the cell surface in an unusual way by prostate cancer cells in response to the tumor microenvironment. If so, is this related to the cause (a viral oncogene in the mouse model used by Savage *et al.*) of the cancer? Is histone H4 also recognized as an antigen in spontaneous human prostate cancers (and in other murine models of prostate cancer)? No self-reactivity or harmful effects by the immune system occurred in normal mice, even with the abundance of T cells ($CD8^+$ subtype) expressing receptors specific for histone H4. T cells localized and proliferated in the cancerous tissue in response to the peptide, but failed to produce cytotoxic effector molecules or cytokines (such as interferon-γ) that could further boost the immune response,

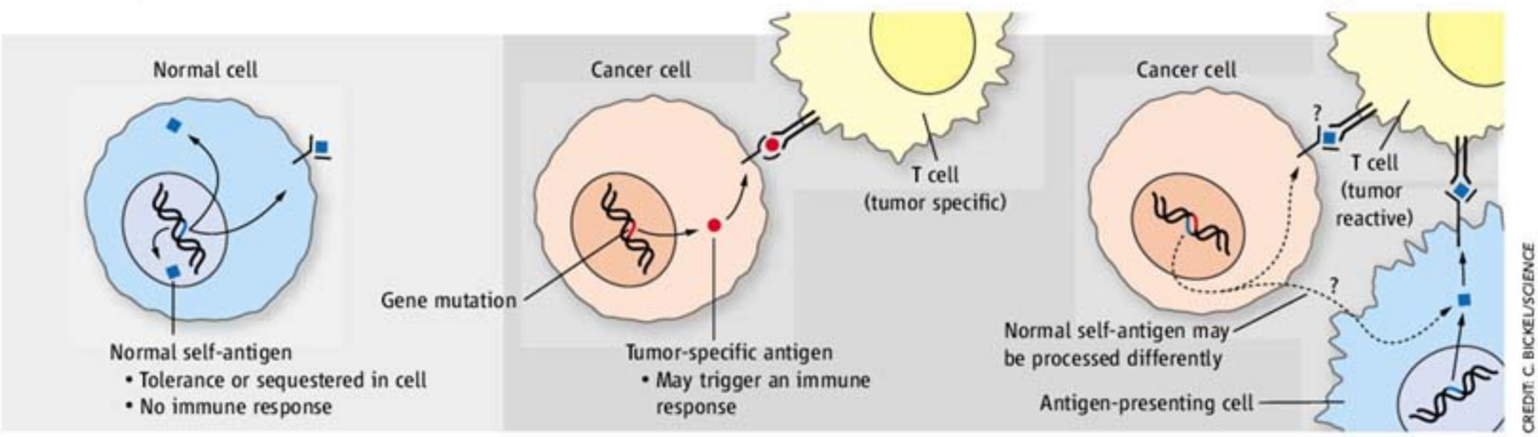

Not so normal. New molecules synthesized in cancer cells may elicit a tumor-specific immune response. Cancer cells can also express genes encoding self-molecules that are released and presented to T cells by antigen-presenting cells in the tumor. Self-molecules may also be aberrantly processed and recognized by immune cells. Factors in the tumor microenvironment could trigger these effects.

CREDIT: C. BICKEL/SCIENCE

and there was no increase in animal survival. The reason for this immunity breakdown is unclear.

Antibodies to growth factors (such as vascular endothelial growth factor), growth factor receptors (such as HER-2), or self-antigens (such as CD20, expressed by B cells) have become important in the therapy of other cancers. It is unclear, however, whether T cells that target self-antigens on tumors could be similarly effective, even if normal cells expressing those antigens were dispensable. Self-reactive T cells are readily deleted and/or functionally inactivated, and when not deleted, have a reduced capacity to recognize target antigens (*8*). When self-reactive T cells are made effective (*9*), fatal autoimmune damage may occur. Even though one can generate T cells bearing receptors with high (nanomolar) affinity for self-antigens that are highly expressed in cancers, it is difficult to predict whether autoimmune damage will occur if used therapeutically. Much depends on whether the self-antigen is only expressed on dispensable normal tissues.

Whether ubiquitous, normal self-proteins are sufficiently selective antigenic targets on prostate cancer to allow tumor eradication without detrimental autoimmune responses by the therapeutic T cells will become apparent once any functional defects of the antigen-specific T cells have been identified and reversed. Similarly, for use in adoptive T cell therapy in which autologous human T cells are activated, expanded in vitro, transduced to express antigen-specific T cell receptors, and reinfused into the patient, it will be necessary to compare mutated and normal self-antigens for efficacy as targets. Although the feasibility and safety of such engineered T cells have been demonstrated in studies targeting the normal melanocyte-differentiation antigen MART-1 (*10*), only 2 of 17 patients responded to treatment. The autologous T cells expanded in vitro and reinfused into these patients likely contained variable numbers of T cells that recognized tumor-specific antigens. Procedures are therefore needed for expanding a patient's T cells in vitro so that they recognize the autochthonous tumor cells specifically. Such T cells may not only be therapeutic upon infusion but also may be used to elucidate the genetic origins of mutated tumor-specific antigens.

As effective drugs are generated to target specific mutated proteins, and as cancer treatments become "personal" (*11*), it is ironic that individual specificity still has to conquer the field of cancer immunology. After all, it was the discovery of individually distinct tumor-specific antigens that ended gloom in the field over 30 years ago (*12*).

References

1. P. A. Savage *et al.*, *Science* **319**, 215 (2008).
2. M. Miettinen, *Adv. Exp. Med. Biol.* **587**, 99 (2006).
3. B. S. Worley *et al.*, *Cancer Res.* **61**, 6868 (2001).
4. D. Mumberg, M. Wick, H. Schreiber, *Semin. Immunol.* **8**, 289 (1996).
5. L. D. Wood *et al.*, *Science* **318**, 1108 (2007).
6. B. A. Weir *et al.*, *Nature* **450**, 893 (2007).
7. G. Klein, H. O. Sögren, E. Klein, K. E. Hellström, *Cancer Res.* **20**, 1561 (1960).
8. Z. Yu *et al.*, *J. Clin. Invest.* **114**, 551 (2004).
9. B. Ludewig *et al.*, *J. Exp. Med.* **191**, 795 (2000).
10. R. A. Morgan *et al.*, *Science* **314**, 126 (2006).
11. P. A. Kiberstis, J. Travis, *Science* **312**, 1157 (2006).
12. M. A. Basombrio, *Cancer Res.* **30**, 2458 (1970).

1031126/cience.1153713

BIOCHEMISTRY

Dicey Assemblies

Site-directed mutagenesis allows the symmetry of protein assemblies to be directed in a systematic manner.

Joël Janin

Proteins are made of polypeptide chains that may associate to form so-called quaternary structures (*1*). More than 40 years ago, Jacques Monod and co-workers developed the theory of allostery that explains how the activity of proteins can be efficiently regulated. The quaternary structure allows proteins to have symmetries that play a central role in allostery (*2*, *3*). Can this symmetry be manipulated by site-directed mutagenesis? On page 206, Grueninger *et al.* prove that it can (*4*). Their experiments confirm some of the basic arguments made by Monod *et al.*

Monod *et al.* noted that, in an symmetrical oligomer (a protein made of several polypeptide chains) with identical sequences, every structural feature or interaction is repeated a number of times. Thus, any change in contact between two subunits will affect all symmetry-related contacts. For example, in the eight-dice assembly shown in the figure, the dice form two layers, each with a C_4 (cyclic four-fold) symmetry. The layers are related by two-fold axes that give the assembly a D_4 (dihedral four-fold) symmetry. The sixes form the interface between the layers. If one dot in each six is removed, that interface will lose a total of eight dot-dot contacts.

Monod's dice. The dimerization mutants of the urocanase and Rua proteins prepared by Grueninger *et al.* display the symmetries illustrated here by assemblies of *n* dice. (**Left**) Dihedral two-fold (D_2) symmetry ($n = 4$), (**middle**) dihedral four-fold (D_4) symmetry ($n = 8$), (**right**) cyclic three-fold (C_3) symmetry ($n = 3$). Each die represents a polypeptide chain.

Monod *et al.* remarked that "mutations which abolish the interactions should frequently be found to result in stabilization of a monomeric state" (*3*) and cited examples of mutations of that type identified by classical genetics. Yet when molecular genetics allowed the introduction of such mutations in a rational way, converting an oligomer into a stable monomer proved to be difficult. Most attempts yielded products that were highly unstable and insoluble, because nonpolar (and hence water-repelling) protein surfaces become exposed to water when subunit interfaces are disrupted. The few successful cases all involve multiple mutations that make the interface less water-repelling (*5*).

The author is at Yeast Structural Genomics, Institut de Biochimie et Biophysique Moléculaire et Cellulaire, Bat. 430 UMR 8619 CNRS, Université Paris-Sud, 91405 Orsay, France. E-mail: joel.janin@u-psud.fr

PHOTO CREDIT: HENRI BUC/INSTITUT PASTEUR, PARIS

However, Monod *et al.*'s reasoning applies not only to the destruction of a symmetrical oligomer but also to its creation: Any change that can generate a favorable subunit contact in an oligomer with cyclic n-fold symmetry (C_n) will do so $2n$ times, leading to dimerization, if the contact is compatible with dihedral n-fold (D_n) symmetry. Contacts not compatible with such a symmetry can still promote subunit association but will generate an infinite helical fiber rather than a closed structure. A classical example is sickle-cell anemia, in which a point mutation in the β chain of hemoglobin causes the protein to polymerize.

In other systems, conformation changes rather than mutations may cause the formation of a fiber, and this can also lead to dimerization. The prion protein implicated in neurodegenerative diseases (such as bovine spongiform encephalopathy in cows and Creutzfeldt-Jakob disease in humans) undergoes both types of self-association under different conditions (*6*). Thus, fiber formation and dimerization are related, frequently observed, and possibly competing natural processes.

Grueninger *et al.* have now achieved both dimerization and fiber formation by site-directed mutagenesis, engineering new subunit contacts in five different bacterial proteins. They used the known crystal structure of these proteins to model assemblies with a two-fold symmetry and to select amino acid substitutions that introduce nonpolar side chains at the modeled interface. They then generated the mutations, purified the corresponding mutant proteins, and checked their molecular weight by size-exclusion chromatography and dynamic light scattering. They also crystallized several mutants and elucidated their structures to validate their solution data.

In the cases of 6-phospho-β-galactosidase and *O*-acetylserine sulfhydrylase, several mutant proteins showed various degrees of dimerization in solution but did not crystallize. In the cases of urocanase and L-rhamnulose-1-phosphate aldolase (Rua), substitution of one or a few residues resulted in complete dimerization, and crystal structures confirmed the presence of extensive new subunit interfaces involving the designed contacts. Urocanase is a C_2 dimer; substitution of three surface residues yields a tetramer with approximate D_2 symmetry. Rua is a C_4 tetramer; single substitutions convert it to two different octamers (one with the D_4 symmetry of Monod's eight-dice assembly, the other with a lower symmetry). A different Rua variant with three substitutions aggregates into fibers.

In another system described by Grueninger *et al.*—the bacterial MspA porin—dimerization results from a deletion. The porin (a membrane-bound C_8 octamer) becomes a soluble D_8 16-mer after the membrane-immersed part is deleted. A crystal structure confirms that the contact between octamers involves the large protein surface, mostly nonpolar, revealed by the deletion. Thus, the set of proteins prepared by Grueninger *et al.* shows a variety of responses to point mutations. Not all the engineered assemblies have the expected symmetry; some are only marginally stable, or they aggregate instead of dimerizing. But on the whole, the data indicate that it is relatively easy to convert a protein with n identical subunits into one with twice that number, at least for $n > 1$.

The successful dimerization of three bacterial proteins by Grueninger *et al.* has implications for the evolution of protein quaternary structures. The new subunit contacts created by mutation or deletion must show some specificity, because the mutant proteins do not aggregate in the crowded bacterial cytoplasm, where they fold and assemble correctly. How can specificity arise in the absence of natural selection?

The answer may be negative selection (*7*). In a cytoplasmic protein with n subunits and C_n symmetry, nonpolar side chains must be disallowed at any surface site where they could stabilize an assembly with $2n$ subunits and D_n symmetry. Mutations not compatible with that symmetry still promote aggregation, but a helical fiber lacks the multiple contacts that create cooperative effects in a D_n assembly. Thus, a single mutation may not suffice to stabilize a fiber, unless the protein is present at a very high concentration, such as hemoglobin in red blood cells.

References

1. K. U. Linderström-Lang, J. A. Schellman, in *The Enzymes*, P. D. Boyer, Ed. (Academic Press, New York, ed. 2, 1959), vol. 1, pp. 443–510.
2. J. Monod, J. P. Changeux, F. Jacob, *J. Mol. Biol.* **6**, 306 (1963).
3. J. Monod, J. Wyman, J. P. Changeux, *J. Mol. Biol.* **12**, 88 (1965).
4. D. Grueninger *et al.*, *Science* **318**, 206 (2008).
5. T. V. Borchert, R. Abagyan, R. Jaenicke, R. K. Wierenga, *Proc. Natl. Acad. Sci. U.S.A.* **91**, 1515 (1994).
6. M. J. Bennett, M. R. Sawaya, D. Eisenberg, *Structure* **14**, 811 (2006).
7. D. B. Lukatsky, B. E. Shakhnovich, J. Mintseris, E. I. Shakhnovich, *J. Mol. Biol.* **365**, 1596 (2007).

10.1126/science.1152930

GEOPHYSICS

What Triggers Tremor?

Tidal forces and distant earthquakes can increase the low-frequency rumbling that occurs where tectonic plates collide.

Eliza Richardson and Chris Marone

An enduring mystery in geophysics is why the periodic stresses of tides do not commonly trigger earthquakes. If earthquakes simply represent reaching some threshold for the failure of rock, tidal forces should often trigger faults near failure by pushing them over the threshold. However, many studies show that this is not the case, except in special situations (*1*, *2*). Now, on page 186, Rubinstein *et al.* report that a seismic activity called nonvolcanic tremor is indeed triggered by lunar-solar tides (*3*) and, in some cases, as reported on page 173 by Gomberg *et al.*, by distant earthquakes (*4*). Discovering how dynamic stresses trigger fault failure may provide important clues about the onset of earthquake rupture.

Earth tremor episodes involve quasi-continuous emissions of low-frequency seismic energy that last longer than ordinary earthquakes. Tremor is well known in volcanic settings, where it is associated with magma movement and fluid-cavity resonance (*5*, *6*). The recent discovery of tremor in nonvolcanic settings (*7*) has inspired multiple groundbreaking studies (*8*–*14*). An emerging question is how nonvolcanic tremor relates to aseismic (that is, radiating no measurable seismic energy) fault slip; they occur simultaneously and in predictable, periodic episodes in at least two locations where they have been studied extensively (*8*, *15*, *16*). The association of nonvolcanic tremor with fault slip suggests the tantalizing possibility that tremor could be used in earthquake forecasting, as it is in predicting volcano eruption (*5*).

The authors are at the Istituto Nazionale di Geofisica e Vulcanologia, Rome, Italy, and the Department of Geosciences, Pennsylvania State University, University Park, PA 16802, USA. E-mail: eliza@geosc.psu.edu

Rubinstein *et al.* found a clear correlation between the dominant tidal forcing (at periods of 12.4 and 24 hours) and the amplitude of tremor along the Cascadia subduction zone offshore Vancouver Island, Canada. Tremor and aseismic fault slip recur periodically every 14 months in this area (*8*, *13*), and tidal stressing modulates tremor amplitude only during times of active tremor (*3*). This is an important point. The work of Rubinstein *et al.* shows that tides are not sufficient to trigger tremor at arbitrary times during the cycle of repeated failure. In this sense, their result is actually quite similar to tidal triggering of volcanoes and ordinary earthquakes, when tides primarily trigger earthquakes during times of extreme activity, for example, just before or after large earthquakes (*1*, *2*, *17*).

In contrast, a recent study (*14*) shows that the Cascadia tremor was triggered early in the failure cycle by the passage of surface waves from the magnitude 7.8 Denali, Alaska, earthquake on 3 November 2002. The Denali earthquake triggered the Cascadia tremor roughly 3 months before the predicted tremor episode in February 2003. Surface waves from Denali caused a spike in shear stress on the subduction interface at Cascadia (*14*), much higher than the stress from tides (*3*). This implies that tremor can be induced at arbitrary times during the seismic cycle as long as the perturbation amplitude is sufficient and its orientation is favorable to shear failure. Laboratory observations of triggered frictional stick-slip corroborate the idea that larger-amplitude perturbations are needed to trigger failure earlier in the seismic cycle (*18*). In addition, both laboratory experiments and earthquake studies suggest that a complex combination of amplitude and frequency of dynamic stressing determines the triggering threshold (*19*).

The mechanism of nonvolcanic tremor is poorly understood. Before the work of Gomberg *et al.*, all studies except one (*9*) have observed tremor where tectonic plates are subducting. As a result, explanations have focused on fluid migration and thermal release of volatile elements in subduction zones. The discovery by Gomberg *et al.* that surface waves from the Denali earthquake triggered tremor in multiple locations along the North America-Pacific plate boundary in California suggests that these may not be the only viable mechanisms. Theoretical studies based on laboratory data suggest that transient, aseismic slip can arise spontaneously given the right fault rheology (*20*). This scenario is consistent with recent studies in Japan (*10*–*12*) suggesting that nonvolcanic tremor arises from shear failure on quasi-dynamic slip patches that radiate low-frequency seismic energy. Shelly *et al.* (*12*) show that tremor can be explained as a swarm of slow, low-frequency earthquakes. Thus, a central remaining question is: What causes slow fault slip? Special conditions appear to be necessary to limit acceleration during shear instability (*21*), yet seismic observations of slow and silent earthquakes indicate that this mode of deformation is widespread (*22*, *23*).

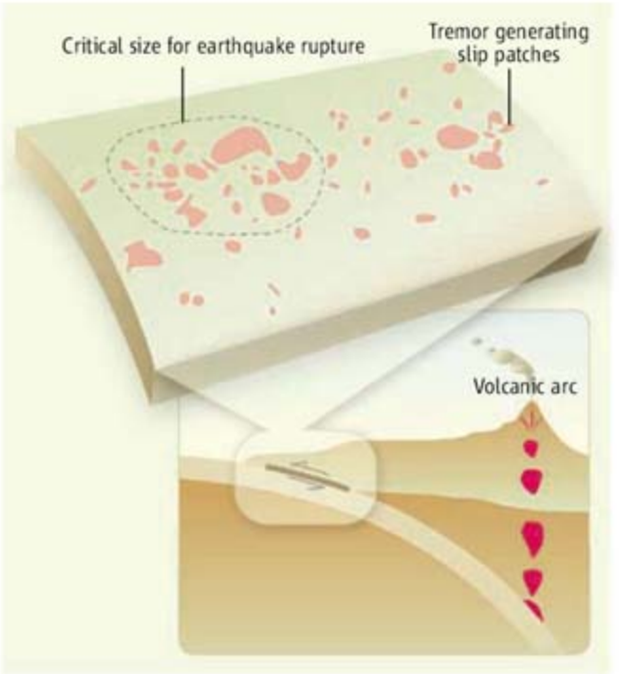

Tides and temblors trigger tremor. Volcanic earth tremor is often generated by movement of magma. Nonvolcanic tremor may represent swarms of small slip patches (red shaded regions) that radiate only low-frequency energy. Rubinstein *et al.* and Gomberg *et al.* show that periodic stress caused by tides and remote seismic activity can increase nonvolcanic tremor. The patches may then coalesce (dashed line) to produce large earthquakes.

Tremor may provide clues about the onset of earthquake rupture. All earthquakes are thought to nucleate as small patches of unstable slip, with some events becoming large earthquakes given the right combination of energy release and spatial homogeneity of fault strength. Tremor may represent slip on a series of subcritical fault patches that radiate low-frequency energy (see the figure), reflecting slip acceleration before reaching a critical size associated with fully unstable behavior and high-frequency seismic radiation. This idea is consistent with results from studies of small earthquakes, which document the acceleration of rupture velocity and the resulting initiation of high-frequency energy radiation associated with fast earthquake rupture (*24*, *25*).

The studies by Rubinstein *et al.* and Gomberg *et al.* can guide future efforts to characterize nonvolcanic tremor, both in terms of observations and through laboratory experiments. For example, how widespread is the occurrence of tremor far from subduction zones? Is nonvolcanic tremor triggered by small earthquakes or vice-versa? What is the recipe for triggering tremor via stress transients (i.e., what roles do amplitude, frequency, time during the seismic cycle, or orientation of the remote perturbation play?)? How do tremor, earthquakes, low-frequency seismicity, and aseismic slip interact in time and space? Earth tremor represents one of a wide spectrum of behaviors ranging from aseismic fault creep to ordinary fast earthquakes. Future geodetic and seismic networks should help us learn much more about these phenomena.

References

1. M. F. Tolstoy, F. Vernon, J. Orcutt, F. Wyatt, *Geology* **30**, 503 (2002).
2. E. S. Cochran, J. E. Vidale, S. Tanaka, *Science* **306**, 1164 (2004).
3. J. L. Rubinstein, M. La Rocca, J. E. Vidale, K. C. Creager, A. G. Wech, *Science*, **319**, 186 (2008).
4. J. Gomberg *et al.*, *Science* **319**, 173 (2008).
5. S. R. McNutt, *Ann. Rev. Earth Planet. Sci.* **33**, 461 (2005).
6. L. Burlini *et al.*, *Geology* **35**, 183 (2007).
7. K. Obara, *Science* **296**, 1679 (2002).
8. G. Rogers, H. Dragert, *Science* **300**, 1942 (2003).
9. R. M. Nadeau, D. Dolenc, *Science* **307**, 389 (2005).
10. D. R. Shelly, G. C. Beroza, S. Ide, S. Nakamula, *Nature* **442**, 188 (2006).
11. S. Ide, D. R. Shelly, G. C. Beroza, *Geophys. Res. Lett.* **34**, 10.1029/2006GL028890 (2007).
12. D. R. Shelly, G. C. Beroza, S. Ide, *Nature* **446**, 305 (2007).
13. M. Brudzinski, R. M. Allen, *Geology*, **35**, 907 (2007).
14. J. L. Rubinstein *et al.*, *Nature*, **448**, 579 (2007).
15. M. M. Miller, T. Melbourne, D. J. Johnson, W. Q. Sumner, *Science* **295**, 2423 (2002).
16. K. Obara, H. Hirose, F. Yamamizu, K. Kasahara, *Geophys. Res. Lett.* **31**, 10.1029/2004GL020848 (2004).
17. J. Kasahara, *Science* **297**, 348 (2002).
18. H. Savage, C. Marone, *J. Geophys. Res.* 112, B02301, 10.1029/2005JB004238 (2007).
19. R. M. Harrington, E. E. Brodsky, *Bull. Seismol. Soc. Am.* **96**, 871 (2006).
20. J. R. Rice, J.-C. Gu, *Pure Appl. Geophys.* **121**, 187 (1983).
21. M. Roy, C. Marone, *J. Geophys. Res.* **101**, 13919 (1996).
22. G. C. Beroza, T. Jordan, *J. Geophys. Res.* **95**, 2485 (1990).
23. J. J. McGuire, M. Boettcher, T. H. Jordan, *Nature* **434**, 457 (2005).
24. E. Richardson, T. H. Jordan, *Bull. Seismol. Soc. Am.* **92**, 1766 (2002).
25. R. E. Abercrombie, J. R. Rice, *Geophys. J. Int.* **162**, 406 (2005).

10.1126/science.1152877

CHEMISTRY

Not So Simple

A molecular-beam study of a classic organic reaction shows that its mechanism is more complex than previously assumed.

John I. Brauman

The details of molecular transformations are often referred to as chemical reaction mechanisms. These mechanisms can be characterized in terms of the number of molecules involved, geometric and structural features (including stereochemistry), the presence or absence of intermediates, and the timing of individual steps. Knowledge of mechanism is critical for predicting how molecules may react and for inventing or developing new reactions. On page 183 of this issue, Mikosch *et al.* (*1*) reveal details of the timing, structural changes, and energy exchange in a paradigmatic reaction: the displacement reaction $Cl^- + CH_3I \longrightarrow CH_3Cl + I^-$. The work elegantly combines experiment and theory.

The reaction studied by the authors is a simple example of a nucleophilic displacement (S_N2) reaction, which has an exceptional place in organic chemistry because of its apparent simplicity and its utility. In this reaction, the nucleophile X^- reacts with RY, which can be any of a wide variety of organic chemical structures, giving the products RX and the leaving group Y^-.

The S_N2 reaction is sensitive to the conditions under which it is carried out (*2*), such as whether it is performed in solution or in the gas phase (see the figure). Because the gas-phase reaction occurs at low pressure, there is enough energy to cross the reaction barrier. The solution reaction is much slower, because the reactants are stabilized by solvation more than the transition state is; only a small fraction of the reactants has enough energy to proceed to products at any given time (*3*).

Mikosch *et al.* now use molecular beams to provide a detailed analysis of this reaction in the gas phase. In these experiments, the temperature and collision velocity of the reacting molecules can be controlled separately. The directional distribution and velocity of the products reveals much about the times involved in the reaction and—from considerations of conservation of energy—the distribution of energy in the products as kinetic energy or internal (vibrational) energy. Recent advances in detection allow the data to be accumulated and displayed as images that reflect the relative amounts of product produced at each energy in every direction (*4*). This technique has been used to study reactions of neutral molecules (*5*, *6*). The authors now apply it to reactions of ions with molecules.

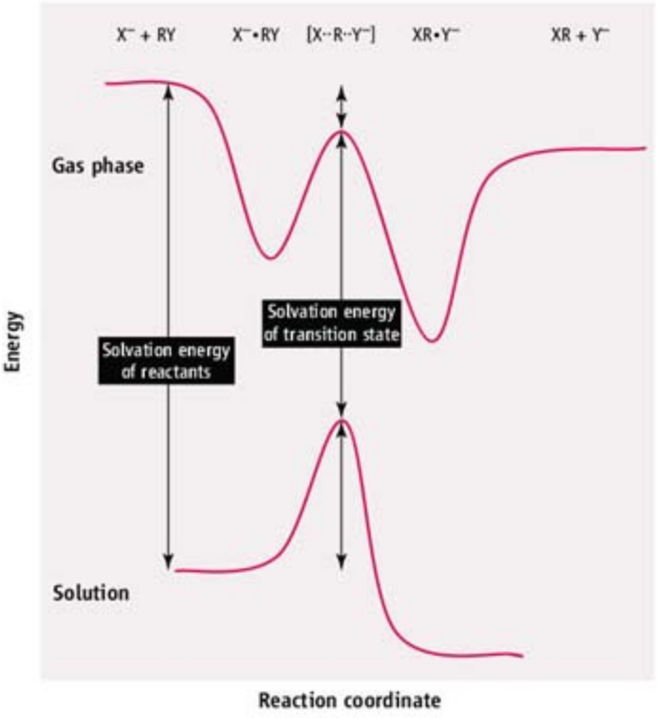

Images and insights. The ability to image the dynamics of ion-molecule reactions in the gas phase allows new insights into the details of a classic organic chemical reaction, as reported by Mikosch *et al.* in this issue.

The details of solution reactions are often inferred rather than directly observed, because collisions with solvent control the trajectories of the molecules, so that the behavior of the initially formed products cannot be determined. In the current case, the solution reaction is essentially a simple, one-step process in which the nucleophile attacks the neutral substrate from the back side and gives a product with stereochemical inversion of configuration relative to the starting material. Molecular dynamics simulations show, however, that interactions with solvent can cause products to return to reactants and cross back and forth many times before finally completing the reaction (*7*).

Mikosch *et al.* now provide considerable detail about the reaction in the gas phase. At low collision energy, the reaction products are distributed isotropically—that is, equally probable in all directions—showing that intermediate X^-•RY complexes persist long enough to undergo many rotations.

At higher collision energies, a new mechanism appears: The I^- departs directly along the axis from which the Cl^- enters, and most of the energy is retained as kinetic energy in the I^- product. In this "direct" reaction, the complexes do not last long enough to rotate before the reaction occurs. Depending on the collision energy, the original process and the new processes compete, with the direct reaction becoming increasingly important as the collision energy is increased.

Direct dynamics trajectory simulations also reported by Mikosch *et al.* are consistent with the experiments in terms of energetics, but also show important details that the experiments do not completely reveal. At even higher collision energy, the indirect reaction reappears, but with an unexpected twist: The incoming Cl^- collides with and induces a rotation of CH_3I, followed by backside attack and displacement. This process can involve multiple rotations of the CH_3I, and a small fraction of the trajectories show transient trapping in the postreaction complex. The study by Mikosch *et al.* illustrates the exceptional insights into details of reaction dynamics that can be obtained with molecular beams. As more reactions are studied with this technique, it should become possible to generalize and make predictions prior to detailed experiments or calculations.

The author is in the Department of Chemistry, Stanford University, Stanford, CA 94305, USA. E-mail: brauman@stanford.edu

References

1. J. Mikosch *et al.*, *Science* **319**, 183 (2008).
2. E. V. Anslyn, D. A. Dougherty, *Modern Physical Organic Chemistry* (University Science Books, Sausalito, CA, 2006), chap. 11.
3. M. L. Chabinyc, S. L. Craig, C. K. Regan, J. I. Brauman, *Science* **279**, 1882 (1998).
4. J. Mikosch *et al.*, *Phys. Chem. Chem. Phys.* **8**, 2990 (2006).
5. K. Liu, *Annu. Rev. Phys. Chem.* **52**, 139 (2001).
6. M. S. Elioff, J. J. Valentini, D. W. Chandler, *Science* **302**, 1940 (2003).
7. J. P. Bergsma, B. J. Gertner, K. R. Wilson, J. T. Hynes, *J. Chem. Phys.* **86**, 1356 (1987).

10.1126/science.1152387

Climate Change, Deforestation, and the Fate of the Amazon

Yadvinder Malhi,[1]* J. Timmons Roberts,[1,2] Richard A. Betts,[3] Timothy J. Killeen,[4] Wenhong Li,[5] Carlos A. Nobre[6]

The forest biome of Amazonia is one of Earth's greatest biological treasures and a major component of the Earth system. This century, it faces the dual threats of deforestation and stress from climate change. Here, we summarize some of the latest findings and thinking on these threats, explore the consequences for the forest ecosystem and its human residents, and outline options for the future of Amazonia. We also discuss the implications of new proposals to finance preservation of Amazonian forests.

The forests of Amazonia (*1*) covered about 5.4 million km^2 in 2001, approximately 87% of their original extent (*2*), with 62% in Brazil. They host perhaps a quarter of the world's terrestrial species (*3*) and account for about 15% of global terrestrial photosynthesis (*4*). Evaporation and condensation over Amazonia are engines of the global atmospheric circulation, having downstream effects on precipitation across South America and further afield across the Northern Hemisphere (*5*, *6*). Amazonian forests have been an important and continuous part of Earth system functioning since the Cretaceous (*7*).

By 2001, about 837,000 km^2 of Amazonian forests had been cleared (*2*), with 1990s gross rates of ~25,000 km^2 year^{-1} (*8*). Clearance is concentrated in the "arc of deforestation" on the southern and eastern margins, driven primarily by expansion of cattle and soybean production, and along the Andean piedmont. Amazonia lies inside nine nations, but 80% of deforestation has been in Brazil (*2*) and 70% of that is provoked by cattle ranching. From 1988 to 2006, deforestation rates in Brazilian Amazonia averaged 18,100 km^2 year^{-1}, recently reaching 27,400 km^2 year^{-1} in 2004. Brazilian deforestation rates had more than halved by 2007 to ~11,000 km^2 year^{-1} because of a combination of falling prices for soy, increased strength of the Brazilian currency, and active Brazilian government intervention (*9*). Roughly 6% of deforested land has remained in cropland, 62% in pastures, and 32% in regrowing vegetation (*10*). The overall direct footprint of human activity in Amazonia is much greater than deforestation alone and includes logging, hunting, and fire leakage (see supporting online text).

Global Drivers of Amazonian Climate Change

In recent decades, the rate of warming in Amazonia (*11*) has been about 0.25°C decade^{-1}. Under midrange greenhouse-gas emission scenarios, temperatures are projected to rise 3.3°C (range 1.8 to 5.1°C) this century, slightly more in the interior in the dry season (*12*), or by up to 8°C if substantial forest dieback affects regional biophysical properties (*13*). At the end of the last glacial period, Amazonia warmed (*14*) at only ~0.1°C century^{-1}.

Changes in precipitation, particularly in the dry season, are probably the most critical determinant of the climatic fate of the Amazon. There has been a drying trend in northern Amazonia since the mid-1970s and no consistent multidecadal trend in the south (*15*), but some global climate models (GCMs) project significant Amazonian drying over the 21st century. Pacific sea surface temperature (SST) variation, dominated by the El Niño–Southern Oscillation (ENSO), is particularly important for wet-season rainfall: El Niño events (warm eastern Pacific) suppress convection in northern and eastern Amazonia. However, dry-season rainfall is strongly influenced by the tropical Atlantic north-south SST gradient; intensification of the gradient (warming of northern SSTs relative to the south) shifts the Intertropical Convergence Zone northwards (interannual time scales) and strengthens the Hadley Cell circulation (longer time scales), enhancing the duration and intensity of the dry season in much of southern and eastern Amazonia (*16*), as occurred in 2005. Interannual variability in the Atlantic gradient is influenced by remote forcing such as ENSO and the North Atlantic Oscillation, as well as by variations in evaporation induced by strengthening/weakening of the local trade winds (*17*). On longer time scales, the Atlantic SST gradient may be strengthened by changes in the north Atlantic, such as changes of the thermohaline circulation driven by subpolar melting (*18*), or a warmer north Atlantic associated with warmer northern hemisphere continents.

Forest Influences on Regional and Global Climate

Amazonian forests have a substantial influence on regional and global climates. Hence, their removal by deforestation can itself be a driver of climate change and a positive feedback on externally forced climate change. They store 120 ± 30 Pg C in biomass carbon (*19*), of which 0.5 Pg C year^{-1} (0.3 to 1.1) were released through deforestation in the 1990s (*10*). Similar or greater amounts may be held in soil carbon, but these are less vulnerable to loss after deforestation (*20*). In addition, forest plot studies suggest that intact forests are a carbon sink (~0.6 Pg C year^{-1}) (*21*), particularly in more fertile western Amazonia. The existence of this sink is debated (*22*) but is strongly supported by a recent reevaluation of global sources and sinks of atmospheric carbon dioxide (*23*). It may be driven by enhanced productivity associated with CO_2 fertilization, changes in light regime, or other factors not yet identified (*24*).

The extraction of soil water by tree roots up to 10 m deep, and its return to the atmosphere (a "transpiration service"), is perhaps the most important regional ecosystem service. Basin-wide, 25 to 50% of rainfall is recycled from forests (*25*), but this effect is particularly important in regions where most precipitation is derived from local convection (see below). Moderate and localized deforestation may locally enhance convection and rainfall, but large-scale forest loss tends to reduce rainfall (*26*), the magnitude of reduction being dependent on how regional circulation of atmospheric moisture is affected. Some model studies suggest that the regional forest-climate system may have two stable states: Removal of 30 to 40% of the forest could push much of Amazonia into a permanently drier climate regime (*27*). Dry season rainfall, the most critical for determining vegetation patterns, is more often driven by locally generated convection and may be more strongly affected by deforestation.

Loss of forest also results in (i) decreased cloudiness and increased insolation, (ii) increased land surface reflectance, approximately offsetting the cloud effect (*28*), (iii) changes in the aerosol loading of the atmosphere from a hyperclean "green ocean" atmosphere to a smoky and dusty continental atmosphere that can modify rainfall patterns (*29*), and (iv) changes in surface roughness (and hence wind speeds) and the large-scale convergence of atmospheric moisture that generates precipitation (*13*).

Risks of Amazon Forest Loss Due to Global Climate Change

Risks of a drying climate. The climate models employed in the 2007 Intergovernmental Panel on Climate Change (IPCC) Fourth Assessment Report (*12*) show no consistent trend in annual,

[1]Environmental Change Institute, Oxford University Centre for the Environment, South Parks Road, Oxford OX1 3QY, UK. [2]College of William and Mary, Williamsburg, VA 23187, USA. [3]Met Office Hadley Centre, Exeter EX1 3PB, UK. [4]Conservation International, Washington, DC 20036, USA. [5]School of Earth and Atmospheric Sciences, Georgia Institute of Technology, Atlanta, GA 30332–0340, USA. [6]Instituto Nacional de Pesquisas Espaciais, São Jose dos Campos, SP, Brazil.

*To whom correspondence should be addressed. E-mail: yadvinder.malhi@ouce.ox.ac.uk

Amazon-wide rainfall over the 21st century, but a tendency to less dry season rain in the east and more rain in the west and in the wet season (Fig. 1). Taking the ensemble of 23 IPCC models as a crude metric of probabilities, some intensification of dry seasons is about 80% probable in the southeast Amazon and Guyanas, 70% in the east, 60% in the center, and 30% in the west (Fig. 1A). The probabilities of more substantial decline are slightly lower: 70% in the southeast, 60% in the Guyanas, 50% in the east, 40% in the center, and 20% in the west. The probabilities of severe decline in dry season rainfall are 50% in the southeast, 30% in the Guyanas and east, and 10% in the center and west. This metric is not ideal, as models may share systematic biases and vary in their ability to represent current Amazonian climates; further, most underestimate current Amazonian rainfall and most do not incorporate the climatic feedbacks from forest loss. Therefore, a more careful evaluation of model ability to capture key elements of Amazonian climate variability is needed. When the effects of rising temperatures on evapotranspiration are included, almost all models indicate increasing seasonal water deficit in eastern Amazonia (*30*). This drying is exacerbated by ecosystem feedbacks such as forest die-back and reduced transpiration in remaining forests (*13*).

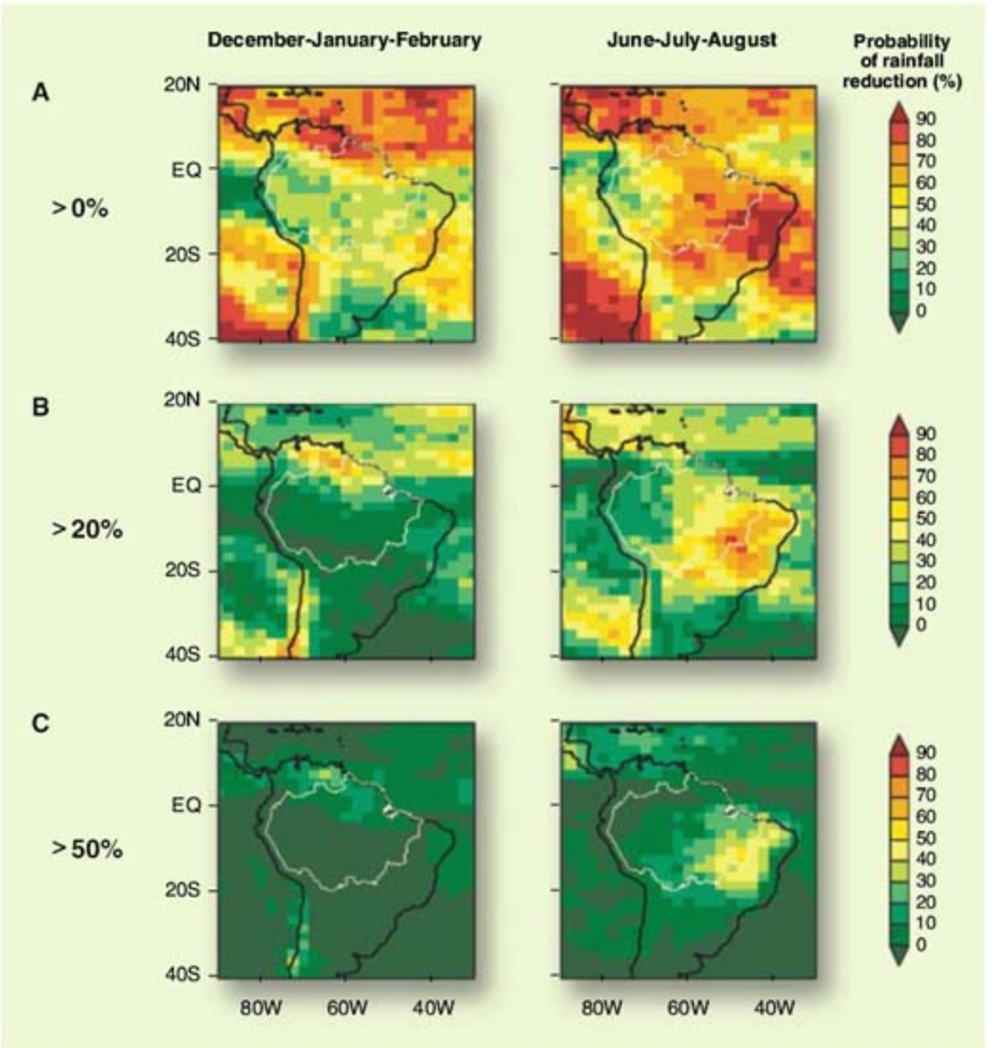

Fig. 1. A metric of the probability of enhanced drought in Amazonia: the proportion of 23 climate models that show a decline in rainfall between 1980 to 1999 and 2080 to 2099 under midrange (A1B) global greenhouse gas emissions scenarios. (**A**) Any decline (rainfall decline > 0%); (**B**) substantial decline (rainfall decline > 20%); (**C**) severe decline (rainfall decline > 50%). Dry season rainfall is particularly important. Left column: December-January-February (dry season in north); right column: June-July-August (dry season in central and southern Amazonia).

The zone of highest drought risk (southeast and east) is also the zone of most active deforestation (Fig. 2). Deforestation-driven changes in precipitation may be strongest in the eastern dry corridor, 700 km inland from the coast, where geographical positioning results in ocean-generated squall lines passing through the region at night and being unable to trigger much rainfall (*31*), leaving a greater fraction of precipitation generated locally. This area includes important agricultural and ranching frontiers that are experiencing high levels of deforestation.

In contrast, the northwestern Amazon is least likely to experience major drought. The high precipitation in this region is controlled by moisture convergence forced by the Andes, although it may be vulnerable to reduced precipitation recycling upwind in eastern Amazonia. This region hosts the highest biodiversity and has been least affected by historical climate variability and land use.

The Andean flank of the Amazon has exceptional rates of biodiversity, adjoins the most biodiverse regions of lowland Amazonia, and also hosts a number of orographic wet spots in otherwise dry areas (*32*). As conditions warmed at the end of the last ice age, the Andes acted as refugia for many "lowland" (now exclusively Andean) tree species that were ill-adapted to warming temperatures (*33*). Andean ecosystems have their own form of vulnerability, however: The cloud forests between 1500 and 3000 m elevation are susceptible to drying as cloud levels rise in the face of warming temperatures (*34*), and higher elevation restricted endemics would be particularly vulnerable.

Resilience of Amazonian forest ecosystems. Understanding of Amazonian forest processes has greatly advanced through the recent Large-Scale Biosphere-Atmosphere program in Amazonia (LBA) (*35*). There is mounting evidence from artificial drought experiments (*36*), flux towers, and satellite remote sensing of forest greenness (*37*) that intact Amazonian forests are more resilient (although not invulnerable) to climatic drying than is currently represented in vegetation-climate models. First, dry season water supply is greatly enhanced by root systems accessing deep soil water and redistributing it into the surface soil through the process of hydraulic lift, enabling the whole forest ecosystem to maintain high transpiration and photosynthesis rates (*38*). Second, plant acclimation to higher temperatures may limit detrimental effects below 45°C [when proteins begin to denature (*39*)], although selective advantage by favored species may cause changes in community composition, as occurred at the last glacial-interglacial transition (*33*). Finally, rising CO_2 may improve plant water use efficiencies and offset the negative transpiration effects of rising temperatures. Southern Amazonia was considerably drier as recently as the early-mid Holocene, yet the region seems to have remained largely forested (*33*).

The Interaction Between Human Pressures and Forest Resilience

The speed and magnitude of current human pressures on forests are affecting forest resilience. Forests close to edges are vulnerable to elevated dessication, tree mortality (*40*), and fire impacts. Rain forests may become seasonally flammable in dry years, but without anthropogenic ignition sources fire is a rare occurrence. Hence, fire has been a weak evolutionary selective force, and as a result many tree species lack adaptations

that allow them to survive even low-intensity fires (*41*).

Fire use for land management is nearly ubiquitous in rural Amazonia. About 28% of the Brazilian Amazon faces incipient fire pressure, being within 10 km of a fire source (*42*). Logging and forest fragmentation also increase the flammability of forests by providing substantial combustion material, opening up the canopy and drying the understory and litter layer and greatly increasing the amount of dry fire-prone forest edge. This synergism between fragmentation and fire is becoming increasingly important, with 20,000 to 50,000 km^2 of new forest edge being created annually in Brazilian Amazonia alone (*43*). Once burnt, a forest becomes more vulnerable to further burns (*44*), loses many primary forest species, and decreases sharply in biomass (*41*). A tipping point may be reached when grasses can establish in the forest understory, providing a renewable source of fuel for repeated burns.

In scenarios of increased drying, it is possible to see this logging, fragmentation, dessication, and repeated burning as a likely fate for many of Amazonia's forests. The 2005 drought provides evidence of this in southwest Amazonia: Remote forests remained fairly unaffected, but there was substantial penetration of fires from agricultural areas into surrounding, temporarily flammable forests (*45*).

Despite the very recent slowdown in deforestation rates, there is potential for extensive deforestation in Amazonia, as more roads (both official and unplanned) are built through its core and connect across to Pacific ports and as international demand for tropical timber, soybeans, and free-range beef continues to grow, particularly from rapidly expanding Asian economies (*2*, *46*, *47*). Existing pressures might be exacerbated by accelerating worldwide demand for biofuels. Current plans for infrastructure expansion and integration could reduce forest cover from 5.4 million km^2 (2001, 87% of original area) to 3.2 million km^2 (53%) by 2050 (*2*) (Fig. 2A). This exceeds the likely threshold for rainfall maintenance and would emit 32 ± 8 Pg of carbon. Deforestation will be more concentrated in the south and east, with >50% forest loss, and along the Andean piedmont, isolating the warming lowlands from potential biotic refuges in the cooler mountains (*46*). In this scenario, the northwestern Amazon is protected by its remoteness and wetness, but longer term, this region is also vulnerable to hydrocarbon exploration and oil-palm plantations that are suitable for wet climates and acidic soils and have already replaced many of Asia's tropical rainforests (*46*). Drying of Amazonia, whether caused by local or global drivers, could greatly expand the area suitable for soy, cattle, and sugarcane, accelerating forest disappearance.

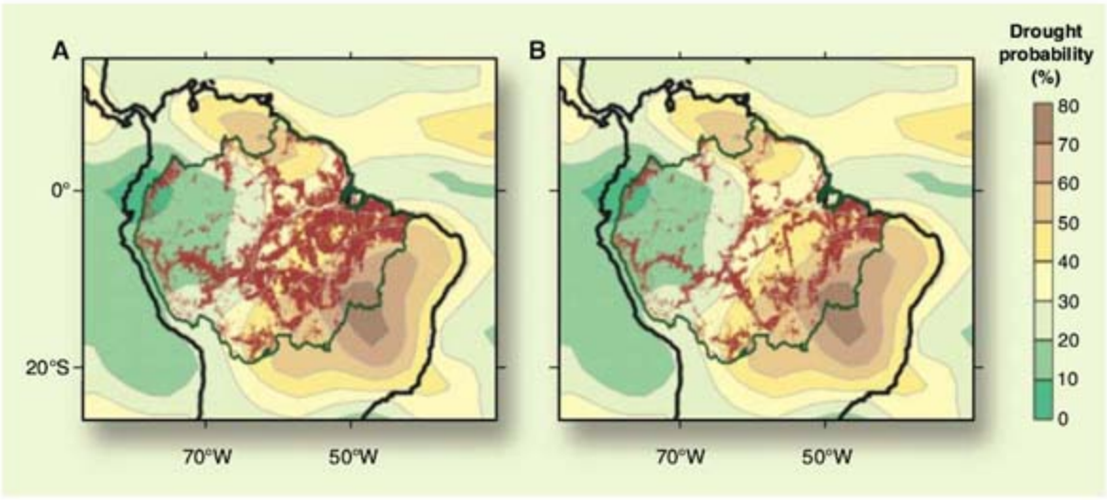

Fig. 2. The potential overlap between deforestation and climate change. Potential loss in forest cover (brown) by 2050 under (**A**) business as usual and (**B**) increased governance scenarios [derived from (*2*)], superimposed on the probability of substantial drought, which is defined as a >20% reduction in dry-season rainfall by the late 21st century, as shown in Figure 1B. The dry season is defined as from December to February (south of the equator) and from June to August (north of the equator). Precipitation scenarios are from mid-range (A1B) global greenhouse gas emissions scenarios, from the 21 climate models employed in IPCC Fourth Assessment Report [extracted and modified from (*15*)].

Planning for Climate Change

The probability of substantially enhanced drought (Fig. 1B) under mid-range greenhouse gas emissions scenarios ranges from >60% in the southeast to <20% in the west. The severity of this potential threat merits planning for development, conservation, and adaptation in all regions. Even if the drought does not come, a well-conceived and implemented plan will have built resilience into the Amazon social ecological system.

It is almost inevitable that substantial further conversion of forest into agricultural and pasture lands will occur as part of the economic development of Amazonian countries (*2*, *46*). The danger is that degradation of ecosystem services could push some subregions into a permanently drier climate regime and greatly weaken the resilience of the entire region to possible large-scale drought driven by SST changes. Hence, the challenge is to manage the economic development of Amazonia so that it occurs where appropriate and sustainable, in a way that maintains the inherent climatic resilience that the intact forest provides. Simultaneously, this would preserve the region's carbon store and sink and its exceptional biodiversity, contributing both toward mitigating global warming and assisting that biodiversity to adapt to climate change.

Key aspects of such a plan for Amazonia could include

(i) Keeping the total extent of deforestation safely below possible climatic threshold values (about 30 to 40% cleared) in a matrix that includes large protected areas with limited fragmentation and managed landscapes that maintain sufficient forest cover and landscape connectivity to preserve species migration corridors and forest transpiration services.

(ii) Controlling fire use through both education and regulation, probably for net economic benefit.

(iii) Maintaining broad species migration corridors in ecotonal areas that are most likely to show early signals of climate impacts, such as those between forest and savanna, between lowlands and the Brazilian and Guyana shield uplands, between the Andean piedmont and montane forest, and between montane forest and highland Andean grasslands.

(iv) Conserving river corridors to act as humid refugia and migration corridors for terrestrial ecosystems and as sedimentation buffers and refugia for aquatic systems. Many of the southern tributaries of the Amazon river run from dry fringes to the wet core and could assist the migration of wet-adapted species.

(v) Keeping the core northwest Amazon largely intact as a biological refuge that hosts the highest biodiversity and is the least vulnerable to climatic drying.

Is such a plan feasible? With the expansion of protected areas and effective legal enforcement of private land use, the projections of loss of 47% of original forest area by 2050 could be reduced to 28% loss (*2*), avoiding ~17 PgC emissions (Fig. 2B). Recent developments suggest that such good governance is achievable. Details of the role that can be played by protected areas, indigenous peoples, smallholders, agroindustries, and governments are discussed in the supporting online text.

Financing a Climate-Resilience Plan for Amazonia

A plan for keeping Amazonia from ecological and climatic decline faces several challenges:

the drive of globalizing market forces, insufficient financial resources, provision of open access to information, limited technical and governance capacity, and ineffective enforcement of rule of law. In particular, new financial incentives are needed to act as a countervailing force to the economic pressures for deforestation.

Such incentives are now a serious possibility through the international markets in carbon spawned by the Kyoto Protocol, such as the European Union's Emissions Trading System. The recently agreed-upon "Bali Roadmap" for extension of the Kyoto Protocol beyond 2012 includes plans for rainforest nations to be paid for reducing emissions from deforestation and degradation (REDD), either through international carbon markets or a voluntary fund (*48*–*50*). Tropical forest carbon credits have particular value within a climate mitigation strategy because they bring additional direct climatic services [cloud formation and precipitation, local cooling by evapotranspiration (*28*)], as well as other ecosystem services such as biodiversity conservation, watershed protection, and pollination.

These plans have the potential to shift the balance of underlying economic market forces that currently favor deforestation (*45*) by raising billions of dollars for the ecosystem services provided by rainforest regions but will require exceptional planning, execution, and long-term follow-through. Such resources could support the expansion of capacity in forest monitoring (e.g., freely available satellite-based monitoring, as already achieved by Brazil) and improved governance and rule-of-law in frontier regions, but in particular would need to ensure that they bring benefits and incentives (e.g., improved social services like health and education) to the individuals and groups making decisions about Amazon land use on a daily basis, be they indigenous peoples, rural subsistence dwellers, smallholder migrants, or large private landholders.

The interaction between global climate change and regional deforestation may make Amazonian forests vulnerable to large-scale degradation. Ironically, it is also this linkage between the global (carbon sequestering) ecosystem service, for which the world may be more willing to pay, and regional (transpiration) services that maintain the region's climate that provides an opportunity to sustain the climatic resilience of Amazonia while contributing toward its conservation and development.

The next few years represent a unique opportunity, perhaps the last, to maintain the resilience, biodiversity, and ecosystem services of Amazonia in the face of a medium threat of significant drying and a high threat of significant deforestation. The best climate, ecological, economic, and social science will be needed to develop, implement, and monitor effective policy responses for securing the region's future. The other key requirement is political will at the local, national, and international levels.

References and Notes

1. Here defined as the Legal Amazon in Brazil and the Amazon river watershed and Guyanas region outside of Brazil.
2. B. S. Soares-Filho *et al.*, *Nature* **440**, 520 (2006).
3. R. Dirzo, P. H. Raven, *Annu. Rev. Env. Res.* **28**, 137 (2003).
4. C. B. Field, M. J. Behrenfeld, J. T. Randerson, P. Falkowski, *Science* **281**, 237 (1998).
5. N. Gedney, P. J. Valdes, *Geophys. Res. Lett.* **27**, 3053 (2000).
6. D. Werth, R. Avissar, *J. Geophys. Res. Atmos.* **107**, 8087 (2002).
7. M. Maslin, Y. Malhi, O. Phillips, S. Cowling, *Trans. Inst. Br. Geogr.* **30**, 477 (2005).
8. F. Achard *et al.*, *Science* **297**, 999 (2002).
9. D. Nepstad *et al.*, *Conserv. Biol.* **20**, 65 (2006).
10. N. Ramankutty *et al.*, *Glob. Change Biol.* **13**, 51 (2007).
11. Y. Malhi, J. Wright, *Philos. Trans. R. Soc. Lond. B Biol. Sci.* **359**, 311 (2004).
12. J. H. Christensen *et al.*, in *Climate Change 2007: The Physical Science Basis. Contribution of Working Group I to the Fourth Assessment Report of the Intergovernmental Panel on Climate Change*, S. D. Solomon *et al.*, Eds. (Cambridge Univ. Press, Cambridge and New York, 2007), chap. 11.
13. R. A. Betts *et al.*, *Theor. Appl. Clim.* **78**, 157 (2004).
14. M. B. Bush, M. R. Silman, D. H. Urrego, *Science* **303**, 827 (2004).
15. J. A. Marengo, *Theor. Appl. Clim.* **78**, 79 (2004).
16. W. H. Li, R. Fu, R. E. Dickinson, *J. Geophys. Res.* **111**, D02111, 10.1029/2005JD006355 (2006).
17. P. Chang, R. Saravanan, L. Ji, *Geophys. Res. Lett.* **30**, 1501 (2003).
18. B. W. Dong, R. T. Sutton, *Geophys. Res. Lett.* **29**, 1728 (2002).
19. Y. Malhi *et al.*, *Glob. Change Biol.* **12**, 1107 (2006).
20. K. W. Holmes *et al.*, *Global Biogeochem. Cycles* **20**, GB3004 (2006).
21. T. R. Baker *et al.*, *Philos. Trans. R. Soc. Lond. B Biol. Sci.* **359**, 353 (2004).
22. S. J. Wright, *Trends Ecol. Evol.* **20**, 553 (2005).
23. B. B. Stephens *et al.*, *Science* **316**, 1732 (2007).
24. S. L. Lewis *et al.*, *Philos. Trans. R. Soc. Lond. B Biol. Sci.* **359**, 421 (2004).
25. E. A. B. Eltahir, R. L. Bras, *Q. J. R. Meteorol. Soc.* **120**, 861 (1994).
26. S. B. Roy, R. Avissar, *J. Geophys. Res.* **107**, 8037 (2002).
27. M. D. Oyama, C. A. Nobre, *Geophys. Res. Lett.* **30**, 2199 (2003).
28. G. Bala *et al.*, *Proc. Natl. Acad. Sci. U.S.A.* **104**, 6550 (2007).
29. M. O. Andreae *et al.*, *Science* **303**, 1337 (2004).
30. L. F. Salazar, C. A. Nobre, M. D. Oyama, *Geophys. Res. Lett.* **34**, L09708 (2007).
31. M. Garstang, H. L. Massie Jr., J. Halverson, S. Greco, J. Scala, *Mon. Weather Rev.* **122**, 608 (1994).
32. T. J. Killeen, M. Douglas, T. Consiglio, P. M. Jorgensen, J. Mejía, *J. Biogeogr.* **34**, 1357 (2007).
33. F. E. Mayle, D. J. Beerling, W. D. Gosling, M. B. Bush, *Philos. Trans. R. Soc. Lond. B Biol. Sci.* **359**, 499 (2004).
34. P. Foster, *Earth Sci. Rev.* **55**, 73 (2001).
35. LBA Web site: http://lba.cptec.inpe.br/lba/site.
36. R. A. Fisher *et al.*, *Glob. Change Biol.* **13**, 2361 (2007).
37. A. R. Huete *et al.*, *Geophys. Res. Lett.* **33**, L06405 (2006).
38. R. S. Oliveira, T. E. Dawson, S. S. O. Burgess, D. C. Nepstad, *Oecologia* **145**, 354 (2005).
39. T. D. Sharkey, S. M. Schrader, in *Physiology and Molecular Ecology of Stress Tolerance in Plants* (Kluwer, Netherlands, 2004), pp. 101–130.
40. W. F. Laurance *et al.*, *Science* **278**, 1117 (1997).
41. J. Barlow, C. A. Peres, *Philos. Trans. R. Soc. Lond. B Biol. Sci.* **359**, 367 (2004).
42. P. Barreto *et al.*, *Human Pressure on the Brazilian Amazon Forests* (World Resources Institute, Washington, DC, USA, and Imazon, Belém, Brazil, 2006).
43. M. A. Cochrane, W. F. Laurance, *J. Trop. Ecol.* **18**, 311 (2002).
44. M. A. Cochrane *et al.*, *Science* **284**, 1832 (1999).
45. L. E. O. C. Aragão *et al.*, *Geophys. Res. Lett.* **34**, L07701 (2007).
46. T. J. Killeen, *Advances in Applied Biodiversity Science No. 7* (Center for Applied Biodiversity Science, Conservation International, Washington, DC, 2007).
47. A. A. C. Alencar, L. A. Solorzano, D. C. Nepstad, *Ecol. Appl.* **14**, S139 (2004).
48. M. Santilli *et al.*, *Clim. Change* **71**, 267 (2005).
49. R. E. Gullison *et al.*, *Science* **316**, 985 (2007).
50. P. Moutinho, S. Schwartzman, *Tropical Deforestation and Climate Change* (IPAM, Belem, Brazil, 2005).

51. This paper is based largely on the conference "Climate Change and the Fate of the Amazon," held at Oriel College, University of Oxford, 20 to 22 March 2007, and funded by the James Martin 21st Century School, the Environmental Change Institute, and the Centre for Brazilian Studies, University of Oxford. Conference presentations are available at www.eci.ox.ac.uk/news/events/070320presentations.php. We thank all participants at the conference, in particular E. Boyd, M. Gloor, P. Harris, J. Lloyd, J. Marengo, D. Nepstad, O. Phillips, and B. Soares, for their comments on this manuscript. Y.M. is supported by the Jackson Foundation, J.T.R. by the James Martin 21st Century School and the College of William and Mary, and R.A.B. by the joint Defra and MoD Integrated Climate Programme. We thank D. Maniatis and P. Zelazowski for assistance in manuscript preparation. We acknowledge the Coupled Model Intercomparison Project and the international modeling groups for providing their data for analysis.

Supporting Online Material

www.sciencemag.org/cgi/content/full/1146961/DC1
SOM Text
References and Notes

Published online 22 November 2007;
10.1126/science.1146961
Include this information when citing this paper.

Widespread Triggering of Nonvolcanic Tremor in California

Joan Gomberg,[1]* Justin L. Rubinstein,[2] Zhigang Peng,[3] Kenneth C. Creager,[2] John E. Vidale,[2] Paul Bodin[2]

Tremor away from volcanoes (*1*), termed nonvolcanic tremor, reflects a fault slip regime different than that of earthquakes. Relative to radiation from earthquakes, tremor signals have longer durations, have fewer or no abrupt wave onsets, and are depleted in high frequencies. Tremor has almost exclusively been found in subduction zones: Cascadia, southwestern Japan, Mexico, Costa Rica, and Alaska; there is only one study documenting tremor outside a subduction-dominated region, on the strike-slip San Andreas Fault in Parkfield, California (*2*). In Japan and Cascadia, nonvolcanic tremor has been shown to occur concurrently with slippage across the interface between subducting and overlying plates, both lasting for days to months (*3*). The pace and amount of slip are much smaller than those during earthquakes that rupture comparably sized fault areas, and thus these slow events radiate less seismic energy. The physical relation between the slow slip and tremor generation remains speculative. Recent studies in subduction zones have identified short bursts of tremor with the same measurable characteristics as those associated with slow slip, but triggered by the strong shaking of distant earthquakes (*4*). Because nonvolcanic tremor is preferentially observed in subduction zones, nearly all causative mechanisms proposed appeal to conditions expected in them. We show that the conditions required for its generation must exist in a wider variety of tectonic environments by presenting observations of nonvolcanic tremor at seven sites along the transform plate boundary in California triggered by the 2002 7.8 moment magnitude Denali Fault, Alaska, earthquake.

We examined all available recordings of the Denali earthquake waves from seismic stations in California. We identified triggered nonvolcanic tremor as high frequency (about 3 to 15 Hz), nonimpulsive seismic energy that pulses with the period of the passing surface waves. This energy is not associated with nearby earthquakes or with the Denali earthquake itself. We identified tremor from seven sources that we located by using tremor envelopes as input to a grid-search algorithm (*5*). These locations range from the desert southeast of Los Angeles to Napa Valley in the north (Fig. 1).

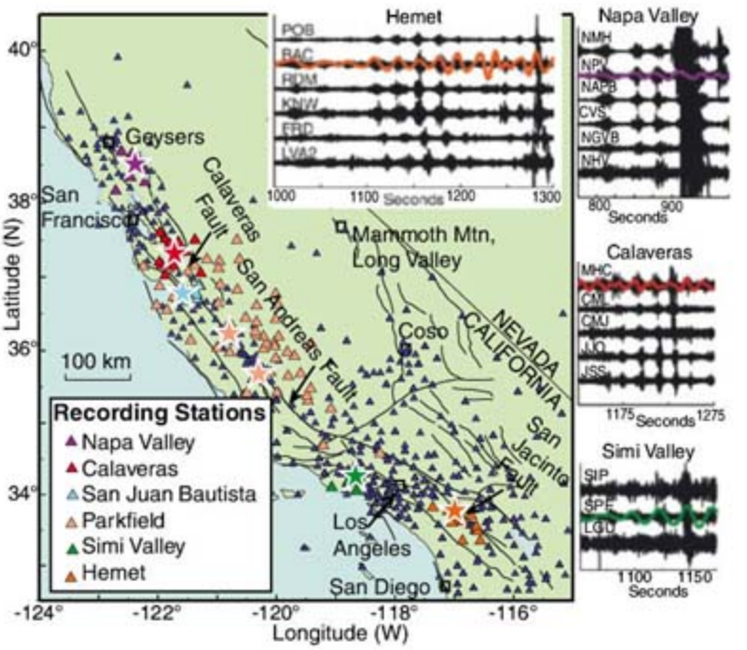

Fig. 1. Map of the locations of tremor sources [stars (*5*)], stations that recorded signals from each tremor source (triangles color coded to the respective sources, see legend), stations that showed no tremor (dark blue triangles), and major faults (black lines). (**Insets**) Examples of the tremor signals associated with four regions where single tremor sources are identified. The Denali surface waves have been filtered out to highlight the tremor (black seismograms), and colored traces show the transverse component of the surface waves from Denali at one unfiltered broadband station in each region, noting that the amplitudes on the radial and vertical components do not differ significantly. Depending on the tremor site, we observed tremor triggering by both Love and Rayleigh waves. The last large bursts in the Hemet and Napa Valley signals are characteristic of nearby earthquakes. Each seismogram has been scaled to make the tremor easily identifiable, times are referenced to the Denali earthquake origin time, and recording stations are labeled.

Although the observed tremor bursts span a large transect of California, five sources locate close to or on dominant strike-slip faults: the San Andreas, the San Jacinto, and the Calaveras faults. The Simi Valley and Napa Valley sources are likely on more minor faults. Some models of tremor associated with slow aseismic slip in subduction zones invoke frictional behaviors expected in regions transitional between where the fault is locked and earthquakes occur and where it is slipping freely below (*6*). Such transition zones also must exist at shallow depths both below the top few km of fault segments known to creep continuously and laterally between locked segments and those that creep for most or all of their depth. The distribution of these various behaviors is known for most faults in California. However, we find no clear correlation between where the faults are creeping, locked, or transitional and where tremor occurs.

Many studies have speculated that aseismic slip and tremor are related to the release of fluids from dehydration of the subducting plate (*1*). Given this expected correlation between fluids and nonvolcanic tremor, we examined the data from stations close to the Coso and Geysers geothermal fields. We identified signals of many triggered earthquakes, but no tremor was apparent. These findings agree with previous work on triggered earthquakes at these sites and at the hydrothermal regions in Long Valley Caldera and Mammoth Mountain (*7*). The lack of triggered tremor in these geothermal regions implies that high fluid pressure and/or temperatures, although they may be necessary, are not alone sufficient to produce tremor.

In interpreting our results, it is important to note where we found triggered tremor as well as where we did not. The paucity of triggered tremor in hydrothermal regions and its lack of correlation with local, ambient slip behavior suggest that very specific conditions (e.g., temperature, pressure, fluid content, and frictional properties) control where tremor and earthquakes occur. The wide geographic extent of the triggered tremor indicates that it is more common than previously recognized and that the necessary conditions exist in a wide range of tectonic environments.

References

1. K. Obara, *Science* **296**, 1679 (2002).
2. R. M. Nadeau, D. Dolenc, *Science* **307**, 389 (2005); published online 9 December 2004 (10.1126/science.1107142).
3. G. Rogers, H. Dragert, *Science* **300**, 1942 (2003); published online 8 May 2003 (10.1126/science.1084783).
4. J. L. Rubinstein *et al.*, *Nature* **448**, 579 (2007).
5. Materials and methods are available as supporting material on *Science* Online.
6. Y. Liu, J. R. Rice, *J. Geophys. Res.* **110**, 10.1029/2004JB003424 (2005).
7. S. Prejean *et al.*, *Bull. Seismol. Soc. Am.* **94**, 5348 (2004).

Supporting Online Material

www.sciencemag.org/cgi/content/full/1149164/DC1
Materials and Methods

13 August 2007; accepted 17 October 2007
Published online 22 November 2007;
10.1126/science.1149164
Include this information when citing this paper.

[1]U.S. Geological Survey, Box 351310, Seattle, WA 98195, USA. [2]Department of Earth and Space Science, University of Washington, Box 351310, Seattle, WA 98195, USA. [3]School of Earth and Atmospheric Sciences, Georgia Institute of Technology, 311 Ferst Drive, Atlanta, GA 30332–0340, USA.

*To whom correspondence should be addressed. E-mail: gomberg@usgs.gov

Stellar Feedback in Dwarf Galaxy Formation

Sergey Mashchenko,* James Wadsley, H. M. P. Couchman

Dwarf galaxies pose substantial challenges for cosmological models. In particular, current models predict a dark-matter density that is divergent at the center, which is in sharp contrast with observations that indicate a core of roughly constant density. Energy feedback, from supernova explosions and stellar winds, has been proposed as a major factor shaping the evolution of dwarf galaxies. We present detailed cosmological simulations with sufficient resolution both to model the relevant physical processes and to directly assess the impact of stellar feedback on observable properties of dwarf galaxies. We show that feedback drives large-scale, bulk motions of the interstellar gas, resulting in substantial gravitational potential fluctuations and a consequent reduction in the central matter density, bringing the theoretical predictions in agreement with observations.

Dwarf galaxies are the most common galaxy type (*1*). In the hierarchical picture of cosmic structure formation, dwarf galaxies form first, later becoming building blocks for larger galaxies. Thanks to their proximity in the local universe (around 18 galaxies are located within 300 kpc of the Sun), several of these galaxies have been studied in detail. Accurate modeling of the mass distribution, based on the observed line-of-sight velocities for hundreds of stars, has revealed features that pose severe challenges for the standard cosmological model. It appears, for example, that the distribution of dark matter (which is the dominant mass component of these galaxies) is of almost constant density in a central region that is comparable in size to the stellar body of the galaxy (*2*–*6*). In the best-studied systems, Fornax and Ursa Minor, the radius of this region is ~ 400 and ~ 300 pc, respectively (*6*). This core is at odds with existing cosmological models, which reliably predict the dark matter to have a divergent density (a cusp) at the galactic center (*7*). Some dwarf spheroidal galaxies also exhibit radial gradients in the stellar population, with stars more deficient in heavy elements (and therefore presumed older) having a more extended distribution and being kinematically warmer than more metal-rich stars (*8*, *9*). Further, the presence of globular clusters in many dwarfs is puzzling, because these massive, compact systems of many thousands of stars would have suffered gravitational drag as they moved through the dark-matter background of the galaxy halo. This dynamical friction would have caused the globular clusters to spiral into the galaxy center on time scales much shorter than the age of the galaxy [the Fornax dwarf spheroidal galaxy is notable in this regard (*5*)].

It is well established that massive stars inject large amounts of energy into the surrounding medium via stellar winds and supernova explosions, resulting in large-scale (hundreds of parsecs in large galaxies) random bulk motions of the interstellar gas at close to sonic speeds (~ 10 km s^{-1} for the typical gas temperature of 10^4 K) (*10*–*12*). The effect of such perturbations is larger for dwarf galaxies, because they have lower gas pressure as a result of the lesser depth of their gravitational potential wells. This stellar feedback has been invoked to explain at least some of the puzzling properties of dwarf galaxies. In particular, there has been considerable debate as to whether or not such feedback can turn the theoretically predicted central dark-matter cusp into a core (*13*–*16*).

Previous theoretical work has included both noncosmological and cosmological modeling. High-resolution, noncosmological numerical models with detailed descriptions of relevant physical processes (*10*, *17*, *18*) suffer from unrealistically symmetric initial conditions and a static description of the dark-matter potential, as well as from the lack of gas accretion from the ambient cosmic medium. Previous attempts at self-consistent hydrodynamic cosmological simulations have tended to focus on the formation of the very first small galaxy progenitors (*19*, *20*) or on dwarf galaxy models without sufficient resolution or the relevant physics to properly model star formation and feedback because of the substantial computational challenges involved in self-consistent modeling (*21*, *22*).

Here we present the results of cosmological simulations of dwarf galaxy formation and evolution that adequately resolve and model the processes of star formation and stellar feedback. In good agreement with our previous semi-analytical results (*16*), our self-consistent model demonstrates that, in small galaxies, random bulk gas motions driven by stellar feedback play a critical role in determining the structure of the galactic center. The key result is the transformation of the central density profile from a cusp to a large core. This is a consequence of resonant heating of dark matter in the fluctuating potential that results from the bulk gas motions. We also demonstrate that the same mechanism can explain other puzzling features of dwarf galaxies, such as the stellar population gradients, low decay rate for globular cluster orbits, and the low central stellar density.

The simulations were run with the cosmological parallel tree code Gasoline (*23*). This code represents dark and stellar matter as a collection of dark-matter and star particles and uses the smoothed particle hydrodynamics formalism to describe gas evolution. A detailed description of the code, including the prescriptions for star formation and supernova feedback, can be found in (*24*, *25*). The very high resolution achieved in our models required the addition of two key features to the standard cosmological code. First, low-temperature (<10^4 K) radiative cooling from the de-excitation of fine structure and metastable lines of heavy elements was necessary to correctly model gas cooling in small galaxies (*25*). Second, because our mass resolution (<200 $M_\odot$) is sufficient to resolve individual supernovae, we introduced an innovative, stochastic prescription for stellar feedback (*25*).

Department of Physics and Astronomy, McMaster University, Hamilton, ON L8S 4M1, Canada.

*To whom correspondence should be addressed. E-mail: syam@physics.mcmaster.ca

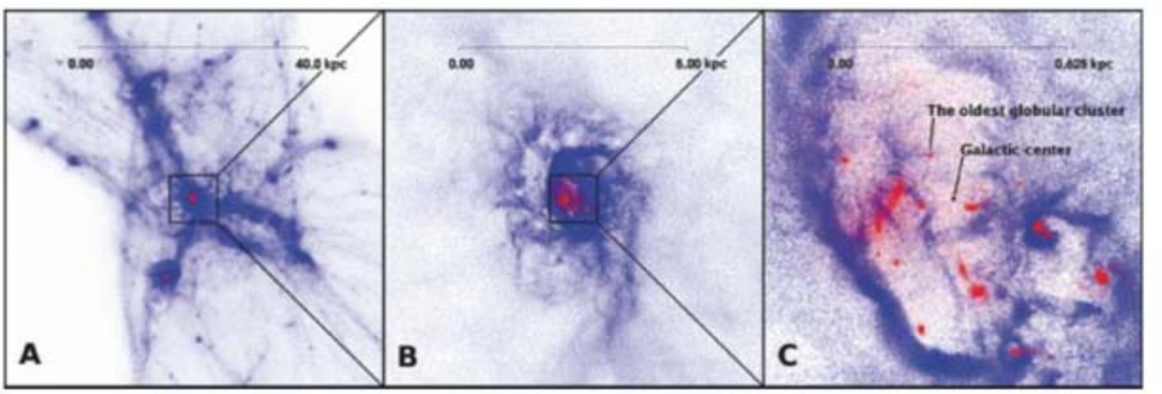

Fig. 1. Zoom-in images of the central part of the simulated forming dwarf galaxy at redshift $z = 5.3$. This time was chosen to illustrate the very clumpy gas distribution after a star burst. Gas is shown in blue and stars are shown in red. (**A**) Global view. (**B**) View of the galaxy. (**C**) The central part of the galaxy. Several star clusters are visible in (C), and the oldest (marked) has an age of 200 My.

We created cosmological initial conditions with input constraints designed to produce a dwarf galaxy with total mass ~ 10^9 $M_\odot$ at redshift $z = 6$ within a box of size 4 co-moving Mpc. A central, high-resolution sphere, with radius 0.4 co-moving Mpc, was populated with gas particles. The particle masses inside the high-resolution sphere were 1900 $M_\odot$ for dark matter and 370 $M_\odot$ for gas. The mass of particles generated to represent stars was ~ 120 $M_\odot$. At the end of the simulations, the total numbers of dark-matter, gas, and star particles were 1.1×10^7, 4.5×10^6, and 4.5×10^5, respectively. The gravitational softening length was held constant at 12 pc. Further model details, including the description of numerical convergence tests and free-parameter studies, can be found in (*25*).

Two primary simulations were run. The first one included all the key physical effects: gas dynamics, star formation, and stellar feedback. [This simulation was by far the most computationally expensive, consuming 6×10^5 central processing unit hours.] The second one was a dark-matter-only control simulation. The simulations started at $z = 150$ and ended at $z = 5$.

In the simulations, the matter distribution develops the classic weblike or filamentary structure on large scales, with the most massive galaxy forming around $z = 10$ at the intersection of the major filaments near the center of the computational box (Fig. 1). The evolution of the galaxy is relatively smooth (i.e., there are no major mergers) between $z = 8$ and 5. The star formation in the dwarf galaxy is very "bursty," with major star bursts repeating roughly every ~ 80 million years (My), which is consistent with the noncosmological models of (*10*). Stars form predominantly in clusters, but many of them quickly disperse. Starting at $z = 6.2$, when the galactic stellar mass reaches ~ 10^7 $M_\odot$, clusters that survive until the end of the simulation start to form. These long-lived clusters have broadly the same sizes (~ 10 pc, essentially unresolved in our simulations), masses (~ 10^5 $M_\odot$), and heavy-element abundance (~ 3% of that of the Sun) as globular clusters observed in the local universe. In the Local Group, no old (early-type) dwarfs with stellar mass $<10^7$ $M_\odot$ have globular clusters, whereas all brighter dwarfs (with the exception of M32, which is severely tidally stripped by its host galaxy, M31) have globular clusters (*1*). This suggests that a galaxy has to be large enough ($>10^7$ $M_\odot$ in baryons) to produce globular clusters, which is in good agreement with our simulations.

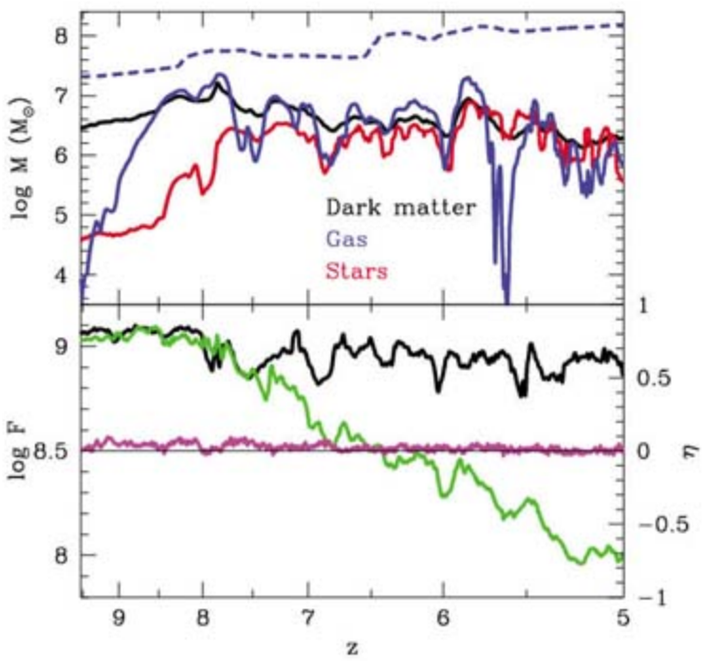

Fig. 2. Evolution of the central quantities in the model dwarf galaxy. (**Top**) Solid lines correspond to changes in the dark-matter (black), gas (blue), and stellar (red) masses enclosed within the central 100 pc as a function of z. The dashed blue line shows the evolution of the enclosed gas mass within the central 1.6 kpc (half the virial radius). (**Bottom**) Green and black lines show the evolution of the central dark-matter phase-space density, F, for the hydrodynamic and dark-matter-only simulations, respectively. We also show the evolution of the velocity anisotropy, η, for the same dark-matter particles as were used to calculate F (magenta line; horizontal black line marks $\eta = 0$). Here, $\eta = (\sigma_r^2 - \sigma_t^2)/(\sigma_r^2 + \sigma_t^2)$, where σ_r and σ_t are, respectively, the one-dimensional radial and tangential velocity dispersions.

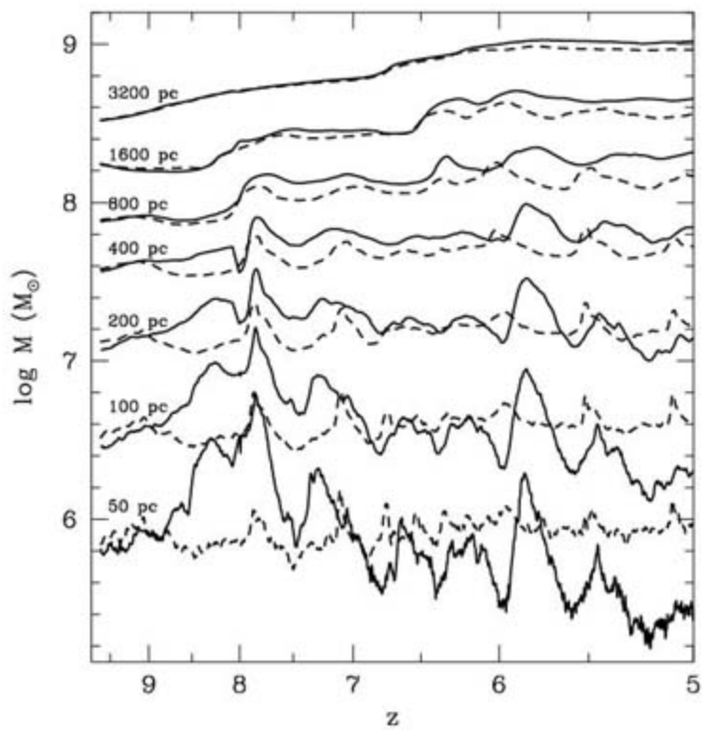

Fig. 3. Evolution of the enclosed dark-matter masses in the model galaxy at different radii. Dashed lines correspond to the dark-matter-only simulation, and solid lines correspond to the hydrodynamic simulation.

Feedback from the bursty and clustered star formation results in a dramatically perturbed interstellar gas distribution on large scales (hundreds of parsecs) (Figs. 1 and 2 and movie S1). This is consistent with the observed (irregular) distribution of gas in dwarf galaxies (*1*). At high redshift, this feedback does not expel gas from the galaxy, in contrast to the maximum stellar feedback mechanism (*14*). Instead, supernova explosions compress gas into large shells and filaments, which are confined to the central part of the galaxy and move with speeds ~ 10 to 20 km s^{-1} (which are comparable to the speeds of dark-matter particles). We showed previously (*16*) that gas motion with these characteristics results in efficient gravitational heating of the central dark matter and flattening of the cusp.

The heating of dark matter in our model dwarf galaxy is highly effective (Figs. 2 to 4). Whereas both density, ρ, and velocity dispersion, σ, of the particles are strongly affected by the variable content of gas and stars at the galactic center, the phase-space density, $F = \rho/\sigma^3$, is much less sensitive to adiabatic compression of dark matter by baryons (Fig. 2). In the dark-matter-only simulation, F stays roughly constant, whereas in the hydrodynamic simulation, F gradually decreases with time as the result of the stellar feedback and, at the end of the evolution, becomes 10 times as low as the value for the dark-matter-only simulation.

The dark-matter density is strongly affected by the stellar feedback only in the central region of the galaxy (Fig. 3). This is the region in which the enclosed gas mass occasionally dominates that of the dark matter and is where the gas is most strongly affected by the feedback. At the end of the hydrodynamic simulations, the dark-matter density at the smallest resolved ra-

dius becomes seven times as small as the density obtained in the dark-matter-only simulations.

Whereas the dwarf galaxy halo in the dark-matter-only simulation develops a central cusp with logarithmic slope −0.95, which is consistent with previous predictions of the standard model (*7*), in the hydrodynamic simulations, resonant heating resulting from stellar feedback turns the cusp into a flat core with radius 400 pc (Fig. 4) and average density 0.2 $M_\odot$ pc^{-3}. These core parameters are close to those inferred for Fornax: ~ 400 pc (*6*) and ~ 0.1 $M_\odot$ pc^{-3} (*1*), respectively. The same mechanism produces a core of somewhat smaller radius (~ 300 pc) in the distribution of stars and, notably, pushes newly formed globular clusters away from the galactic center. The four oldest globular clusters, for example, were born with radial distance dispersion 37 pc (essentially at the galactic center), but after ~ 200 My of evolution, this distance had grown to a time-averaged value of 280 pc (which is comparable to the stellar core radius). We suggest that resonant gravitational heating can at least partially explain why globular clusters in Fornax, and in some other dwarfs, are located at large distances from the galactic center (*5*). Two mechanisms contribute to the effect: (i) The feedback flattens the central cusp, which reduces the efficiency of dynamical friction in the central regions (*5*), and (ii) stellar feedback would have continued to heat the globular cluster orbits until stars stopped forming, around 200 million years ago in Fornax (*9*).

The distribution of velocities is isotropic within the core and shows slight radial anisotropy outside the core (Fig. 4), whereas the core remains isotropic throughout the evolution (Fig. 2). This behavior is inconsistent with a mechanism (*26*) making use of massive gas clouds, passively orbiting (i.e., not driven by feedback) near the galactic center, which flatten the dark-matter cusp via heating resulting from dynamical friction. It has been shown (*27*) that this would result in the development of substantial tangential anisotropy within the core, which is not observed in our simulations. On the other hand, the gravitational resonance heating (*16*) naturally produces isotropic cores because the feedback-driven bulk gas motions have random directions.

These results also provide a natural explanation for the stellar population gradients seen in many early-type dwarfs (*8*, *9*). In our simulations, star formation is concentrated toward the galactic center. Over time, feedback gradually heats the population of stars, resulting in older (and more metal-poor) stars being kinematically warmer and having a larger spatial extent than younger (and more metal-rich) stellar populations. Hence, we can reproduce, qualitatively, the age, metallicity, and velocity-dispersion gradients observed in dwarf galaxies.

Our simulations were stopped at $z = 5$, because continuing beyond this point would require a much larger computational box (to correctly model the growth of larger structures) and an infeasible increase in computation time. Furthermore, the impact of external ionizing radiation, which was ignored in our model, can become substantial after $z = 6.5$. Nevertheless, we can reasonably infer the subsequent evolution of our model galaxy. If it is to become one of the early-type galaxies in the local universe (which are gas-poor), some mechanism will have to remove most or all of its interstellar medium. Some combination of a powerful star burst, increased metagalactic ionizing radiation, and ram-pressure stripping could result in the dwarf losing most of its gas (*28*). It is also likely that only a fraction of its star clusters will survive until the present time. As a result, our model galaxy would end up resembling a large dwarf spheroidal galaxy in the local universe: low stellar density; metal-poor, with old stellar populations having pronounced radial population gradients; large stellar and dark-matter cores (which are comparable in size and density to those in dwarf spheroidals); and perhaps a few globular clusters. In many respects, the galaxy would resemble the Fornax dwarf.

Our noncosmological modeling (*16*) suggested that stellar feedback can be directly responsible for the absence of dark-matter cusps only in small galaxies, with total masses < 10^{10} $M_\odot$: In larger galaxies, the dark-matter particle velocities become substantially larger than the velocity of the random bulk gas motions, which is ~ 10 km s^{-1}. Our current, cosmological simulations are consistent with this result (the mass of our galaxy reaches 2×10^9 $M_\odot$ by $z = 5$). Numerical simulations (*29*) have suggested that a universal halo density profile (either cuspy or cored), once set, is preserved through subsequent hierarchical evolution (which is consistent with the analytical result that the collisionless dark-matter phase-space density can only decrease over time), implying that our mechanism may also lead to dark-matter cores in larger galaxies.

Our simulations indicate that the gravitational heating of matter resulting from feedback-powered bulk gas motions is a critical determinant of the properties of dwarf galaxies. Large dark-matter cores are an unavoidable consequence of early star formation in dwarf galaxies. Our model indicates that, in primordial dwarf galaxies, globular clusters are formed in the most natural place—near the center, where the gas pressure is highest—and are then pushed by feedback to much larger distances. This mechanism also ensures that globular clusters and unclustered stars have a comparable distribution, as is observed in early-type dwarfs (*30*). Additionally, the low stellar density and stellar population gradients observed in dwarf galaxies are also expected from the model. Finally, large cores have serious implications for direct searches of dark matter, because a flat core will produce a much weaker gamma-ray annihilation signal than that produced by a cusp.

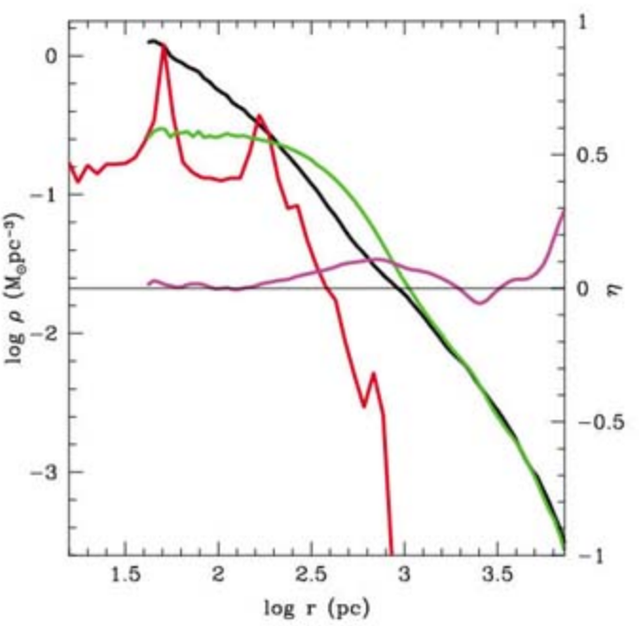

Fig. 4. Radial profiles for the model galaxy at redshift $z = 5.2$. At this time, the central gas density is very low, minimizing the adiabatic compression of dark matter resulting from baryons (which makes it appropriate for comparison with presently observed gas-poor dwarfs). Green and red lines show the dark-matter and stellar density (ρ) profiles, respectively, in the hydrodynamic simulation. The black line corresponds to the dark-matter density profile for the dark-matter-only simulation. The magenta line shows the η profile for the dark matter (in the hydrodynamic simulation).

References and Notes

1. M. L. Mateo, *Annu. Rev. Astron. Astrophys.* **36**, 435 (1998).
2. W. J. G. de Blok, S. S. McGaugh, V. C. Rubin, *Astron. J.* **122**, 2396 (2001).
3. J. T. Kleyna, M. I. Wilkinson, G. Gilmore, N. W. Evans, *Astrophys. J.* **588**, L21 (2003).
4. G. Gentile, A. Burkert, P. Salucci, U. Klein, F. Walter, *Astrophys. J.* **634**, L145 (2005).
5. T. Goerdt, B. Moore, J. I. Read, J. Stadel, M. Zemp, *Mon. Not. R. Astron. Soc.* **368**, 1073 (2006).
6. G. Gilmore *et al.*, *Astrophys. J.* **663**, 948 (2007).
7. J. F. Navarro *et al.*, *Mon. Not. R. Astron. Soc.* **349**, 1039 (2004).
8. E. Tolstoy *et al.*, *Astrophys. J.* **617**, L119 (2004).
9. G. Battaglia *et al.*, *Astron. Astrophys.* **459**, 423 (2006).
10. F. I. Pelupessy, P. P. van der Werf, V. Icke, *Astron. Astrophys.* **422**, 55 (2004).
11. A. D. Slyz, J. E. G. Devriendt, G. Bryan, J. Silk, *Mon. Not. R. Astron. Soc.* **356**, 737 (2005).
12. M. A. de Avillez, D. Breitschwerdt, *Astron. Astrophys.* **436**, 585 (2005).
13. J. F. Navarro, V. R. Eke, C. S. Frenk, *Mon. Not. R. Astron. Soc.* **283**, L72 (1996).
14. O. Y. Gnedin, H. Zhao, *Mon. Not. R. Astron. Soc.* **333**, 299 (2002).
15. J. I. Read, G. Gilmore, *Mon. Not. R. Astron. Soc.* **356**, 107 (2005).

16. S. Mashchenko, H. M. P. Couchman, J. Wadsley, *Nature* **442**, 539 (2006).
17. F. I. Pelupessy, P. P. Papadopoulos, P. van der Werf, *Astrophys. J.* **645**, 1024 (2006).
18. A. Marcolini, A. D'Ercole, F. Brighenti, S. Recchi, *Mon. Not. R. Astron. Soc.* **371**, 643 (2006).
19. T. Abel, G. L. Bryan, M. L. Norman, *Science* **295**, 93 (2002).
20. N. Yoshida, T. Abel, L. Hernquist, N. Sugiyama, *Astrophys. J.* **592**, 645 (2003).
21. M. Ricotti, N. Y. Gnedin, *Astrophys. J.* **629**, 259 (2005).
22. J. I. Read, A. P. Pontzen, M. Viel, *Mon. Not. R. Astron. Soc.* **371**, 885 (2006).
23. J. W. Wadsley, J. Stadel, T. Quinn, *New Astron.* **9**, 137 (2004).
24. G. Stinson *et al.*, *Mon. Not. R. Astron. Soc.* **373**, 1074 (2006).
25. Materials and methods are available as supporting material on *Science* Online.
26. A. El-Zant, I. Shlosman, Y. Hoffman, *Astrophys. J.* **560**, 636 (2001).
27. C. Tonini, A. Lapi, P. Salucci, *Astrophys. J.* **649**, 591 (2006).
28. L. Mayer, S. Kazantzidis, C. Mastropietro, J. Wadsley, *Nature* **445**, 738 (2007).
29. S. Kazantzidis, A. R. Zentner, A. V. Kravtsov, *Astrophys. J.* **641**, 647 (2006).
30. J. M. Lotz *et al.*, *Astrophys. J.* **552**, 572 (2001).
31. The simulations reported in this paper were carried out on facilities of the Shared Hierarchical Academic Research Computing Network [(SHARCNET) www.sharcnet.ca]. The authors acknowledge the support of the Canadian Institute for Advanced Research, Natural Sciences and Engineering Research Council of Canada, and SHARCNET. To produce Fig. 1 and movie S1, we used the public domain program IFrIT written by N. Gnedin (Fermilab).

Supporting Online Material

www.sciencemag.org/cgi/content/full/1148666/DC1
Materials and Methods
Figs. S1 to S5
References
Movie S1

1 August 2007; accepted 9 November 2007
Published online 29 November 2007;
10.1126/science.1148666
Include this information when citing this paper.

Superconducting Vortices in $CeCoIn_5$: Toward the Pauli-Limiting Field

Andrea D. Bianchi,[1]*† Michel Kenzelmann,[2,3] Lisa DeBeer-Schmitt,[4] Jon S. White,[5] Edward M. Forgan,[5] Joel Mesot,[3] Markus Zolliker,[6] Joachim Kohlbrecher,[3] Roman Movshovich,[7] Eric. D. Bauer,[7] John L. Sarrao,[7] Zachary Fisk,[1] Cedomir Petrović,[8] Morten Ring Eskildsen[4]

Many superconducting materials allow the penetration of magnetic fields in a mixed state in which the superfluid is threaded by a regular lattice of Abrikosov vortices, each carrying one quantum of magnetic flux. The phenomenological Ginzburg-Landau theory, based on the concept of characteristic length scales, has generally provided a good description of the Abrikosov vortex lattice state. We conducted neutron-scattering measurements of the vortex lattice form factor in the heavy-fermion superconductor cerium-cobalt-indium ($CeCoIn_5$) and found that this form factor increases with increasing field—opposite to the expectations within the Abrikosov-Ginzburg-Landau paradigm. We propose that the anomalous field dependence of the form factor arises from Pauli paramagnetic effects around the vortex cores and from the proximity of the superconducting state to a quantum critical point.

$CeCoIn_5$ is a d-wave, heavy-fermion superconductor with a critical temperature T_c = 2.3 K (*1*). The interaction of Ce with the conduction electrons leads to an enhancement of the effective electron mass by several orders of magnitude. The competition between an instability toward antiferromagnetic ordering (suppressed by superconductivity) and a paramagnetic state leads to a quantum critical point at the upper critical field, H_{c2}, and an associated non–Fermi liquid behavior (*2*, *3*). The heavy electron mass (and, for the field parallel to the planes, the 2d electronic structure) suppresses orbiting supercurrents circling the vortices. Hence, the upper critical field at low temperature in $CeCoIn_5$ is not determined by the usual orbital depairing. Instead, it is limited by the Pauli spin susceptibility of the electrons, which favor the electron spins to line up parallel to a magnetic field, which is in competition with the antiparallel alignment required for Cooper pairing in a singlet superconductor (*4*). In $CeCoIn_5$, the Pauli-limiting field is smaller than the orbital upper critical field H_{c2}^{orb} by a factor of >2.5, as extrapolated from measurements near T_c (*5*), and the transition to the normal state at low temperatures becomes first-order (*5*, *6*). Finally, $CeCoIn_5$ can be prepared as an ultraclean superconductor with an electron mean free path (ℓ) of several micrometers, three orders of magnitude larger than the superconducting coherence length (*7*, *8*).

The Ginzburg-Landau (GL) model is a phenomenological description of a superconducting phase with only two parameters: the coherence length ξ of the superconducting order parameter, and the penetration depth λ of magnetic fields into the superconducting phase. Abrikosov showed that the GL model describes the mixed state of type II superconductors (*9*), where quantum flux tubes with a core size of ~ξ penetrate the superconductor in a regular vortex lattice (VL). The Abrikosov-Ginzburg-Landau (AGL) picture gives a good description of the mixed-state properties of orbitally limited superconductors, but it is not known to what extent the AGL model applies for Pauli-limited superconductors, particularly close to the upper critical field.

One of the predicted scenarios for the superconducting Cooper pairs in Pauli-limited superconductors at high fields is that they are no longer formed by a pairing of spin-up and spin-down electrons carrying opposite momenta; instead, the superconducting order parameter carries a finite momentum, giving rise to an inhomogeneous superconducting state known as the Fulde-Ferrell-Larkin-Ovchinnikov (FFLO) state (*10*, *11*). In the Larkin-Ovchinnikov form of such a state, the superconducting order parameter is expected to develop regularly spaced planar nodes perpendicular to the vortex lines (*12*). A number of experiments on $CeCoIn_5$ provide evidence for a phase transition inside the superconducting state near H_{c2} consistent with a FFLO state (*12*). Although the majority of these measurements were performed with the field parallel to the basal plane of the tetragonal unit cell, the possible existence of an FFLO state has also been reported for an applied field along the *c* axis (*12*–*14*).

In our experiment, the VL was imaged by small-angle neutron scattering (SANS), using the direct coupling of the magnetic moment of the neutron to the spatial variation of the magnetic field created by the VL (*15*). Figure 1 shows the evolution of the VL diffraction patterns with increasing magnetic field at 50 mK. The VL in real space has the same symmetry as its diffraction pattern but is rotated by 90° about the field axis. At the lowest fields, the VL of $CeCoIn_5$ has a distorted hexagonal symmetry, giving two equivalent domain orientations and hence 2×6 first-order reflections, which are symmetric with respect to the [110] crystallographic direction (Fig. 1, A and D). With increasing field, the VL undergoes a first-order transition at H_1 = 0.55 T to a rhombic symmetry indicated by 2×4 Bragg reflections (Fig. 1, B and E). Upon further increasing the field, the VL continuously transforms into an ideal, single-domain square symmetry (Fig. 1, C and F) at H_2 = 1.1 T. This evolution of the VL symmetry is in agreement with our earlier studies conducted in fields up to 2 T (*16*, *17*). At higher fields, this sequence of phase transitions reverses (Fig. 1, G and H), with the VL undergoing a transition to a rhombic

[1]Department of Physics and Astronomy, University of California, Irvine, CA 92697, USA. [2]Laboratory for Solid State Physics, ETH Zürich, CH-8093 Zürich, Switzerland. [3]Laboratory for Neutron Scattering, ETH Zürich and Paul Scherrer Institute, CH-5232 Villigen PSI, Switzerland. [4]Department of Physics, University of Notre Dame, Notre Dame, IN 46556, USA. [5]School of Physics and Astronomy, University of Birmingham, Birmingham B15 2TT, UK. [6]Laboratory for Developments and Methods, Paul Scherrer Institute, CH-5232 Villigen PSI, Switzerland. [7]MPA-10, Los Alamos National Laboratory, Los Alamos, NM 87545, USA. [8]Condensed Matter Physics and Materials Science Department, Brookhaven National Laboratory, Upton, NY 11973, USA.

*Present address: Département de Physique, Université de Montréal, Montréal, Quebec H3C 3J7, Canada.
†To whom correspondence should be addressed. E-mail: andrea.bianchi@umontreal.ca

(at $H_2' = 3.4$ T) and finally a distorted hexagonal symmetry (at $H_3 = 4.4$ T).

Further measurements taken at higher temperatures establish the field-temperature VL structural phase diagram (Fig. 2). We note that the phase boundary of the high-field "hexagonal" phase does not intersect with the onset of the first-order nature of H_{c2} (*5*), nor does it coincide with the proposed FFLO phase boundary (*12*, *14*). At higher temperatures, where thermal excitation reduces the effects of anisotropy, fewer VL phases are observed. We also note that the sequence of VL phase transitions is qualitatively similar to that in $TmNi_2B_2C$ (*18*), where localized-moment antiferromagnetic order interacts with the superconducting order parameter. Both compounds have a strong paramagnetic response, which suggests that this may be the driving force leading to the sequence of phase transitions. However, unlike $TmNi_2B_2C$, which has well-ordered local moments, in $CeCoIn_5$ superconductivity is thought to supersede magnetism (*2*).

The VL structural transitions in Fig. 2 at low field and temperature may be understood in the following terms: In the limit of large distances, the vortex lines are isotropic around the screening current plane, as this is the tetragonal crystal basal plane. As the field is increased and the vortices move closer together, there are two effects that can lead to the hexagonal-rhombic-square sequence of transitions: (i) d-wave effects (*19*, *20*), and (ii) the nonlocal relation between supercurrent density **j** and vector potential **A** due to a finite coherence length (*21*). If the square VL is due to d-wave effects, then the nearest neighbors should be aligned along the nodal directions of the d-wave order parameter (*22*), consistent with the $d_{x^2-y^2}$ pairing reported for $CeCoIn_5$ (*23*).

More surprising is the reversal of the sequence of phase transitions, back to a nearly isotropic hexagonal VL, as the field approaches H_{c2} (which is a region not accessible in the d-wave high-T_c superconductors). A reentrant square VL phase has been predicted theoretically, attributed to opposing anisotropies of the Fermi surface and the energy gap (*24*) or to strong fluctuations near H_{c2} (*25*). However, neither of these theories is clearly applicable to $CeCoIn_5$. We propose instead that a quite different mechanism becomes important when the vortex spacing becomes comparable to the core size. A qualitative explanation for the weakening of the fourfold anisotropy at high fields may lie in the observation that, by continuity, the field at the center of a vortex must exhibit cylindrical symmetry, just as it does at large distances; the "four-leaved clover" anisotropy is strong only at intermediate distances [see, e.g., (*26*)]. The proposed tendency toward isotropy at large fields is seen in free energy calculations (*20*), and this tendency may be amplified by the Pauli limiting process that becomes increasingly important near H_{c2}, with induced paramagnetic moments in the vortex cores that are less sensitive than the orbital supercurrents to the crystallographic directions.

We now analyze the diffracted intensity arising from the spatial variation of the magnetic field due to the VL. The total intensity of a diffraction peak, integrated over angle as the VL is rocked through the Bragg condition (*15*), is proportional to the square modulus of the VL form factor $F(\mathbf{q}_{hk})$, which is the Fourier transform at wave vector $\mathbf{q}_{hk}$ of the two-dimensional magnetic flux density of the VL. In the limit of very low fields, the London approach with negligible vortex core effects should apply, and $|F|^2$ depends only on λ with the value $[\sqrt{3}\phi_0/(8\pi^2\lambda^2)]^2$, where ϕ_0 is the flux quantum. Our measured $|F|^2$

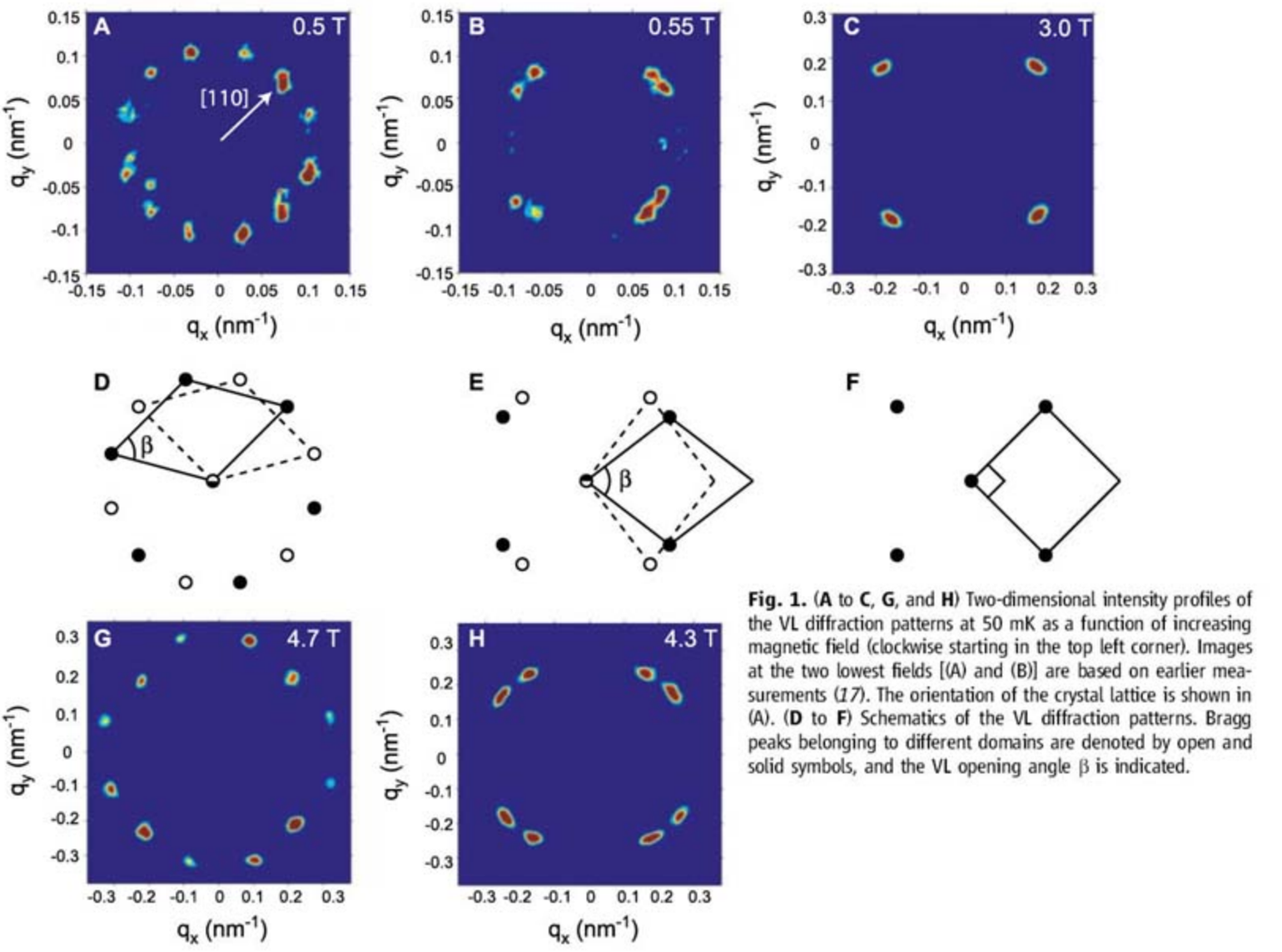

Fig. 1. (**A** to **C**, **G**, and **H**) Two-dimensional intensity profiles of the VL diffraction patterns at 50 mK as a function of increasing magnetic field (clockwise starting in the top left corner). Images at the two lowest fields [(A) and (B)] are based on earlier measurements (*17*). The orientation of the crystal lattice is shown in (A). (**D** to **F**) Schematics of the VL diffraction patterns. Bragg peaks belonging to different domains are denoted by open and solid symbols, and the VL opening angle β is indicated.

implies a value of $\lambda = 4650$ Å, about double the values obtained in zero field by other techniques (*27*, *28*); the cause of this difference is not clear at present. Since the early work on Nb (*29*), it has been observed that $|F|^2$ decreases monotonically as the vortices move closer together and their field distributions overlap. Both the GL model and numerical calculations predict an approximately exponential decrease of the form factor at low and intermediate fields for both s- and d-wave superconductors (*20*, *30*). Near H_{c2} Abrikosov's solution to the GL equations predicts that $|F|^2$ falls quadratically to zero (*31*). Figure 3 shows the measured form factor in $CeCoIn_5$ at $T = 50$ mK and 0.5 K, which is in striking contrast to typical AGL field dependence shown by the dashed lines. Below 2 T, $|F|^2$ is essentially constant, in agreement with previous reports (*17*), followed by a monotonic increase by a factor of ~4 with field up to 4.5 T at both 50 and 500 mK. An additional testimony to the increasing form factor is given by the fact that a strong VL diffraction pattern was observed even at 4.9 T (within 50 mT of H_{c2}).

The GL picture can be generalized by allowing the characteristic lengths to vary with field. This was the approach of earlier work, which, motivated by theoretical predictions for ultraclean superconductors (*32*), used a field-dependent core size ξ to explain the unexpected constancy of $|F|^2$ below 2 T (*17*). With the increase in $|F|^2$ reported here, however, a parameterization of our results between 0.5 and 4.5 T by a field-dependent ξ would require a decrease of the core size by a factor of more than 5. In comparison, previous experimental reports of core contraction show that it occurs mainly at low vortex densities (*33*), and although ξ decreases, the ratio of the core size to the vortex separation increases with field, causing $|F|^2$ to decrease. Within the Bardeen-Cooper-Schrieffer (BCS) and GL approach, the BCS coherence length ξ_0 is field-independent and $\xi_{GL} \propto \hbar v_F/k_B T_c$ (where $\hbar$ is the Planck constant divided by 2π, v_F is the Fermi velocity, and k_B is the Boltzmann constant). To explain our results strictly in such terms would require a large increase of the pairing interaction with field (which we regard as very unlikely) or would require a decrease in the Fermi velocity, which would entail an increase in λ and a decrease of $|F|^2$. We also exclude the possibility that an increase in $|F|^2$ could be explained by a decrease in λ, as this would imply a superfluid density increasing toward H_{c2}. Thus, our results present a clear departure from the AGL paradigm. This conclusion is also indirectly supported by observations of an unusual broadening of the nuclear magnetic resonance line shape in the mixed state of $CeCoIn_5$ [see (*12*), references 28 and 120].

Instead, we ascribe the increase in $|F|^2$ at large fields to a contribution of electron spin polarization to the magnetic induction in the vortex cores. A similar process has been studied in the borocarbide superconductor $TmNi_2B_2C$, which has localized magnetic moments (*34*).

In a strongly Pauli-limited superconductor, it is expected that parallel spin alignment of the quasi-particles would be greater in the cores, where the Cooper pairs are broken. This conclusion is strengthened by recent first-principles calculations, which indeed show an increase in $|F|^2$ with field arising from paramagnetic effects (*35*). However, there is not complete agreement, as an increasing form factor requires a ratio between the Pauli limiting field and the orbital limiting field, which is larger than the one found experimentally for $CeCoIn_5$. This discrepancy may arise from the fact that the magnetic susceptibility in the c direction is twice that for the basal plane (*6*), whereas the heat capacity in the normal state is approximately independent of field direction, suggesting an additional enhancement of paramagnetic effects for fields along the c axis. Alternatively, it may be the quantum critical point at $H_{c2}(T = 0)$ that leads to a divergence of the heavy fermion masses as measured by de Haas–van Alphen measurements (*36*) and heat capacity (*2*), possibly leading both to an enhancement of the paramagnetic effect and to a limitation of the vortex core size, both of which would tend to maintain a large form factor to high fields.

Finally, we draw attention to the drop in $|F|^2$ just below H_{c2} shown in our lowest-temperature data in Fig. 3. This drop does not coincide with a VL structure change. However, it does occur in the field and temperature region where other measurements have been interpreted as evidence for a FFLO phase with field direction parallel to the c axis (*12*–*14*). Certainly, the additional zeroes in the order parameter in a spatially modulated FFLO state would be expected to

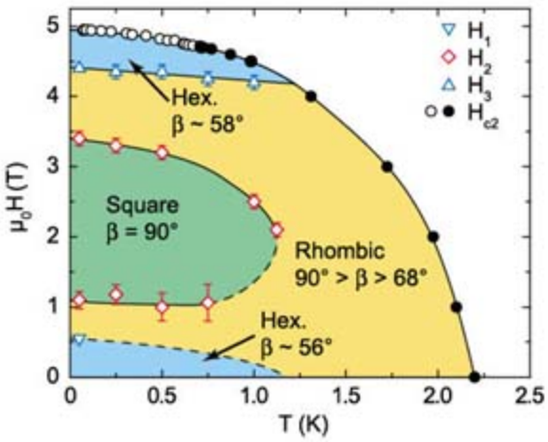

Fig. 2. Structural phase diagram for the VL in $CeCoIn_5$ with the magnetic field parallel to the c axis. The exact location of the hexagonal to rhombic transition H_1 was reliably determined only at base temperature, and the dashed line thus denotes our best estimate at higher temperatures. Likewise, there is some uncertainty in the lower branch of the square to rhombic transition H_2 between 0.75 and 1.25 K. The upper critical field is from (*5*). Above 0.7 K, H_{c2} is second order (solid circles). Below 0.7 K, the transition from the superconducting to the normal state becomes first order (open circles) because of the combination of high cleanliness and dominating Pauli paramagnetic limiting.

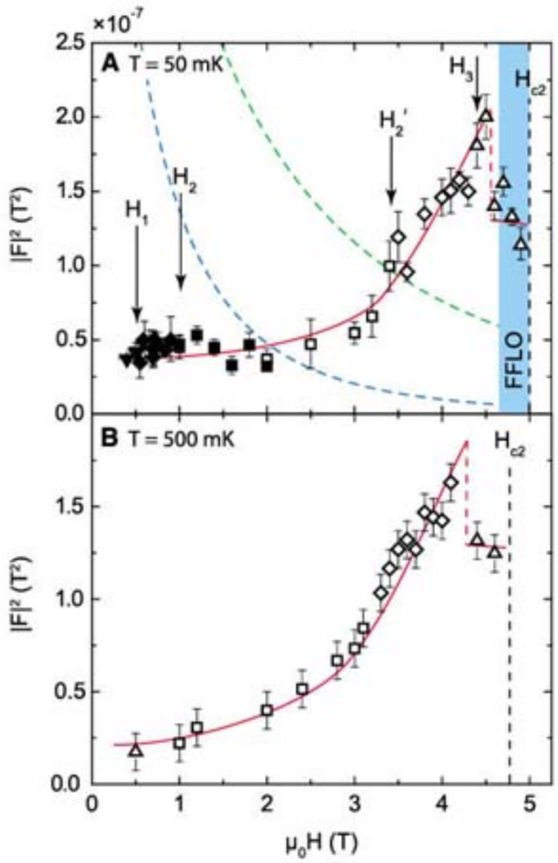

Fig. 3. Field dependence of the VL form factor for the (1,0) Bragg reflection at 50 mK (**A**) and 0.5 K (**B**). Solid symbols indicate earlier results obtained below 2 T (*17*). The lines through the data are guides to the eye. The VL symmetry transition fields H_1, H_2, and H_3 at 50 mK are indicated by arrows, and the upper critical field is shown by the vertical dashed lines. The green and blue dashed lines in the upper panel correspond to $|F|^2$ calculated from the Clem model (*30*) using a constant $\lambda = 235$ nm and $\xi_{c2} = 8.1$ nm (blue) or $\xi_{orb} = 5.0$ nm (green). The blue shaded region in the upper panel indicates the fields above which a FFLO phase has been reported on the basis of magnetization measurements (*14*).

reduce the form factor. Even without this indirect evidence for the predicted FFLO state, our main conclusion remains that in this strongly Pauli-limited superconductor with a quantum critical point at $H_{c2}(T = 0)$, the mixed state departs in many respects from the classical Abrikosov VL.

References and Notes

1. C. Petrović *et al.*, *J. Phys. Condens. Matter* **13**, L337 (2001).
2. A. Bianchi, R. Movshovich, I. Vekhter, P. G. Pagliuso, J. L. Sarrao, *Phys. Rev. Lett.* **91**, 257001 (2003).
3. M. A. Tanatar, J. Paglione, C. Petrović, L. Taillefer, *Science* **316**, 1320 (2007).
4. A. M. Clogston, *Phys. Rev. Lett.* **9**, 266 (1962).
5. A. Bianchi *et al.*, *Phys. Rev. Lett.* **89**, 137002 (2002).
6. T. Tayama *et al.*, *Phys. Rev. B* **65**, 180504 (2002).
7. R. Movshovich *et al.*, *Phys. Rev. Lett.* **86**, 5152 (2001).
8. Y. Kasahara *et al.*, *Phys. Rev. B* **72**, 214515 (2005).
9. A. A. Abrikosov, *Sov. Phys. JETP* **5**, 1174 (1957).
10. A. I. Larkin, Y. N. Ovchinnikov, *Sov. Phys. JETP* **20**, 762 (1965).
11. P. Fulde, R. A. Ferrell, *Phys. Rev. A* **550**, 135 (1964).
12. Y. Matsuda, H. Shimahara, *J. Phys. Soc. Jpn.* **76**, 051005 (2007), and references therein.
13. A. Bianchi, R. Movshovich, C. Capan, P. G. Pagliuso, J. L. Sarrao, *Phys. Rev. Lett.* **91**, 187004 (2003).
14. X. Gratens *et al.*, http://arxiv.org/abs/cond-mat/0608722 (2006).
15. See supporting material on *Science* Online.
16. M. R. Eskildsen, C. D. Dewhurst, B. W. Hoogenboom, C. Petrović, P. C. Canfield, *Phys. Rev. Lett.* **90**, 187001 (2003).
17. L. DeBeer-Schmitt, C. D. Dewhurst, B. W. Hoogenboom, C. Petrović, M. R. Eskildsen, *Phys. Rev. Lett.* **97**, 127001 (2006).
18. M. R. Eskildsen *et al.*, *Nature* **393**, 242 (1998).
19. M. H. S. Amin, I. Affleck, M. Franz, *Phys. Rev. B* **58**, 5848 (1998).
20. M. Ichioka, A. Hasegawa, K. Machida, *Phys. Rev. B* **59**, 8902 (1999).
21. V. G. Kogan *et al.*, *Phys. Rev. B* **55**, R8693 (1997).
22. S. P. Brown *et al.*, *Phys. Rev. Lett.* **92**, 067004 (2004).
23. A. Vorontsov, I. Vekhter, *Phys. Rev. Lett.* **96**, 237001 (2006).
24. N. Nakai, P. Miranović, M. Ichioka, K. Machida, *Phys. Rev. Lett.* **89**, 237004 (2002).
25. A. Gurevich, V. G. Kogan, *Phys. Rev. Lett.* **87**, 177009 (2001).
26. M. Franz, C. Kallin, P. I. Soininen, A. J. Berlinsky, A. L. Fetter, *Phys. Rev. B* **53**, 5795 (1996).
27. R. J. Ormeno, A. Sibley, C. E. Gough, S. Sebastian, I. R. Fisher, *Phys. Rev. Lett.* **88**, 047005 (2002).
28. S.Özcan *et al.*, *Europhys. Lett.* **62**, 412 (2003).
29. J. Schelten, H. Ullmaier, W. Schmatz, *Phys. Status Solidi B* **48**, 619 (1971).
30. J. R. Clem, *J. Low Temp. Phys.* **18**, 427 (1975).
31. E. M. Forgan *et al.*, *Phys. Rev. Lett.* **88**, 167003 (2002).
32. V. G. Kogan, N. V. Zhelezina, *Phys. Rev. B* **71**, 134505 (2005).
33. J. E. Sonier, *J. Phys. Condens. Matter* **16**, S4499 (2004).
34. L. DeBeer-Schmitt *et al.*, *Phys. Rev. Lett.* **99**, 167001 (2007).
35. M. Ichioka, K. Machida, *Phys. Rev. B* **76**, 064502 (2007).
36. R. Settai *et al.*, *J. Phys. Condens. Matter* **13**, L627 (2001).

37. This work is based on experiments performed at the Swiss spallation neutron source SINQ, Paul Scherrer Institute, Villigen, Switzerland. Supported by NSF grant NSF-DMR-0600742 (A.D.B. and Z.F.), the Alfred P. Sloan Foundation (M.R.E.), the European Commission under the 6th Framework Programme through the Key Action: Strengthening the European Research Area, Research Infrastructures (contract RII3-CT-2003-505925), the Swiss National Science Foundation (contract PP002-102831), the Swiss National Center of Competence in Research program "Materials with Novel Electronic Properties," the UK Engineering and Physical Sciences Research Council, and the U.S. Department of Energy, Office of Basic Energy Sciences. Part of this work was carried out at the Brookhaven National Laboratory, which is operated for the U.S. Department of Energy by Brookhaven Science Associates (DE-Ac02-98CH10886). We thank L. N. Bulaevskii, C. Capan, V. G. Kogan, K. Machida, and I. Vekhter for discussions during the preparation of the manuscript.

Supporting Online Material

www.sciencemag.org/cgi/content/full/319/5860/177/DC1
Materials and Methods
Fig. S1

17 September 2007; accepted 21 November 2007
10.1126/science.1150600

Self-Assembled Water-Soluble Nucleic Acid Probe Tiles for Label-Free RNA Hybridization Assays

Yonggang Ke,[1,3] Stuart Lindsay,[1,3,4] Yung Chang,[2,5] Yan Liu,[1,3] Hao Yan[1,3]*

The DNA origami method, in which long, single-stranded DNA segments are folded into shapes by short staple segments, was used to create nucleic acid probe tiles that are molecular analogs of macroscopic DNA chips. One hundred trillion probe tiles were fabricated in one step and bear pairs of 20-nucleotide-long single-stranded DNA segments that act as probe sequences. These tiles can hybridize to their targets in solution and, after adsorption onto mica surfaces, can be examined by atomic force microscopy in order to quantify binding events, because the probe segments greatly increase in stiffness upon hybridization. The nucleic acid probe tiles have been used to study position-dependent hybridization on the nanoscale and have also been used for label-free detection of RNA.

The detection of low levels of gene expression (*1*) has been enabled by technologies such as DNA microarrays (*2*, *3*) and reverse transcription polymerase chain reaction (RT-PCR) (*4*). Nonetheless, these technologies are still expensive (*5*), require probe labeling, and are hard to scale down to sample volumes comparable to those of single cells. Sample volumes have been reduced and sensitivities have been increased, but target detection still relies heavily on enzymatic manipulation and amplification to create detectable signals. We present an alternative that complements benchtop arrays in which individual self-assembled nucleic acid "tile" molecules, formed by "stapling" long, single-stranded DNA segments with shorter strands into shapes, can act as hybridization probes for molecules such as mRNAs in solution. After binding, the tiles can be adsorbed onto mica surfaces and are detected by atomic force microscopy (AFM). Thus, the probe tiles are reagents that are hybridized in solution and then titrated to quantify the targets.

Because the probes are placed on each nucleic acid tile with nanometer-scale precision, the effects of probe placement can be explored with molecular resolution. We found that the exact position of the probe made a substantial difference to hybridization efficiency. We circumvented this problem by manufacturing "bar-coded" tiles in which all of the probes were placed in an optimal position, and each type of nucleic acid tile was distinguished with a distinctive code represented by a group of dumbbell-shaped DNA loops protruding out of the tile surface as topographic registration markers; each coded tile detected one gene product.

Our ability to detect single-molecule hybridization with AFM appears to be enabled by the difference in the elastic properties of single- and double-stranded DNA or of the RNA-DNA hybrid. Detection sensitivity was, in this case, limited only by nucleic acid tile concentration down to the 200 pM levels, which we were able to image readily.

The design of the nucleic acid probe tiles and the read-out mechanism for the target binding are illustrated in Fig. 1. The foundation of the tile design was based on "scaffolded DNA origami" (Fig. 1A): a self-assembling technique for one-step synthesis of fully addressable DNA nanostructures (*6*). Rothemund (*6*) demonstrated that a long, single-stranded viral DNA scaffold can be folded and stapled by a large number of short synthetic "helper strands" into nanostructures that display complex patterns. A one-step nanomolar-scale synthesis yields $>10^{14}$ origami tiles with nearly 100% yield.

We used a simple, rectangular-shaped design, and its layout is shown schematically in Fig. 1A. Three different sequences of capture probes were included on the origami tile, corresponding to a region of three genes—*Rag-1*, *c-myc*,

[1]Center for Single Molecule Biophysics, Arizona State University, Tempe, AZ 85287, USA. [2]Center for Infectious Diseases and Vaccinology, The Biodesign Institute, Arizona State University, Tempe, AZ 85287, USA. [3]Department of Chemistry and Biochemistry, Arizona State University, Tempe, AZ 85287, USA. [4]Department of Physics, Arizona State University, Tempe, AZ 85287, USA. [5]School of Life Sciences, Arizona State University, Tempe, AZ 85287, USA.

*To whom correspondence should be addressed. E-mail: hao.yan@asu.edu

and β-*actin*—expressed in the murine progenitor B cell line (*7*, *8*). A sequence not found in the mouse genome was added as a control. Twelve copies of each probe were arranged into each line on the tile, with an interprobe distance within the lines of 5 nm and a spacing between the lines of 20 nm (Fig. 1A). Six copies of the control probes form a shorter line on the left side of the tile. An "index spot" was placed in the top left corner. We used six of the 28-nucleotide-long dumbbell-shaped structures [described elsewhere (*6*)] as "permanent" features to break the symmetry of the tile, so that the images of the tiles could be oriented unambiguously. Detailed sequences of the probes, control, and indexes can be found in the supporting online material (*9*).

The tiles were self-assembled in solution: We used the single-stranded M13 viral genome scaffold strand to nucleate both the probe-modified and nonmodified helper strands. An aliquot of the solution (2 μl) was dropped onto the mica surface for AFM imaging (Fig. 1B). In our probe design, selected pairs of neighboring helper strands are modified so that each contains a single-stranded fragment of 20 nucleotides that protrudes out of the tile surface (Fig. 1C). Each dangling single strand in the pair serves as a half-probe for a single RNA target of 40 bases. Upon hybridization of the target to a pair of half-probes, the strands form a stiff V-shaped structure [see (*9*) for molecular dynamics simulation]. This local stiffening is readily sensed mechanically with an AFM cantilever and appears in the image as local high-spot (Fig. 1C). We have tried various different probe designs (*9*), and this V-shaped junction design provides the best AFM signal of target binding.

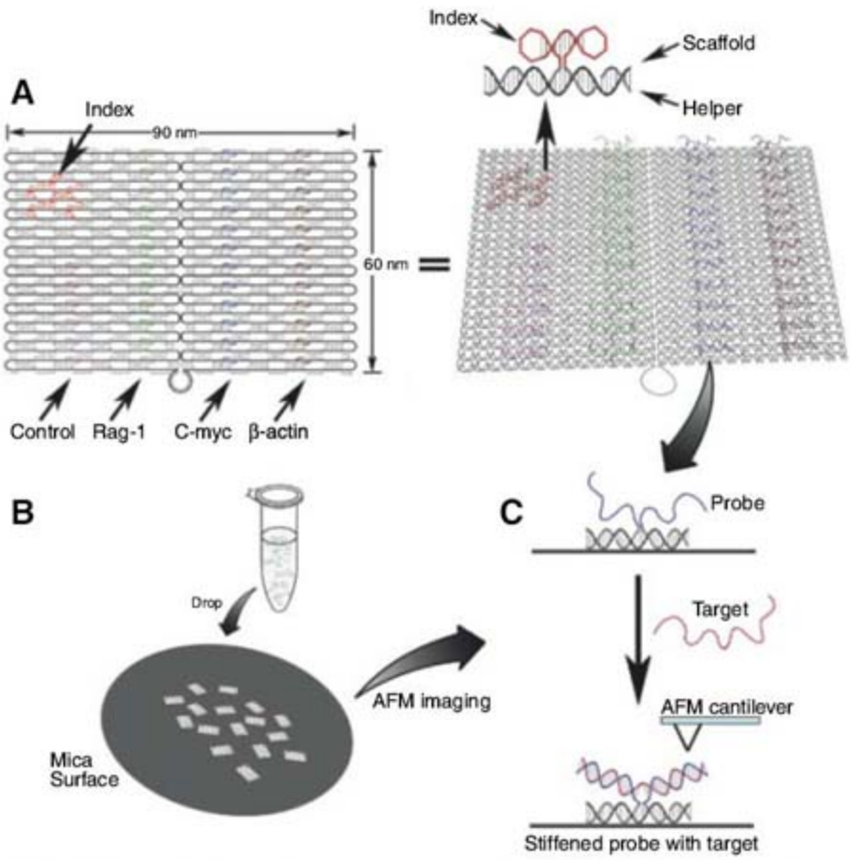

Fig. 1. (**A**) (Left) Schematic layout of the indexed nucleic acid probe tiles bearing three different probes (for targets *Rag-1*, *C-myc*, and β-*actin*) and a control probe. A simple, rectangular-shaped DNA origami tile was used, in which a circular single-stranded M13 viral DNA (black lines), composed of 7249 bases, is folded and stapled, with the help of >200 short synthetic DNA strands, to form the desired two-dimensional (2D) tile. Helper strands without probe modifications are shown (gray lines), and helper strands modified with probe sequences and control sequences are shown in different colors. This rectangular-shaped probe tile has dimensions of 90 nm by 60 nm. Twelve copies of the specific probes are spaced at 5-nm intervals in a line, and lines of probes are separated by 20 nm. Six control probes are arranged in a shorter line. An index spot, composed of six closely packed dumbbell-shaped bulge loops at the top left corner, is designed to give the AFM topological feature with which to orient the AFM image of each individual tile. (Right) Tilted view of the tile (drawn in DNA helix style) to illustrate the 3D view of the probe tile layout. (**B**) Illustration of the process (not drawn to scale) for the use of probe tiles for target detection. Probe tiles are self-assembled in solution, hybridized with targets, and then dropped onto the mica surface for AFM imaging. (**C**) Probe design and detection mechanism. A pair of neighboring helper strands is extended out of the surface of the tile, with each 20-base-long extension bearing a half of the target sequence. These single-stranded probes are flexible and do not produce a visible feature under AFM imaging. Upon target hybridization with the pair of half-probes, the double helix of the DNA-RNA duplex forms, and the stiffer V-shaped junction is readily detected with the AFM cantilever.

In a test of the initial design, tiles with all three probes and a control (Fig. 1A) were assembled with 10 nM of the M13 viral genome as the scaffold strand and a fivefold excess of short helper strands. Because the existence of the excess helper strands (some of which contain the probe sequences) will interfere with the target hybridization, the tiles were purified with Microcon centrifugal filter devices [MWCO 100,000 (Millipore, Bedford, MA)] to remove the small oligonucleotides. We adjusted the final concentration of the tile by using optical absorption at 260 nm. We then mixed 10 nM of the tiles with 600 nM {a [probe]/[target] ratio of 1:5} of each of the three different targets. AFM images of these hybridized tiles revealed that the target hybridization depends strongly on the probe positions in the tile. The probes on the edge (β-*actin* at position 3) give the best hybridization efficiency, whereas the probes in the middle of the tile (*Rag-1* at position 1) give the worst binding efficiency (fig. S5).

To confirm that this positional effect does not depend on the sequence of the probes, we put the same probes with the worst binding (*Rag-1*) at all three positions and found again that the probes on the edge (position 3) gave the best hybridization efficiency (Fig. 2 and fig. S6). Because electric-charge repulsions between the target and the underlying tile, as well as repulsions between probes, are stronger in the middle of the tile than at the edge of the tile, and because steric hindrance is weakest at the tile's edge, these factors presumably play a role in our observed results. In the DNA microarray, interprobe spacing is not controlled at the single-molecule level. Hybridization on a solid surface is not only kinetically slow but also less efficient (*10*, *11*). Our probe tile design now permits the study of the positional effect of probes on their efficiency of target binding. The precise interprobe-distance control and the hybridization in solution also make the binding kinetically fast, with full hybridization within 30 min with no stirring at room temperature.

The self-assembling nucleic acid tile (*12*–*14*) allows accurate control of probe placement (*15*, *16*). We designed four different bar-coded tiles (Fig. 3A), each of which carried a line of probes: one for each of the three targets and one as a control. The probes were placed along one edge of the tiles to optimize the hybridization efficiency, and a bar-coded region was added, in which combinations of different index geometries were used to distinguish the tile. An equimolar mix of the four types of tiles was used for simultaneous multiplex detection. Typical AFM images (Fig. 3A, middle panel) show that each bar-coded tile can be distinguished by its own bar code, without targets.

We used these bar-coded probe tiles to test the detection of single and multiple targets (Fig. 3, A and B, and fig. S9). The detection of the three different targets is highly specific, with no binding of the control sequence. Each probe also serves as a control for the other two probes and revealed no nonspecific cross-hybridization. To

demonstrate that our system can detect a synthetic RNA target in the presence of a large amount of cellular RNA, we performed a spike experiment in our hybridization by mixing the synthetic RNA with 2 mg/ml total cellular RNA. The target hybridization can still be visualized (Fig. 3B, right panel), and the excess amount of cellular RNA did not interfere with the specific target hybridization. The use of the tile probes for RNA detection is also sensitive to the amount of targets added. Figure 3C shows the obvious difference of the hybridization efficiency between low and high target concentrations.

Because the nucleic acid probe tiles are themselves reagents, it is possible to titrate the probes against the targets and obtain quantitative results, as shown in Fig. 4 for two different tile concentrations (10 nM and 200 pM). The plots of hybridization efficiency versus [target]/[probe] ratios at these two tile concentrations show a similar trend: a nearly linear increase at [target]/[probe] < 1 that reaches saturation at [target]/[probe] > 1. This non–Michaelis-Menten (i.e., linear) binding shows that the detection is limited only by the concentration of the tiles; every target molecule is bound by a probe at these concentrations. This result is expected, given that the hybridization free energy is about −50 kcal/mol (*17*), and it is a clear indication that the intrinsic hybridization efficiency is 100% and that the kinetics are not limiting.

Our current sensitivity is limited by our use of large substrates for AFM imaging and by conventional micropipette handling of reagents. To improve the detection for profiling gene expression of single cells, we propose that further developments are needed to deposit a smaller amount of tiles onto a tiny spot for AFM imaging. For example, if tiles as small as 1 nl of 1 pM solution (the tiles are dilutable) could be placed on an optically indexed AFM stage for imaging, it would bring the detection limit down to ~ 1000 molecules, which would be adequate for label-free and PCR-free detection of the product of gene expression in a single cell. Although this approach does not yet compete with existing arrays for analysis with hundreds of thousands of probes, it can probe the effects of nanometer-scale changes in geometry, as demonstrated by our measurements of the position dependence of hybridization. Such investigations need not be limited to DNA or RNA analysis. For example, we have shown that proteins can be placed onto these tiles with nanometer-scale precision using DNA aptamers (*18*). Thus,

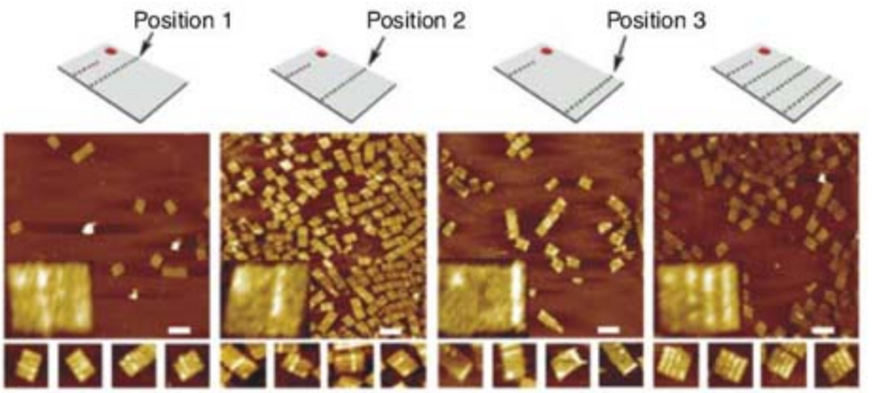

Fig. 2. The effect of the probe positions on the efficiency of target binding. The three lines (positions 1 to 3) are all composed of the same probes for *Rag-1*. Four different DNA tiles are constructed: three tiles with probes at one of the three positions, and one tile with the same probes at all three positions. The target-binding efficiency is measured by analyzing the height images by AFM (*9*). Topographic illustrations of the tile design and their corresponding AFM images with a [target]/[probe] ratio of 5:1 in all cases are shown. Scale bars, 150 nm. Four representative zoom-in images are shown in the bottom of each large-area scan. An enlarged zoom-in image is also shown in the bottom-left corner of the large-area scan. Additional enlarged images and a plot of hybridization percentage versus probe positions can be found in (*9*).

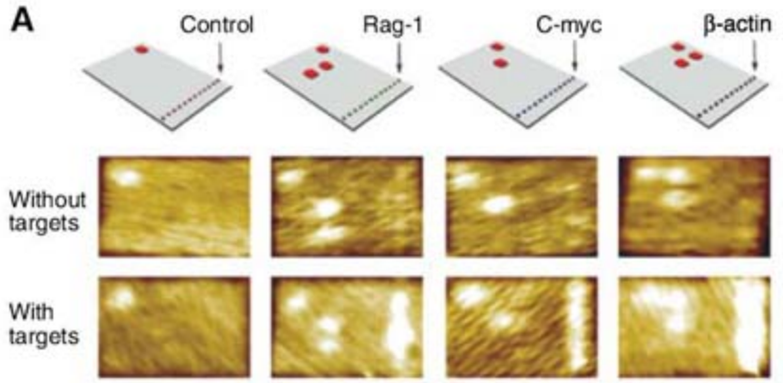

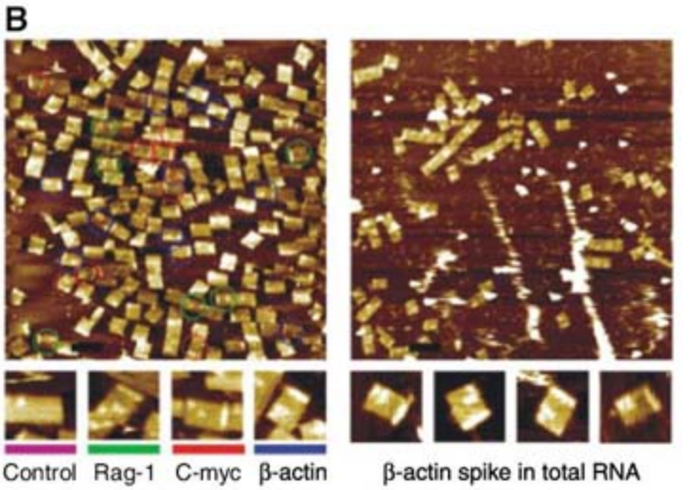

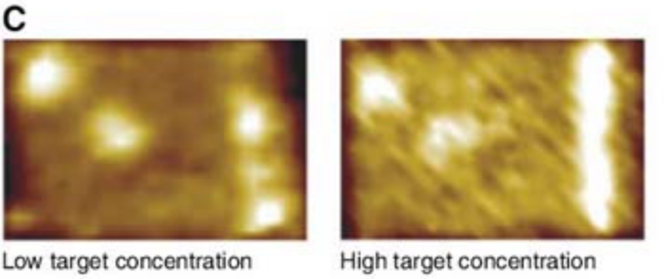

Fig. 3. (**A**) (Top) Topographic illustration of the bar-coded tile designs. The top left corners of the tiles are modified with one to three groups of topological features that form distinctive bar codes for each tile. Each tile carries a line of probes positioned near the right edge of the tile to optimize target-binding efficiency. (Middle and Bottom) Typical zoom-in AFM images of the bar-coded tiles without targets (Middle) and with targets (Bottom); each type of tile is readily identified by its bar code. (**B**) (Left) AFM images of an equimolar mix of the bar-coded tiles with combinations of the three gene targets. The tiles marked by red, green, blue, and pink circles are identified from their bar codes as carrying the *C-myc*, *Rag-1*, β-*actin*, and control probes, respectively. Each probe shows specific target binding in the presence of their targets. The control probes and the probes for the absent targets do not show any nonspecific binding. (Right) β-*actin* RNA spike experiment in the presence of 2 mg/ml cellular total RNA extract. The detection efficiency of the β-*actin* target is not interfered by the presence of a high concentration of the cellular RNA. Scale bars, 150 nm. (**C**) Typical AFM images showing the sensitivity of the probe tile to target concentration (with the *C-myc* target as an example). The [target]/[probe] ratios of 0.2:1 (left) and 2:1 (right) are shown. Dimensions of each tile in all images were measured to be ~ 60 nm by 90 nm.

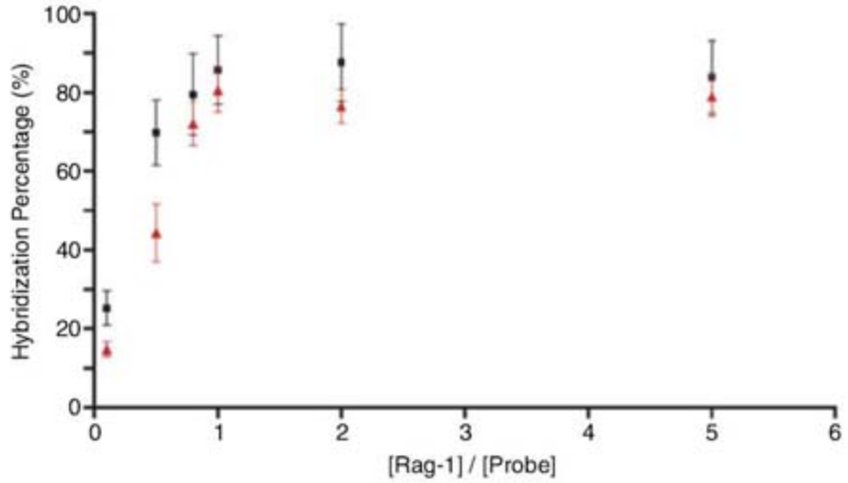

Fig. 4. Hybridization percentage as a function of the [target]/[probe] ratio. The tile used is the one shown in Fig. 3A carrying the *Rag-1* probes. Two different tile concentrations are used: 10 nM (black squares) and 200 pM (red triangles). Each error bar represents SD calculated from measurements on 50 tiles.

it should be possible to probe the spatial dependence of binding interactions involving multiple biomolecular components.

References and Notes

1. D. R. Meldrum, *Science* **292**, 515 (2001).
2. U. R. Mueller, D. V. Nicolau, *Microarray Technology and its Applications* (Springer-Verlag, Berlin, 2004).
3. M. Schena, D. Shalon, R. W. Davis, P. O. Brown, *Science* **270**, 467 (1995).
4. S. A. Bustin, T. Nolan, in *Real-Time PCR: An Essential Guide*, K. Edwards, J. Logan, N. Saunders, Eds. (Horizon Bioscience, Norfolk, UK, 2004).
5. Y. H. Yang, T. Speed, *Nat. Rev. Genet.* **3**, 579 (2002).
6. P. W. K. Rothemund, *Nature* **440**, 297 (2006).
7. Y. Chang, M. L. Brown, *Proc. Natl. Acad. Sci. U.S.A.* **96**, 191 (1999).
8. E. A. Jacobsen, O. Ananieva, M. L. Brown, Y. Chang, *J. Immunol.* **176**, 6831 (2006).
9. See supporting material on *Science* Online.
10. A. W. Peterson, R. J. Heaton, R. M. Georgiadis, *Nucleic Acids Res.* **29**, 5163 (2001).
11. Y. Gao, L. K. Wolf, R. M. Georgiadis, *Nucleic Acids Res.* **34**, 3370 (2006).
12. N. C. Seeman, *Nature* **421**, 427 (2003).
13. E. Winfree, F. Liu, L. A. Wenzler, N. C. Seeman, *Nature* **394**, 539 (1998).
14. H. Yan, S. H. Park, G. Finkelstein, J. H. Reif, T. H. LaBean, *Science* **301**, 1882 (2003).
15. K. Lund, Y. Liu, S. Lindsay, H. Yan, *J. Am. Chem. Soc.* **127**, 17606 (2005).
16. S. H. Park *et al.*, *Angew. Chem. Int. Ed.* **45**, 735 (2006).
17. M. Zuker, D. H. Mathews, D. H. Turner, in *RNA Biochemistry and Biotechnology*, J. Barciszewski, B. F. C. Clark, Eds. (Kluwer Academic, Dordrecht, Netherlands, 1999), pp. 11–43.
18. R. Chhabra *et al.*, *J. Am. Chem. Soc.* **129**, 10304 (2007).

19. This research is partly supported by funding from NIH (to S.L. and H.Y.) and from NSF, Office of Naval Research, and U.S. Air Force Office of Scientific Research (to H.Y.).

Supporting Online Material

www.sciencemag.org/cgi/content/full/319/5860/180/DC1
Materials and Methods
Sequence Information
Figs. S1 to S16

4 September 2007; accepted 21 November 2007
10.1126/science.1150082

Imaging Nucleophilic Substitution Dynamics

J. Mikosch,[1] S. Trippel,[1] C. Eichhorn,[1] R. Otto,[1] U. Lourderaj,[2] J. X. Zhang,[2] W. L. Hase,[2] M. Weidemüller,[1] R. Wester[1]*

Anion-molecule nucleophilic substitution (S_N2) reactions are known for their rich reaction dynamics, caused by a complex potential energy surface with a submerged barrier and by weak coupling of the relevant rotational-vibrational quantum states. The dynamics of the S_N2 reaction of $Cl^- + CH_3I$ were uncovered in detail by using crossed molecular beam imaging. As a function of the collision energy, the transition from a complex-mediated reaction mechanism to direct backward scattering of the I^- product was observed experimentally. Chemical dynamics calculations were performed that explain the observed energy transfer and reveal an indirect roundabout reaction mechanism involving CH_3 rotation.

Bimolecular nucleophilic substitution is a fundamental reaction mechanism in chemistry (*1*). The reaction's equation, X + R-Y → X-R + Y, summarizes bond formation by the attacking nucleophile X with the moiety R and concerted bond cleavage of the substituted leaving group Y. S_N2 reactions are widely used in preparative organic synthesis (*2*). Low-energy negative-ion reactions, most likely nucleophilic substitution, are suggested to cause the large amount of DNA double strand breaks in the wake of ionizing particles (*3*).

Anion-molecule S_N2 reactions may be the most prominent type of ion-molecule reactions, studied extensively both experimentally (*4*, *5*) and computationally (*6*, *7*). Rate coefficients for these reactions depend strongly on the surrounding solvent (*4*), making experiments on isolated gas-phase systems a crucial reference point in distinguishing solvent effects from the intrinsic dynamics of the reaction. The low rate coefficients observed in the gas phase, which are much smaller than the classical Langevin capture rate expected for a barrier-less ion-molecule reaction, are qualitatively well understood to stem from two wells (Fig. 1) on the potential energy hypersurface (*8*). This characteristic potential energy landscape is attributed to the formation of ion-dipole collision complexes on both sides of the reaction barrier. The barrier itself, which represents a transition state that corresponds to inversion at the reaction center, has a substantial influence on the reaction kinetics even though it most often lies submerged with respect to the energy of the reactants.

Studies of anion-molecule S_N2 reactions have determined reaction rates as a function of temperature (*9*, *10*) and energy (*11*) and probed the dynamics of the pre- and postreaction ion-dipole complexes (*12*, *13*). An important finding from these studies is that the reaction kinetics and dynamics are often inadequately described by statistical theories (*14*–*16*, *12*, *17*), a result supported by classical (*6*, *18*) and quantum (*19*, *7*, *20*) chemical dynamics simulations. An illustrative example of nonstatistical behavior is the strong dependence of the $Cl^- + CH_3Br$ reaction rate on the relative translational energy of the reactants, despite insensitivity to their internal temperature (*14*). Such dynamics contradict the statistical assumption of rapid randomization of all the available energy in the $Cl^- \cdot CH_3Br$ prereaction complex. Nonstatistical dynamics of the ion-dipole complexes are also evident in the product energy partitioning for the $Cl^- \cdot CH_3I$ unimolecular decomposition (*13*), the mode-specific dynamics of the $Cl^- \cdot CH_3Br$ complex (*12*, *21*), and the $Cl^- + CH_3Br$ reaction rate dependence on collision energy (*11*). Therefore, a detailed analysis of the flow of energy during the course of the reaction is required (*6*).

[1]Physikalisches Institut, Universität Freiburg, Hermann-Herder-Straße 3, 79104 Freiburg, Germany. [2]Department of Chemistry and Biochemistry, Texas Tech University (TTU), Lubbock, TX 79409, USA.

*To whom correspondence should be addressed. E-mail: roland.wester@physik.uni-freiburg.de

Until recently, many details of the S_N2 dynamics of bimolecular anion-molecule reactions could only be obtained from chemical dynamics simulations. However, with recent experimental advances (*22*), insight into the reaction dynamics may be obtained from measurements of correlated angle- and energy-differential cross sections. Specifically, the probabilities for energy redistribution within the ion-dipole complexes, their dependences on initial quantum states, the branching into different product quantum states, and the role of tunneling through the central barrier pose open questions to be probed experimentally.

We report kinematically complete reactive scattering experiments of the anion-molecule S_N2 reaction $Cl^- + CH_3I \rightarrow CH_3Cl + I^-$ (Fig. 1) with use of our ion-molecule crossed beam imaging spectrometer (*22*). In this way, we extended the successful crossed beam imaging experiments of neutrals (*23*) to ionic reactions. These single-collision experiments measure directly the velocity vector of the product anion, which reveals the energy- and angle-differential reaction cross section. By using reactants with well-defined relative kinetic energy and momentum, we can determine energy transfer during the reaction, which yields the fraction of total available energy partitioned to internal modes of the molecular product. For comparison with the experimental results, we have performed high-level trajectory simulations.

In the experiment, we produced slow pulses of Cl^- anions with a tunable well-defined kinetic energy between 0.2 and 5 eV in a compact electron-impact supersonic expansion ion source (*22*). The ion pulses crossed a supersonic neutral jet of CH_3I seeded in helium, whereby a few of the Cl^- anions induced nucleophilic substitution and liberated I^- anions. The interaction region of the crossed beam experiment was placed in a pulsed-field velocity map imaging spectrometer, which maps the velocity of the I^- product anion

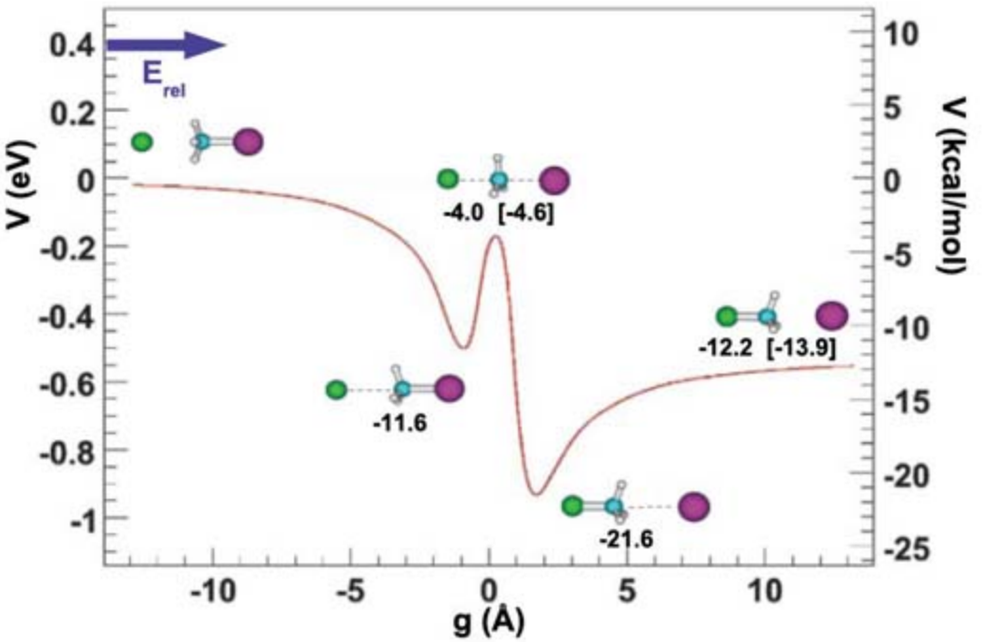

Fig. 1. Calculated MP2(fc)/ECP/aug-cc-pVDZ Born-Oppenheimer potential energy along the reaction coordinate $g = R_{C-I} - R_{C-Cl}$ for the S_N2 reaction $Cl^- + CH_3I$ and obtained stationary points. The reported energies do not include zero-point energies. Values in brackets are from (*28*).

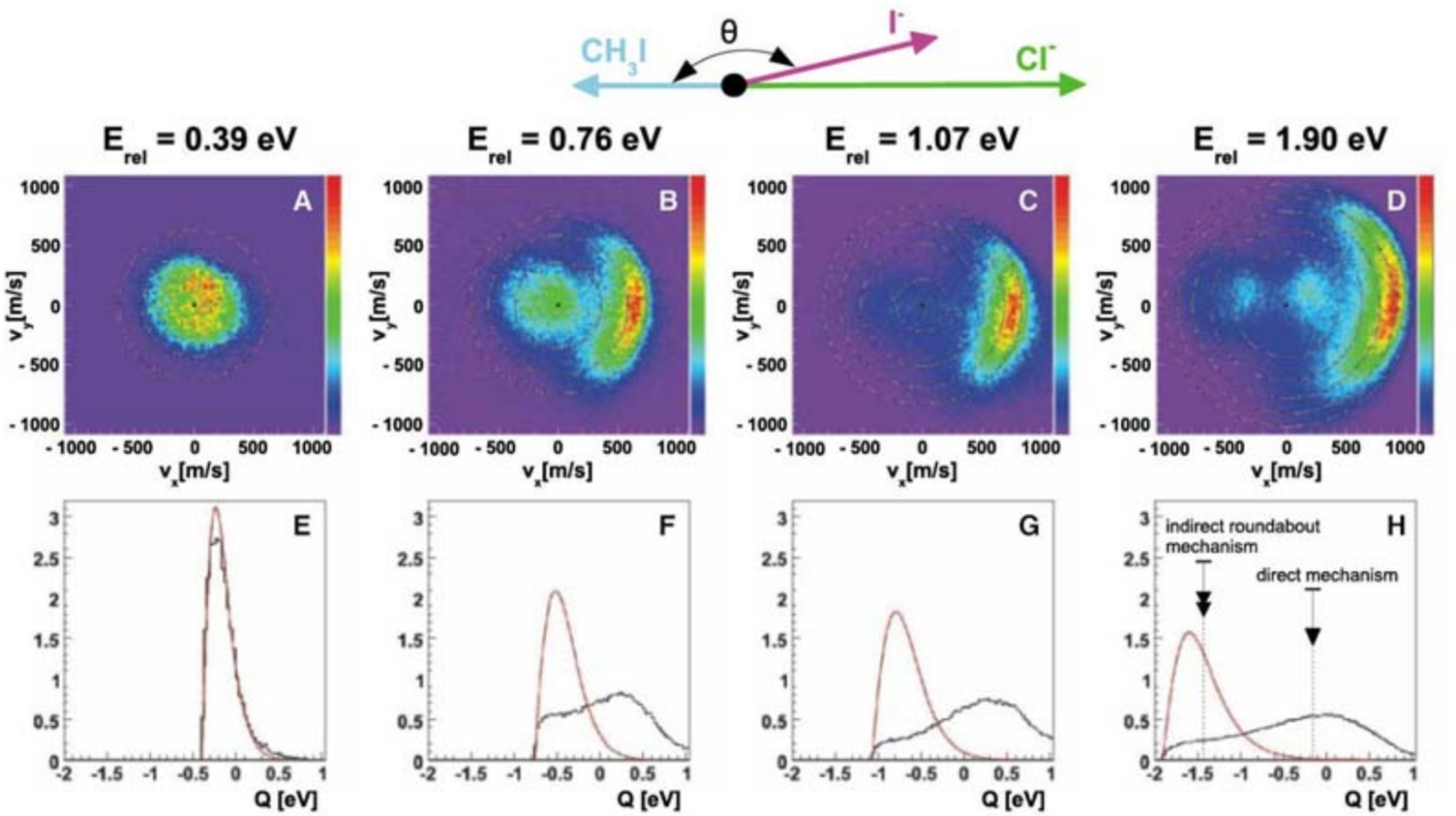

Fig. 2. (**A** to **D**) Center-of-mass images of the I^- reaction product velocity from the reaction of Cl^- with CH_3I at four different relative collision energies. The image intensity is proportional to $[(d^3\sigma)/(dv_x\ dv_y\ dv_z)]$: Isotropic scattering results in a homogeneous ion distribution on the detector. (**E** to **H**) The energy transfer distributions extracted from the images in (A) to (D) in comparison with a phase space theory calculation (red curve). The arrows in (H) indicate the average Q value obtained from the direct chemical dynamics simulations.

onto a position-sensitive detector. With the use of slice imaging (*23*) implemented by activating the detector only during a short time window, we imaged only scattering events for which the velocity vectors of the products lie within the plane defined by the reactant velocities. Because of the cylindrical symmetry of the scattering cross section, this procedure yielded the velocity magnitude- and angle-differential cross sections directly, without resorting to Abel-inversion-type algorithms. The neutral product does not need to be detected because its properties can be inferred from conservation of energy and momentum (*24*).

The top row of Fig. 2 shows maps of the I^- product ion velocities from the $Cl^- + CH_3I \rightarrow CH_3Cl + I^-$ reaction at four different relative collision energies between $E_{rel} = 0.39$ eV and $E_{rel} = 1.90$ eV, which were chosen because they span the distinct reaction dynamics observed in this energy range. The only data processing applied to the ion impact position on the detector is a linear conversion from position to ion speed and a transformation into the center of mass frame. Consequently, the velocity vectors of the two reactants, the Cl^- anion and the CH_3I neutral, line up horizontally and point in opposite directions, indicated by the arrows in Fig. 2. Each velocity image represents a histogram summed over 10^5 to 10^6 scattering events. The total energy available to the reaction products is given by the relative translational energy, E_{rel}, of the reactants plus the exoergicity, 0.55 eV, of the reaction (Fig. 1). I^- products reach the highest velocity when all the available energy is converted to translational energy. The outermost circle in Fig. 2 represents this kinematic cutoff for the velocity distribution. The other concentric rings display spheres of the same translational energy and hence also the same internal product excitation, spaced at 0.5-eV intervals.

The images in Fig. 2 reveal many details of the reaction dynamics. For the lowest relative collision energy of 0.39 eV, there is an isotropic distribution of product velocities centered around zero with all scattering angles equally probable. This pattern points to the traditional reaction mechanism (*8*) mediated by a collision complex whose lifetime is long compared to the time scale of its rotation. The complex-mediated mechanism is accompanied by a velocity distribution that drops to zero far before the kinematic cutoff is reached, as can be inferred from the position of the outermost ring in the image. Thus, the largest fraction of the available energy is partitioned to internal rovibrational energy of the CH_3Cl product.

A distinctly different reaction mechanism becomes dominant at the higher relative collision energy of 0.76 eV (Fig. 2B): The I^- product is back-scattered into a small cone of scattering angles. This pattern indicates that direct nucleophilic displacement dominates. The Cl^- reactant attacks the methyl iodide molecule at the concave center of the CH_3 umbrella and thereby drives the I^- product away on the opposite side. The direct mechanism leads to product ion velocities close to the kinematic cutoff. In addition, part of the product flux is found at small product velocities with an almost isotropic angular distribution, indicating that for some of the collisions there is a significant probability of forming a long-lived complex.

At a collision energy of 1.07 eV (Fig. 2C), the complex-mediated reaction channel is not observed any more. The reaction proceeds almost exclusively by the direct mechanism, with a similar velocity and a slightly narrower angular distribution relative to the 0.76-eV case. At an even higher collision energy of 1.90 eV, the dominating backward scattering pattern of the I^- ion spreads over an increased range of scattering angles. The inserted rings demonstrate a concomitant broadening of the velocity distribution. In addition, a new feature appears that consists of two distinct low-velocity peaks symmetric in the forward and the backward directions with respect to the center of mass. As detailed below, these peaks represent reactions that occur via a roundabout mechanism. At relative energies above 2 eV, new dissociative channels open and influence the scattering dynamics, and so we restricted the current presentation to collision energies up to 1.9 eV.

For a quantitative analysis, we calculated the energy transfer $Q = E_{kin,final} - E_{kin,initial}$ for the reaction events. For the lowest collision energy of 0.39 eV, Fig. 2E shows that the observed distribution vanishes for Q values far below the kinematic cutoff at +0.55 eV. A theoretical phase-space calculation (red line in Fig. 2E) (*25*), which assumes that the available energy is distributed statistically among all degrees of freedom of the reaction products, shows excellent agreement with the data after convolution with the experimental resolution stemming from the velocity spread of the reactant beams. The observation of statistical energy partitioning at this finite collision energy is unexpected, given the reported nonstatistical unimolecular decomposition of metastable $Cl^-{\cdot}CH_3I$ S_N2 complexes (*13*). We found that 84% of the total available energy is trapped in internal excitation of the CH_3Cl reaction product, which amounts to $E_{int} = 0.79$ eV. At all the higher relative collision energies (Fig. 2, F to H), the phase space model cannot reproduce the observed dynamics. Here, the Q value distribution peaks near its maximum value of +0.55 eV. The mean internal excitation in absolute and in relative numbers is given by 0.5 eV (40%), 0.45 eV (25%), and 0.95 eV (40%). At 1.07 eV relative collision energy, a minimum is found both in the absolute and the relative amount of internal excitation, which is a sign of subtle changes in the translation-vibration coupling during the reaction.

To complement the above experimental study of the $Cl^- + CH_3I$ reaction dynamics, we performed a trajectory simulation at the MP2(fc)/ECP/aug-cc-pVDZ (*26*) level of theory by a computational approach directly using this theory (*27*). As shown in Fig. 1, this theory gives energies for the reaction's stationary points in good agreement with previous values based on rate coefficient measurements (*28*). These simulations are computationally expensive and only practical at the highest collision energies where both the encounter time is short and the reaction probability appreciable. Here, we report results for the 1.9-eV collision energy and CH_3I rotational and vibrational temperatures of 75 K and 360 K, respectively, which are the approximate experimental conditions.

Although the reaction has no overall barrier, the simulations show a quite low reaction probability at 1.9 eV, decreasing from 0.065, 0.05,

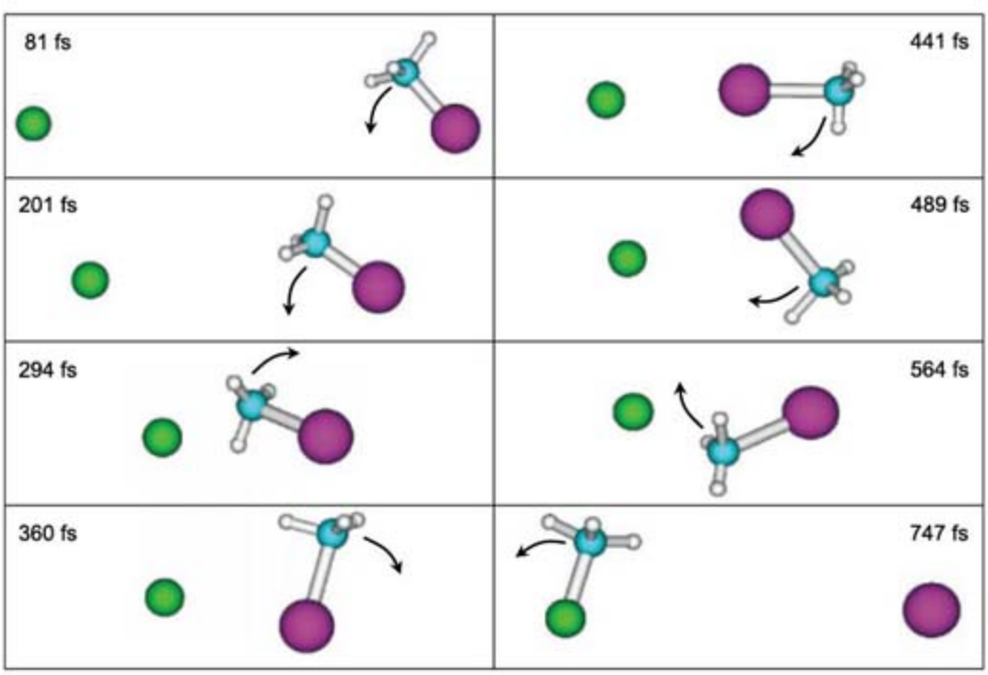

Fig. 3. View of a typical trajectory for the indirect roundabout reaction mechanism at 1.9 eV that proceeds via CH_3 rotation.

0.03, to 0.005 as the collision impact parameter, b, is increased from 0.0, 1.0, 2.0, to 3.0 Å. On the basis of the centrifugal potential at the central barrier, the maximum impact parameter for reaction is estimated as 5.2 Å, but the low reaction probability at $b > 2$ Å makes it computationally intractable to sample the complete range of b. Nevertheless, important details of the reaction dynamics are found. The reaction occurs by both direct and indirect mechanisms, with a direct fraction of 0.4, 0.8, 0.8, and ~1.0 for impact parameters of 0.0, 1.0, 2.0, and 3.0 Å, respectively, suggesting the direct reaction dominates at the larger b values. The product energy partitioning for the direct reaction is the same for these four impact parameters, with average fractions of 0.04, 0.23, and 0.73 for rotation, vibration, and translation, respectively. For the indirect trajectories, the average fractions of energy partitioning to rotation (0.28), vibration (0.56), and translation (0.16) are quite different. Because the direct reaction is expected to dominate when trajectories are averaged over all impact parameters, an overall fraction partitioned to translation in the range of 0.6 to 0.7 is expected. This partitioning corresponds to a mean internal excitation of about 0.85 eV, which agrees well with the experimental value of 0.95 eV as given above. The much higher internal excitation for indirect reactions amounts to about 1.9 eV, which is in good agreement with the average energy of the two low-velocity peaks observed in the experiment (Fig. 2D and Fig. 2H, left arrow).

The atomic-level mechanisms for the direct and indirect reactions at 1.9 eV collision energy are substantially different. The direct reaction occurs by the classical S_N2 reaction path, with Cl^- attacking the backside of CH_3I and directly displacing I^- (*8*). The indirect reaction occurs via a roundabout mechanism involving a CH_3 rotation. The principal mode for this mechanism is depicted in Fig. 3, where Cl^- first strikes the side of the CH_3 group, causing it to rotate around the more massive I atom. Then, after one CH_3 revolution, Cl^- attacks the C atom backside and directly displaces I^-. The time between the initial Cl^--CH_3 collision and the departure of I^- ranges around 400 fs. Two variants of the roundabout mechanism, of much lesser importance and with intermediate lifetimes of 1 to 4 ps, were also found. One is identical to the roundabout mechanism, except the departing I^- becomes transiently trapped in the post–reaction potential energy well (Fig. 1). The other is similar to the roundabout mechanism, except CH_3 rotates twice about the I atom. The translational energy partitioning for the roundabout mechanism approximates that of phase space theory (Fig. 2H), which assumes statistical dynamics. This suggests that this mechanism may participate in the statistical product energy partitioning observed for the $Cl^- + CH_3I$ S_N2 reaction at lower collision energies.

This combined experimental and computational study has identified a previously unknown roundabout, CH_3-rotation mechanism for gas-phase S_N2 nucleophilic substitution reactions. This mechanism may also play a role for other S_N2 reactions, such as the $Cl^- + CH_3Br$ reaction, where an energy-dependent change in the reaction mechanism has been discussed (*11*, *29*). It will be of particular interest to determine the role of the roundabout mechanism in other and more complex ion-molecule reactions.

References and Notes

1. See, for example, K. P. C. Vollhardt, N. E. Schore, *Organic Chemistry, Structure and Function* (Pallgrave Macmillan, Basingstoke, UK, 2007).
2. N. Merceron-Saffon, A. Baceiredo, H. Gornitzka, G. Bertrand, *Science* **301**, 1223 (2003).
3. B. Boudaïffa, P. Cloutier, D. Hunting, M. A. Huels, L. Sanche, *Science* **287**, 1658 (2000).
4. M. L. Chabinyc, S. L. Craig, C. K. Regan, J. I. Brauman, *Science* **279**, 1882 (1998).
5. J. K. Laerdahl, E. Uggerud, *Int. J. Mass Spectrom.* **214**, 277 (2002).
6. W. L. Hase, *Science* **266**, 998 (1994).
7. S. Schmatz, *ChemPhysChem* **5**, 600 (2004).
8. W. N. Olmstead, J. I. Brauman, *J. Am. Chem. Soc.* **99**, 4219 (1977).
9. C. H. DePuy, S. Gronert, A. Mullin, V. M. Bierbaum, *J. Am. Chem. Soc.* **112**, 8650 (1990).
10. J.-L. Le Garrec, B. R. Rowe, J. L. Queffelec, J. B. A. Mitchell, D. C. Clary, *J. Chem. Phys.* **107**, 1021 (1997).
11. L. A. Angel, K. M. Ervin, *J. Am. Chem. Soc.* **125**, 1014 (2003).
12. D. S. Tonner, T. B. McMahon, *J. Am. Chem. Soc.* **122**, 8783 (2000).
13. S. T. Graul, M. T. Bowers, *J. Am. Chem. Soc.* **116**, 3875 (1994).
14. A. A. Viggiano, R. A. Morris, J. S. Paschkewitz, J. F. Paulson, *J. Am. Chem. Soc.* **114**, 10477 (1992).
15. S. L. Craig, J. I. Brauman, *Science* **276**, 1536 (1997).
16. S. L. VanOrden, R. M. Pope, S. W. Buckner, *Org. Mass Spectrom.* **26**, 1003 (1991).
17. R. Wester, A. E. Bragg, A. V. Davis, D. M. Neumark, *J. Chem. Phys.* **119**, 10032 (2003).
18. L. Sun, K. Song, W. L. Hase, *Science* **296**, 875 (2002).
19. C. Hennig, S. Schmatz, *J. Chem. Phys.* **122**, 234307 (2005).
20. D. C. Clary, *Science* **279**, 1879 (1998).
21. P. Ayotte, J. Kim, J. A. Kelley, S. B. Nielsen, M. A. Johnson, *J. Am. Chem. Soc.* **121**, 6950 (1999).
22. J. Mikosch *et al.*, *Phys. Chem. Chem. Phys.* **8**, 2990 (2006).
23. J. J. Lin, J. Zhou, W. Shiu, K. Liu, *Science* **300**, 966 (2003).
24. Special care is taken to suppress formation of clusters in the supersonic expansion, as identified by photodissociation with ultraviolet (UV) laser light. Extraction fields are multistage to enable velocity mapping and spatial focusing of product ions spread over a large volume. The velocity distribution of the anion reactant beam is measured before and after recording each of the product velocity images. The velocity distribution of the neutral beam is measured by ionization with a pulsed electron beam and subsequent velocity map imaging. The beam spreads represent the largest contribution to the experimental resolution, such that effects of imperfect velocity mapping and slicing can be neglected. A few product anions are formed per bunch crossing; the repetition rate of the experiment is 10 Hz. We accounted for the decreased signal of fast product ions by using a one-dimensional, experimentally determined efficiency function.
25. W. J. Chesnavich, M. T. Bowers, *J. Chem. Phys.* **66**, 2306 (1977).
26. The aug-cc-pVDZ basis set was used for the C, H, and Cl atoms. For iodine, the Wadt and Hay effective core potential (ECP) was used for the core electrons and an uncontracted 3s,3p basis set for the valence electrons (*30*). This iodine basis was augmented by a d-polarization function with a 0.262 exponent and s, p, and d diffuse functions with exponents of 0.034, 0.039, and 0.0873, respectively (*31*). This basis is denoted as ECP/aug-cc-pVDZ in the text.
27. U. Lourderaj, K. Song, T. L. Windus, Y. Zhuang, W. L. Hase, *J. Chem. Phys.* **126**, 044105 (2007).
28. M. N. Glukhovtsev, A. Pross, L. Radom, *J. Am. Chem. Soc.* **118**, 6273 (1996).
29. Y. Wang, W. L. Hase, H. Wang, *J. Chem. Phys.* **118**, 2688 (2003).
30. W. R. Wadt, P. J. Hay, *J. Chem. Phys.* **82**, 284 (1985).
31. W.-P. Hu, D. G. Truhlar, *J. Phys. Chem.* **98**, 1049 (1994).

32. This work is supported by the Deutsche Forschungsgemeinschaft under contract no. WE 2661/4-1 and by the Eliteförderprogramm der Landesstiftung Baden-Württemberg. We thank U. Frühling and D. Schwalm for their support in setting up the experiment. The contribution from TTU is based on work supported by the NSF under grant no. CHE-0615321 and the Robert A. Welch Foundation under grant no. D-0005. Support was also provided by the TTU High-Performance Computing Center.

7 September 2007; accepted 12 November 2007
10.1126/science.1150238

Tidal Modulation of Nonvolcanic Tremor

Justin L. Rubinstein,[1]* Mario La Rocca,[2] John E. Vidale,[1] Kenneth C. Creager,[1] Aaron G. Wech[1]

Episodes of nonvolcanic tremor and accompanying slow slip recently have been observed in the subduction zones of Japan and Cascadia. In Cascadia, such episodes typically last a few weeks and differ from "normal" earthquakes in their source location and moment-duration scaling. The three most recent episodes in the Puget Sound/southern Vancouver Island portion of the Cascadia subduction zone were exceptionally well recorded. In each episode, we saw clear pulsing of tremor activity with periods of 12.4 and 24 to 25 hours, the same as the principal lunar and lunisolar tides. This indicates that the small stresses associated with the solid-earth and ocean tides influence the genesis of tremor much more effectively than they do the genesis of normal earthquakes. Because the lithostatic stresses are 10^5 times larger than those associated with the tides, we argue that tremor occurs on very weak faults.

Shortly after the discovery of both nonvolcanic tremor (*1*) and recurring slow-slip events (*2*, *3*), Rogers and Dragert determined that these two phenomena occur coincident with each other at regular intervals in the Cascadia subduction zone (*4*). They termed this phenomenon episodic tremor and slip (ETS). Soon thereafter, ETS was also observed in the Nankai Trough in Japan (*5*). ETS falls into a newly identified class of geophysical phenomena that are distinct from "normal" earthquakes. For these slow-slip phenomena, seismic moment scales with event duration (*6*), whereas for earthquakes, moment scales with the cube of event

duration (*7*). The relative locations of nonvolcanic tremor and earthquakes also indicate that they are different processes. In Cascadia, tremor appears to fill volumes of crust that have little or no seismicity (*8*), whereas on the San Andreas Fault, tremor is found below crustal seismicity (*9*). Precise locations of low-frequency earthquakes in Japan, which have been shown to make up a substantial part of nonvolcanic tremor (*10*), place them well above the only nearby seismicity (*11*).

ETS has been interpreted by many as intermittent accelerated slip located between the locked and freely slipping portions of subduction megathrust faults, possibly mediated by pressure fluctuations of fluids rising from the subducting slab (*4*–*6*, *10*, *11*). However, a wide range of other physical mechanisms for ETS remains on the table. Here we spotlight a striking difference from normal earthquakes: The amplitude of tremor strongly correlates with tidal stresses. Many have sought a correlation between earthquakes and the stress fluctuations induced by the tides, but only those examining the most favorable conditions for triggering (*12*–*17*) see any correlation of earthquakes with the tides. Careful studies of large earthquake data sets find no such correlation (*18*–*21*).

The ETS episodes in the portion of the Cascadia subduction zone near Puget Sound and southern Vancouver Island have a periodicity of approximately 14 months, with each episode lasting 2 to 3 weeks. The last three major ETS episodes in this region were in July 2004, September 2005, and January 2007. Although each event had its own characteristics, they all covered approximately the same region from southern Puget Sound to southern Vancouver Island (Fig. 1). Before each of these events, we deployed focused seismic arrays to better locate and characterize ETS. Each array recorded one ETS event. The arrays had 5 to 11 stations and their apertures ranged from 0.6 to 2.0 km. In this study, we used five of these arrays (Fig. 1) to filter out noise and to closely examine how the amplitude of tremor varies with time (*22*). This allowed us investigate whether nonvolcanic tremor has a tidal periodicity. Two additional arrays that were deployed (LO in 2004 and BD in 2007) and two individual stations (SE-1 and PA-15) were not used because they were dominated by cultural noise.

The amplitude of the tremor varied over time and from array to array (Fig. 2). The recorded amplitude of the tremor depended on both the strength of the tremor and the proximity of the array to the migrating tremor source. For example, it is evident that the 2007 ETS episode migrated from the south to the north, because early in the ETS event, the amplitudes were larger at the southern array PL than at array BS. A few days later, amplitudes were largest at array BS (Fig. 2C).

When examining the amplitude of the tremor for the 2004 and 2007 ETS episodes, one can clearly identify a twice-a-day pulsing of tremor activity, and there are suggestions of such a periodicity in the 2005 episode (Fig. 2 and fig. S1). Once-a-day periods are also visible in several of the time series. The likely signals from tidal stresses would be roughly once- and twice-a-day signals from the gravitational influence of the Sun and Moon. As with all seismic data, we also have to contend with cultural noise that has a daily cycle and often a week/weekend cycle. These signals are visible, for example, in the nontremor interval at the PA array (Fig. 2).

To present a more quantitative evaluation of the periodicity of the tremor, we took a 13-day window of the tremor and computed its spectrum (*22*). The approximately twice-daily periodicity visible in the amplitude time series for each array (Fig. 2) is even more clear when we examine the spectra during ETS episodes (Fig. 3). At all five arrays, there is a strong peak in the spectral amplitude at 12.4 hours, the period of the principal lunar tide. This is in contrast with the characterization of the noise at these same arrays, many of which have a much weaker peak at periods of approximately 12 hours. The strongest tidal forcing is at a period of 12.4 hours, so, given its presence in all three ETS episodes, its absence at other times, and the lack of alternative sources, we can confidently identify the 12.4-hour peaks as due to tidal stresses. The strong 12.4-hour periodicity of the tremor amplitudes is evident when one compares the tremor amplitudes to a sinusoid with 12.4-hour periodicity (fig. S1). Many peaks in the tremor amplitude line up with peaks in an aligned 12.4-hour–period sinusoid.

To quantify the influence of the 12.4-hour lunar tide on the tremor, we examined the relationship between tremor amplitude and its phasing in a best-fit 12.4-hour periodic model (Fig. 4). To do this, we converted time into a phase angle, given a function with a 12.4-hour periodicity. This means that we can now express tremor amplitude as a function of phase instead of time. For each degree of phase, we computed the mean amplitude of the tremor over all ~25 times that particular phase angle repeated in the 13-day window. We then stacked these curves for all five arrays deployed to get an overall sense of how the tides influenced the amplitude of tremor. Using this calculation, we find that tremor amplitude varies smoothly as a function of phase in a sinusoidal fashion. Tremor amplitude varies strongly with phase; the variance of the amplitude is 33.4% from the mean. This is in strong contrast with the results from same methodology applied to the noise. The noise shows no significant amplitude variation with phase, having a variance of 3.3% from the mean.

During the ETS episodes, we also identified a strong peak in the spectra at a range of periods from 24 to 25 hours, the period of the lunisolar and lunar declination tides (Fig. 3). This peak is more difficult to interpret than those at 12.4 hours, because this is the period at which we would expect to identify cultural noise. In fact, we expect that the rather strong source at a period of 24 hours during periods without ETS is a result of cultural noise (Fig. 3C). Fortunately, we have no reason to believe that the cultural

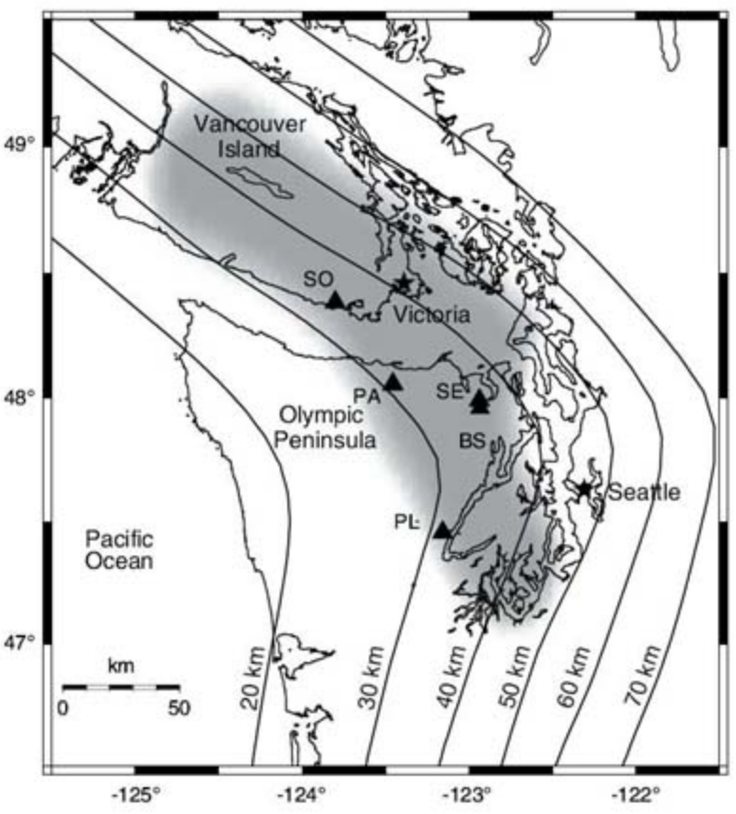

Fig. 1. Map of the study region. Seismic arrays used to record tremor (triangles), the approximate source region of Puget Sound/southern Vancouver Island ETS episodes (shaded region), and isodepths of the plate interface between the Juan de Fuca and North American plates (lines) are indicated on the map.

[1]Department of Earth and Space Science, University of Washington, Box 351310, Seattle, WA 98195, USA. [2]Istituto Nazionale di Geofisica e Vulcanologia–Osservatorio Vesuviano, Via Diocleziano, 328-80124 Napoli, Italy.

*To whom correspondence should be addressed. E-mail: justin@ess.washington.edu

noise that we observe at our sites should be variable from any one period of time to another. Therefore, the much larger spectral amplitudes at periods of 24 to 25 hours during ETS than when ETS is not occurring indicate that tremor is being strongly forced at a daily periodicity in addition to the twice-daily periodicity discussed earlier. We also note that the peaks in tremor amplitude that have an ~24-hour periodicity do not correlate with daylight hours, when cultural noise is at a maximum. This lends further support to our argument that the 24-hour periodicity of the tremor is real. Because of the complication of having two sources of energy that are periodic at 24 hours and do not have the same phasing, we elected not to examine the relationship between amplitude and phase at these periods, because the noise and tremor would interfere with each other.

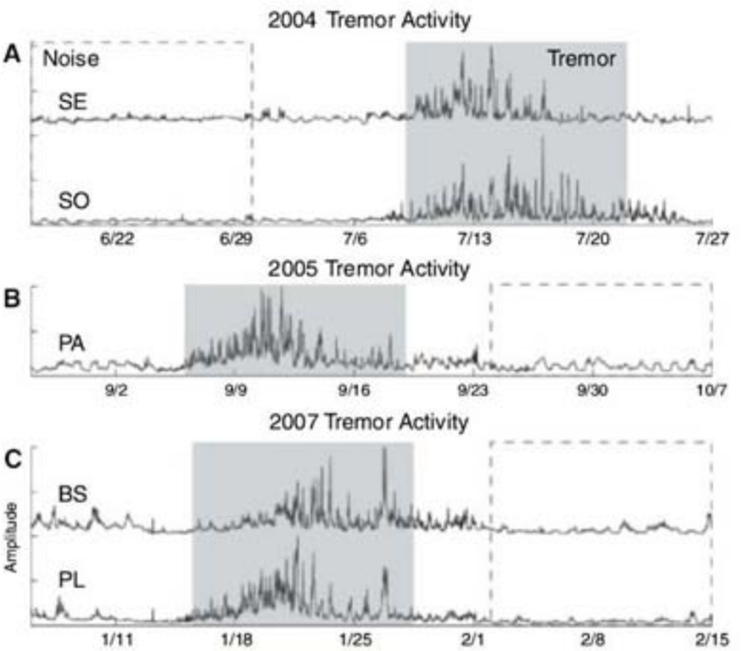

Fig. 2. Tremor amplitudes for ETS episodes in 2004 (**A**), 2005 (**B**), and 2007 (**C**). Each line represents the amplitude of a stack of envelope amplitudes for a single array, each of which recorded a single ETS episode. These stacks were low-pass filtered at a period of 1 hour to distill signals at the frequencies we are interested in. Earthquakes and glitches were removed before stacking. Before computing the envelope, seismograms were band-pass filtered between 1 and 8 Hz. The shaded regions represent a 13-day period during each ETS episode when tremor was strongest at the arrays we were using. The ETS episodes for these events lasted longer than the 13-day windows highlighted; we focused on the periods when recordings of tremor were strongest, when the ETS sources were passing near the arrays. These shaded regions are the regions used to analyze the periodicity of tremor. The dashed-boxed regions represent a 13-day window in which there was no substantial tremor and were used to characterize the noise. Amplitude was normalized at each array by maximum amplitude.

We have conducted exploratory modeling of the ocean tidal stresses, finding peak-to-peak values of 15 KPa on the Cascadia subduction interface at depth. Solid-earth tides are also likely to be important, inducing stresses on the order of 5 KPa (*13*). A direct correlation of tremor with the phase of stressing proved beyond the scope of this study. Such correlation would require tidal stress calculations that account for the complexities of tremor as a moving source (*4*), variability in the orientation and even polarity of tidal stresses across the source region, and variability with depth for the appropriate loading geometry. We did compare tremor amplitude and tidal heights (fig. S2), because the normal stress effect of water loading is simple: An increment in water increases normal stress with a diminishing effect with depth. We found that tremor is stronger at periods of high water and therefore periods of increased normal stress. This is in line with the findings of Shelly *et al.* (*23*), who argue that the increment in water height above the subducting slab will slightly decouple the subduction zone and thus allow for increased tremor. An alternate explanation is to consider that the increase in water height above the overriding plate (and the tremor) is increasing friction on the already slipping subduction zone, causing the slow-slip event to radiate more energy. There are undoubtedly other viable explanations for this correlation, but they require knowledge of the shear stresses associated with ocean loading or the earth tides, which will both have a constant phase relative to the ocean tides and the tremor.

Other recent studies have shown twice-daily tidal periodicities in ETS tremor in Japan (*23*, *24*). To explain the propensity for tremor at certain periods of time, they suggest that solid-earth tides (*24*) and ocean tides (*23*) increase the Coulomb failure stress on the plate interface. We do not yet know whether the Coulomb model can explain our observations.

We have shown that tidal modulation at both daily and twice-daily frequencies is a pervasive feature of all three recent episodes in the best-instrumented tremor source region in Cascadia. The stresses associated with these tides are on the order of 15 KPa, approximately 10^5 times smaller than the lithostatic stresses at the depth where tremor radiates. Although it seems improbable that such small stress changes would have such a dramatic effect, there is supporting evidence that small stress changes can influence the genesis of nonvolcanic tremor. A recent study (*25*) has shown that nonvolcanic tremor was triggered in Cascadia by the surface waves of the moment magnitude 7.8 Denali earthquake, which imparted shear stress changes of ~40 Kpa. Similar observations of teleseismic earthquakes triggering tremor have also been made in California (*26*) and Japan (*27*–*29*).

Our observation that tremor is strongly modulated by the tides shows that the physical pro-

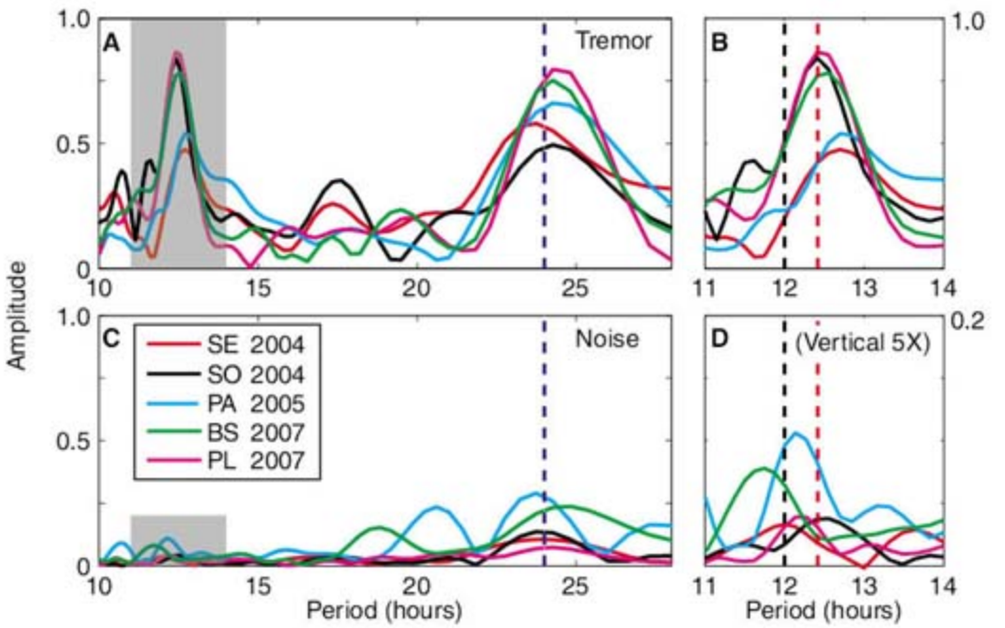

Fig. 3. Spectra of the 13-day windows of tremor (**A** and **B**) and noise (**C** and **D**). Shaded regions in (A) and (C) represent the region that is shown in a zoom in (B) and (D). (D) has been rescaled by a factor of 5. Amplitudes in each panel have been normalized so that the area under each curve in (A) is equal. The variation in amplitudes of the noise [(C) and (D)] indicates the variation in the signal-to-noise ratios at individual arrays; that is, arrays with higher amplitudes of noise have lower signal-to-noise ratios. Dashed vertical lines indicate the strong tidal periods of 12, 12.4, and 24 hours.

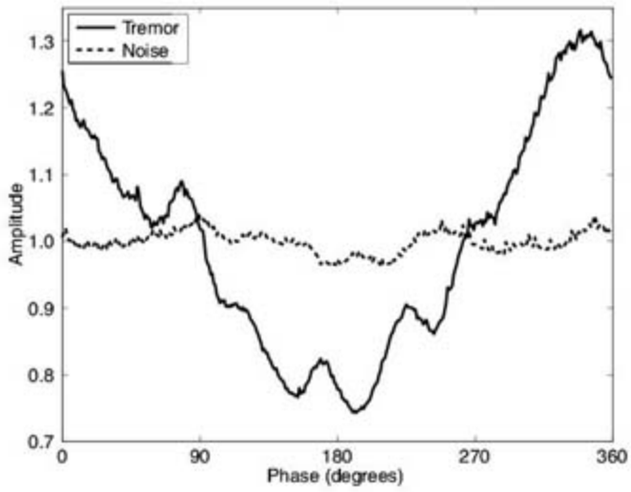

Fig. 4. Amplitude versus phase for a 12.4-hour tidal cycle. In this figure, we compare the variation of the amplitude of tremor during the 13-day ETS windows (solid line) and the 13-day noise windows (dotted line) according to phase in the best-fitting 12.4-hour–period tidal cycle. Phase for each array was determined by cross-correlating a 12.4-hour–period cosine function with the tremor and noise amplitude functions. The amplitude for each degree at each array was averaged over the 25 to 26 times that phase occurred in the 13-day window examined. The amplitudes at the five arrays were averaged for both noise and tremor and were then normalized so that the mean of each curve is 1.

cesses underpinning nonvolcanic tremor are substantially different from those governing earthquakes, which are not typically affected by the tides. ETS appears to represent slow ongoing failure, and thus any increment in stress should affect the failure rate, regardless of the stress state. We believe that this failure is occurring on very weak faults, because small stresses will have a much larger effect on a low-stress fault than a high-stress one. These faults could be very low-friction or, similarly, occur in the presence of near-lithostatic pore pressures.

References and Notes

1. K. Obara, *Science* **296**, 1679 (2002).
2. H. Dragert, K. L. Wang, T. S. James, *Science* **292**, 1525 (2001).
3. M. M. Miller, T. Melbourne, D. J. Johnson, W. Q. Sumner, *Science* **295**, 2423 (2002).
4. G. Rogers, H. Dragert, *Science* **300**, 1942 (2003).
5. K. Obara, H. Hirose, F. Yamamizu, K. Kasahara, *Geophys. Res. Lett.* **31**, L23602 (2004).
6. S. Ide, G. C. Beroza, D. R. Shelly, T. Uchide, *Nature* **447**, 76 (2007).
7. H. Houston, *J. Geophys. Res.* **106**, 11137 (2001).
8. H. Kao *et al.*, *Nature* **436**, 841 (2005).
9. R. M. Nadeau, D. Dolenc, *Science* **307**, 389 (2005).
10. D. R. Shelly, G. C. Beroza, S. Ide, *Nature* **446**, 305 (2007).
11. D. R. Shelly, G. C. Beroza, S. Ide, S. Nakamula, *Nature* **442**, 188 (2006).
12. D. Emter, in *Tidal Phenomena, Lecture Notes in Earth Sciences*, H. Wilhelm, W. Zurn, H.-G. Wenzel, Eds. (Springer-Verlag, Berlin, 1997), vol. 66, pp. 293–309.
13. E. S. Cochran, J. E. Vidale, S. Tanaka, *Science* **306**, 1164 (2004).
14. S. R. McNutt, R. J. Bevan, *Nature* **294**, 615 (1981).
15. W. S. D. Wilcock, *Geophys. Res. Lett.* **28**, 3999 (2001).
16. M. Tolstoy, F. L. Vernon, J. A. Orcutt, F. K. Wyatt, *Geology* **30**, 503 (2002).
17. D. F. Stroup, D. R. Bohnenstiehl, M. Tolstoy, F. Waldhauser, R. T. Weekly, *Geophys. Res. Lett.* **34**, L15301 (2007).
18. M. McNutt, T. H. Heaton, *Calif. Geol.* **34**, 12 (1981).
19. E. S. Cochran, J. E. Vidale, *Geophys. Res. Lett.* **34**, L04302 (2007).
20. J. E. Vidale, D. C. Agnew, M. J. S. Johnston, D. H. Oppenheimer, *J. Geophys. Res.* **103**, 24567 (1998).
21. M. Kennedy, J. E. Vidale, M. Parker, *Seismol. Res. Lett.* **75**, 607 (2004).
22. Materials and methods are available as supporting material on *Science* Online.
23. D. R. Shelly, G. C. Beroza, S. Ide, *Geochem. Geophys. Geosyst.* **8**, Q10014 (2007).
24. R. Nakata, N. Suda, H. Tsuruoka, *Eos* **87**, Fall Meet. Suppl., Abstract V41A-1700.
25. J. L. Rubinstein *et al.*, *Nature* **448**, 579 (2007).
26. J. Gomberg *et al.*, *Science* **319**, 173 (2008).
27. M. Miyazawa, E. E. Brodsky, paper presented at the Seismological Society of Japan 2007 Fall Meeting, Sendai, Japan, 25 October 2007.
28. M. Miyazawa, J. Mori, *Geophys. Res. Lett.* **32**, L10307 (2005).
29. M. Miyazawa, J. Mori, *Geophys. Res. Lett.* **33**, L05303 (2006).
30. C. W. Ulberg, thesis, Carleton College, Northfield, MN (2007).

31. A summer undergraduate project (*30*) paved the road for parts of this study. Incorporated Research Institutions for Seismology, Earthscope, and Istituto Nazionale di Geofisica e Vulcanologia provided instruments for the various deployments. D. Agnew provided invaluable help and insight into the tides. J. Sweet assisted with the mapping of the tremor episodes. J. Gomberg, S. Malone, H. Houston, and two anonymous reviewers provided comments that improved this manuscript.

Supporting Online Material

www.sciencemag.org/cgi/content/full/1150558/DC1
Materials and Methods
Figs. S1 and S2

17 September 2007; accepted 13 November 2007
Published online 22 November 2007;
10.1126/science.1150558
Include this information when citing this paper.

Isotopic Evidence for Glaciation During the Cretaceous Supergreenhouse

André Bornemann,[1,2]* Richard D. Norris,[1] Oliver Friedrich,[1,3] Britta Beckmann,[4] Stefan Schouten,[5] Jaap S. Sinninghe Damsté,[5] Jennifer Vogel,[1] Peter Hofmann,[4] Thomas Wagner[6]

The Turonian (93.5 to 89.3 million years ago) was one of the warmest periods of the Phanerozoic eon, with tropical sea surface temperatures over 35°C. High-amplitude sea-level changes and positive $\delta^{18}O$ excursions in marine limestones suggest that glaciation events may have punctuated this episode of extreme warmth. New $\delta^{18}O$ data from the tropical Atlantic show synchronous shifts ~91.2 million years ago for both the surface and deep ocean that are consistent with an approximately 200,000-year period of glaciation, with ice sheets of about half the size of the modern Antarctic ice cap. Even the prevailing supergreenhouse climate was not a barrier to the formation of large ice sheets, calling into question the common assumption that the poles were always ice-free during past periods of intense global warming.

Despite the extreme warmth of the Turonian (*1–3*) [93.5 to 89.3 million years ago (Ma) (*4*)], it has been argued that there may have been several stages of continental ice growth during the period, reflected in both erosional surfaces and geochemical records associated with possible glaciation-induced sea-level falls (*5–7*). Rapid decreases (<1 million years) in sea level are known from diverse locations in the Turonian of northern Europe, North America, and the Russian Platform and are estimated at magnitudes of 25 to 40 m (*7*, *8*) or even more (*9*). These rapid changes in sea level are too fast and too widespread to be accounted for by tectonic processes and were therefore plausibly triggered by glacioeustasy (*7*, *10*). Further evidence comes from positive $\delta^{18}O$ excursions in marine, but diagenetically altered, limestone sequences (*5*, *11*) and brachiopod isotope data (*6*). However, evidence from sedimentological findings such as ice-rafted debris is still lacking, and unequivocal $\delta^{18}O$ records of well-preserved open-ocean foraminifera are rare, are of low resolution, or do not support the idea of Late Cretaceous ice sheets (*12*). Moreover, there is only a poor understanding of how large ice sheets might grow in a period when tropical sea surface temperatures (SSTs) exceed 35°C (*3*, *13*) and high-latitude temperatures are in excess of 20°C (*2*, *14*).

We used two independent techniques to estimate SSTs during the early Late Cretaceous. One proxy is the $\delta^{18}O$ paleothermometer, which we applied to monospecific planktic foraminiferal samples from a 40-m-thick, organic carbon–rich, laminated marlstone succession of Turonian to Santonian age from the western equatorial Atlantic at Demerara Rise [Ocean Drilling Program (ODP) Site 1259]. These sediments contain planktic foraminifera with a "glassy" appearance and pristine, well-preserved wall textures (*15*).

This state of preservation is ideal for an extensive geochemical investigation in order to reconstruct past SSTs (*16*). Comparison of the $\delta^{18}O$ values of planktic and benthic foraminifera was also used to provide information on the global isotopic composition of oceans when compared against a salinity-independent temperature proxy: the tetraether index of lipids with 86 carbon atoms (TEX_{86}), which is based on the distribution of crenarchaeol membrane lipids (*17*, *18*). Because the growth of continental ice enriches seawater in ^{18}O, the $\delta^{18}O$ chemistry, when constrained by TEX_{86} temperature estimates, can be further used to estimate the size of continental ice sheets.

Our tropical $\delta^{18}O$-derived SST estimates range from ~34° to ~37°C [–4.2 to –4.9 per mil (‰), Vienna Pee Dee belemnite (VPDB) standard] in the Turonian and from ~31.5° to ~35°C (–3.65 to –4.4‰ VPDB) in the late Coniacian and Santonian (Fig. 1A). These values are in good agreement with earlier estimates from spot measurements from the western Atlantic (*1*, *3*) and with low-resolution data from the organic paleothermometer TEX_{86} (*13*). Newly generated TEX_{86} data indicate high SSTs of up to 36°C during the Turonian, followed by a shift to cooler temperatures during the Coniacian and Santonian (Fig. 1B). Today, temperatures in the western tropical Atlantic range from 28° to 29°C (*19*), so our data suggest that the Turonian surface ocean was 5° to 9°C warmer than at present.

The Turonian warmth was punctuated by a short-lived decrease in the $\delta^{18}O$ content of planktic foraminifera ~91.34 Ma [523 meters of composite depth (mcd)] and a pronounced positive $\delta^{18}O$ excursion centered on the CC11/CC12 calcareous nannofossil biozone boundary ~91.2 Ma (521.5 mcd) (Figs. 1A and 2A). The most negative $\delta^{18}O$ ratios in our record are found ~91.34 Ma, but the implied SST peak (>36°C) is not reflected in either the benthic foraminiferal $\delta^{18}O$ or the TEX_{86} data (Fig. 2). Evidently, this $\delta^{18}O$ event reflects an episode of acceleration of the hydrological cycle, causing a decrease in the local sea surface salinity (Fig. 2C), and was followed at ~91.2 Ma by a synchronous positive shift in $\delta^{18}O$ in both planktic and benthic foraminifera, which lasted for ~200,000 years. The magnitude of the positive $\delta^{18}O$ excursion in planktic foraminifera is >1‰, whereas it is up to 0.7‰ in benthic foraminifera.

Because TEX_{86} temperature estimates are independent of changes in seawater $\delta^{18}O$ (δ_W), we calculated temperature anomalies based on paired measurements of both $\delta^{18}O$ and TEX_{86} to quantify the change in δ_W (Fig. 2C) produced by the possible growth of continental ice. The TEX_{86} data display only a 1°C decrease in surface ocean temperatures associated with the 91.2 Ma planktic oxygen isotope shift. Therefore the remaining 0.4 to 0.6‰ anomaly during the 91.2 Ma event in planktic foraminiferal $\delta^{18}O$, which is similar to the range suggested by the benthic foraminifera (0.3 to 0.7‰), must primarily reflect changes in δ_W rather than ocean temperature alone. Both the surface ocean and the deep sea floor (estimated to be at depths >1500 m) (*20*) show the positive $\delta^{18}O$ anomaly, making it unlikely that this signal reflects local changes in surface ocean salinity. It is much more likely that the synchronous change in benthic and planktic foraminiferal $\delta^{18}O$ was produced by sequestering ^{16}O in glacial ice, causing a whole-ocean increase in δ_W.

The middle Turonian is characterized by a series of short-term relative sea-level changes (*9*, *21*) that are consistent with our glacioeustatic interpretation of the isotopic record. Two major widespread unconformities, Tu-2 at 91.2 Ma and Tu-3 at 90.9 Ma (*21*, *22*), correspond to sea-level falls of at least 25 m (*9*, *21*) and occur close to the CC11/CC12 nannofossil zone boundary (91.2 Ma) (*4*). Data from the Russian Platform (*8*) suggest a drop in sea level of up to 40 m at ~91 Ma, and a further drop by ~25 to 30 m is reported from the New Jersey margin at the CC11/CC12 boundary (*7*, *10*). The sea-level record from the Russian Platform is particularly important because this region is generally regarded as tectonically stable, making it a particularly good place to estimate global sea-level changes. A large-scale unconformity has also been reported from the Western Interior Basin (*23*) and northwest Europe (*24*) in the late middle Turonian. Because of stratigraphic uncertainties and the lack of sophisticated supraregional stratigraphic concepts, it is not clear which of these unconformities correspond to the observed positive $\delta^{18}O$ shift. However, the widespread occurrence of high-amplitude relative sea-level changes sup-

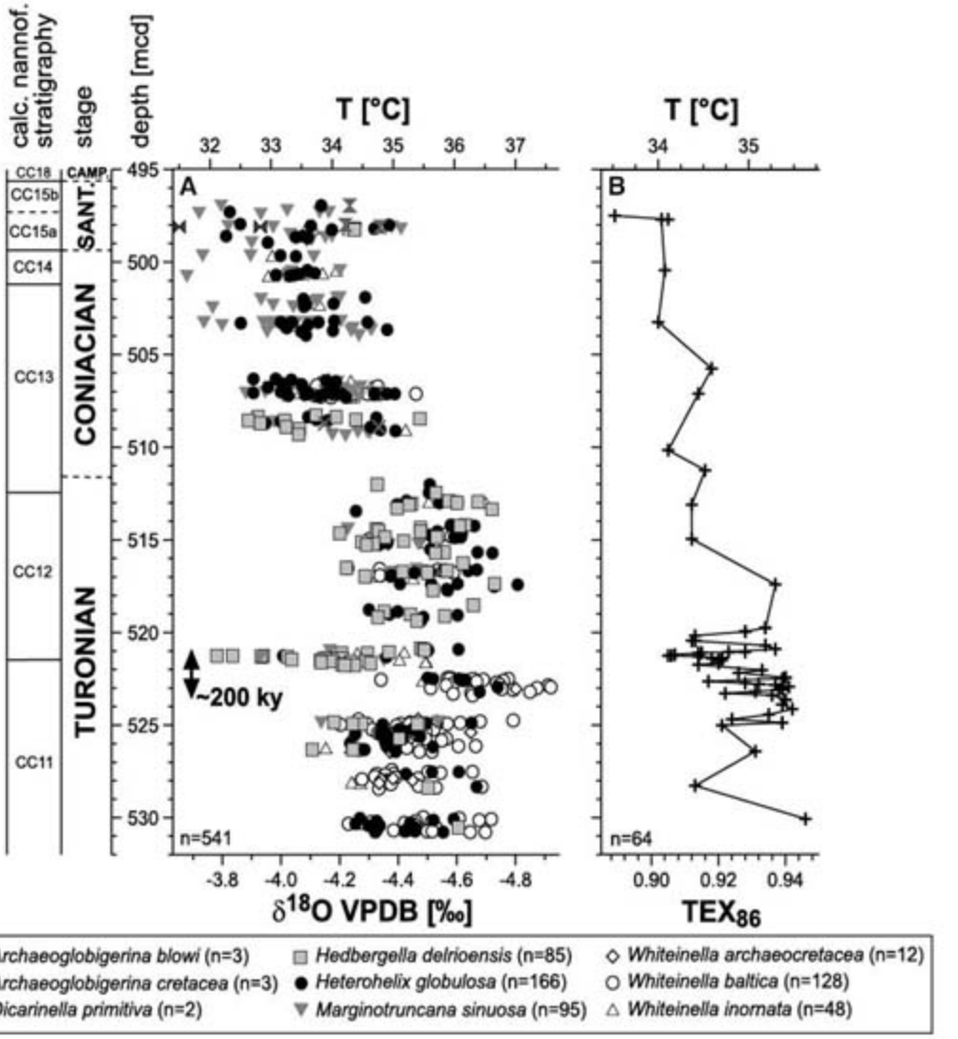

Fig. 1. Stratigraphy and calculated SSTs based on planktic foraminiferal $\delta^{18}O$ and TEX_{86} data for the Turonian to Santonian interval at ODP Site 1259 (*33*), Demerara Rise, western equatorial Atlantic. (**A**) $\delta^{18}O$ data based on monospecific planktic foraminiferal and corresponding conservative SST estimates. (**B**) TEX_{86} values and the calculated SSTs. The late Turonian $\delta^{18}O$ peak interval is estimated to represent ~200,000 years (200 ky). *T*, temperature.

[1]Scripps Institution of Oceanography, University of California, San Diego, Geosciences Research Division, 9500 Gilman Drive, La Jolla, CA 92093–0244, USA. [2]Institut für Geophysik und Geologie, Universität Leipzig, Talstraße 35, D-04103 Leipzig, Germany. [3]School of Ocean and Earth Science, National Oceanography Centre, European Way, Southampton SO14 3ZH, UK. [4]Institut für Geologie und Mineralogie, Universität Köln, Zülpicher Straße 49a, D-50674 Köln, Germany. [5]Department of Marine Biogeochemistry and Toxicology, Royal Netherlands Institute for Sea Research, Post Office Box 59, 1790 AB Den Burg, Texel, Netherlands. [6]School of Civil Engineering and Geosciences, Newcastle University, Newcastle upon Tyne NE1 7RU, UK.

*To whom correspondence should be addressed. E-mail: a.bornemann@uni-leipzig.de

ports the hypothesis that continental ice may have formed in the middle Turonian. Our biostratigraphy and the $\delta^{13}C$ record (fig. S2) suggest that the positive $\delta^{18}O$ shift is synchronous with the Pewsey Event in western Europe (*25*, *26*), which is considered to have been associated with regional cooling based on bulk-rock $\delta^{18}O$ data and faunal patterns from western Europe (*11*).

The magnitude of the sea-level fall associated with the 91.2 Ma $\delta^{18}O$ shift is constrained by four variables: (i) our 0.3 to 0.7‰ δ_W anomaly, (ii) the magnitude of the late Turonian sea-level fall [~25 to 40 m (*7*, *8*)], (iii) an estimate of the relationship between sea level and $\delta^{18}O$ [0.11‰ VPDB $\delta^{18}O$ per 10 m of sea-level fall in the Quaternary (*27*) and 0.075‰ VPDB $\delta^{18}O$ per 10 m of sea-level fall in a warm climate scenario (*7*)], and (iv) the estimated $\delta^{18}O$ composition of Cretaceous ice. The first three variables are well known, whereas the isotopic composition of Cretaceous ice can be constrained between the average modern value for the Antarctic ice cap [–44‰ Vienna standard mean ocean water (VSMOW)] (*7*) and the predicted ice composition for past warm climates (–30‰ VSMOW) (*7*, *28*). Given the modern $\delta^{18}O$ composition of the Antarctic ice cap, the observed $\delta^{18}O$ anomaly is consistent with a sea-level fall of 27 to 64 m. Today, the Antarctic ice sheet stores sufficient water to change global sea level by 61 m (*29*). Therefore, our calculated volume of the Cretaceous ice sheet is equivalent to 44 to 105% that of the modern Antarctic ice sheet. If Cretaceous ice had a $\delta^{18}O$ composition of –30‰ VSMOW, the 91.2 Ma event would be consistent with a sea-level fall of 40 to 93 m and an ice volume 66 to 152% that of modern Antarctica.

We propose that any large Turonian ice sheet was probably located on Antarctica, given the polar position of the continent and the widespread areas of elevated terrain (with altitudes of 1500 to 2500 m) when the modern ice cap is isostatically removed (*30*). However, the uplift history of the Transantarctic Mountains before the Cenozoic is very poorly known and may have commenced during the Cretaceous (*31*) or the Eocene (*32*). Warm tropical and subpolar SSTs in the Turonian (*1*–*3*) would seem to preclude substantial ice development at or near sea level, even on Antarctica, emphasizing the need for further work on the paleoelevation history of the continent.

It is unlikely that an ice sheet of the size of the modern Antarctic ice cap existed in the Cretaceous, both because of the warm surface temperatures noted above and because there is no evidence for the ice-rafted debris that should be present in the Southern Ocean if all of Antarctica had been glaciated. However, an ice cap of up to ~60% the size of the modern Antarctic ice sheet is plausible given the constraints imposed by the sea-level record, as well as our estimate of the change in mean ocean δ_W and our –44‰ VSMOW estimate for the isotopic composition of glacial ice. These results also imply that the $\delta^{18}O$ composition of Turonian polar precipitation was not substantially heavier than today and contradict expectations that greenhouse warming should decrease fractionation during vapor transport from mid- to high latitudes (*7*, *28*).

We are left with the apparent paradox that the prevailing extraordinarily high tropical temperatures during the Turonian were not a barrier to the initiation and growth of large continental ice sheets. The development of these ice sheets could be attributed to an increase in the activity of the hydrological cycle, which must have initiated more humid conditions and enhanced precipitation in the high latitudes. As with periods of Cenozoic ice growth, the initiation of Cretaceous ice expansion may have been triggered by orbital dynamics, because the ~200,000-year duration of the 91.2 Ma event is similar to the half period of the 400,000-year eccentricity cycle. Our results suggest that fairly large ice sheets could grow and decay equally rapidly, which is very much the same pattern as during the Pleistocene. However, unlike the Pleistocene, Cretaceous ice sheets were apparently not a regularly recurring phenomenon, possibly because the extreme warmth of the Turonian, the paleoelevation of Antarctica, and the orbital configuration allowed the initiation of ice sheet development only under certain rare conditions. Our results further suggest that the common assumption that ice sheets did not exist during periods of past supergreenhouse climates should be reexamined, with implications for paleotemperature estimation, the determination of the past isotopic composition of seawater, and high-latitude terrestrial climate reconstruction.

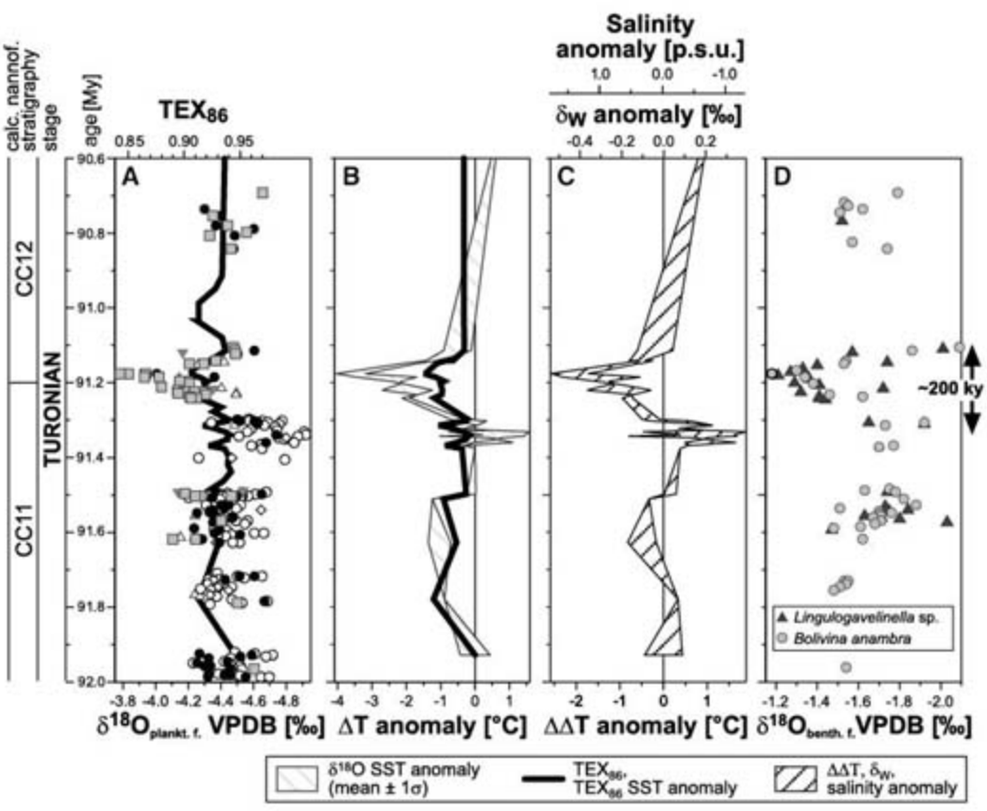

Fig. 2. Detailed data from the CC11 and CC12 calcareous nannofossil biozone interval of ODP Site 1259 (*33*). Data are plotted against absolute age (*4*) (table S1) and cover the interval from 518.02 to 530.78 mcd in Fig. 1. (**A**) The raw planktic foraminiferal $\delta^{18}O$ data (see Fig. 1 for symbol explanation) and TEX_{86} data; both are plotted on the same scale with respect to the estimated SSTs in Fig. 1. (**B**) $\delta^{18}O$ and TEX_{86} anomalies were calculated in reference to sample 1259B-22-4, 75–76.5 cm (530.08 mcd, 91.93 My). In (B) and (**C**), only those samples are shown from which both proxy data types ($\delta^{18}O$ and TEX_{86}) are available. These anomalies were then converted to expected δ_W anomalies (C) by application of a $\delta^{18}O/T$ relationship of –0.208‰/°C. The resulting δ_W anomaly was then assumed to reflect changes corresponding to surface water salinity changes due to shifts in the precipitation/evaporation balance. The salinity anomaly field represents a δ_W/salinity relationship of 0.30‰/practical salinity units (p.s.u.) (*33*). (**D**) $\delta^{18}O$ data from two benthic foraminiferal taxa show a positive $\delta^{18}O$ shift of 0.3 to 0.7‰ within ~200,000 years, which parallels the δ_W anomaly.

References and Notes

1. P. A. Wilson, R. D. Norris, M. J. Cooper, *Geology* **30**, 607 (2002).
2. K. L. Bice, B. T. Huber, R. D. Norris, *Paleoceanography* **18**, 10.1029/2002PA000848 (2003).
3. K. L. Bice *et al.*, *Paleoceanography* **21**, 10.1029/2005PA001203 (2006).
4. F. Gradstein, J. Ogg, A. Smith, Eds., *A Geologic Time Scale 2004* (Cambridge Univ. Press, Cambridge, 2004).
5. H. M. Stoll, D. P. Schrag, *Geol. Soc. Am. Bull.* **112**, 308 (2000).
6. S. Voigt, A. S. Gale, S. Flögel, *Paleoceanography* **19**, 10.1029/2004PA001015 (2004).
7. K. G. Miller, J. D. Wright, J. V. Browning, *Mar. Geol.* **217**, 215 (2005).

8. D. Sahagian, O. Pinous, A. Olferiev, V. Zakharov, *Am. Assoc. Pet. Geol. Bull.* **80**, 1433 (1996).
9. B. U. Haq, J. Hardenbol, P. R. Vail, *Science* **235**, 1156 (1987).
10. K. G. Miller *et al.*, *Science* **310**, 1293 (2005).
11. S. Voigt, F. Wiese, *J. Geol. Soc.* **157**, 737 (2000).
12. B. T. Huber, R. D. Norris, K. G. MacLeod, *Geology* **30**, 123 (2002).
13. A. Forster, S. Schouten, M. Baas, J. S. Sinninghe Damsté, *Geology* **35**, 919 (2007).
14. A. B. Herman, R. A. Spicer, *Nature* **380**, 330 (1996).
15. A. Bornemann, R. D. Norris, *Mar. Micropaleontol.* **65**, 32 (2007).
16. P. N. Pearson *et al.*, *Nature* **413**, 481 (2001).
17. S. Schouten, E. C. Hopmans, E. Schefuss, J. S. Sinninghe Damsté, *Earth Planet. Sci. Lett.* **204**, 265 (2002).
18. C. Wuchter, S. Schouten, M. J. L. Coolen, J. S. Sinninghe Damsté, *Paleoceanography* **19**, 10.1029/2004PA001041 (2004).
19. J. I. Antonov, S. Levitus, T. P. Boyer, M. E. Conkright, T. O'Brien, *World Ocean Atlas 1998* (National Oceanic and Atmospheric Administration, Silver Spring, MD, 1998), vol. 1.
20. M. A. Arthur, J. H. Natland, in *Deep Drilling Results in the Atlantic Ocean: Continental Margins and Paleoenvironment*, M. Talwani, W. W. Hay, W. B. F. Ryan, Eds. (American Geophysical Union, Washington, DC, 1979), pp. 375–401.
21. J. Hardenbol, J. Thierry, M. B. Farley, P.-C. De Graciansky, P. R. Vail, in *Mesozoic and Cenozoic Sequence Chronostratigraphic Framework of European Basins*, P. C. De Graciansky, J. Hardenbol, T. Jacquin, P. Vail, Eds. (Society for Sedimentary Geology, Tulsa, OK, 1998), vol. 60, pp. 3–13.
22. Absolute ages are adopted from TSCreator (www.stratigraphy.org), based on (*21*), recalibrated after (*4*).
23. B. B. Sageman, J. Rich, M. A. Arthur, G. E. Birchfield, W. E. Dean, *J. Sediment. Res.* **67**, 286 (1997).
24. J. M. Hancock, *Proc. Geol. Assoc.* **100**, 565 (1989).
25. A. S. Gale, *Geol. Soc. Spec. Publ.* **103**, 177 (1996).
26. I. Jarvis, A. S. Gale, H. C. Jenkyns, M. A. Pearce, *Geol. Mag.* **143**, 561 (2006).
27. R. G. Fairbanks, R. K. Matthews, *Quat. Res.* **10**, 181 (1978).
28. H. K. Coxall, P. A. Wilson, H. Pälike, C. H. Lear, J. Backman, *Nature* **433**, 53 (2005).
29. P. Huybrechts, D. Steinhage, F. Wilhelms, J. Bamber, *Ann. Glaciol.* **30**, 52 (2000).
30. R. M. DeConto, D. Pollard, *Nature* **421**, 245 (2003).
31. P. Fitzgerald, *Roy. Soc. New Zeal. Bull.* **35**, 453 (2002).
32. U. S. ten Brink, R. I. Hackney, S. Bannister, T. A. Stern, Y. Makovsky, *J. Geophys. Res.* **102**, 27603 (1997).
33. Materials, methods, and data are available as supporting material on *Science* Online.

34. This research used samples and data provided by the ODP. The ODP was sponsored by NSF and participating countries under the management of Joint Oceanographic Institutions (JOI). We thank P. Worstell for sample preparation and C. Charles (Scripps Institution of Oceanography) and D. Andreasen (University of California Santa Cruz) for their assistance with the mass spectrometers. Financial support was provided by the German Research Foundation (A.B., O.F., and T.W.) and JOI/U.S. Science Support Program (R.D.N.). T.W. acknowledges the Royal Society–Wolfson Research Merit Award.

Supporting Online Material

www.sciencemag.org/cgi/content/full/319/5860/189/DC1
Materials and Methods
Figs. S1 and S2
Tables S1 to S4
References and Notes

3 August 2007; accepted 16 November 2007
10.1126/science.1148777

Breakdown of an Ant-Plant Mutualism Follows the Loss of Large Herbivores from an African Savanna

Todd M. Palmer,[1,2,4]* Maureen L. Stanton,[2,3,4] Truman P. Young,[2,4,5] Jacob R. Goheen,[1,4,6] Robert M. Pringle,[4,7] Richard Karban[8]

Mutualisms are key components of biodiversity and ecosystem function, yet the forces maintaining them are poorly understood. We investigated the effects of removing large mammals on an ant-*Acacia* mutualism in an African savanna. Ten years of large-herbivore exclusion reduced the nectar and housing provided by plants to ants, increasing antagonistic behavior by a mutualistic ant associate and shifting competitive dominance within the plant-ant community from this nectar-dependent mutualist to an antagonistic species that does not depend on plant rewards. Trees occupied by this antagonist suffered increased attack by stem-boring beetles, grew more slowly, and experienced doubled mortality relative to trees occupied by the mutualistic ant. These results show that large mammals maintain cooperation within a widespread symbiosis and suggest complex cascading effects of megafaunal extinction.

Obligate mutualistic relationships among species are ubiquitous and central to ecological function and the maintenance of biodiversity (*1*–*5*). The symbiosis between ants and plants, which involves many species throughout the tropics, was the first coevolved mutualism to be thoroughly elucidated by ecologists (*6*). Many studies have shown the efficacy of ant mutualists in deterring herbivory (*7*) and explored the costs and benefits accruing to the interacting partners (*8*). However, although the importance of large herbivores in the evolution and maintenance of these interactions has been hypothesized (*9*, *10*), it has never been shown.

We investigated the effects of large mammalian herbivores on an ant-*Acacia* mutualism in an African savanna. The whistling-thorn tree, *Acacia drepanolobium*, dominates heavy-clay soils across large expanses of upland East Africa (*11*). At branch nodes, *A. drepanolobium* produces either slender stipular thorns or hollow swollen thorns that serve as ant housing ("domatia"). The tree also secretes a carbohydrate-rich nectar from extrafloral glands located near the bases of leaves (*12*). At our study site in Kenya, four species of ants (*Crematogaster mimosae*, *C. sjostedti*, *C. nigriceps*, and *Tetraponera penzigi*) compete for exclusive possession of host trees and vary strongly in both their defense of the host trees and their use of the tree's "rewards" [i.e., domatia and nectar (*11*, *13*)]. *Crematogaster mimosae* aggressively defends host trees from herbivores and relies heavily on swollen-thorn domatia, where they raise brood, house workers, and occasionally tend honeydew-producing scale insects (Coccidae) (*11*). In contrast, *C. sjostedti* is a less-aggressive defender of host plants (*13*) and, exclusively among the four ant species, does not nest in domatia but rather in stem cavities excavated by the larvae of long-horned beetles (Cerambycidae). Under natural conditions, *C. mimosae* is the most abundant ant symbiont, occupying ~52% of all trees at our sites, whereas *C. sjostedti* occupies ~16% of host plants.

The remaining two ant species, *C. nigriceps* and *T. penzigi*, also occur in relatively low abundance (~15% and ~17% of trees, respectively), and each uses distinctive behaviors that reduce the likelihood of hostile takeover by the competitively superior *C. mimosae* and *C. sjostedti*. *Crematogaster nigriceps* is an effective defender (*13*, *14*) but also prunes axillary buds and kills apical meristems, which reduces lateral canopy spread and thus the likelihood of contact with trees occupied by hostile colonies (*15*). *Tetraponera penzigi*, an intermediate protector, destroys its host-plants' nectaries: a "scorched-earth" strategy that reduces the probability of takeover by neighboring nectar-dependent *Crematogaster* colonies (*16*). All three *Crematogaster* species derive at least some of their energy by foraging off-tree for insects; in contrast, *T. penzigi* seldom leaves its host and appears to subsist by gleaning small food items (e.g., pollen and fungal spores) from the surfaces of its host (*17*).

In 2005, we sampled *A. drepanolobium* trees (1.8 to 3.0 m in height) in 12 plots (4 ha each)

[1]Department of Zoology, University of Florida, Gainesville, FL 32611, USA. [2]Center for Population Biology, University of California, Davis, CA 95616, USA. [3]Section of Evolution and Ecology, University of California, Davis, CA 95616, USA. [4]Mpala Research Centre, Box 555, Nanyuki, Kenya. [5]Department of Plant Environmental Sciences, University of California, Davis, CA 95616, USA. [6]Department of Zoology, University of British Columbia, Vancouver, BC V6T 1Z4, Canada. [7]Department of Biological Sciences, Stanford University, Stanford, CA 94305, USA. [8]Department of Entomology, University of California, Davis, CA 95616, USA.

*To whom correspondence should be addressed. E-mail: tmpalmer@zoo.ufl.edu

situated within three replicate blocks of the Kenya Long-Term Exclosure Experiment (KLEE) (*18*). In each block, two plots were accessible to all wildlife, and in the other two (hereafter called "exclosures"), all wild herbivores >15 kg had been excluded continuously since 1995 (*18*, *19*). This gave us six replicates per treatment, divided among three blocks in a stratified random design (*19*, *20*).

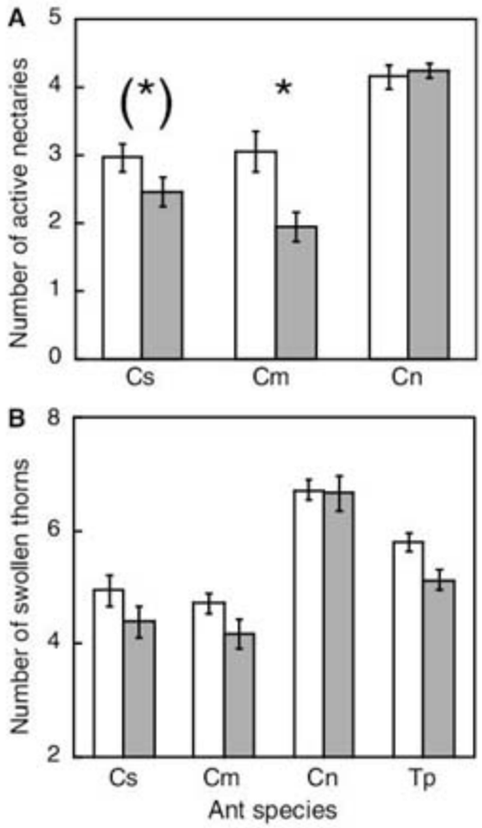

Fig. 1. Rewards produced in the presence (white bars) and absence (gray bars) of large herbivores by *A. drepanolobium* occupied by different species of *Acacia* ants. Ant species' abbreviations are indicated as: Cs, *C. sjostedti*; Cm, *C. mimosae*; Cn, *C. nigriceps*; Tp, *T. penzigi*. All means shown are averages across six plots ± SEM. "Ant species," herbivore-exclusion treatment ("treatment"), and their interaction all had significant effects on the production of host-tree rewards [multivariate analysis of variance (MANOVA), Wilk's lambda; for ant species: $F_{6,74} = 80.7$, $P < 0.0001$; for treatment: $F_{2,37} = 7.54$, $P < 0.002$; for the interaction: $F_{6,74} = 2.3$, $P = 0.04$]. There was no significant block effect on overall reward production by host plants ($P > 0.30$). (**A**) ANOVA revealed a significant ant species × treatment effect ($F_{2,28} = 4.3$, $P = 0.01$) on mean production of active nectaries by host plants. There was no significant block effect on mean nectary production ($P = 0.4$). Asterisks indicate significant differences in planned contrasts of mean production of active nectaries by species between treatments. (*), $P = 0.06$; *, $P < 0.001$. Nectary data are not shown for *T. penzigi* because this species actively destroys all host-plant nectaries (*16*). (**B**) Both ant species (ANOVA, $F_{3,38} = 39.5$, $P < 0.0001$) and herbivore-exclusion treatment (ANOVA, $F_{1,38} = 8.0$, $P < 0.01$) were significant sources of variation in the mean number of swollen thorns produced by host plants. There were no ant species × treatment ($P > 0.5$) or block ($P > 0.2$) effects on mean swollen-thorn production.

In the absence of browsing by large herbivores, *A. drepanolobium* trees decreased their investment toward supporting symbiotic ants. A single decade of herbivore exclusion resulted in reduced rewards (both extrafloral nectaries and swollen thorns) provided to ants by trees (Fig. 1). Within exclosures, reduction of leaf nectar gland rewards was strongest for trees occupied by *C. sjostedti* and *C. mimosae*, whereas the abundance of "active" nectaries (*11*) did not decline significantly on trees occupied by *C. nigriceps* (Fig. 1A). From the plant's perspective, the pruning behavior of *C. nigriceps* may simulate browsing by herbivores, inducing host trees to provide more rewards to *C. nigriceps* symbionts even in the absence of browsers (*11*, *20*, *21*). Production of domatia by host trees was also significantly reduced by herbivore exclusion (Fig. 1B). Similar to the observed reductions that occurred for nectaries, reductions in swollen-thorn densities for host plants occupied by *C. nigriceps* were negligible relative to trees occupied by the other three ant species. Differences in the density of active nectaries and swollen thorns between exclosure treatments almost certainly do not result from trait-specific variation in tree recruitment or survivorship over the 10-year duration of this experiment; sampled host trees are estimated to be 47 to 70 years old (*18*), and there were no significant differences in tree density among treatments within this size class of trees [analysis of variance (ANOVA), for treatment: $F_{1,6} = 0.37$, $P = 0.56$] (*18*). Rather, reductions in swollen-thorn and nectar provisioning likely represent phenotypically plastic responses by host plants to the reduction of browsing pressure (*18*), as with previous studies demonstrating both the relaxation and experimental re-inducibility of stipular thorns in *A. drepanolobium* in the mammal exclosures (*21*).

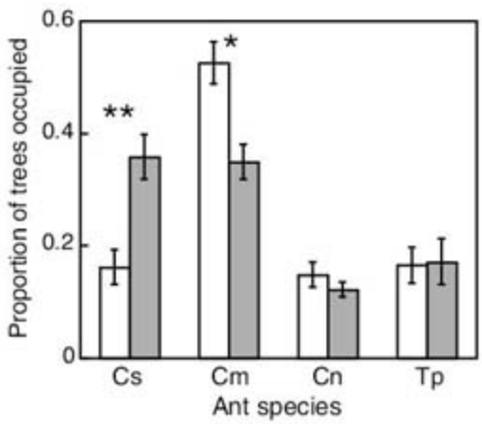

Fig. 2. The proportion of host trees occupied by the four *Acacia*-ant species in the presence of large herbivores (white bars) and in plots from which large herbivores had been excluded (gray bars) for 10 years. Means shown are averages across six plots ± SEM. MANOVA revealed significant differences in *Acacia*-ant species composition in plots with and without large herbivores (Wilk's lambda, $F_{4,3} = 17.9$, $P < 0.02$). There were no significant block ($P = 0.13$) or treatment × block ($P = 0.65$) effects on *Acacia*-ant species composition. Asterisks indicate significant differences in planned contrasts of the relative abundance of each ant species between treatments. **, $P < 0.003$; *, $P < 0.01$.

The experimental exclusion of large herbivores caused marked shifts in the community of symbiotic ants occupying *A. drepanolobium* (Fig. 2). In the absence of browsing by large herbivores, the proportion of trees occupied by *C. sjostedti* doubled, with this species becoming the most abundant symbiont (*18*). In contrast, the proportion of trees occupied by *C. mimosae* decreased by more than 30% (Fig. 2). There were no significant differences between treatments in the proportion of host trees occupied by the less-common guild members *C. nigriceps* ($P = 0.4$) and *T. penzigi* ($P = 0.9$) (*18*). Herbivore exclusion also reduced the average size of individual *C. mimosae* colonies by 47% (planned contrasts, $P < 0.001$), while having no significant effect on average colony size for *C. sjostedti* ($P = 0.5$), *C. nigriceps* ($P = 0.9$), or *T. penzigi* ($P = 0.5$) (*18*).

In addition to shifting the community structure and competitive relationships among ant symbionts, the exclusion of large herbivores increased the frequency of apparently antagonistic behavior by *C. mimosae*. After reductions in the production of leaf nectar glands within the herbivore-exclusion treatment, *C. mimosae* was twice as likely, on average, to tend sap-sucking homopteran scale insects (scale insects were tended on 19.4 versus 9.7% of branches surveyed for exclosures versus open plots, respectively; logistic regression, for treatment: chi-square = 12.30, df = 1, $P = 0.007$) (*18*).

In addition, aggressive recruitment in response to experimental disturbances of host plants was 50% lower for *C. mimosae* workers in herbivore exclosures versus unfenced plots (fig. S1; planned contrasts, $P << 0.0001$) (*18*), whereas herbivore exclusion had no significant effects on host-defending behaviors in the three other *Acacia*-ant species (planned contrasts, $P > 0.4$ for all comparisons) (*18*). Thus, trees occupied by *C. mimosae* within exclosures are likely to experience both increased costs (due to increased tending of scale insects by their associate ants) and decreased benefits (due to the ants' reduced aggression in response to experimentally induced disturbance).

Changes in *Acacia*-ant community structure and *C. mimosae* colony size appear to be driven by differences among the four ant species in the degree to which they depend on host-plant rewards. The greater reliance of *C. mimosae* and *C. nigriceps* on nectar rewards from host trees, relative to that of *C. sjostedti*, is indicated by their much higher rates of attendance at active nectaries [mean number of workers attending nectaries (± SEM) = 2.02 (± 0.37), 3.76 (± 0.38), and 0.1 (± 0.06) for *C. mimosae*, *C. nigriceps*,

and *C. sjostedti*, respectively; ANOVA, $F_{2,148} = 61.04$, $P < 0.0001$] (*18*) and by their relatively lower values of ∂^{15}N [a stable-isotope signature indicating that *C. sjostedti* derives a greater proportion of its diet from higher trophic levels (*22*), namely other arthropods (*23*, *24*)]. When large herbivores are excluded, a reduction in the availability of active nectaries on trees appears to reduce average colony size, defense of host plants, and the relative abundance of nectar-dependent *C. mimosae*, all in favor of its parasitic competitor, *C. sjostedti*. In contrast, although *C. nigriceps* also depends heavily on nectaries, branch pruning by this species appears to maintain the production of active nectaries by its host trees (Fig. 1A), even where herbivores are absent (*15*, *20*, *21*).

The reduction in ant domatia on host trees that resulted from herbivore exclusion also had a disproportionate negative impact on *C. mimosae*. This species depends entirely on swollen thorns for nest space, whereas *C. sjostedti* houses eggs, larvae, and pupae exclusively within stem cavities excavated by cerambycid beetle larvae. Again, although *C. nigriceps* also raises young exclusively in domatia, pruning by this species may help to maintain domatia production by host trees. Finally, the relative abundance of *T. penzigi* was not influenced by herbivore exclusion. Because this species destroys its host-plant's nectaries (*16*), very rarely undergoes aggressive colony expansion (*25*), and is often able to resist invasion by neighboring ant colonies (*13*), *T. penzigi* is less affected by variation in host-plant rewards than *C. mimosae*.

Because *C. sjostedti* derives much of its diet from terrestrial invertebrates, increased arthropod abundance after mammal exclusion might favor that species. However, this is unlikely to explain our results. Extensive sampling within experimental plots (*18*) demonstrated that neither the mean abundances of arboreal, herbaceous, and terrestrial non-ant arthropods, nor the mean biomass of herbaceous and terrestrial non-ant arthropods, differed significantly between herbivore-exclusion and control plots (*t* tests, $P > 0.1$ for all comparisons) (*18*). This finding is consistent with a previous study showing no differences in total arthropod abundance across these treatments (*26*).

Thus, herbivore exclusion effects dramatic changes in the *Acacia*-ant community, but how do these changes feed back to the host plants themselves? Counterintuitively, the loss of large herbivores that browse on *A. drepanolobium* is likely to have strong negative impacts on the growth and survival of these trees, mediated through changes in the abundance of dominant ant symbionts. Eight years of longitudinal data for >1750 marked *A. drepanolobium* individuals (*18*) show that trees occupied by *C. sjostedti* grow markedly more slowly and suffer twice the mortality as compared with trees occupied by the other three ant species (Fig. 3). The reduced vigor and higher mortality of *C. sjostedti*–occupied trees are likely tied to stem damage by wood-boring cerambycid beetles that create nesting spaces for *C. sjostedti*. An ant-removal experiment (*18*) revealed that *C. sjostedti* actively facilitates attack of its host trees by cerambycid beetles. After 18 months, attack by long-horned beetles decreased by 77% on trees from which *C. sjostedti* had been removed, relative to trees where colonies were left intact (Fig. 4). In contrast, *C. nigriceps* and *C. mimosae* appear to actively protect their host trees from attack by these beetles (Fig. 4). The facilitation of these highly destructive (*27*) tree-boring insects by *C. sjostedti* provides a mechanism for the negative impact of this ant on tree growth and survival.

Our results indicate that the large herbivores typical of African savannas have driven the evolution and maintenance of a widespread ant-*Acacia* mutualism and that their experimentally simulated extinction rapidly tips the scales away from mutualism and toward a suite of antagonistic behaviors by the interacting species. Browsing by large herbivores induces greater production of nectary and domatia rewards by trees, and these rewards in turn influence both the behavior of a specialized, mutualistic ant symbiont and the outcome of competition between this mutualist and a non-obligate host-plant parasite. Where herbivores are present, the carbohydrate subsidy provided by host trees plays a key role in the dominance of the strongly mutualistic *C. mimosae*, which is consistent with the hypothesis that plant exudates fuel dominance of canopy ant species that are specialized users of these abundant resources (*28*). In the absence of large herbivores, reduction in host-tree rewards to ant associates results in a breakdown in this mutualism, which has strong negative consequences for *Acacia* growth and survival. Ongoing anthropogenic loss of large herbivores throughout Africa (*29*, *30*) may therefore have strong and unanticipated consequences for the broader communities in which these herbivores occur.

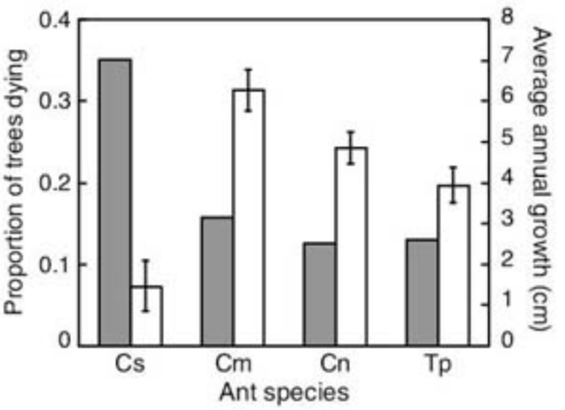

Fig. 3. Average annual growth (white bars ± SEM) and cumulative mortality (gray bars) for host trees occupied by the four *Acacia*-ant species over an 8-year observation period. Average annual growth increments were calculated for trees continuously occupied over an 8-year period by each ant species, with n = 158, 192, 162, and 75 for trees occupied by *C. sjostedti*, *C. mimosae*, *C. nigriceps*, and *T. penzigi*, respectively.

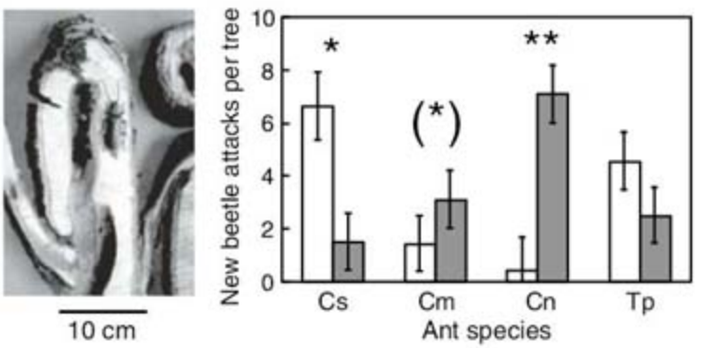

Fig. 4. Long-horned beetle (Cerambycidae) attack on ant-removal (gray bars ± SEM) and control trees (white bars ± SEM) occupied by the four *Acacia*-ant species (n = 9 to 12 trees per ant species per treatment). Significance levels for effects of ant removal on new beetle damage sites are shown for one-way ANOVA models conducted separately on each ant species, after the discovery of a highly significant interaction (*18*) between ant species and the ant-removal treatment. (*), $P = 0.07$; *, $P = 0.02$; **, $P = 0.005$. The left panel shows cavities excavated by boring beetle larvae within a longitudinal cross section of a main stem of *A. drepanolobium*. An adult cerambycid beetle discovered within this stem is also shown.

References and Notes

1. D. A. Wardle *et al.*, *Science* **304**, 1629 (2004).
2. G. P. Jones, M. I. McCormick, M. Srinivasan, J. V. Eagle, *Proc. Natl. Acad. Sci. U.S.A.* **101**, 8251 (2004).
3. A. M. Klein *et al.*, *Proc. R. Soc. London Ser. B* **274**, 303 (2007).
4. R. W. F. Hardy, U. D. Havelka, *Science* **188**, 633 (1975).
5. J. L. Sachs, E. L. Simms, *Trends Ecol. Evol.* **21**, 585 (2006).
6. D. H. Janzen, *Univ. Kans. Sci. Bull.* **47**, 315 (1967).
7. M. Heil, D. McKey, *Annu. Rev. Ecol. Syst.* **34**, 425 (2003).
8. M. E. Frederickson, *Oecologia* **143**, 387 (2005).
9. D. H. Janzen, *Ecology* **53**, 885 (1972).
10. W. L. Brown Jr., *Ecology* **41**, 587 (1960).
11. T. P. Young, C. H. Stubblefield, L. A. Isbell, *Oecologia* **109**, 98 (1997).
12. B. Hocking, *Trans. R. Entomol. Soc. London* **122**, 211 (1970).
13. T. M. Palmer, T. P. Young, M. L. Stanton, E. Wenk, *Oecologia* **123**, 425 (2000).
14. L. Stapley, *Oecologia* **115**, 401 (1998).
15. M. L. Stanton, T. M. Palmer, T. P. Young, A. Evans, M. L. Turner, *Nature* **401**, 578 (1999).
16. T. M. Palmer, T. P. Young, M. L. Stanton, *Oecologia* **133**, 372 (2002).
17. W. M. Wheeler, I. W. Bailey, *Trans. Am. Philos. Soc.* **22**, 235 (1920).

18. Materials and methods are available as supporting material on *Science* Online.
19. T. P. Young, B. D. Okello, D. Kinyua, T. M. Palmer, *Afr. J. Range Forage Sci.* **14**, 94 (1998).
20. M. Huntzinger, R. Karban, T. P. Young, T. M. Palmer, *Ecology* **85**, 609 (2004).
21. T. P. Young, M. L. Stanton, C. E. Christian, *Oikos* **101**, 171 (2003).
22. T. M. Palmer, *Ecology* **84**, 2843 (2003).
23. B. J. Peterson, B. Fry, *Annu. Rev. Ecol. Syst.* **18**, 293 (1987).
24. D. M. Post, *Ecology* **83**, 703 (2002).
25. M. L. Stanton, T. M. Palmer, T. P. Young, *Ecol. Monogr.* **72**, 347 (2002).
26. R. M. Pringle, T. P. Young, D. I. Rubenstein, D. J. McCauley, *Proc. Natl. Acad. Sci. U.S.A.* **104**, 193 (2007).
27. E. G. Brockerhoff, A. M. Liebhold, H. Jactel, *Can. J. For. Res.* **36**, 263 (2006).
28. D. W. Davidson, *Biol. J. Linn. Soc.* **61**, 153 (1997).
29. J. T. Du Toit, D. H. M. Cumming, *Biodiversity Conserv.* **8**, 1643 (1999).
30. W. K. Ottichilo, J. De Leeuw, A. K. Skidmore, H. H. T. Prins, M. Y. Said, *Afr. J. Ecol.* **38**, 202 (2000).
31. We thank J. Lemboi and the excellent staff at Mpala Research Centre and Mpala Ranch for logistical support, students from The Kenya Wildlands Program for field assistance, and the Gordon Lab (Stanford University), Koch Lab (University of California), Silliman Lab (University of Florida), K. Rudolph, and four anonymous reviewers for helpful comments on the manuscript. This work was funded by NSF grants DEB-0089706 and DEB-0444741 to T.M.P., M.L.S., and T.P.Y. The KLEE plots were built and maintained with grants from the James Smithson Fund of the Smithsonian Institution (to A. Smith), the National Geographic Society (4691-91), NSF (BSR-97-07477 and BSR-03-16402), and the African Elephant Program of the U.S. Fish and Wildlife Service (98210-0G563) (to T.P.Y.). This research was carried out under the auspices of the Ministry of Education, Science, and Technology of the Republic of Kenya (Permit number MOEST 13/001/34 17). This paper is dedicated to the memory of Otis Trout Palmer, a true mutualist.

Supporting Online Material
www.sciencemag.org/cgi/content/full/319/5860/192/DC1
Materials and Methods
Fig. S1
References

10 October 2007; accepted 28 November 2007
10.1126/science.1151579

Endothelial Progenitor Cells Control the Angiogenic Switch in Mouse Lung Metastasis

Dingcheng Gao, Daniel J. Nolan, Albert S. Mellick, Kathryn Bambino, Kevin McDonnell, Vivek Mittal*

Angiogenesis-mediated progression of micrometastasis to lethal macrometastasis is the major cause of death in cancer patients. Here, using mouse models of pulmonary metastasis, we identify bone marrow (BM)–derived endothelial progenitor cells (EPCs) as critical regulators of this angiogenic switch. We show that tumors induce expression of the transcription factor Id1 in the EPCs and that suppression of Id1 after metastatic colonization blocked EPC mobilization, caused angiogenesis inhibition, impaired pulmonary macrometastases, and increased survival of tumor-bearing animals. These findings establish the role of EPCs in metastatic progression in preclinical models and suggest that selective targeting of EPCs may merit investigation as a therapy for cancer patients with lung metastases.

Disseminated malignant primary tumor cells colonize target secondary organs, through bone marrow (BM)–derived premetastatic niches (*1*, *2*), to form dormant micrometastases (*3*). In some cases, these micrometastases activate the angiogenic switch and progress to macrometastases (*4*, *5*). The cellular and molecular mechanisms regulating the angiogenic switch and the dynamics of vessel assembly during the progression of micrometastases to macrometastases remain poorly understood, which limits the utility of antiangiogenic approaches to controlling metastasis. In this study, we have investigated whether BM-derived endothelial progenitor cells (EPCs) contribute to angiogenesis-mediated progression of micrometastases into deadly macrometastases.

To facilitate tracking of both metastatic tumor cells and BM-derived cells in vivo, we implanted Lewis lung carcinoma cells stably expressing red fluorescent protein (LLC-RFP) into syngeneic mice reconstituted with BM cells expressing green fluorescent protein (GFP^+ BM) (fig. S1A) (*6*). After primary tumor resection (fig. S1B), numerous RFP^+ pulmonary micrometastases (<1 mm in diameter) were detected by stereomicroscopic imaging at day 14 after tumor inoculation (12 on average per animal) (fig. S1C). The total number of metastases increased with time (average 22 and 35 per animal at day 21 and day 28, respectively) (Fig. 1A), with a concomitant increase in macrometastases (≥1 mm in diameter, 47% at day 28) (Fig. 1A), which indicated a time window of micrometastasis to macrometastasis progression. We next determined whether this window of metastasis progression was associated with the angiogenic switch. Immunohistochemical staining showed that the micrometastatic foci (day 14) were largely avascular, as determined by a lack of $CD31^+$ vessels (Fig. 1B, top). In contrast, macrometastatic foci (days 21 to 28) were infiltrated with many $CD31^+$ neovessels of various sizes (Fig. 1B, bottom), which suggested that these lesions had undergone an angiogenic switch during their expansion in size. As expected, many BM-derived GFP^+ cells were recruited to both micro- and macrometastases (fig. S1C and Fig. 1B). Although a majority of these cells represented hematopoietic lineages, as previously described in primary tumors (*7*) (fig. S2A), we focused on BM-derived endothelial cells that directly contribute to neovascularization (*8*). Microscopic analysis of macrometastases showed that a subset of neovessels had incorporated BM-derived endothelial cells [GFP^+CD31^+ (Fig. 1C)]. Luminal incorporation was confirmed by optical sectioning microscopy, which showed that the GFP and CD31 signals were localized to the same individual cell in all three dimensions [supporting online material (SOM) text, Note 1, and (fig. S2B)]. Functional incorporation of BM-derived endothelial cells was quantified by systemic perfusion of fluorescently labeled isolectin GS-IB4, which specifically binds to the luminal surface of endothelial cells in vessels with active blood circulation (*8*, *9*). Macrometastases were dissected from the lungs, and fluorescence activated cell sorting (FACS) analysis showed that the luminally incorporated BM-derived endothelial cells ($GFP^+Lectin^+CD31^+CD11b^-$) represent on average 12.7 ± 2.9% of total endothelial cells ($Lectin^+CD31^+CD11b^-$) (Fig. 1, D and E).

To confirm that these events also occur in a model of spontaneous metastasis, we transplanted syngeneic GFP^+ BM into MMTV-PyMT transgenic mice, a model of breast cancer. Pulmonary micrometastases were detected in the mice at 12 weeks of age, and these lesions progressed into numerous macrometastases by week 16 (Fig. 2A). Notably, GFP^+ BM-derived cells colocalized with the metastatic lesions (Fig. 2B). As observed in the LLC model, the micrometastases were avascular and lacked $CD31^+$ vessels (Fig. 2C), whereas macrometastases were infiltrated by $CD31^+$ neovessels (Fig. 2D), which indicated that these lesions had undergone an angiogenic switch at this defined window. Histology revealed vessel-incorporated GFP^+ $CD31^+$ BM-derived endothelial cells (Fig. 2E). Further quantification showed that 11.7 ± 3.7% of vessels in the metastases contained incorporated GFP^+ BM-derived endothelial cells (Fig. 2F).

We have previously shown that the BM-derived endothelial cells are derived from progenitor cells defined by cell surface expression of vascular endothelial (VE)–cadherin, vascular endothelial growth factor receptor 2 (VEGFR2), dim CD31, and Prominin 1 and lack various hematopoietic markers (*8*). Analysis of micrometastases showed infiltration of BM-derived GFP^+ VE-cadherin$^+$ EPCs in the peripheral region of the lesions (Fig. 3A). FACS analysis of the lungs bearing micro-

Cancer Genome Research Center, Cold Spring Harbor Laboratory, Cold Spring Harbor, NY 11724, USA.

*To whom correspondence should be addressed. E-mail: mittal@cshl.edu

metastases showed a fivefold increase in BM-derived EPCs (GFP$^+$ VE-cadherin$^+$ CD31^{dim} CD11b$^-$), as compared with that of control normal lungs (198.5 ± 29.9 versus 37.3 ± 6.1, $P < 0.0001$) (Fig. 3, B and C). To determine the mechanism underlying EPC recruitment to the sites of neovascularization, we examined metastatic lesions for the expression of adhesion molecules. Nascent vessels confined to the metastatic lesions expressed higher levels of vascular cell adhesion molecule–1 (VCAM-1), and notably, EPCs expressed cognate receptors integrin $\alpha_4\beta_1$ (fig. S3, A, C, and D). Indeed, the presence of EPCs in the proximity of VCAM-1$^+$ vessels (fig. S3B) suggests that interactions between VCAM-1 and integrin $\alpha_4\beta_1$ mediate EPC recruitment, as observed previously for hematopoietic progenitors (*10*–*12*). Taken together, these results demonstrate that an angiogenic switch is associated with the progression of micrometastases to macrometastases, during which BM-derived EPCs are recruited to the metastatic foci and contribute luminally to the neovasculature in metastatic lesions.

To explore whether BM-derived EPCs are required for the progression of micrometastasis to macrometastasis, we studied the effects of loss of EPC function in vivo. We focused on the Id1 transcription factor because Id1 knockout mice (Id1$^{+/-}$ Id3$^{-/-}$) exhibit impaired tumor growth, because of BM-associated angiogenic defects (*13*, *14*). Notably, in response to a tumor challenge, we detected a ~2.5-fold up-regulation in Id1 mRNA expression in the BM cells (Fig. 3D). More important, Id1 expression was confined to EPCs and was not seen in other BM cells upon tumor challenge (Fig. 3E and fig. S4A), which suggests that Id1 may be critical for EPC function in the context of metastasis. To dissect the role of Id1 in EPC-mediated progression of metastatic lesions, we used a lentiviral-based synthetic microRNA (miR-30)–based short hairpin RNA (shRNA) expression system whose activity could be induced by doxycycline (Dox) to target Id1 expression in vivo (fig. S5). This approach allowed us to generate acute Id1 suppression in the BM selectively during metastasis progression without compromising the contribution of BM-derived endothelial cells to the growth of primary tumor, which cannot be achieved in the Id1 knockout

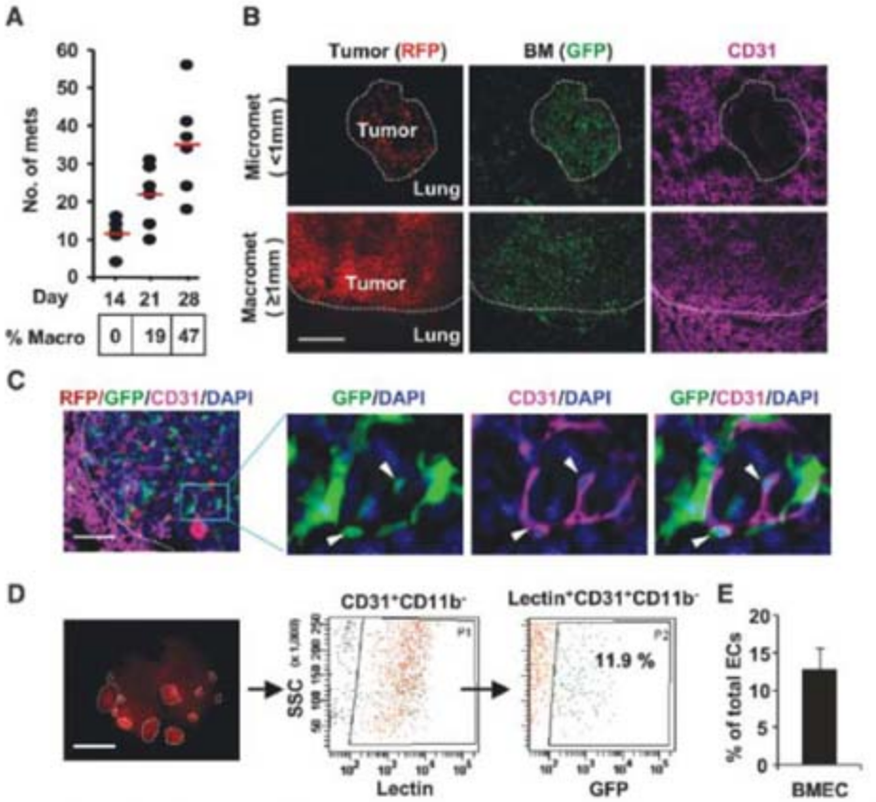

Fig. 1. BM-derived endothelial cells contribute to the angiogenic switch in mice transplanted with LLC cells. (**A**) Quantification of total metastatic colonies in the lung after tumor inoculation. The percentage of macrometastases (≥1 mm in diameter) is indicated; $n = 6$ per time point. (**B**) Microscopy showing avascular micrometastases (top, day 14) and a vascularized macrometastasis (bottom, day 21). Blood vessels were detected by CD31-specific antibody. Dotted line separates the host tissue from the tumor in this and subsequent figures. Scale bar, 200 μm. (**C**) Vessel incorporated BM-derived endothelial cells (GFP$^+$ CD31$^+$, arrows) in RFP$^+$ macrometastasis stained with DAPI (4′,6′-diamidino-2-phenylindole). Scale bar, 100 μm. (**D**) Scatter plot depicting contribution of BM-derived endothelial cells in functional vessels of microdissected macrometastasis. P1 gate, total functional endothelial cells (CD31$^+$ Isolectin$^+$ CD11b$^-$); P2 gate, BM-derived endothelial cells (GFP$^+$ CD31$^+$ Isolectin$^+$ CD11b$^-$). Results obtained by analyzing 1×10^6 cells. SSC, side-scatter values. (**E**) Quantification of FACS analysis showing percentage of BM-derived endothelial cells (BMEC) in vessels of macrometastases. Data are means ± SD; $n = 5$ per group.

Fig. 2. BM-derived endothelial cells contribute to the angiogenic switch in MMTV-PyMT mice, a model of spontaneous metastasis. (**A** and **B**) Representative lung images showing metastasis progression (weeks 12 to 16) in MMTV-PyMT mice reconstituted with GFP$^+$ BM; $n = 20$ mice. Scale bar, 5 mm. CD31 staining of pulmonary micrometastases (**C**) and macrometastases (**D**) in MMTV-PyMT mice. Dotted line, as in Fig. 1. Scale bar, 200 μm. (**E**) Incorporated BM-derived endothelial cells (GFP$^+$ CD31$^+$, arrows) in the vessels in macrometastases in MMTV-PyMT mice. Scale bar, 20 μm. (**F**) Quantification of vessels containing GFP$^+$ BM-derived endothelial cells. Data are means ± SD. (A total of 2418 vessels were counted; $n = 38$ metastases derived from six animals).

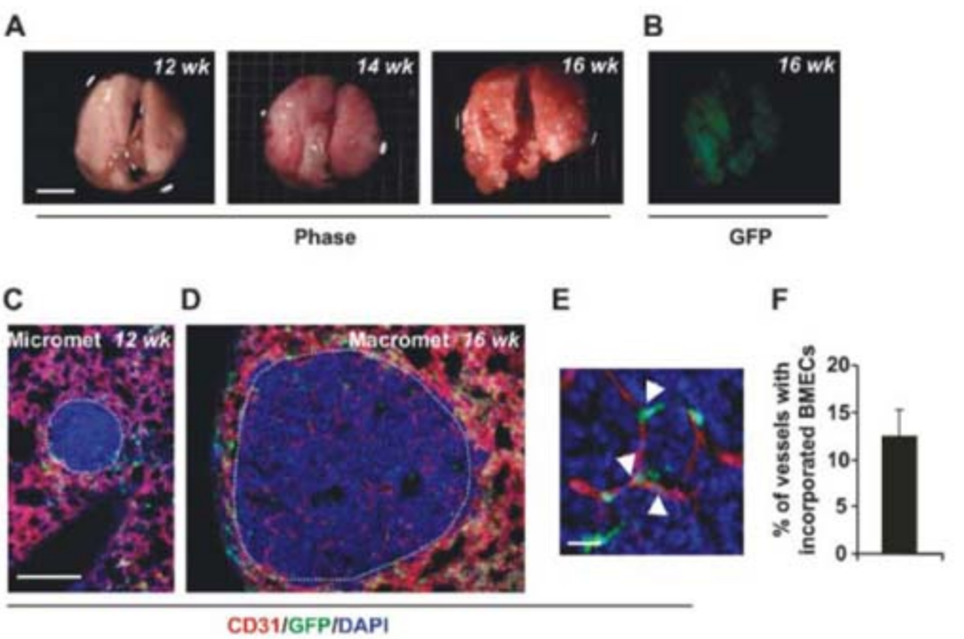

mice. An effective shRNA that reduced endogenous Id1 mRNA and protein levels (>95% reduction) (fig. S4, B and C) was cloned into a Dox–inducible expression vector (fig. S4D). The specific and tight regulation of Id1 shRNA expression by the inducible system was established in the context of genomic integration in vitro (fig. S4, E and F).

To determine the impact of Id1 gene suppression on metastasis progression, lineage negative (Lin^-) cells derived from ROSA26 reverse tetracycline transactivator (rtTA) transgenic mice (*15*) were transduced ex vivo with lentivirus expressing either the Id1 shRNA or the nonspecific shRNA and transplanted into lethally irradiated recipient mice according to the scheme in fig. S5A. No significant change in primary tumor growth was observed in these animals (fig. S5B) before Dox administration. However, Dox-mediated induction of Id1 shRNA expression substantially reduced the total number of metastases in animals having an Id1 shRNA bone marrow transplant (BMT) (28 ± 6 in –Dox versus 8 ± 5 in +Dox) as compared with nonspecific shRNA-

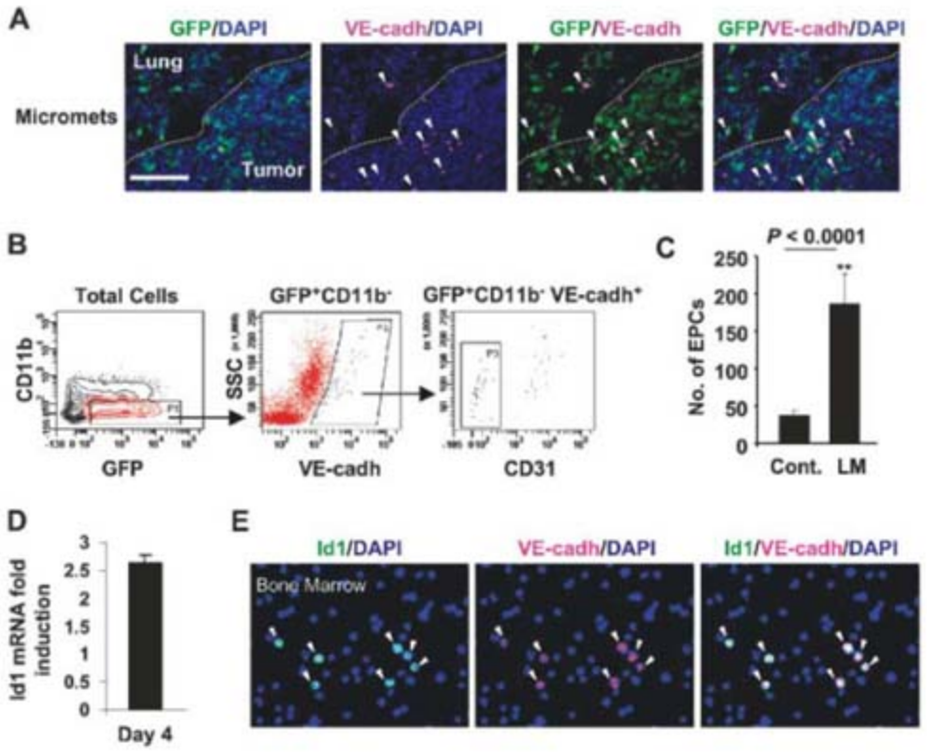

Fig. 3. $Id1^+$ EPCs contribute to early metastatic lesions in mice. (**A**) Microscopy showing recruitment of BM-derived EPCs (GFP^+ VE-$cadherin^+$) at the periphery of LLC micrometastases in the lung (day 14). Dotted line is as in Fig. 1. Scale bar, 100 μm. (**B**) FACS analysis of EPC recruitment from lungs bearing micrometastases (day 14). Of the total lung cells, BM-derived non-hematopoietic cells (GFP^+ $CD11b^-$) cells were gated (P1), from which BM-derived total endothelial cells (GFP^+ VE-$cadherin^+$ $CD11b^-$) were determined (P2). A subset of these cells are EPCs (GFP^+ VE-$cadherin^+$ $CD31^{dim}$ $CD11b^-$) represented by (P3). (**C**) Quantification of FACS analysis showing EPC recruitment to metastatic lungs (LM) (day 14) versus control lungs (Cont.). Results are from analysis of 1×10^6 cells per animal. Means ± SD; $n = 5$ per group. (**D**) Quantitative RT-PCR analysis showing Id1 mRNA levels in Lin^- BM cells harvested from tumor challenged versus unchallenged mice. (**E**) Microscopy showing that Id1 expression is confined to VE-$cadherin^+$ EPCs in tumor-challenged BM (arrows).

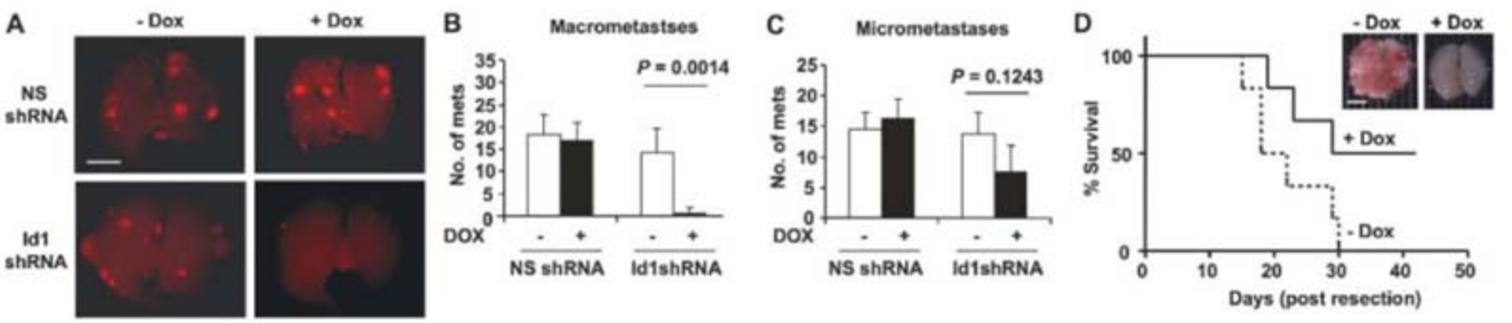

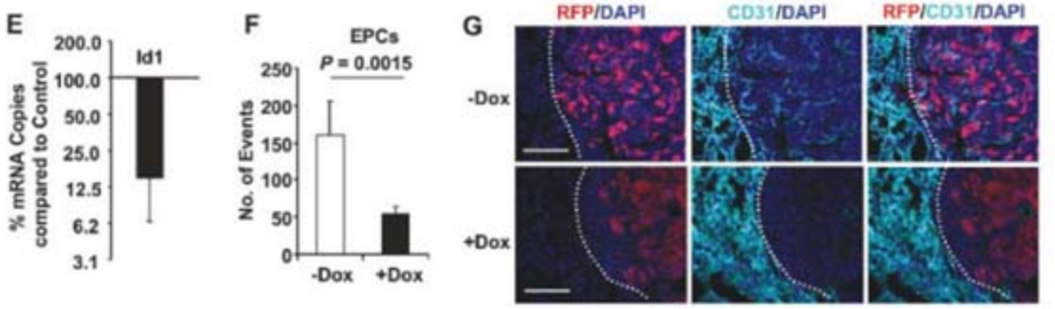

Fig. 4. Inducible RNAi-mediated suppression of Id1 in the BM impairs the formation of pulmonary macrometastases in mice. (**A**) Microscopy showing RFP^+ pulmonary metastases (day 28) in mice with BMT of nonspecific shRNA (top) or Id1 shRNA (bottom) in the absence (–Dox) or presence (+Dox) of Dox. Scale bar, 5 mm. (**B** and **C**) Quantification of macrometastases (≥1 mm in diameter) and micrometastases (<1 mm in diameter) in the lungs. Data are means ± SD; $n = 10$ per group. (**D**) Survival curve comparing untreated (–Dox) and treated (+Dox) Id1 shRNA–BMT mice. (Insets) Representative lungs isolated from –Dox (day 30 post resection) and +Dox (day 42 post resection) mice. Scale bar, 5 mm. (**E**) Quantitative RT-PCR analysis showing Id1 mRNA levels in the BM harvested from the treated (+Dox) versus untreated (–Dox) Id1 shRNA–BMT mice. Data are means ± SD; $n = 10$ per group. (**F**) FACS analysis of the circulating EPCs (c-kit^+VEGFR2$^+$$CD11b^-$) in peripheral blood of untreated (–Dox) and treated (+Dox) Id1 shRNA–BMT mice (day 21). A total of 1×10^6 cells were analyzed per animal. Data are means ± SD; $n = 10$ per group. Note, that because FACS did not detect GFP expression, circulating EPC levels in the peripheral blood were determined in the context of c-Kit expression as described (*21*). (**G**) CD31 staining showing the vascularization defects in pulmonary metastases in treated (+Dox) versus untreated (–Dox) Id1 shRNA–BMT animals (day 28). Scale bar, 100 μm. Dotted line separates the RFP^+ metastases from the host lung.

BMT animals [32 ± 7 in –Dox versus 33 ± 6 in +Dox (Fig. 4A)]. This reduction was due primarily to a decrease in macrometastases in Dox-treated Id1 shRNA–BMT animals [13.8 ± 6.1 in –Dox versus 0.6 ± 1.3 in +Dox, $P = 0.0014$ (Fig. 4B)]. No significant reduction in micrometastases was observed in the lungs of these animals (Fig. 4C), which suggested that the inducible Id1 suppression did not affect initial lung colonization by tumor cells, but impaired their progression into macrometastases. Furthermore, tumor-bearing Id1 shRNA–BMT mice treated with Dox outlived the untreated mice [$P = 0.0233$ (Fig. 4D)]. Necropsy revealed that the untreated mice had collapsed lungs containing numerous macrometastatic lesions (Fig. 4D, insert –Dox), which suggested that pulmonary macrometastasis was the main cause of death.

Inducible suppression of Id1 gene expression in vivo was confirmed by quantitative real-time polymerase chain reaction (RT-PCR), which showed a reduction in Id1 mRNA levels in the BM of the Dox-treated Id1 shRNA–BMT mice to one-fifth those of untreated mice (Fig. 4E). More important, conditional Id1 suppression resulted in reduction in the level of circulating EPCs (c-kit$^+$VEGFR2$^+$CD11b$^-$) to one-third the circulating EPCs in those without doxycycline (Fig. 4F). The reduction in EPCs was specific, as we detected no significant change in the levels of BM-derived hematopoietic cells, including B cells, T cells, and myeloid and VEGFR1$^+$ cells (figs. S6 to S8). Our data also suggest that a decrease in lymphocytes in resting Id1 knockout mice recently reported by Nimer and colleagues (*16*) was most likely due to developmental compensations associated with the knockout mice. Overall, our study provides evidence that BM-derived EPCs play a direct role in angiogenesis-mediated progression of metastatic lesions, but they have no effect on metastatic initiation, which is dependent on VEGFR1$^+$ cells. Notably, impaired mobilization of EPCs resulted in a dramatic reduction in vessel density in metastatic lesions in Dox-treated Id1 shRNA–BMT mice [22.2 ± 4.7% in –Dox versus 4.1 ± 2.9% in +Dox (Fig. 4G)]. Although we have observed that a reduction in the levels of circulating EPCs correlates with impaired angiogenesis, our study does not address whether local lung resident progenitors or dedifferentiation of committed hematopoietic cells also contribute to EPC population as reviewed in (*17*).

This study illustrates the critical role of EPCs as novel regulators of the angiogenic switch in metastatic progression and points to a direct role of Id1 in mediating EPC mobilization and recruitment. Although only 12% of the neovessels in the metastatic lesions showed luminal incorporation by BM-derived endothelial cells, it is noteworthy that blocking EPC mobilization caused severe angiogenesis inhibition and significantly impaired the formation of lethal macrometastases, which suggested that EPCs may have additional proangiogenic properties in mediating the angiogenic switch. Notably, gene expression analysis of FACS-purified EPCs from tumor tissue revealed up-regulation of a variety of key proangiogenic genes including growth factors, receptors, chemokines, and ECM modifiers (table S1). Together, these findings support the rationale for the antiangiogenic treatment of metastatic cancer and suggest that the efficacy of antiangiogenic inhibitors currently used in clinical trials, such as blocking antibodies to VEGF and VEGFR2, may be a consequence of directly targeting BM-derived EPCs, as well as the nascent tumor vasculature. This hypothesis is bolstered by studies that have shown that antiangiogenic drugs also suppress the mobilization and levels of EPCs (*18*). Given that BM-derived endothelial cells also contribute to vessels in humans (*19*, *20*) and that initial metastatic colonization has usually occurred by the time of the primary tumor diagnosis, our results suggest that targeting BM-derived EPCs, perhaps in combination with conventional chemotherapeutics, may provide a feasible therapeutic approach for cancer patients with lung metastases. It is important to note, however, that in the clinical setting it can sometimes take years for dormant micrometastases to progress to lethal micrometastases, a time course that is not recapitulated in our mouse models.

References and Notes

1. R. N. Kaplan *et al.*, *Nature* **438**, 820 (2005).
2. S. Hiratsuka, A. Watanabe, H. Aburatani, Y. Maru, *Nat. Cell Biol.* **8**, 1369 (2006).
3. J. L. Townson, A. F. Chambers, *Cell Cycle* **5**, 1744 (2006).
4. L. Holmgren, M. S. O'Reilly, J. Folkman, *Nat. Med.* **1**, 149 (1995).
5. G. N. Naumov, L. A. Akslen, J. Folkman, *Cell Cycle* **5**, 1779 (2006).
6. Materials and methods are available as supporting material on *Science* Online.
7. H. G. Kopp, C. A. Ramos, S. Rafii, *Curr. Opin. Hematol.* **13**, 175 (2006).
8. D. J. Nolan *et al.*, *Genes Dev.* **21**, 1546 (2007).
9. L. Laitinen, I. Virtanen, L. Saxen, *J. Histochem. Cytochem.* **35**, 55 (1987).
10. A. G. Arroyo, J. T. Yang, H. Rayburn, R. O. Hynes, *Cell* **85**, 997 (1996).
11. B. Garmy-Susini *et al.*, *J. Clin. Invest.* **115**, 1542 (2005).
12. H. Jin *et al.*, *J. Clin. Invest.* **116**, 652 (2006).
13. D. Lyden *et al.*, *Nat. Med.* **7**, 1194 (2001).
14. M. B. Ruzinova *et al.*, *Cancer Cell* **4**, 277 (2003).
15. K. Hochedlinger, Y. Yamada, C. Beard, R. Jaenisch, *Cell* **121**, 465 (2005).
16. V. Jankovic *et al.*, *Proc. Natl. Acad. Sci. U.S.A.* **104**, 1260 (2007).
17. G. A. Prindull, E. Fibach, *Exp. Hematol.* **35**, 691 (2007).
18. P. Beaudry *et al.*, *Clin. Cancer Res.* **11**, 3514 (2005).
19. B. A. Peters *et al.*, *Nat. Med.* **11**, 261 (2005).
20. S. Jiang *et al.*, *Proc. Natl. Acad. Sci. U.S.A.* **101**, 16891 (2004).
21. F. Bertolini, Y. Shaked, P. Mancuso, R. S. Kerbel, *Nat. Rev. Cancer* **6**, 835 (2006).

22. We thank R. Jaenisch, L. Eisenbach, R. Dickins, S. Elledge, R. Benezra, and D. Trono for reagents and R. Stephen for technical assistance. Supported by funds from the NIH, Robert I. Goldman Foundation, and the Berkowitch Foundation.

Supporting Online Material

www.sciencemag.org/cgi/content/full/319/5860/195/DC1
Materials and Methods
SOM Text
Figs. S1 to S8
Table S1
References

7 September 2007; accepted 28 November 2007
10.1126/science.1150224

Dendritic Cell–Induced Memory T Cell Activation in Nonlymphoid Tissues

Linda M. Wakim,[1] Jason Waithman,[1] Nico van Rooijen,[2] William R. Heath,[3]* Francis R. Carbone[1]*

Secondary lymphoid organs are dominant sites of T cell activation, although many T cells are subsequently retained within peripheral tissues. Currently, these nonlymphoid compartments are viewed as sites only of effector T cell function, without the involvement of renewed induction of immunity via the interactions with professional antigen-presenting cells. We describe a method of reactivation of herpes simplex virus to examine the stimulation of tissue-resident T cells during secondary challenge. The results revealed that memory CD8$^+$ T cell responses can be initiated within peripheral tissues through a tripartite interaction that includes CD4$^+$ T cells and recruited dendritic cells. These findings lend evidence for the existence of a sophisticated T cell response mechanism in extra-lymphoid tissues that can act to control localized infection.

The activation of T cells during localized infection takes place within the draining lymph nodes, where the bulk of T cell priming is thought to occur (*1*). However, peripheral nonlymphoid tissues harbor a sizable proportion of the overall T cell pool, primarily consisting of long-lived memory T cells (*2*, *3*). During infection, peripheral tissues invariably represent the first point of contact with a wide range of pathogens, with resident T cells considered as critical to local infection control (*4*). Indeed, it has been suggested that such sites should be viewed as an extension of the secondary lymphoid compartment, and the term effector-lymphoid tissue (ELT) has been used in their description (*5*). Nevertheless, the contribution of the individual components within the ELT

[1]Department of Microbiology and Immunology, University of Melbourne, Melbourne, Victoria 3010, Australia. [2]Faculty of Medicine, Department of Molecular Cell Biology, Vrije Universiteit, 1081 BT, Amsterdam, Netherlands. [3]Division of Immunology, Walter and Eliza Hall Institute of Medical Research, Melbourne, Victoria 3050, Australia.

*To whom correspondence should be addressed. E-mail: fcarbone@unimelb.edu.au (F.R.C.); heath@wehi.edu.au (W.R.H.)

and the nature of the local responses remain poorly defined. Furthermore, it is commonly assumed that peripheral responses occur solely through the elaboration of effector molecules in the absence of new lymphocyte proliferation (*6*, *7*). However, local expansion has been reported in certain situations (*8*), and it remains possible that dendritic cells (DCs) are involved because these cells are known to aid in memory T cell activation (*9*). Such DCs might be resident within peripheral tissues (*10*) or could derive from infiltrating monocytes in response to inflammation (*11*).

Transplantation of peripheral tissues containing T cells into naïve recipients provides one convenient means of studying local responses, because it permits identification of the memory cells originating from these nonlymphoid sites while allowing recruitment of other cells that may be critical for their optimal activation. We selected sensory dorsal root ganglia (DRGs) from mice that had been infected with herpes simplex virus (HSV) in their flank, because these tissues retain infiltrating T cells well after resolution of acute infection (*12*–*14*). In addition, these ganglia harbor HSV in a latent form, which is typically reactivated as a consequence of surgical extraction (*15*), providing an effective means of local virus challenge. Ganglia taken 20 and 40 days after infection had detectable numbers of virus-specific T cells and no infectious virus at the time of extraction (*13*). Excision and transplantation provided a robust level of virus reactivation over the course of 5 or 6 days (fig. S1). To track virus-specific T cells, we seeded mice (to be used as DRG donors before HSV infection) with low numbers of T cells from animals expressing transgenic T cell receptors specific for the class I–restricted immunodominant peptide of HSV glycoprotein B (gBT-I cells). Within two days of transplantation, the numbers of T cells in the DRGs fell sharply, in most cases to undetectable levels (Fig. 1, A and B) in a fashion similar to that observed recently (*16*). This decline was followed by a rise in specific T cell numbers, beginning around days 5 or 6 after transplantation (Fig. 1A). The peak in numbers of gBT-I cells at

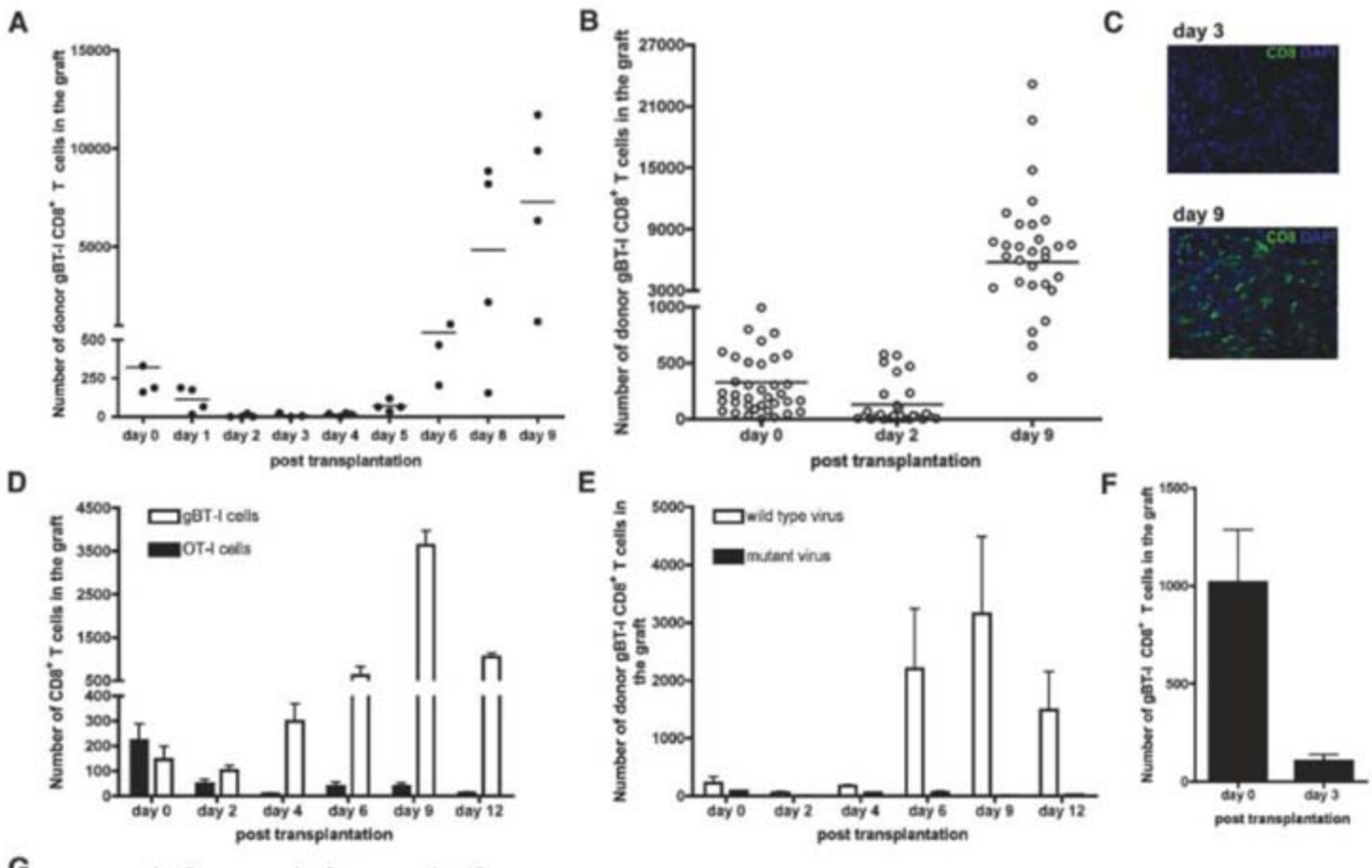

Fig. 1. Expansion of tissue-resident T cells after HSV reactivation. (**A** and **B**) B6 mice seeded with naïve gBT-I.CD45.1$^+$ CD8$^+$ T cells were infected with HSV. DRGs from these mice harboring latent HSV infection were transplanted under the kidney capsule of naïve recipients. Numbers of gBT-I.CD45.1$^+$ CD8$^+$ T cells within each graft were enumerated by flow cytometry. Data points represent individual mice from a single experiment (A) and pooled data from seven experiments (B). Horizontal bars indicate the mean. (**C**) Sections of the graft on days 3 and 9 after transplantation, stained for CD8 (green) and 4′,6′-diamidino-2-phenylindole (DAPI) (blue nuclear staining). (**D**) B6 mice were seeded with in vitro activated gBT-I cells and OT-I.CD45.1$^+$ CD8$^+$ T cells 4 days after HSV infection. Latently infected DRGs from these mice were transplanted under the kidney capsule of recipients. Grafts were recovered, and the numbers of gB-specific and ovalbumin-specific CD8$^+$ T cells were enumerated. Error bars represent the mean + SEM with five mice per group. (**E** and **F**) B6 mice seeded with naïve gBT-I.CD45.1$^+$ CD8$^+$ T cells were infected with either a thymidine kinase mutant HSV incapable of viral reactivation or the wild-type parental strain. Latently infected DRGs were transplanted under the kidney capsule of recipient mice and, at the indicated times, the number of gBT-I.CD45.1$^+$ CD8$^+$ T cells within the graft was determined. The data in (E) represent the mean + SEM with five mice per group. The decay in the number of donor gBT-I.CD45.1$^+$ CD8$^+$ T cells within the graft after transplantation of ganglia latently infected with a thymidine kinase mutant HSV is shown in (F). The data in (F) represent the mean + SEM with eight mice per group. (**G**) Donor gBT-I.CD45.1$^+$ CD8$^+$ T cells could not be detected within the spleen or kidney-draining lymph nodes (LN) of transplant recipients.

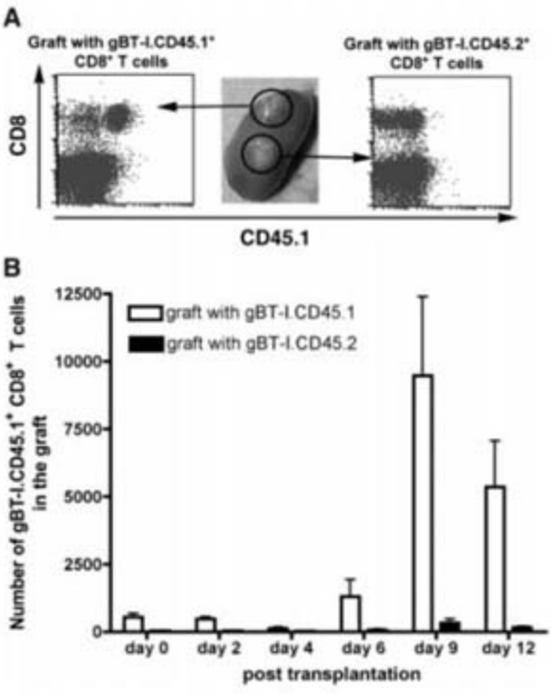

Fig. 2. Local reexpansion of resident memory CD8$^+$ T cells. B6 mice seeded with either gBT-I.CD45.1$^+$ or gBT-I.CD45.2$^+$ CD8$^+$ T cells were infected with HSV. Latent DRGs harboring these different T cells were harvested and placed in different locations under a single kidney capsule. (**A**) Plots of lymphocytes isolated from the grafts in different locations on day 9 after transplantation. (**B**) The numbers of gBT-I.CD45.1$^+$ CD8$^+$ T cells within both transplants, at the indicated times. The data represent the mean + SEM with seven mice per group.

day 9 represented a 17-fold increase over starting cell numbers and at least a 45-fold difference over those found at the day 2 post-transplant nadir (Fig. 1B). Histological comparison of ganglia at days 3 and 9 after transplantation (Fig. 1C) confirmed that these cells were undetectable in ganglia at the earlier time.

To verify that the expansion of T cells was antigen-specific, we seeded donor mice with activated gBT-I cells and control ovalbumin-specific T cells (OT-I cells). Because T cell infiltration of infected DRGs is nonspecific, reliant solely on an activated T cell phenotype (*13*), transplanted DRGs initially contained roughly equal numbers of HSV-specific gBT-I cells and irrelevant OT-I cells. However, only the gBT-I cells responded to reactivation (Fig. 1D). Infection with a thymidine kinase mutant virus, which does not reactivate from neuronal tissue (*17*), failed to drive any T cell expansion (Fig. 1E), showing that the response required overt infection. In contrast, reactivation was not necessary for the loss of the resident T cells (Fig. 1F), which

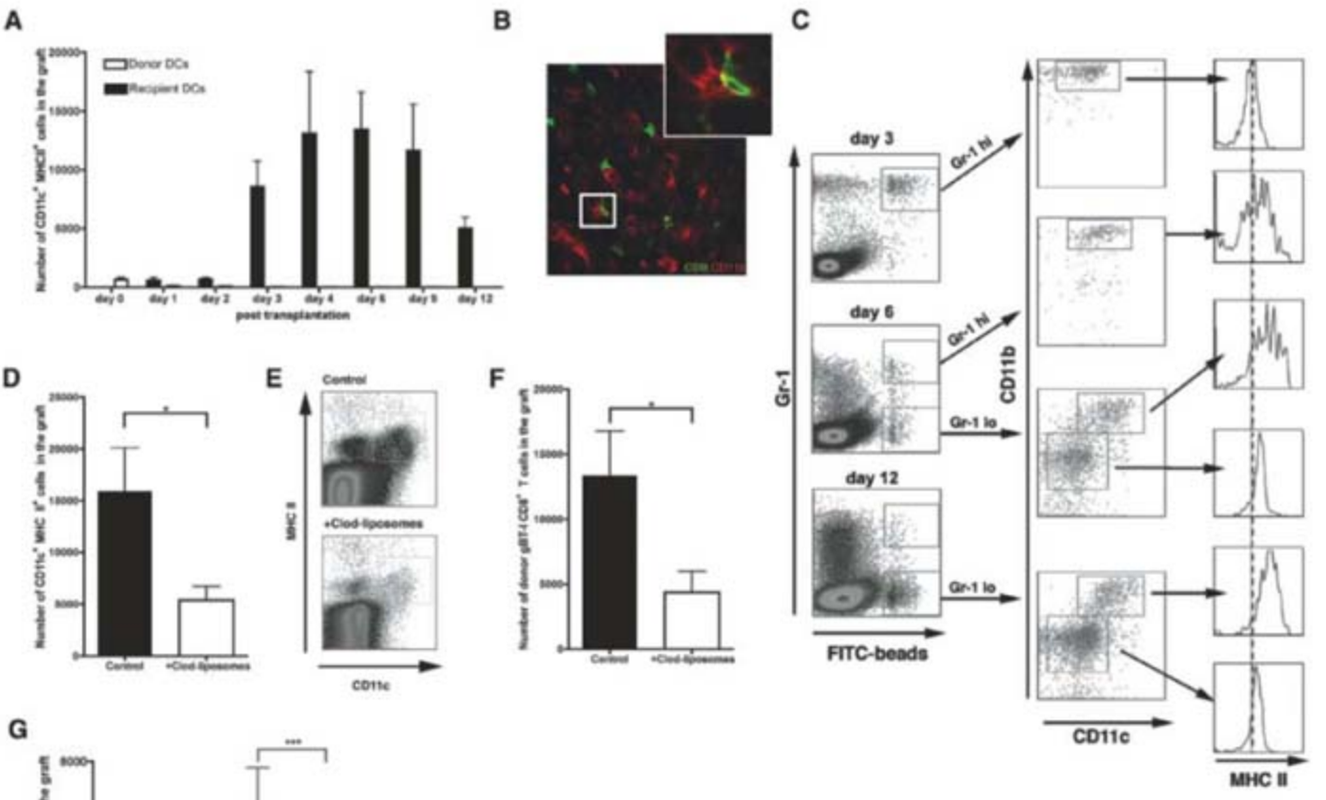

Fig. 3. Stimulation of resident memory CD8$^+$ T cells is dependent on recruited APCs. (**A**) Latently infected DRGs harvested from B6 donor mice were transplanted under the kidney capsule of CD45.1 recipients. The number of donor (CD45.1$^-$) and recipient (CD45.1$^+$) DCs (CD11c$^+$MHCII$^+$) was determined at the indicated times after transplantation. Error bars represent the mean + SEM with four mice per group. (**B**) Section of the graft on day 9 after transplantation, stained for CD8 (green) and CD11c (red). (**C**) Latent ganglia were grafted into recipient mice containing fluorescein isothiocyanate (FITC)–bead-labeled Gr-1^{hi} monocytes. The level of expression of Gr-1, CD11b, CD11c, and MHC II on the bead-positive cells in the grafts was determined at the indicated times. (**D** to **F**) Latent DRGs containing gBT-I.CD45.1$^+$ CD8$^+$ T cells were grafted into recipient mice depleted of circulating monocytes via the administration of clodronate-loaded liposomes (+Clod-liposomes). On day 9 after transplantation, the number of CD11c$^+$MHCII$^+$ cells [(D) and (E)] and gBT-I.CD45.1$^+$ CD8$^+$ T cells (F) in the graft was determined by flow cytometry. The data in (D) and (F) represent the mean + SEM with seven mice per group. *, $P = 0.0262$ in (D); *, $P = 0.0175$ in (F). (**G**) Latent DRGs from HSV-infected mice containing gBT-I.CD45.1$^+$ CD8$^+$ T cells were transplanted into either B6→B6 or bm3→B6 bone marrow chimeras. The number of gBT-I.CD45.1$^+$ CD8$^+$ T cells within the graft was enumerated at the time of transplantation (day 0) or 9 days after transplantation. The data represent the mean + SEM of the combined experiments shown in fig. S5. The difference between groups was determined to be statistically significant with a Mann-Whitney test. ***, $P = 0.0002$.

suggests that these cells were probably dying as a consequence of the surgical trauma. Finally, at all times examined, gBT-I cells were absent from the spleen and renal lymph nodes (Fig. 1G), arguing that the antigen-specific increase in T cell numbers resulted from local proliferation.

Despite our inability to detect circulating T cells, the numerical increase in gBT-I cells within the ganglia could nonetheless have resulted from stimulation within lymphoid tissues, followed by rapid recruitment into infected ganglia. To exclude this possibility, we infected two different groups of mice: one received HSV-specific cells tagged with the CD45.1 allelic marker (gBT-I.CD45.1 T cells) before infection, whereas the second group received CD45.2-bearing gBT-I cells (gBT-I.CD45.2 T cells). All mice were infected with HSV, and on resolution of primary infection, ganglia from each group were transplanted into distinct regions under the kidney capsule of a C57BL/6 (B6) recipient. The reisolated DRGs largely contained either one or the other T cell subset, showing little cross-migration of T cells between DRGs (Fig. 2, A and B). Such strict segregation would not be evident if T cell expansion occurred in lymphoid organs with subsequent infiltration of DRGs. Thus, the local response is maintained in each tissue, with few of the T cells released into the wider circulation.

Transplantation of ganglia into bone marrow irradiation chimeras suggested that parenchyma was not the dominant driver of T cell expansion. For these experiments, bm3 animals carrying the non–gBT-I cell–stimulating K^{bm3} major histocompatibility complex class I (MHC I) molecule (*13*) were reconstituted with B6 bone marrow. These B6→bm3 chimeras were then used as donors, because they permit gBT-I cell priming by B6 DCs and their subsequent infiltration into infected ganglia. A robust glycoprotein B (gB)–specific T cell expansion was measured in the transplanted B6→bm3 ganglia (fig. S2), despite infected neurons being of nonpresenting bm3 origin. Antigen-presenting cells (APCs), most likely DCs, were thus responsible for the effective T cell stimulation. Analysis of CD45.2-reactivating ganglia transplanted into CD45.1 recipients showed recruitment of substantial numbers of recipient-derived $CD11c^+$ cells after a 2-day delay (Fig. 3A). These cells expressed a range of DC markers (fig. S3) and were sometimes found in close proximity to $CD8^+$ cells (Fig. 3B).

DCs recruited into sites of inflammation are derived from a subset of circulating monocytes that develop into DCs once they enter peripheral tissues (*18*–*21*). To investigate whether such DCs were formed in reactivating DRGs, we took advantage of the finding that $Gr1^{hi}$ monocytes that convert into DCs can be labeled with fluorescent beads after eliminating an interfering noninfiltrating subset via the administration of clodronate-containing liposomes (*22*). Figure 3C shows that such bead-labeled cells mature in reactivating ganglia to a $Gr1^{lo}$ population containing $CD11b^{hi}CD11c^{hi}$ DCs expressing high levels of MHC II molecules. Similar recruitment of blood-derived DCs is seen after primary infection (fig. S4), and these cells are the likely source of the low number of persisting DCs found in the latent ganglia (Fig. 3A). To formally show monocyte-derived DC involvement in T cell expansion, we eliminated their precursors by repeatedly administering clodronate-containing liposomes after transplantation (*23*). Despite incomplete DC ablation (Fig. 3, D and E), treatment inhibited the level of T cell expansion (Fig. 3F). A contribution from other presenting cells during T cell stimulation may explain the residual expansion, although blood-derived APCs clearly make a substantial contribution to the observed response.

It was possible that the cells recruited from the circulation were driving T cell expansion solely by some indirect means rather than by direct antigen presentation. To exclude this possibility, we transplanted latent ganglia from HSV-infected B6 mice containing gBT-I cells into bm3→B6 bone marrow chimeras that contain DCs unable to stimulate the gBT-I cells. These chimeras suffered from a high degree of variability (fig. S5), although on average, T cell expansion was much reduced in the bm3→B6 recipients as compared with that in the B6→B6 controls (Fig. 3G), which is consistent with a host APC contribution. Again, inhibition was incomplete, which suggests some contribution by donor APCs.

Donor $CD4^+$ T cells, which persist within latent ganglia, also expanded within transplanted

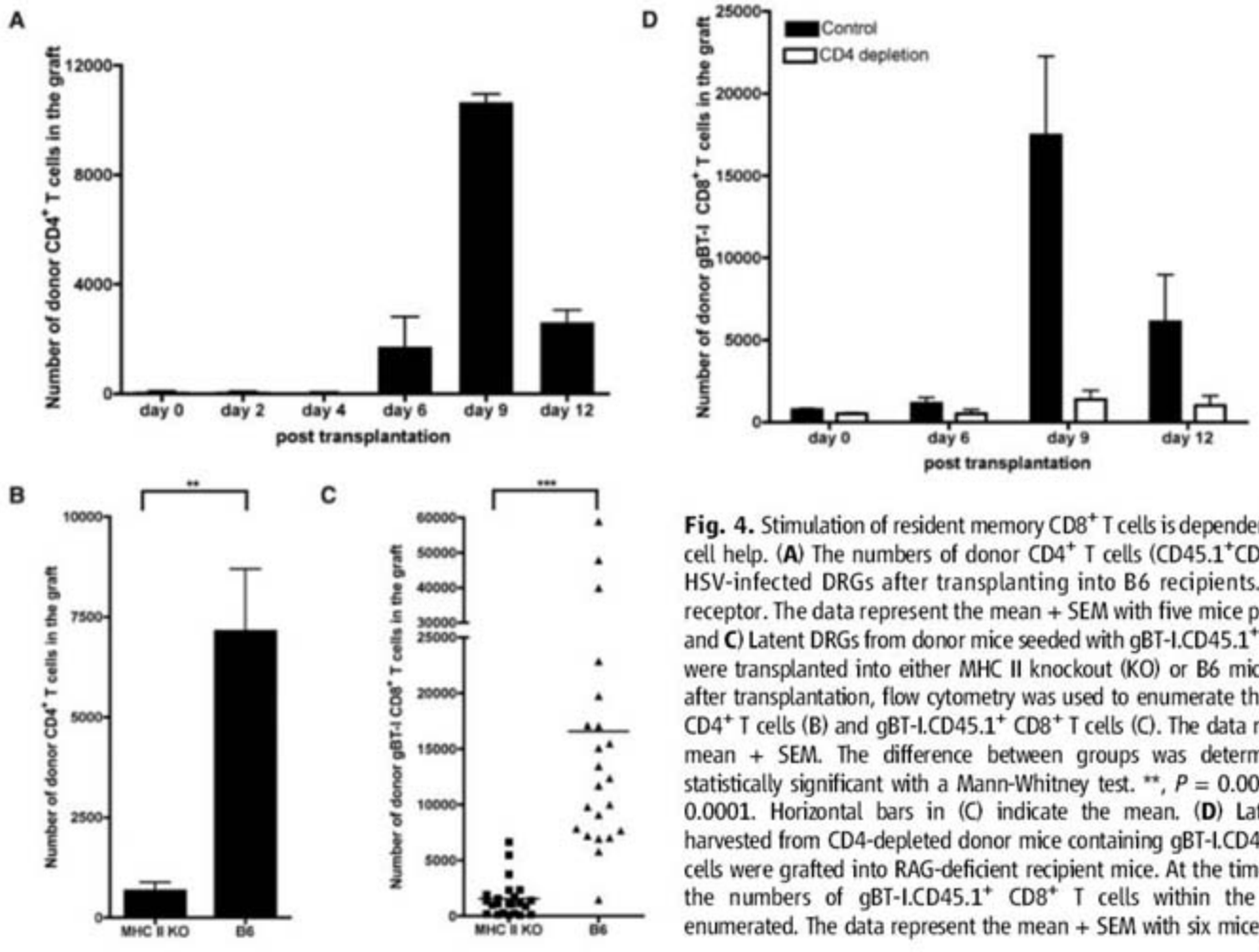

Fig. 4. Stimulation of resident memory $CD8^+$ T cells is dependent on $CD4^+$ T cell help. (**A**) The numbers of donor $CD4^+$ T cells ($CD45.1^+CD4^+\beta TCR^+$) in HSV-infected DRGs after transplanting into B6 recipients. TCR, T cell receptor. The data represent the mean + SEM with five mice per group. (**B** and **C**) Latent DRGs from donor mice seeded with gBT-I.$CD45.1^+$ $CD8^+$ T cells were transplanted into either MHC II knockout (KO) or B6 mice. On day 9 after transplantation, flow cytometry was used to enumerate the number of $CD4^+$ T cells (B) and gBT-I.$CD45.1^+$ $CD8^+$ T cells (C). The data represent the mean + SEM. The difference between groups was determined to be statistically significant with a Mann-Whitney test. **, $P = 0.0012$; ***, $P < 0.0001$. Horizontal bars in (C) indicate the mean. (**D**) Latent ganglia harvested from CD4-depleted donor mice containing gBT-I.$CD45.1^+$ $CD8^+$ T cells were grafted into RAG-deficient recipient mice. At the times indicated, the numbers of gBT-I.$CD45.1^+$ $CD8^+$ T cells within the graft were enumerated. The data represent the mean + SEM with six mice per group.

grafts after viral reactivation (Fig. 4A). This $CD4^+$ T cell proliferation was significantly reduced after transplantation into MHC II–deficient recipients as compared with such proliferation in B6 controls, implying a further role for blood-recruited APCs in local T cell activation (Fig. 4B). Unexpectedly, these MHC II–deficient recipients also showed attenuated expansion of DRG-resident gB-specific T cells (Fig. 4C), arguing that the local memory $CD8^+$ T cell activation was itself $CD4^+$ helper T cell–dependent. To confirm this finding, we grafted latent ganglia, taken from donor mice depleted of $CD4^+$ cells just before harvest, into recombination-activating gene (RAG)–deficient mice. Eliminating the $CD4^+$ T cells inhibited $CD8^+$ T cell expansion on secondary antigen encounter (Fig. 4D), although it did not compromise their intrinsic responsiveness because the cells were still able to produce interferon-γ after in vitro stimulation (fig. S6). The tissue-resident $CD4^+$ T cells alone were sufficient to elicit help because the RAG-deficient recipients are otherwise devoid of T cells. It should be noted that primary HSV-specific $CD8^+$ T cell activation is also helper T cell–dependent (*24*).

At face value, our results appear to contradict findings arguing that antigen encounter within nonlymphoid tissues does not result in local T cell proliferation (*6*, *7*). However, it may prove that such a lack of proliferation is only seen under certain conditions: for example, during activation of the T cells by parenchymal cells or where the virus is rapidly brought under control by resident T cells (*25*). As a consequence, we propose that local responses are tailored to the level of inflammation or the extent of infection. In settings with limited inflammation or where presentation of virus antigen is confined to the parenchyma, pure elaboration of effector function results in little overall T cell expansion. If, however, infection progresses and DC recruitment comes into play, then local T cells proliferate in situ. Finally, our results provide insight into HSV immune evasion during reactivation. Virus-specific $CD8^+$ T cells, thought capable of suppressing reactivation (*12*, *26*), are lost from latent ganglia in situations that promote virus recrudescence (*16*). The natural delay in DC infiltration and local T cell expansion affords a natural opportunity for transient HSV replication before the virus is once again brought under renewed immune control.

References and Notes

1. U. H. von Andrian, C. R. Mackay, *N. Engl. J. Med.* **343**, 1020 (2000).
2. R. L. Reinhardt, A. Khoruts, R. Merica, T. Zell, M. K. Jenkins, *Nature* **410**, 101 (2001).
3. D. Masopust, V. Vezys, A. L. Marzo, L. Lefrancois, *Science* **291**, 2413 (2001).
4. H. Hikono *et al.*, *Immunol. Rev.* **211**, 119 (2006).
5. N. van Panhuys, R. Perret, M. Prout, F. Ronchese, G. Le Gros, *Trends Immunol.* **26**, 242 (2005).
6. K. H. Ely *et al.*, *J. Immunol.* **170**, 1423 (2003).
7. N. L. Harris, V. Watt, F. Ronchese, G. Le Gros, *J. Exp. Med.* **195**, 317 (2002).
8. J. E. Moyron-Quiroz *et al.*, *Immunity* **25**, 643 (2006).
9. D. J. Zammit, L. S. Cauley, Q. M. Pham, L. Lefrancois, *Immunity* **22**, 561 (2005).
10. J. Banchereau, R. M. Steinman, *Nature* **392**, 245 (1998).
11. G. J. Randolph, K. Inaba, D. F. Robbiani, R. M. Steinman, W. A. Muller, *Immunity* **11**, 753 (1999).
12. T. Liu, K. M. Khanna, X. Chen, D. J. Fink, R. L. Hendricks, *J. Exp. Med.* **191**, 1459 (2000).
13. A. L. van Lint *et al.*, *J. Virol.* **79**, 14843 (2005).
14. Materials and methods are available as supporting material on *Science* Online.
15. J. G. Stevens, M. L. Cook, *Science* **173**, 843 (1971).
16. M. L. Freeman, B. S. Sheridan, R. H. Bonneau, R. L. Hendricks, *J. Immunol.* **179**, 322 (2007).
17. R. B. Tenser, K. A. Hay, W. A. Edris, *J. Virol.* **63**, 2861 (1989).
18. F. Tacke, G. J. Randolph, *Immunobiology* **211**, 609 (2006).
19. B. Leon, M. Lopez-Bravo, C. Ardavin, *Immunity* **26**, 519 (2007).
20. S. L. Bailey, B. Schreiner, E. J. McMahon, S. D. Miller, *Nat. Immunol.* **8**, 172 (2007).
21. F. Ginhoux *et al.*, *Nat. Immunol.* **7**, 265 (2006).
22. F. Tacke *et al.*, *J. Exp. Med.* **203**, 583 (2006).
23. M. Le Borgne *et al.*, *Immunity* **24**, 191 (2006).
24. S. R. Jennings, R. H. Bonneau, P. M. Smith, R. M. Wolcott, R. Chervenak, *Cell. Immunol.* **133**, 234 (1991).
25. R. J. Hogan *et al.*, *J. Exp. Med.* **193**, 981 (2001).
26. K. M. Khanna, R. H. Bonneau, P. R. Kinchington, R. L. Hendricks, *Immunity* **18**, 593 (2003).

27. The authors thank R. Allan, L. Eidsmo, T. Gebhardt, K. Shortman, J. Villadangos, W. Halford, and B. Gebhardt for helpful discussions. This work was supported by the Australian National Health and Medical Research Council and the Howard Hughes Medical Institute.

Supporting Online Material

www.sciencemag.org/cgi/content/full/319/5860/198/DC1
Materials and Methods
Figs. S1 to S6
References

17 October 2007; accepted 16 November 2007
10.1126/science.1151869

DNA Oxidation as Triggered by H3K9me2 Demethylation Drives Estrogen-Induced Gene Expression

Bruno Perillo,[1]*† Maria Neve Ombra,[1]* Alessandra Bertoni,[2] Concetta Cuozzo,[3] Silvana Sacchetti,[3] Annarita Sasso,[2] Lorenzo Chiariotti,[2] Antonio Malorni,[1] Ciro Abbondanza,[4] Enrico V. Avvedimento[2]†

Modifications at the N-terminal tails of nucleosomal histones are required for efficient transcription in vivo. We analyzed how H3 histone methylation and demethylation control expression of estrogen-responsive genes and show that a DNA-bound estrogen receptor directs transcription by participating in bending chromatin to contact the RNA polymerase II recruited to the promoter. This process is driven by receptor-targeted demethylation of H3 lysine 9 at both enhancer and promoter sites and is achieved by activation of resident LSD1 demethylase. Localized demethylation produces hydrogen peroxide, which modifies the surrounding DNA and recruits 8-oxoguanine–DNA glycosylase 1 and topoisomerase IIβ, triggering chromatin and DNA conformational changes that are essential for estrogen-induced transcription. Our data show a strategy that uses controlled DNA damage and repair to guide productive transcription.

Estrogens control growth and survival of hormone-sensitive cells by inducing expression of genes important for cell cycle progression (*1*) and apoptosis (*2*). The hormone 17β-estradiol (E2) regulates transcription of target genes by binding to cognate estrogen receptors (ERα and ERβ), which then bind with high affinity to estrogen-responsive DNA elements (EREs) (*3*–*5*). After hormone activation, ERα interacts with transcription co-activators that covalently modify histone proteins within nucleosomes (*6*) and contribute to the control of gene expression (*7*).

We examined the molecular mechanism by which specific methylation and demethylation of lysines in histone H3 governs hormone-induced transcription. We studied the anti-apoptotic *bcl-2* gene that contains two EREs in the coding region (*2*) and validated our findings with the prototypic E2-target gene *pS2* (*4*, *5*). With chromatin immunoprecipitation (ChIP) analysis, we assessed DNA binding of estrogen receptors in $ERα^+$ human breast cancer MCF-7 cells (*8*). Figure 1A shows that DNA fragments from the *bcl-2* ERE enhancer region (enh.) and the upstream promoter (pr.), which are 1.5 kb apart (*9*), are bound by ERα after treatment of quiescent cells with 10 nM E2 for 30 min.

Binding of both regions that reside on different fragments in sonicated DNA suggests loop formation between the *bcl-2* promoter and the ERE enhancer. To test this hypothesis, we used the chromosome conformation capture (3C) technique, which detects transcription-dependent chromatin looping caused by dynamic interactions between distant DNA segments. Briefly, after cross-linking of proteins with formaldehyde, we ligated restriction-digested DNA ends: DNA circles were generated by ligation of sites not contiguous on linear DNA (*10*). Figure 1B shows that the *bcl-2* promoter and enhancer were bridged (when co-amplified with divergent primers) only in chromatin harboring activated ERα (45 min of E2). The promoter-enhancer loop (or ligated DNA circle in the 3C) was lost by 60 min of E2 addition. Moreover, the receptor was essential in this process because DNA bending was inhibited by treatment with the antiestrogen ICI 182,780 that prevents receptor binding to the DNA (Fig. 1B).

Assembly of productive ERα transcription complex between 30 and 45 min (fig. S1) was marked by a substantial increase of dimethyl-Lys[4] in histone H3 (H3K4me2) on promoter and enhancer regions of *bcl-2* or *pS2* gene, whereas presence of H3K9me2 was appreciably found in hormone-starved cells or after 60 min of E2 treatment, concurrent with loss of receptor from chromatin (Fig. 1C and fig. S1). Binding of the K4-specific histone methyl transferase (HMT) SET9 (*11*) and the K9-specific HMT Suv39H1 (*12*) peaked at 30 min and 60 min of E2 exposure, respectively (Fig. 1C).

We show that H3K9me2 demethylation at the promoter and enhancer sites is achieved by the lysine-specific demethylase LSD1, known to relieve transcriptional repression by demethylating K9me and K9me2 (*13*). In fact, LSD1 was found to be present on chromatin in both the presence and the absence of estrogens (Fig. 2A), and disappearance of K9me2 was prevented by treatment of cells with the monoamine oxidase inhibitor pargyline (*13*) or by LSD1 knockdown with specific small interfering RNAs (siRNAs) (Fig. 2A).

LSD1 is also responsible for demethylation of H3K4me2 (*14*) observed 60 min after E2 addition and in hormone-starved cells, and this step is mediated by ERα (Fig. 2, B and C). In fact, in the ERα$^-$ MDA-231 breast cancer cells and in fibroblasts, H3K4 and H3K9 are both dimethylated at these sites (Fig. 2C), as also observed for surrounding chromatin in MCF-7 cells (fig. S2). Expression of the receptor in quiescent MDA-231 cells resulted in specific loss of H3K4me2 (Fig. 2C). Therefore, in the absence of hormone, ERα contacts and transiently activates LSD1, leading to local H3K4 demethylation. However, under these conditions, LSD1 is unable to trigger demethylation of H3K9me2 and transcription initiation. In fact, a transcriptionally unproductive cycle has been described, solely driven by the receptor (*5*).

Local demethylation of H3K9me2 was triggered by recruitment of liganded ERα to chromatin (*15*) that was also required for RNA polymerase II (pol II) assembly on the promoter (Fig. 2D). Inhibition of LSD1 activity in the presence of hormone prevented chromatin looping (Fig. 2E) and estrogen-dependent transcription (Fig. 2F), even though the receptor was bound to the EREs (Fig. 2A).

Demethylation by LSD1 of H3K9me2 is an oxidative process that results in the production of hydrogen peroxide (H_2O_2) (*16*). To explore the possibility that formation of H_2O_2 is a signal induced by estrogens to drive transcription initiation, we measured the main DNA product induced by the peroxide: the 8-oxo-guanine (8-oxo-G) that is removed by base excision repair (BER) enzymes (*17*). As shown in Fig. 3A, estrogens caused a rapid nuclear accumulation of 8-oxo-Gs in discrete foci, mimicked by treatment with H_2O_2 and inhibited by scavengers of reactive oxygen species (ROS), such as N-acetylcysteine (NAC). Production of 8-oxo-Gs was tightly linked to LSD1 activation (hence demethylation of H3K9me2) because it was inhibited by pargyline or LSD1 knockdown (Fig. 3, A to C). Furthermore, oxidation of Gs was dependent on ERα because the fluorescent signal was detected in

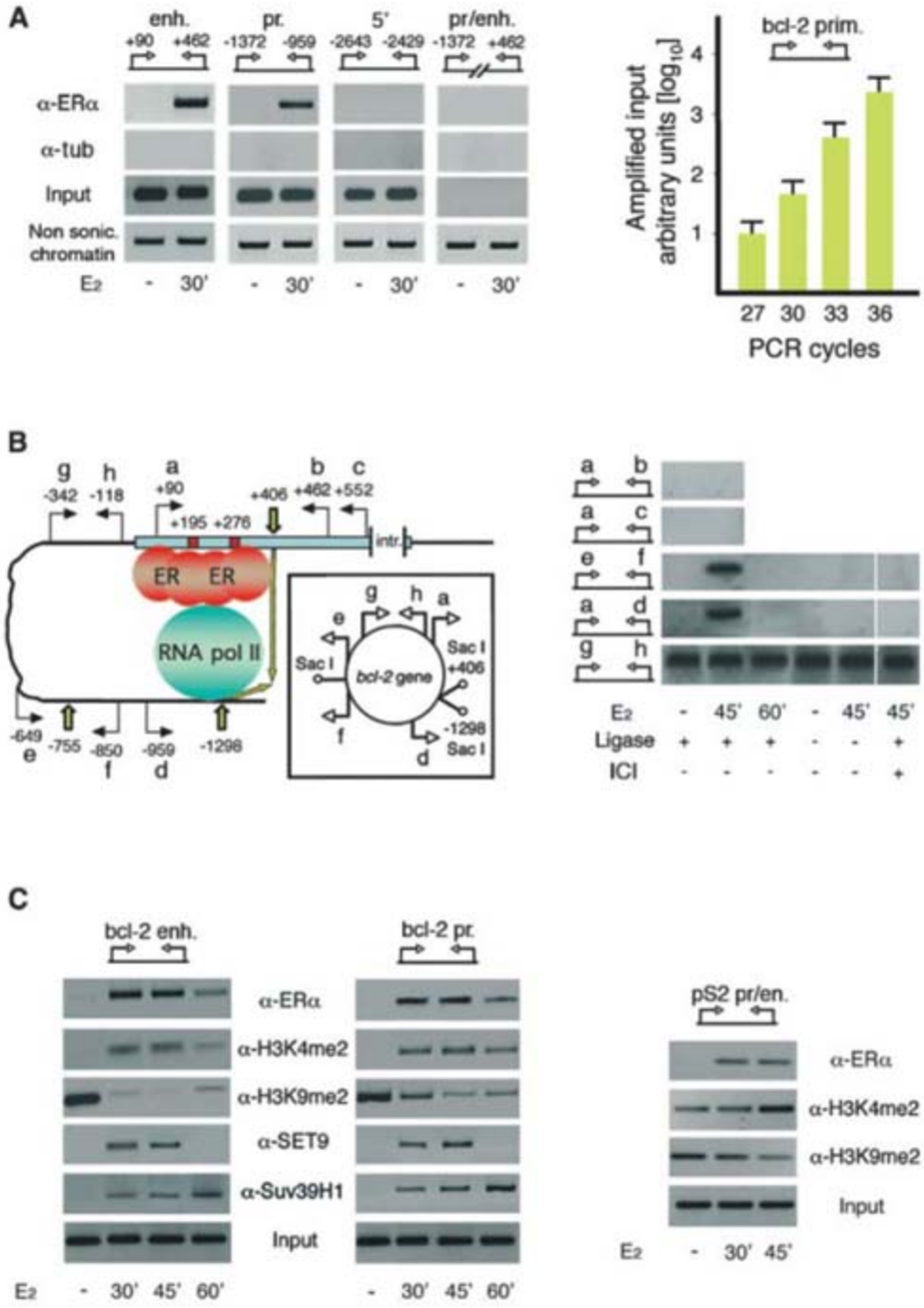

Fig. 1. Dynamics of estrogen-dependent chromatin modifications. (**A**) (Left) ChIP experiments performed with antibodies to ERα (α-ERα) or α-tubulin (α-tub) and with primers spanning the *bcl-2* gene. Primers are numbered relative to the translation start site (+1). enh., enhancer; pr., promoter; 5', upstream DNA. pr/enh., DNA including promoter and enhancer. Input, DNA extracted from sonicated (sonic.) chromatin before immunoprecipitation and used to quantify PCR reactions at different cycles and with different primer (prim.) pairs (right). Error bars indicate SEM. (**B**) (Left) Simplified structure of *bcl-2* gene showing the boxed coding region with EREs (red). intr., intron. *Sac I* restriction sites (yellow arrows) and primers used for PCRs in 3C experiments (thin arrows) are reported. The square box includes the circle generated by DNA ligation in the 3C. (Right) PCRs performed with divergent (a to d) or convergent (e and f) primers. The a-d (655 bp) or the e-f (202 bp) bands were absent in amplifications realized on *Sac I*–digested naked DNA. (**C**) Kinetic ChIP experiments realized on cells stimulated for 30, 45, and 60 min with 10 nM E2.

[1]Istituto di Scienze dell'Alimentazione, Consiglio Nazionale delle Ricerche (C.N.R.), 83100 Avellino, Italy. [2]Dipartimento di Biologia e Patologia Cellulare e Molecolare "L. Califano," Università degli Studi "Federico II," 80131 Naples, Italy. [3]Naples Oncogenomic Center, Centro di Ingegneria Genetica (CEINGE), Biotecnologie Avanzate, 80131 Naples, Italy. [4]Dipartimento di Patologia Generale, Seconda Università degli Studi di Napoli, 80138 Naples, Italy.

*These authors contributed equally to this paper.
†To whom correspondence should be addressed. E-mail: perillo@unina.it (B.P.); avvedim@unina.it (E.V.A.)

Fig. 2. Histone H3K9me2 demethylation by LSD1 is essential for DNA bending induced by activated ERα. (**A**) ChIP experiments on *bcl-2* and *pS2* promoters with indicated antibodies in cells exposed to E2 in the absence or presence of pargyline or control scrambled (scram.) RNAs or siRNAs targeting LSD1 coding region (LSD1-1). (**B**) Effect of pargyline addition on H3K4me2 demethylation, assessed by ChIP. (**C**) ChIPs showing presence of H3K4me2 and K9me2 in MDA-231 cells, expressing (ERα$^+$) or not (wild type, WT) ERα, or in human primary fibroblasts. (**D**) Effect of prevention of ERα binding to DNA by 1 μM ICI on LSD1 activation and RNA pol II recruitment to *bcl-2* promoter. (**E**) 3C assessing the effect of LSD1 inhibition on DNA loop formation. Primers used in PCRs are the same as in Fig. 1B. (**F**) Transcription of *bcl-2* and *pS2* genes measured by nuclear run on in cells stimulated with E2. β-actin was used as hormone-unresponsive control.

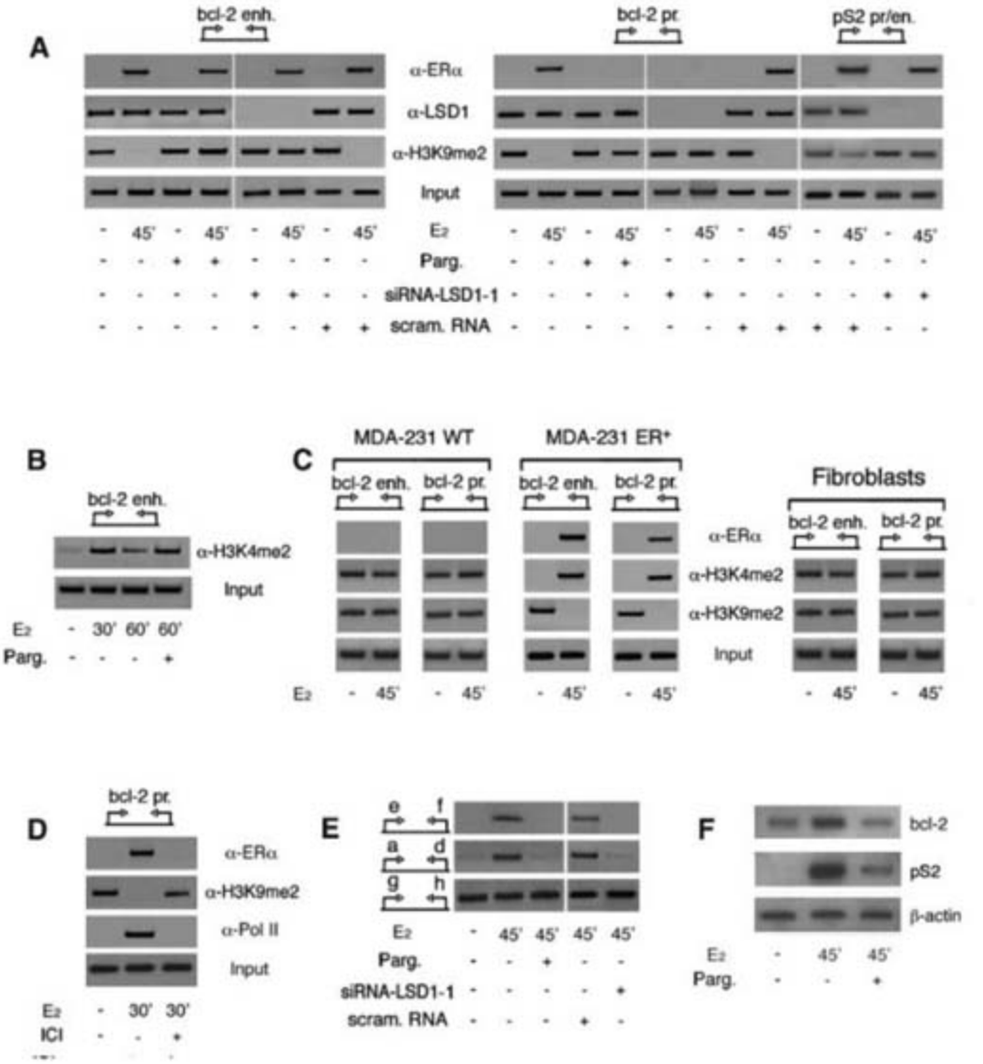

Fig. 3. Estrogens induce a burst of nuclear 8-oxo-Gs and recruitment of OGG1 and topoisomerase IIβ (Topo IIβ) to the promoter and ERE region of E2-responsive genes. (**A** to **C**) Immunofluorescence detection of 8-oxo-Gs by the fluorescein-tagged 8-oxo-G–binding protein. (A) Effect of pargyline or NAC addition to hormone-exposed cells. (B and C) Assessment of LSD1 knockdown, with two different siRNAs targeting the coding region (LSD1-1 and LSD1-5), on accumulation of 8-oxo-Gs. Scrambled (scram.) RNA was used as control. Red fluorescent protein (DsRed1-N1) was added to visualize transfected cells (B). (**D**) ChIP assays with reported antibodies. Topo I, topoisomerase I. The lower supplement shows the location of *bcl-2* DNA regions used in ChIP analysis (indicated by arrows pairs) The histogram on the right is from four different experiments. A representative gel with the *pS2* promoter is also shown. Error bars indicate SEM.

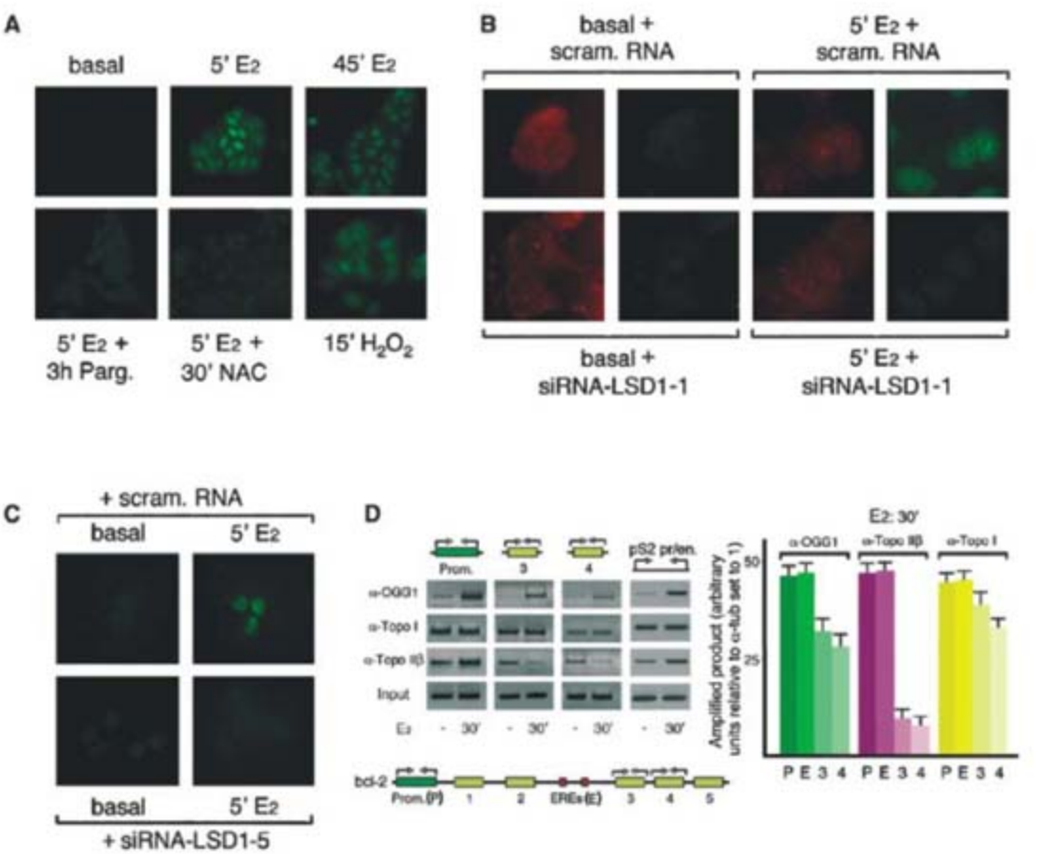

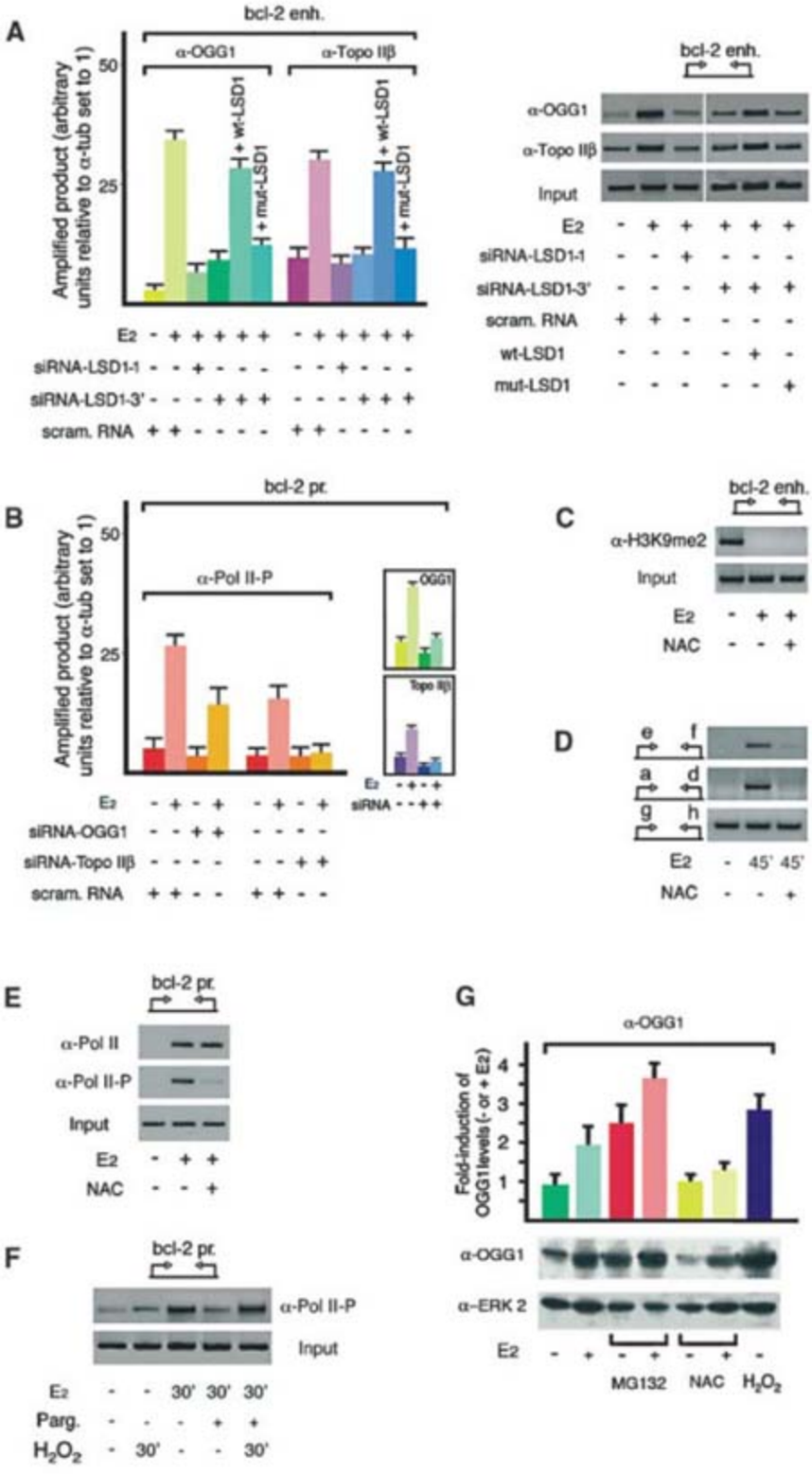

Fig. 4. E2-induced demethylation of H3K9me2 by LSD1 is necessary for OGG1 and topoisomerase IIβ recruitment and assembly of productive transcription initiation complex. (**A**) ChIPs showing OGG1 and topoisomerase IIβ recruitment to *bcl-2* EREs in cells treated with two different siRNAs, targeting the LSD1 coding (LSD1-1) or the 3′-untranslated region (LSD1-3′). scram., scrambled RNA. The rescue by exogenous wild-type (wt) or catalytically inactive (mut) LSD1 in siRNA-LSD1-3′–treated cells is also reported. (**B**) Effect of OGG1 or topoisomerase IIβ knockdown with specific siRNAs on accumulation of Ser^5-phosphorylated RNA pol II (Pol II-P) on *bcl-2* promoter, assessed by ChIP. (Insets) siRNA-dependent down-regulation of presence of each enzyme at the same site. The diagrams in (A) and (B) are from three independent experiments. Error bars indicate SEM. Effect of treatment with NAC (**C**) on H3K9me2 demethylation, (**D**) on formation of chromatin loop assessed by 3C, and (**E**) on accumulation of active RNA pol II (Pol II-P) on *bcl-2* promoter measured by ChIP. (**F**) ChIP assessing the role of H_2O_2 on assembly of transcribing RNA pol-II on *bcl-2* promoter. (**G**) Induction of OGG1 by E2, by inhibition of proteasome activity with MG132, and by ROS. The histogram shows the quantitative analysis from three experiments in which normalized OGG1 levels in the absence of E2 were set to 1. Error bars indicate SEM.

MDA-231 cells exclusively after receptor expression (fig. S3). This is noteworthy because 100 nM E2 treatment for 2 hours has been reported to induce accumulation of oxidized bases in the DNA of responsive cells in the absence of active receptor (*18*).

Because 8-oxo-Gs are specifically recognized and removed by the 8-oxo-guanine–DNA glycosylase 1 (OGG1) (*19*), we looked for OGG1 presence on *bcl-2* and *pS2* promoter and ERE regions. OGG1 engaged both sites concomitantly with recruitment of ERα to chromatin (Fig. 3D). On the other hand, E2 presence did not induce joining of the BER enzyme to the promoter of the androgen-sensitive, ERE⁻ *PSA* gene, notwithstanding the presence of LSD1 (*13*) (fig. S4). We also measured assembly to the complex of topoisomerases I and IIβ and found that, whereas the former bound chromatin independently of hormone treatment, topoisomerase IIβ, required for estrogen-dependent *pS2* transcription (*20*), was targeted to both promoters after E2 addition (Fig. 3D). Systematic analysis of chromatin downstream from *bcl-2* EREs revealed that OGG1 and topoisomerase IIβ accumulated preferentially at the promoter and ERE sites (Fig. 3D). Moreover, with suitable polymerase chain reactions (PCRs) and primer extension experiments, we found that the density of 8-oxo-Gs was higher on the noncoding strand within the region surrounding *bcl-2* EREs, although this observation might be due to the particular chromatin conformation at this site (fig. S5).

Recruitment of OGG1 and topoisomerase IIβ to the *bcl-2* and *pS2* promoter/EREs was dependent on E2-induced activation of LSD1 (Fig. 4A). Moreover, inhibition with siRNAs of topoisomerase IIβ appreciably reduced loading of the actively transcribing RNA pol II phosphorylated at Ser^5 on the promoter, whereas inhibition of OGG1 affected assembly of the phospho–RNA polymerase by 30 to 40% (Fig. 4B), indicating that transcription initiation was driven by targeting of both enzymes to these sites. The partial inhibition of transcription observed after OGG1 knockdown is not surprising in light of the evidence that inactivation in vivo of OGG1 does not induce accumulation of 8-oxo-Gs (*21*) because it can be replaced by other BER enzymes (*22*). Moreover, presence of 8-oxo-Gs is scarcely mutagenic because their removal is very efficient (*22*), and this may explain the effectiveness of coupling transcription initiation to repair of oxidative lesions.

Because it has been shown that topoisomerase II recognizes and repairs a single-stranded DNA break in double-stranded substrates (*23*), we propose that removal of the oxidized bases generates transient nicks that function as entry points for the enzyme. In this way, topoisomerase IIβ relaxes the DNA strands and favors chromatin bending to accommodate the transcription initiation complex.

ROS contribute to assembly of the RNA pol II complex. In fact, treatment of E2-stimulated

cells with NAC that did not prevent H3K9me2 demethylation (Fig. 4C) inhibited chromatin bending (Fig. 4D) and, hence, inhibited accumulation of active polymerase on promoter (Fig. 4E) and transcription (fig. S6). On the other hand, H_2O_2, besides enhancing per se recruitment of phosphorylated RNA pol II, also restored its E2-dependent promoter assembly in cells with pargyline added (Fig. 4F). Therefore, ERα plays a pivotal role in directing the oxidative signal to the promoter. Subsequently, OGG1 and topoisomerase IIβ (but with different efficiencies) are recruited to the promoter after peroxide accumulation; in the absence of hormone, however, their targeting is dispersed throughout chromatin, without the selective gradient imposed by bound receptor: H_2O_2 does not substitute for ERα (fig. S6).

Estrogens induce high OGG1 protein levels, and this induction is prevented by NAC or mimicked by H_2O_2 (Fig. 4G). Moreover, the proteasome inhibitor MG132 similarly induces high OGG1 levels (Fig. 4G). Because the proteasome catalytic subunit LMP2 assembles with the ERα complex and is essential for estrogen-induced transcription (*24*), we suggest that the oxidative burst, initiated by H3K9me2 demethylation, inhibits the proteasome activity and increases the intracellular concentration of OGG1. Thereafter, extinction of the demethylation-ROS wave leads to proteasome reactivation and degradation-release of the receptor (60 min after E2 stimulation) (Fig. 1C). Production of H_2O_2 is temporally limited and strictly localized (*25*).

H3K9me2 demethylation at the promoter and enhancer regions selectively marks the site where transcription initiation complex is assembled to drive the cycle of estrogen-induced gene expression (movie S1). Hence, the RNA pol II complex intimately associates with DNA repair enzymes to initiate hormone-dependent gene expression. Local lysine demethylation, with its associated oxidative burst, may indeed represent the initial signal at other inducible promoters.

References and Notes

1. S. F. Doisneau-Sixou *et al.*, *Endocr. Relat. Cancer* **10**, 179 (2003).
2. B. Perillo, A. Sasso, C. Abbondanza, G. Palumbo, *Mol. Cell. Biol.* **20**, 2890 (2000).
3. D. J. Mangelsdorf *et al.*, *Cell* **83**, 835 (1995).
4. Y. Shang, X. Hu, J. DiRenzo, M. A. Lazar, M. Brown, *Cell* **103**, 843 (2000).
5. R. Metivier *et al.*, *Cell* **115**, 751 (2003).
6. B. D. Strahl, C. D. Allis, *Nature* **403**, 41 (2000).
7. T. Jenuwein, C. D. Allis, *Science* **293**, 1074 (2001).
8. M. Shanmugam *et al.*, *Mol. Cell. Endocrinol.* **148**, 109 (1999).
9. R. L. Young, S. J. Korsmeyer, *Mol. Cell. Biol.* **13**, 3686 (1993).
10. A. Ansari, M. Hampsey, *Genes Dev.* **19**, 2969 (2005).
11. H. Wang *et al.*, *Mol. Cell* **8**, 1207 (2001).
12. O. Vaute, E. Nicolas, L. Vandel, D. Tronche, *Nucleic Acids Res.* **30**, 475 (2002).
13. E. Metzger *et al.*, *Nature* **437**, 436 (2005).
14. Y. Shi *et al.*, *Cell* **119**, 941 (2004).
15. I. Garcia-Bassets *et al.*, *Cell* **128**, 505 (2007).
16. F. Forneris, C. Binda, M. A. Vanoni, A. Mattevi, E. Battaglioli, *FEBS Lett.* **579**, 2203 (2005).
17. A. P. Grollman, M. Moriya, *Trends Genet.* **9**, 246 (1993).
18. N. Rajapakse, M. Butterworth, A. Kortenkamp, *Environ. Mol. Mutagen.* **45**, 397 (2005).
19. T. Roldan-Arjona *et al.*, *Proc. Natl. Acad. Sci. U.S.A.* **94**, 8016 (1997).
20. B.-G. Ju *et al.*, *Science* **312**, 1798 (2006).
21. M. T. Russo *et al.*, *Cancer Res.* **64**, 4411 (2004).
22. S. S. David, V. L. O'Shea, S. Kundu, *Nature* **447**, 941 (2007).
23. P. E. Kroeger, N. Osheroff, T. C. Rowe, *J. Biol. Chem.* **268**, 16449 (1993).
24. H. Zhang *et al.*, *EMBO J.* **25**, 4223 (2006).
25. Q. Felty *et al.*, *Biochemistry* **44**, 6900 (2005).

26. This work has been supported by the Ministero dell'Università e delle Ricerca (MUIR), RBNE0157EH, by Associazone Italiana per la Ricerca sul Cancro (AIRC), and by Federazione Italiana per la Ricerca sul Cancro (FIRC), NOGEC (Naples Oncogenomic Center), CEINGE. We are grateful to the memory of G. Salvatore, S. Varrone, and J. Guardiola.

Supporting Online Material

www.sciencemag.org/cgi/content/full/319/5860/202/DC1
Materials and Methods
Figs. S1 to S6

11 July 2007; accepted 19 November 2007
10.1126/science.1147674

Designed Protein-Protein Association

Dirk Grueninger, Nora Treiber, Mathias O. P. Ziegler, Jochen W. A. Koetter, Monika-Sarah Schulze, Georg E. Schulz*

The analysis of natural contact interfaces between protein subunits and between proteins has disclosed some general rules governing their association. We have applied these rules to produce a number of novel assemblies, demonstrating that a given protein can be engineered to form contacts at various points of its surface. Symmetry plays an important role because it defines the multiplicity of a designed contact and therefore the number of required mutations. Some of the proteins needed only a single side-chain alteration in order to associate to a higher-order complex. The mobility of the buried side chains has to be taken into account. Four assemblies have been structurally elucidated. Comparisons between the designed contacts and the results will provide useful guidelines for the development of future architectures.

In a cell, permanently associated proteins guarantee mechanical integrity, whereas transient associations are indispensable for metabolism and the regulation thereof. Our study focused on permanent contacts, many of which have been established at atomic resolution (*1*). Extensive analyses (*2*–*8*) showed that these contacts are diversified and that only a few rather general rules can be extracted: The contact area should be larger than about 600 Å^2, and the contacting surfaces should be complementary and predominantly nonpolar. Moreover, the contribution of hydrogen bonds and salt bridges at the contact rim is negligible. It is rather easy to destroy a contact by introducing a bulky side chain that is sterically incompatible. It is also comparatively simple to produce weak contacts randomly, as demonstrated by many examples using surface mutations to induce proteins to crystallize (*9*, *10*). However, the creation of a desired permanent contact is a more difficult task (*11*, *12*). Whereas establishing tight contacts by screening is well known from the antigen-antibody system that has also been applied in engineered complexes (*13*), the designed production of a tight novel contact has to our knowledge only been tried once, but the system failed to crystallize (*14*). However, in a number of cases, a given contact was modified by mutations (*15*–*18*). Here, we report the production and analysis of designed permanent *homo* oligomers of five proteins.

The importance of symmetry for the association of identical protein subunits was recognized some time ago (*19*). At the lowest symmetry level, a single contact patch has to provide the whole binding energy, which usually involves a large number of residues. As a consequence, the creation of such a contact requires numerous mutations. Because these contacts also generally form infinite helices that cannot be crystallized (Fig. 1A), we did not try to construct such an assembly. In contrast, a C_2-symmetric dimer (*20*) has a contact multiplicity of 2 and therefore requires only half the number of mutations. Moreover, it is usually globular and thus crystallizable (Fig. 1A). The same applies to higher symmetries. Associating two C_2-symmetric dimers along their molecular axes results in a D_2 tetramer with a contact multiplicity of 4 (*20*), whereas C_4 tetramer units give rise to D_4 octamers with a multiplicity of 8 (fig. S4). Obviously, the higher the symmetry, the fewer mutations are required, which explains the abundance of symmetry in natural *homo* oligomers.

Whereas the symmetry concerns the framework of a design, the actual production of *homo* oligomers was based on the exchange of side chains on the surface. We refrained from touching any main chains, because the corresponding structural changes are much more difficult to predict. Because contacts rigidify the involved

Institut für Organische Chemie und Biochemie, Albert-Ludwigs-Universität, Albertstrasse 21, 79104 Freiburg im Breisgau, Germany.

*To whom correspondence should be addressed. E-mail: georg.schulz@ocbc.uni-freiburg.de

side chains, the side-chain mobility describes part of the entropy reduction required for associations (*21*, *22*). Therefore, if possible, mobile side chains have to be identified and eliminated. Because the mobility of a side chain depends on its environment, its derivation from a single crystal structure is difficult. However, for the enzyme L-rhamnulose-1-phosphate aldolase (Rua) (*23*) 10 high-resolution crystal structures with different packing arrangements are available (*24*). Within this group, we compared the side-chain torsion angles χ_1 and χ_2 for each relevant residue, derived the angular spread in the 10 structures, and defined it as the side-chain mobility (*24*). The resulting mobility distribution over the surface contained surprisingly few hot spots (Fig. 1B). Unfortunately, it was not available when we designed our contacts, but we were able to use it for the assessment of an unexpected contact (see below).

The production of *homo* oligomers was tried at increasing levels of symmetry. In our attempt to make dimers of monomeric 6-phospho-β-galactosidase (Pga) (*25*), we enriched two crystal contacts across local twofold axes (Fig. 1, C and D) with nonpolar residues. In order to design tetramers from dimeric *O*-acetylserine sulfhydrylase (Oas) (*26*) and urocanase (Uro) (*27*), we aligned the dimers along their molecular axes and performed a one-dimensional search along the relative rotation angle (fig. S4), which yielded two suitable orientations for Oas and one for Uro (Fig. 1, E to G). The same was carried out for Rua (*23*) and its molecular fourfold axis (Fig. 1H and fig. S4B). The alignment along an axis allows three arrangements of the contacting partners, which we designated head-head, tail-tail, and head-tail (equals tail-head), defining an arbitrary end as the head. With Oas and Uro, we performed only a tail-tail association, whereas all three types of association were assayed with Rua. The D_8-symmetric tail-tail association of an engineered fragment of the mycobacterial porin MspA (Myp) (*28*) was fully unexpected.

Guided by one of the crystal contacts of Pga, we produced the two mutants Pga-A and Pga-B (*24*) that yielded about 3% dimer, as shown by size-exclusion chromatography (SEC) and dynamic light scattering (DLS) (Fig. 2A and Table 1). The Pga-A dimer was stable in rechromatography and in DLS. Crystallization attempts of the dimer fraction failed. The single dimer peak in the rechromatography (Fig. 2A) demonstrated that the obtained dimer was stable. Its structure is certainly similar to that shown in Fig. 1C because the contact is defined by the applied mutations. Following the other crystal contact, we constructed the two mutants Pga-C and Pga-D (*24*) that resulted in about 50% dimer (Fig. 2B).

Table 1. Protein-protein associations (*24*). Double prime entries indicate the same entry as in the line above; dash entries indicate that a small number of experiments were unsuccessful; none means no success in a very large number of experiments.

Protein	Native number of residues	Designed (observed) total contact area (Å²)	Newly introduced residues	Oligomer fraction (%)	Observed oligomer		
					SEC	DLS	Crystal
Pga-A	1 × 468	750	Phe_2	3	2	2	–
Pga-D	"	860	Phe_2, Trp, Met	56	2	2	none
Oas-A	2 × 303	1080	Asn, Thr, Ile, Val	6	4	4	–
Oas-C	"	1200	Asn_2, Ile, Leu_2	5	4	4	2
Uro-A	2 × 557	1760 (1570)	Ile_2, Ala	80	4	4	4
Rua-A	4 × 274	3060 (4040)	Phe	100	8	8	8
Rua-B	"	3250 (1970)	Tyr	100	8	8	8
Rua-D	"	1410	Trp, Ser	60	8	8	4
Rua-E	"	4470	Phe, Trp, Ser	100	poly	poly	fiber
Myp-A	8 × 184	(2480)	52-deletion	100	16	–	16

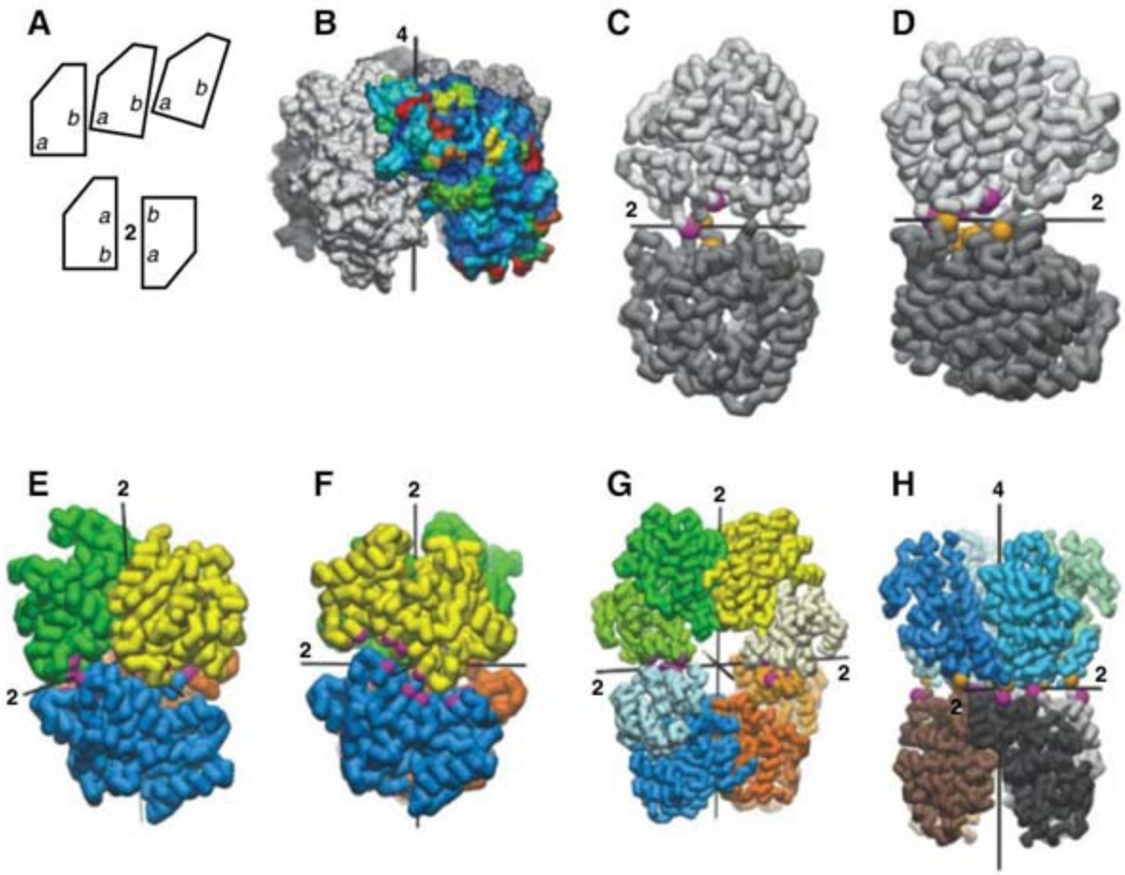

Fig. 1. Design of protein assemblies (*24*). The proteins in (C) to (H) are depicted as thick-lined Cα plots at various scales with mutated residues as colored spheres. (**A**) Sketch of an asymmetric interface between patches a and b, which, in general, gives rise to an infinite helix (top). A C_2-symmetric interface also between patches a and b doubles the numbers of contacts and forms a globular complex (bottom). Along the same lines, the reported D_2, D_4, and D_8 oligomers have 4-, 8-, and 16-fold contacts, respectively (fig. S4). (**B**) Side-chain mobility of the C_4-symmetric Rua, color-coded from 0° (blue) to 90° (red) angular spread in the torsion angles χ_1 and χ_2 (*24*). The C- and N-terminal domains are at the top and bottom, respectively. (**C**) Pga-A and -B designed in crystal contact a-a (*25*). (**D**) Pga-C and -D designed in crystal contact f-f (*25*). (**E**) Oas-A and -B planned as a D_2 tetramer at a rotation angle of 86° around a common molecular twofold axis (vertical). (**F**) Oas-C designed as a D_2 tetramer at an alternative rotation angle of 29°. (**G**) Designed D_2 tetramer of Uro-A around a common molecular twofold axis (vertical). The designed contact is between the NAD^+-binding domains (residues 142 to 343), which are given in lighter hues. (**H**) Designed octameric Rua-D with a head-head contact.

Both dimers were stable in rechromatography and in DLS (Table 1). However, neither of them yielded crystals, although a total of 24 mg of dimer was used in crystallization screens. Again, the dimer structure is most likely close to that of Fig. 1D.

On the basis of the molecular twofold axis of native Oas, we designed a D_2-symmetric tetramer by axis alignment and rotation angle adjustment. We chose a tail-tail association and constructed the three mutants Oas-A, -B, and -C (*24*) for association at rotation angles of 86° and 29° (Fig. 1, E and F). The obtained tetramer fractions ranged around 6% (Fig. 2C). For all three mutants, rechromatography resulted in pure tetramers, indicating that they were stable, and adopted structures similar to those of Fig. 1, E and F, as defined by the positions of the mutations. We produced a total of 35 mg of tetramers, which we used in various crystallization screens. These attempts yielded a number of initial crystals. Among them, one Oas-C crystal form grew to sizes suitable for an x-ray analysis. Unfortunately, it contained only dimers (Table 1 and tables S1 and S2).

With Uro we followed the same approach as with Oas. We chose a tail-tail association at the nicotinamide adenine dinucleotide (NAD^+) domains and found a suitable rotation angle of 65° (Fig. 1G). We introduced two small nonpolar side chains in place of two polar side chains and adjusted one nonpolar side chain in order to improve the fit. The resulting mutant, Uro-A, formed a tetramer fraction of 80% or more (Fig. 2D). The purified tetramer was stable in SEC and DLS (Table 1). It was crystallized, and the structure was established at high resolution (*24*). The actual tetramer followed the design in general terms (Fig. 3A). An analysis showed that the two observed contacts between the four NAD^+ domains were nearly identical, which confirmed that they were highly specific. However, the contact that was actually produced deviated from that which was designed by a relative shift of about 1.5 Å between the contact partners, and this shift was incompatible with the designed D_2 symmetry (Fig. 1G).

Apparently, the designed contact was so strong that this incompatibility caused a disruption of the associated proteins themselves rather than preventing contact formation. The observed new contact caused two of the four NAD^+ domains to be lifted off the protein cores, one in each dimer. This was unexpected because the native contact area between core and NAD^+ domain was much larger than the newly formed interface. As a consequence, the designed global D_2 symmetry broke up into four local C_2 symmetries, the axes of which were tilted by about 10° and displaced by about 2 Å in relation to the D_2 design (Fig. 3A). However, the tetramer kept a global C_2 symmetry defined by the twofold axis pointing toward the viewer.

Rua is a C_4-symmetric tetramer that is associated via its C-terminal domains, whereas its N-terminal domains dangle like tails into the solvent (Fig. 1H). We designed the D_4-symmetric tail-tail complexes Rua-A, Rua-B, and Rua-C with interdigitating tails and very large interfaces (Table 1 and table S1). Given the contact multiplicity of 8 for the design, single point mutations in Rua-A and -B and a double mutation in Rua-C sufficed to yield 100% octamer in SEC and DLS (Fig. 2E). Moreover, all three mutants crystallized. The high-resolution structures showed that Rua-A formed the designed octamer (Fig. 3B), whereas Rua-B formed an octamer with displaced fourfold axes (Fig. 3C) and Rua-C dissociated into tetramers during crystallization (*24*). Surprising-

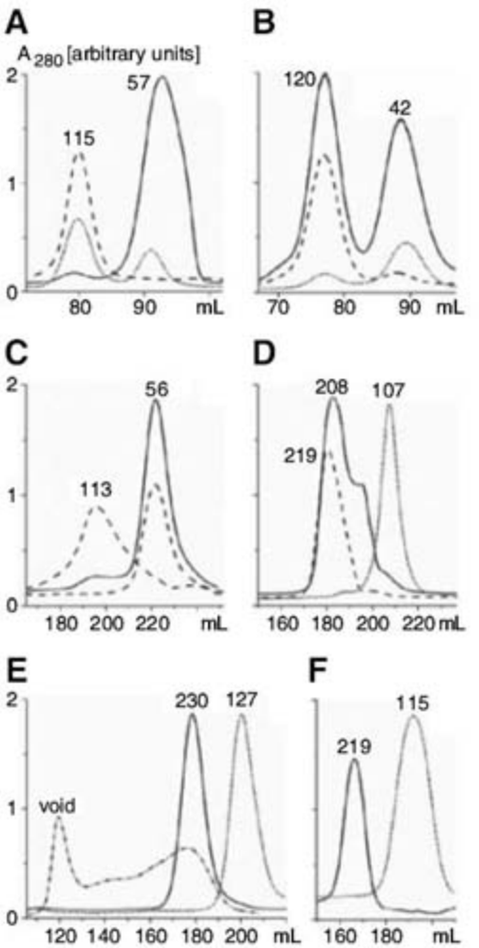

Fig. 2. SEC of modified and native proteins (*24*). Each peak is labeled with its apparent mass (kD). Initial runs are given in solid lines, rechromatographed fractions in dashed lines, and standards in dotted lines. (**A**) Pga-A with monomer and covalent-dimer standard (*24*). (**B**) Pga-D with monomer and covalent-dimer standard (*24*). (**C**) Oas-A with rechromatographed tetramer and dimer. (**D**) Uro-A with wild-type standard. (**E**) Rua-A and Rua-E (dash-dot line) with wild-type standard. The Rua-B and Rua-C distributions were identical to that of Rua-A. (**F**) Hexadecameric Myp-A with octameric Myp-B as standard (*24*).

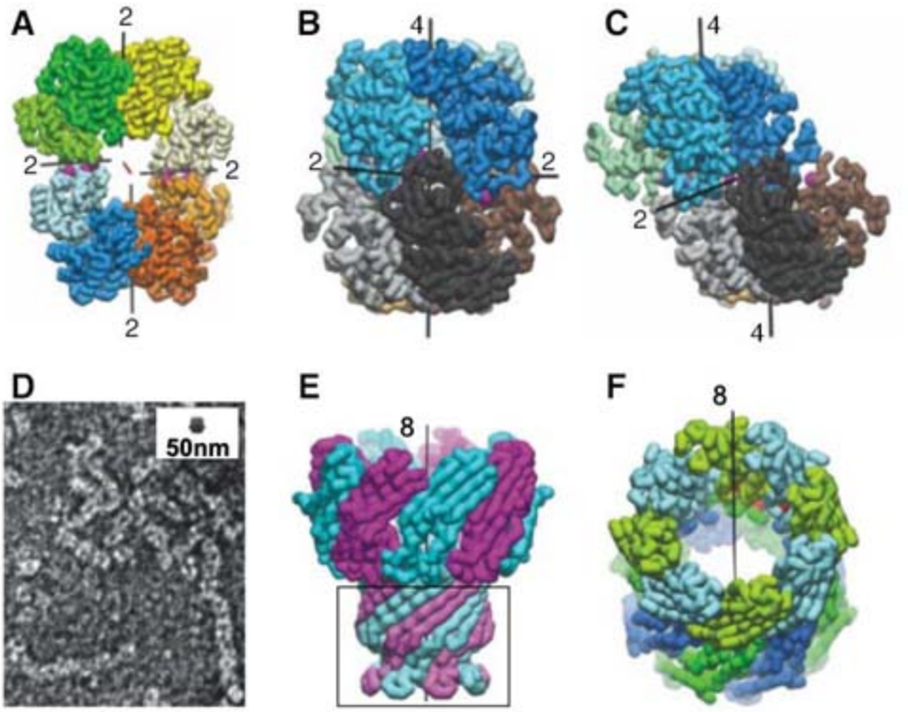

Fig. 3. Established oligomer structures (*24*). All mutations are marked by purple spheres. (**A**) Crystal structure of C_2-symmetric Uro-A showing the twofold molecular symmetry axis (red) and four local twofold axes relating the cores (darker colors) and the NAD^+ domains (light colors) to their counterparts. The interface between core and NAD^+ domains was broken in the lower left and upper right chains. (**B**) D_4-symmetric octamer Rua-A. (**C**) C_2-symmetric octamer Rua-B. (**D**) Negatively stained electron micrograph of Rua-E showing the fiber association and a Rua-A octamer (B) at the scale defined by the box edge. (**E**) Native mycobacterial porin (*28*). The encircled membrane-immersed part was deleted, giving rise to Myp-A. (**F**) D_8-symmetric association of two Myp-A molecules (top and bottom ring). The positions of the 52-residue deletions are marked by red spheres (fig. S1D).

ly, the observed contact area of the Rua-B octamer was only 60% of the planned one, and its symmetry was merely C_2 (Table 1). However, it turned out that its average side-chain mobility was 32° (angular spread) compared to 43° of the respective area of the designed contact (Fig. 1B). We therefore suggest that the unexpected contact is explained by a lesser reduction of the side-chain mobility, which amounts to a lesser entropy reduction on association.

Following the successful tail-tail association, we designed the D_4-symmetric head-head octamer Rua-D (Fig. 1H), which showed an octameric fraction of 60% confirmed by SEC and DLS (Table 1). However, the octamer fraction yielded crystals that contained only tetramers. In the next step, we combined the tail-tail mutant Rua-A with the head-head mutant Rua-D, resulting in the head-tail mutant Rua-E. With its contact surfaces at both ends of the fourfold axis, Rua-E was designed to form polymers. The polymerization was confirmed by SEC (Fig. 2E). Moreover, electron micrographs demonstrated that these polymers formed the expected fibers (Fig. 3D).

In a separate project, our aim was to produce a soluble carrier for large nonpolar molecules, such as organic catalysts, by removing the membrane-immersed part of the mycobacterial porin MspA (*28*). A 52-residue deletion yielded Myp-A (Fig. 3, E and F). To our surprise, Myp-A formed a soluble hexadecameric complex instead of the expected octameric ring. The hexadecamer was identified by SEC of Myp-A in comparison with the octameric mutant Myp-B (*24*) (Fig. 2F). Myp-A was crystallized and structurally elucidated, showing a D_8-symmetric double ring associated at the position of the deletion (Fig. 3F).

Reviewing our data, we find that the introduction of large nonpolar side chains is an efficient means of constructing permanent contacts. Our experience with Pga-A, -B, -C, and -D was that only a few of them were necessary to produce contacts with very low dissociation and association rates at 4°C under physiological conditions. However, such side chains tend to reduce the protein yield (*24*), presumably because of folding problems. Moreover, these easily obtained contacts were most likely not well defined because extensive crystallization attempts with Pga-C and Pga-D dimers never resulted in crystals (*24*), which is uncommon for rigid proteins but a well-known problem with, for instance, fusion proteins (*29*). We conclude that it is relatively easy to form complexes by introducing large nonpolar side chains, such as phenylalanines or tryptophans, but rather difficult to construct a rigid one.

In light of our observations with Pga, we introduced smaller nonpolar residues such as valines and isoleucines into dimeric Oas and dimeric Uro. The mutants of Oas were tetramers in solution and yielded small crystals. However, it was only possible to establish a crystal structure containing a native dimer. Along the same lines, the Rua-C and Rua-D octamers found at pH = 7.0 in SEC and DLS yielded crystals at this pH that contained only native tetramers (*24*) (Table 1).

Moreover, a second crystal form of Rua-A grown at pH = 4.9 in a low-polarity solvent contained only tetramers, although Rua-A formed 100% octamers in this pH range in SEC and DLS. The same applies for a second crystal form of Rua-B grown at pH = 5.0 in a low-polarity solvent. In both cases, the tetramers observed in the crystals were confirmed by SEC analyses at conditions close to those of the respective crystal forms. We conclude that the produced Rua octamers were strong enough in a mild physiological environment but failed to withstand harsher crystallization conditions in, for example, high salt concentrations, extreme pH values, or low-polarity solvents. Achieving stability in a broad range of unphysiological conditions is a more difficult task.

Symmetry is an important factor in protein association because it enhances the multiplicity of a single point mutation (Fig. 1A). The highly symmetric Rua octamers with a contact multiplicity of 8 form complexes after merely one or two mutations, and the 16-fold contact of Myp-A required no designed mutations at all. On the other hand, high multiplicity is hazardous for evolving organisms that need to avoid detrimental mutations. This may explain the rare occurrence of C_4 tetramers such as Rua compared to the ubiquitous D_2 tetramers, because C_4 can associate with eightfold contacts whereas the contacts in an association of D_2 symmetric partners are fourfold at most (fig. S4).

To what extent did our constructs follow the design? The answer depends on the details available. For all reported mutants (table S1), the designs (Fig. 1, C to H) were confirmed by the comparatively rough SEC and DLS data. Uro-A fitted the design at low but deviated at high resolution. The same applies for the Pga and Oas complexes, where the mutations most likely form the contacts. The available high resolution of Uro-A revealed that the novel contact deviated slightly from the design but was so strong that it caused the opening of a large, surprisingly weak interface within the protein partners (Fig. 3A). Rua-A followed the design except for a 3 Å shift that did not change the symmetry (Fig. 3B), whereas Rua-B formed an unexpected C_2 symmetric complex with a much smaller contact area (Fig. 3C). Because this Rua-B complex can be explained by the influence of the side-chain mobility, the mobility is probably an important factor in contact design. Our experiments demonstrate that the production of a particular contact is quite feasible, whereas high precision seems difficult to achieve.

References and Notes

1. H. M. Berman *et al.*, *Acta Crystallogr.* **D58**, 899 (2002).
2. C. Chothia, J. Janin, *Nature* **256**, 705 (1975).
3. L. Lo Conte, C. Chothia, J. Janin, *J. Mol. Biol.* **285**, 2177 (1999).
4. I. Halperin, B. Ma, H. Wolfson, R. Nussinov, *Proteins Struct. Funct. Genet.* **47**, 409 (2002).
5. I. M. A. Nooren, J. M. Thornton, *EMBO J.* **22**, 3486 (2003).
6. Y. Ofran, B. Rost, *J. Mol. Biol.* **325**, 377 (2003).
7. D. S. Cerutti, T. Jain, J. A. McCammon, *Protein Sci.* **15**, 1579 (2006).
8. E. Krissinel, K. Henrick, *J. Mol. Biol.* **372**, 774 (2007).
9. A. Pautsch, J. Vogt, K. Model, C. Siebold, G. E. Schulz, *Proteins Struct. Funct. Genet.* **34**, 167 (1999).
10. Z. S. Derewenda, *Structure* **12**, 529 (2004).
11. G. M. Whitesides, B. Grzybowski, *Science* **295**, 2418 (2002).
12. O. Schueler-Furman, C. Wang, P. Bradley, K. Misura, D. Baker, *Science* **310**, 638 (2005).
13. A. Schweizer *et al.*, *Structure* **15**, 625 (2007).
14. J. E. Padilla, C. Colovos, T. O. Yeates, *Proc. Natl. Acad. Sci. U.S.A.* **98**, 2217 (2001).
15. N. L. Ogihara *et al.*, *Proc. Natl. Acad. Sci. U.S.A.* **98**, 1404 (2001).
16. B. S. Chevalier *et al.*, *Mol. Cell* **10**, 895 (2002).
17. J. M. Shifman, S. L. Mayo, *J. Mol. Biol.* **323**, 417 (2002).
18. T. Kortemme *et al.*, *Nat. Struct. Mol. Biol.* **11**, 371 (2004).
19. J. Monod, J. Wyman, J.-P. Changeaux, *J. Mol. Biol.* **12**, 88 (1965).
20. Note that the bottom sketch of Fig. 1A is a special case of the top sketch forming a circle consisting of only two subunits. Similar circles with $n = 3, 4, \ldots$ subunits form the C_n symmetry that has here been used but not created (Fig. 3F). The symbol C_n refers to the symmetry around an n-fold axis. The contact multiplicity in the formation of a C_n circle is 1 per partner. The symbol D_n equals C_n plus n perpendicular twofold axes with all axes running through a common central point (fig. S4). The contact multiplicity in a D_n-symmetric association of two C_n partners is n per partner.
21. C. Cole, J. Warwicker, *Protein Sci.* **11**, 2860 (2002).
22. K. K. Frederick, M. S. Marlow, K. G. Valentine, A. J. Wand, *Nature* **448**, 325 (2007).
23. M. Kroemer, I. Merkel, G. E. Schulz, *Biochemistry* **42**, 10560 (2003).
24. Materials and methods are available on *Science* Online.
25. C. Wiesmann, G. E. Schulz, *Acta Crystallogr.* **D53**, 274 (1997).
26. M. T. Claus, G. E. Zocher, T. H. P. Maier, G. E. Schulz, *Biochemistry* **44**, 8620 (2005).
27. D. Kessler, J. Rétey, G. E. Schulz, *J. Mol. Biol.* **342**, 183 (2004).
28. M. Faller, M. Niederweis, G. E. Schulz, *Science* **303**, 1189 (2004).
29. D. R. Smyth, M. K. Mrozkiewicz, W. J. McGrath, P. Listwan, B. Kobe, *Protein Sci.* **12**, 1313 (2003).

30. Coordinates and structure factors have been deposited in the Protein Data Bank for Oas-C (accession code 2V03), Uro-A (2V7G), Rua-A (2UYU), Rua-B (2UYV), Rua-D (2V9E), Myp-A (2V9U), and for the determination of the side-chain mobility of Rua (1GT7, 2V2B, 2V9F, 2V9I, 2V9L, 2V9M, and 2V9N). We thank the teams of the European Molecular Biology Laboratory (Deutsches Elektronen-Synchrotron, DESY, Hamburg), Berliner Elektronenspeicherring Gesellschaft für Synchrotronstrahlung (BESSY, Berlin), and Swiss Light Source (SLS, Villigen, Switzerland) for their help in data collection as well as F. Becher and U. Rothweiler for contributions at an early stage in the project. The project was supported by Deutsche Forschungsgemeinschaft grant SFB-428.

Supporting Online Material

www.sciencemag.org/cgi/content/full/319/5860/206/DC1
Materials and Methods
Figs. S1 to S4
Tables S1 and S2
References

12 September 2007; accepted 7 November 2007
10.1126/science.1150421

Membrane Phosphatidylserine Regulates Surface Charge and Protein Localization

Tony Yeung,[1] Gary E. Gilbert,[2] Jialan Shi,[2] John Silvius,[3] Andras Kapus,[4] Sergio Grinstein[1]*

Electrostatic interactions with negatively charged membranes contribute to the subcellular targeting of proteins with polybasic clusters or cationic domains. Although the anionic phospholipid phosphatidylserine is comparatively abundant, its contribution to the surface charge of individual cellular membranes is unknown, partly because of the lack of reagents to analyze its distribution in intact cells. We developed a biosensor to study the subcellular distribution of phosphatidylserine and found that it binds the cytosolic leaflets of the plasma membrane, as well as endosomes and lysosomes. The negative charge associated with the presence of phosphatidylserine directed proteins with moderately positive charge to the endocytic pathway. More strongly cationic proteins, normally associated with the plasma membrane, relocalized to endocytic compartments when the plasma membrane surface charge decreased on calcium influx.

The negative surface charge of the inner leaflet of the plasma membrane determines the targeting of proteins containing polycationic motifs (*1*). The unique negativity of the plasmalemmal inner leaflet has been attributed, in part, to its high polyphosphoinositide content. Phosphatidylinositol-4,5-bisphosphate [$PI(4,5)P_2$] and phosphatidylinositol-3,4,5-trisphosphate [$PI(3,4,5)P_3$] are required to target and retain polycationic proteins, such as K-Ras, to the plasma membrane (*2*). Although they are polyvalent, polyphosphoinositides represent only a minor fraction of the phospholipids of the plasma membrane and are less abundant than phosphatidylserine (PS), the predominant anionic species, which represents 10 to 20% of all surface lipid (*3*). The extent to which PS contributes to the targeting and retention of cationic proteins in cells is unclear, because suitable probes to monitor PS distribution in live cells are lacking.

We wanted to develop a probe to monitor the endogenous distribution of PS in intact cells. Lactadherin, a glycoprotein of milk, binds PS in a calcium-independent manner (*4*, *5*), with the major PS-binding motif localized to its C2 domain. We used the C2 domain of lactadherin (Lact-C2) to generate genetically encoded fluorescent biosensors of PS (*6*). Recombinant Lact-C2 was generated in bacteria and purified to test its affinity for PS-containing liposomes by fluorescence resonance energy transfer (*7*) (fig. S1, A and B). We assessed the effectiveness of liposomes of varying composition to displace Lact-C2 from glass microspheres coated by phospholipid bilayers containing 20% PS and 80% phosphatidylcholine (PC) (lipospheres). Liposomes containing 5 to 20% PS reduced Lact-C2 binding to the lipospheres in a concentration-dependent manner (fig. S1C), whereas liposomes containing only PC (fig. S1C) or physiological levels of either phosphatidylinositol (PI) or $PI(4,5)P_2$ had no effect (Fig. 1A). Lact-C2 fused to green fluorescent protein (GFP–Lact-C2) also bound exclusively to PS-coated beads but not to those coated with PC or phosphatidylethanolamine (PE), or with anionic phospholipids such as phosphatidic acid (PA), PI, or $PI(4,5)P_2$ (Fig. 1B), which confirmed the selectivity observed with the bacterially expressed C2 domain.

We next expressed GFP–Lact-C2 in both wild-type and mutant *Saccharomyces cerevisiae* deficient in PS (*8*). GFP–Lact-C2 was observed predominantly on the plasma membrane of the wild-type yeast (Fig. 1C); however, it was cytosolic in the PS-deficient mutant (Fig. 1C). Although a contribution of protein-protein interactions cannot be completely ruled out, these findings demonstrated that most membrane binding of Lact-C2 requires PS.

The plasma membrane of RAW264.7 macrophages was similarly labeled by the GFP–Lact-C2 probe (Fig. 1D). Additionally, intracellular vesicles were decorated with GFP–Lact-C2 (Fig. 1D), and a similar distribution was noted for the C2 domain of factor VIII, which also binds PS (*9*) (fig. S3A). Certain key residues in the C2 domains of factors VIII and V (fig. S2) are required for these proteins to bind PS. Mutation of the equivalent residues in GFP–Lact-C2 obliterated its ability to bind PS in vitro (Fig. 1B) and rendered the construct cytosolic in macrophages (Fig. 1D).

Several lines of evidence indicated that membrane binding of GFP–Lact-C2 was driven specifically by PS and not by negative charge. First, plasmalemmal targeting of GFP–Lact-C2 persisted after $PI(4,5)P_2$ was depleted by either synaptojanin 2 (fig. S4A) or Inp54 (an inositol 5-phosphatase) (fig. S4, B and C). Lact-C2 remained bound to the membrane, despite elimination of $PI(3,4,5)P_3$ with wortmannin (fig. S4, A and C) or when

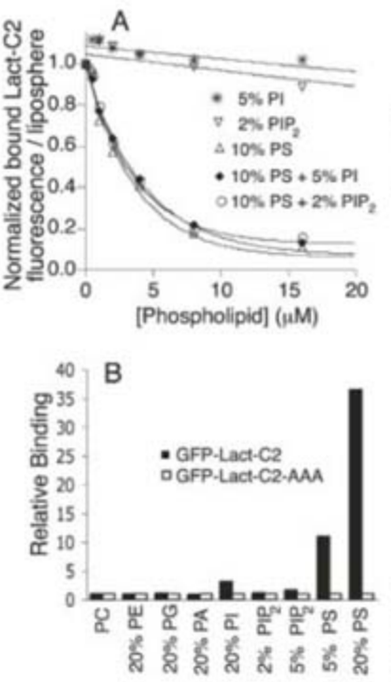

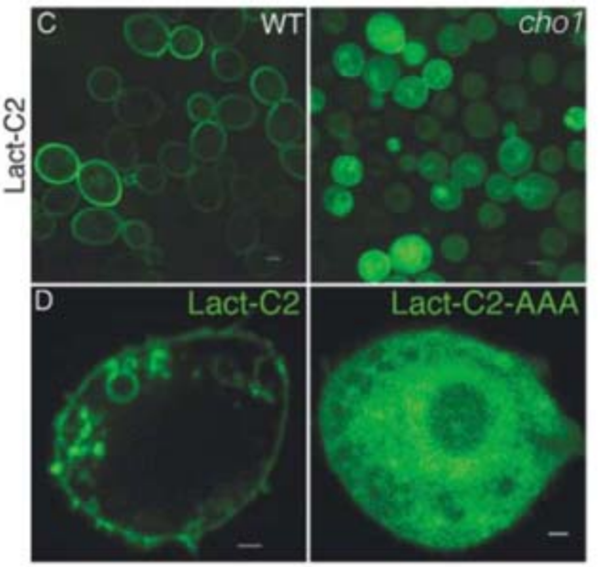

Fig. 1. Characterization of the PS probe Lact-C2. (**A**) Competition for Lact-C2 by liposomes of varying composition. Fluorescein-labeled Lact-C2 (2 nM) was added to a mixture of lipospheres containing 20% PS and 80% neutral lipid with increasing concentrations of liposomes containing the indicated mole fraction of anionic lipids (the balance was PC). (**B**) Binding of wild-type GFP–Lact-C2 (black bars) or GFP–Lact-C2-AAA (*6*, *15*) (white bars) partially purified from HeLa cells to C18-nucleosil beads coated with PC alone or with PE (20%), PG (20%), PA (20%), PI (20%), $PI(4,5)P_2$ (PIP_2) (2%, 5%), or PS (5%, 20%). Data expressed relative to PC-only beads. (**C**) Confocal images of wild-type *S. cerevisiae* (left) and a PS-deficient mutant (*cho1*) (right) expressing GFP–Lact-C2. Scale bars here and elsewhere are 2 μm. (**D**) Confocal images of RAW264.7 macrophages expressing GFP–Lact-C2 (left) or GFP–Lact-C2-AAA (right).

[1]Division of Cell Biology, The Hospital for Sick Children, Toronto M5G 1X8, Canada. [2]Department of Medicine, Department of Veterans Affairs, VA Boston Healthcare System, Brigham and Women's Hospital, Harvard Medical School, Boston, MA 02115, USA. [3]Department of Biochemistry, McGill University, Montreal H3G 1Y6, Canada. [4]Keenan Research Center in the Li Ka Sheng Knowledge Institute of St. Michael's Hospital and Department of Surgery, University of Toronto, Toronto M5B 1W8, Canada.

*To whom correspondence should be addressed. E-mail: sga@sickkids.ca

$PI(4,5)P_2$ and $PI(3,4,5)P_3$ were eliminated by adenosine 5′-triphosphate (ATP) depletion (fig. S4, D and E). Similarly, the accumulation of Lact-C2 on endomembranes remained unchanged when phosphatidylinositol 3-phosphate [PI(3)P] was depleted (fig. S4F). Last, reducing the negativity of the plasma membrane by addition of sphingosine (a membrane-permeant base) or squalamine (a divalent cationic sterol) was without effect on GFP–Lact-C2, but induced a drastic redistribution of surface charge reporters (fig. S5, A and B) (*10*).

Next, we identified the endomembrane organelles bearing PS on their cytosolic surface by colocalization analysis. Mitochondria (Fig. 2A), the Golgi complex (Fig. 2B), and the endoplasmic reticulum (Fig. 2C) did not colocalize significantly with Lact-C2. These findings were unexpected because PS is synthesized, transported, or metabolized in these compartments. The concentration of PS in organelles of the secretory pathway may be lower than that of the plasma membrane, and/or PS may be largely confined to their luminal leaflet. In contrast, extensive overlap was observed between the endocytic pathway and Lact-C2 (Fig. 2D). Various subcompartments of the endocytic pathway were labeled with Lact-C2; early endosomes (fig. S6, A and B), late endosomes (fig. S6C), and lysosomes (fig. S6D) all colocalized with the PS probe.

The presence of PS, an anionic lipid, may confer negative surface charge to endosomes and lysosomes. To test this hypothesis, we expressed a series of surface charge biosensors. These probes combine a hydrophobic farnesyl chain with an adjacent sequence of varying net positive charge (*11*). The most cationic of these biosensors (8+), which is expected to accumulate on membranes with the most-negative surface charge, localized preferentially to the plasmalemma (Fig. 3A), which supports the notion that this membrane bears the most negativity on its inner surface, likely because of the unique accumulation of phosphoinositides (*1*, *12*, *13*). Accordingly, the 8+ probe was observed to relocalize from the plasma membrane to internal organelles after $PI(4,5)P_2$ and $PI(3,4,5)P_3$ depletion (fig. S5C).

By contrast, the least cationic probe (2+), which is targeted predominantly by hydrophobic interactions, associated mainly with intracellular membranes (Fig. 3A). A progressive increase in the number of positive charges should favor interaction of the biosensors with more negatively charged membranes. Indeed, the fraction of the fluorescence associated with the plasma membrane increased gradually along with the charge of the probes (Fig. 3, A and B). This was accompanied by redistribution of the fluorescence in endomembranes. Whereas the farnesylated 2+ probe clearly associated with reticular and juxtanuclear structures, which feature prominently components of the secretory pathway, the 6+ probe bound to the plasmalemma and to a more discrete, vesicular subpopulation (Fig. 3A). A 4+ probe showed an intermediate distribution. Thus, the surface charge of the reticular and juxtanuclear membranes may be less negative than that of the more randomly distributed vesicular membranes.

The nature of the vesicular compartment and the source of its negative surface charge were revealed when we compared the distribution of the charge biosensors with that of Lact-C2. The

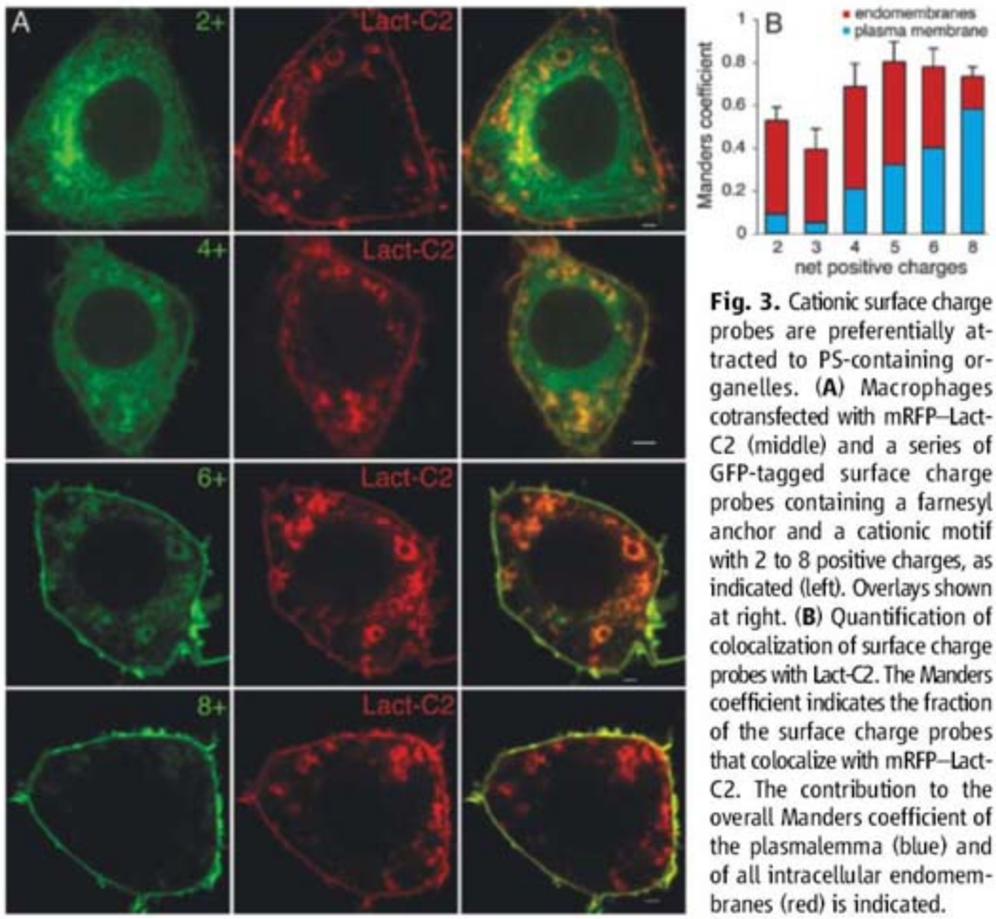

Fig. 3. Cationic surface charge probes are preferentially attracted to PS-containing organelles. (**A**) Macrophages cotransfected with mRFP–Lact-C2 (middle) and a series of GFP-tagged surface charge probes containing a farnesyl anchor and a cationic motif with 2 to 8 positive charges, as indicated (left). Overlays shown at right. (**B**) Quantification of colocalization of surface charge probes with Lact-C2. The Manders coefficient indicates the fraction of the surface charge probes that colocalize with mRFP–Lact-C2. The contribution to the overall Manders coefficient of the plasmalemma (blue) and of all intracellular endomembranes (red) is indicated.

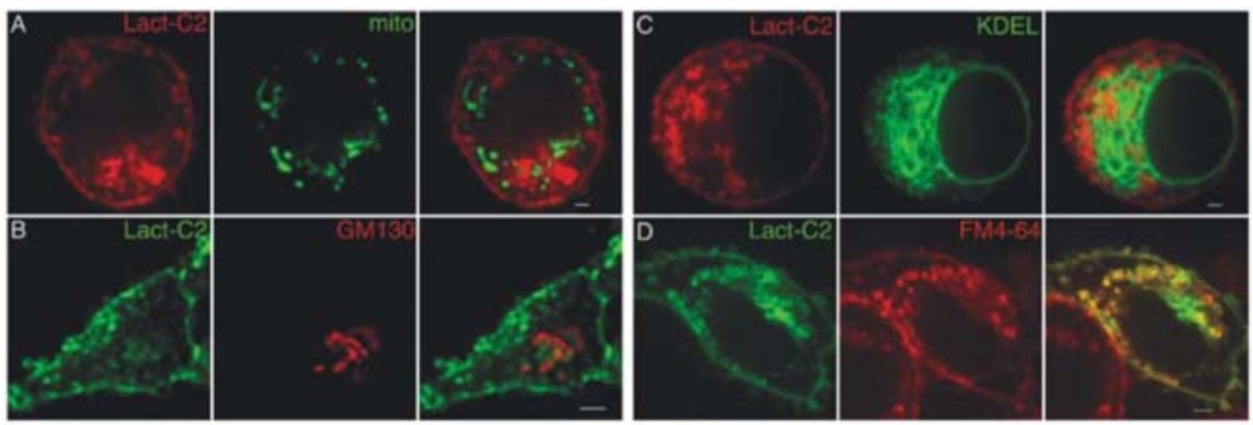

Fig. 2. Subcellular distribution of PS in macrophages. (**A**) Macrophage coexpressing the monomeric form of red fluorescent protein (mRFP)–Lact-C2 (left) and mitochondria-targeted GFP (mito-GFP) (middle). Overlays of both images shown in right panel here and below. (**B**) Macrophages expressing GFP–Lact-C2 (left) were stained with antibodies to GM130 (middle). (**C**) Macrophages coexpressing mRFP–Lact-C2 (left) and the endoplasmic reticulum marker KDEL-GFP (middle). (**D**) Macrophages expressing GFP–Lact-C2 (left) incubated 45 min with FM4-64 to label the endocytic pathway (middle).

compartments of intermediate negative surface charge (lower than that of the plasmalemma, but higher than that of secretory membranes) identified by the 6+ probe were clearly labeled by Lact-C2 (Fig. 3A). Surface charge biosensors with progressively lower positive charge showed steadily decreasing colocalization with the PS probe (Fig. 3, A and B). This implies that the cytosolic leaflet of endosomes and/or lysosomes is negative and that the charge is conferred, at least in part, by PS.

Two additional lines of evidence indicate that PS contributes to the recruitment of charge biosensors to the membranes. First, in ATP and phosphoinositide-depleted cells, the 8+ probe partially relocalized from the plasma membrane to internal organelles (fig. S5C). The redistribution was not random; the 8+ probe was targeted to internal membranes that bound Lact-C2 (fig. S5C). Moreover, a considerable fraction of Lact-C2 remained at the plasmalemma, despite the fact that $PI(4,5)P_2$ and $PI(3,4,5)P_3$ were no longer detectable (fig. S4, D and E). This suggests that PS, which persists in the membrane of ATP-depleted cells, is responsible for retention of the +8 probe. Accordingly, we found that, although the +8 probe is partially retained on the surface membrane of wild-type yeast after ATP depletion, it is largely lost from the membrane of PS-deficient yeast (fig. S7).

The finding that PS-enriched endomembranes recruit proteins bearing sequences with a moderately cationic charge has important functional implications. Although the plasma membrane is the platform where most signal transduction events are initiated, endomembranes are increasingly recognized as sites where signals can be further propagated and amplified (*14*). We therefore analyzed whether the negative charge associated with the enrichment of PS in endocytic compartments contributes to the recruitment of signaling molecules to these loci. Particular attention was given to molecules that, like our charge biosensors, have both a hydrophobic membrane-binding moiety and a cationic motif of intermediate (3+ to 6+) charge. Several well-known signaling molecules fit this description. c-Src, which contains 5+ charges at its myristoylated N terminus, was found at the plasma membrane and in a vesicular compartment that overlapped extensively with Lact-C2 (Fig. 4 and fig. S8). The active forms of Rac1 and Rac2 were similarly found in PS-containing membranes. Of note, the more cationic Rac1 (6+) associated predominantly with the plasmalemma, with a smaller fraction in endomembranes, whereas the converse was true for the less charged (3+) Rac 2 (Fig. 4, A and B). That Rac1 is directed to the surface membrane by its cationic tail is suggested by the observation that a mutant where all six charges were neutralized by replacement of tail cationic amino acids with glutamine (Q) (Rac1-6Q) (*15*) had a widespread distribution reminiscent of the 2+ probe (Fig. 4A). The colocalization of moderately cationic proteins with PS-enriched membranes extends to other Rho family proteins like Cdc42 and to members of the Ras and Rab families (fig. S9). By contrast, guanosine triphosphatases like RheB that bear no positive charge in their tail partition indiscriminately to most cell membranes, setting an upper limit for purely coincidental colocalization with Lact-C2 (Fig. 4).

The electrostatic interaction that targets signaling molecules to PS-enriched endomembranes can be modulated by varying the surface charge of the membrane or by altering the net charge on the protein. K-Ras, which carries 8+ charges at its C-terminal tail, is located primarily at the plasma membrane in resting cells (*16*) (Fig. 4A). When cytosolic calcium rises, plasmalemmal PS is externalized (*17*) and $PI(4,5)P_2$ is hydrolyzed. As a result, the plasmalemmal surface charge decreases and becomes comparable to that of endomembranes, which now compete effectively for binding of K-Ras (Fig. 4, A and B). Conversely, post-translational modifications, like phosphorylation, that reduce the net charge of the cationic tail of K-Ras can also alter its localization (*18*). Accordingly, a phosphomimetic K-Ras mutant with three serine- or threonine-to-glutamate substitutions in its polybasic domain (K-Ras-3E) relocated from the plasmalemma to endomembranes, notably those enriched in PS (Fig. 4).

The presence of sizable pools of PS on the cytosolic leaflet of endosomes and lysosomes implies that these compartments can serve to dock proteins with PS-binding C2-domains, which include a number of important signaling and fusogenic effectors. The accumulation of the anionic lipid also produces the accretion of negative surface charge. As a result, polycationic proteins, particularly those bearing a hydrophobic anchorage site, associate with PS-enriched compartments, including endosomes and/or lysosomes. Electrostatic binding will occur in a manner dependent on both the charge of the membrane and that of the ligand, such that the most-negative membrane (i.e., the plasmalemma) will overwhelmingly accumulate the most cationic proteins, whereas less-positive proteins associate with the plasma membrane and, to a substantial degree, also with membranes of intermediate charge. Because the interaction is dynamic, changes in charge can redirect proteins from one target membrane to another. Thus, diminution of the plasmalemmal charge caused by phospholipid redistribution or metabolism, or phosphorylation of proteins like K-Ras can relocalize them to endocytic membranes, where they could catalyze a different set of reactions.

Clearly, interaction with the surface charge of membranes is but one of the determinants of protein targeting, and other types of interactions must not be neglected. However, the contribution of electrostatic attractions, particularly in endomembranes, should be reevaluated. The electrostatic switch theory (*19*) may be extended to include intermembrane redistribution of ligands in response to charge alteration.

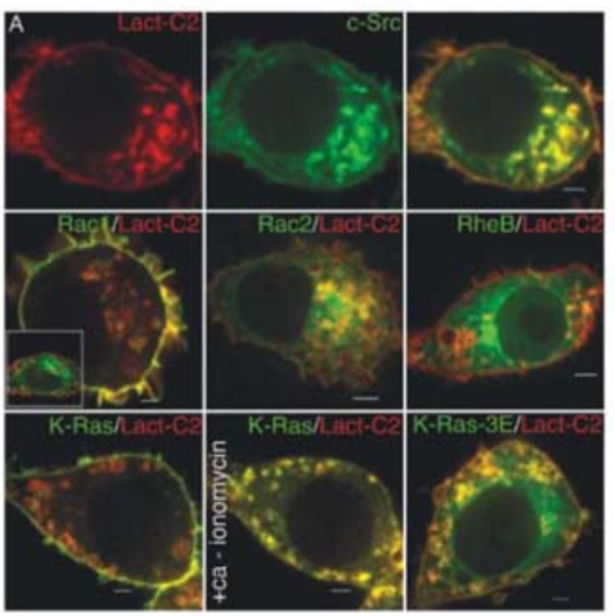

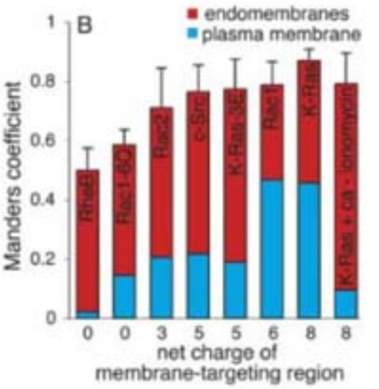

Fig. 4. Proteins with cationic domains are recruited to PS-containing compartments. (**A**) Macrophages coexpressing mRFP–Lact-C2 (red) and one of the following: c-Src–GFP, GFP-Rac1(Q61L), GFP–Rac1(Q61L)-6Q (inset), cyan fluorescent protein (CFP)-Rac2(Q61L), CFP-RheB, GFP–K-Ras(V12)-3E (activated Ras with two tail Ser and one Thr replaced by Glu to mimic phosphorylation), or GFP–K-Ras (green) (*6*). (Top, right) Overlay of mRFP–Lact-C2 and c-Src–GFP. Where indicated, cells were treated with ionomycin. (**B**) Quantification of protein colocalization with the PS probe, measured as the Manders coefficient. The contribution of the plasma membrane (blue) versus that of endomembranes (red) is indicated.

References and Notes

1. S. McLaughlin, D. Murray, *Nature* **438**, 605 (2005).
2. W. D. Heo *et al.*, *Science* **314**, 1458 (2006).
3. J. E. Vance, R. Steenbergen, *Prog. Lipid Res.* **44**, 207 (2005).
4. M. H. Andersen, H. Graversen, S. N. Fedosov, T. E. Petersen, J. T. Rasmussen, *Biochemistry* **39**, 6200 (2000).
5. J. Shi, C. W. Heegaard, J. T. Rasmussen, G. E. Gilbert, *Biochim. Biophys. Acta* **1667**, 82 (2004).
6. Materials and methods are available as supporting material on *Science* Online.
7. G. E. Gilbert, B. C. Furie, B. Furie, *J. Biol. Chem.* **265**, 815 (1990).
8. K. Atkinson, S. Fogel, S. A. Henry, *J. Biol. Chem.* **255**, 6653 (1980).
9. G. E. Gilbert, R. J. Kaufman, A. A. Arena, H. Miao, S. W. Pipe, *J. Biol. Chem.* **277**, 6374 (2002).
10. T. Yeung *et al.*, *Science* **313**, 347 (2006).
11. M. O. Roy, R. Leventis, J. R. Silvius, *Biochemistry* **39**, 8298 (2000).

12. R. Leventis, J. R. Silvius, *Biochemistry* **37**, 7640 (1998).
13. D. Murray *et al.*, *Biochemistry* **37**, 2145 (1998).
14. M. Miaczynska, L. Pelkmans, M. Zerial, *Curr. Opin. Cell Biol.* **16**, 400 (2004).
15. Single-letter abbreviations for the amino acid residues used in this report are as follows: A, Ala; D, Asp; E, Glu; K, Lys; L, Leu; Q, Gln; and R, Arg.
16. J. F. Hancock, H. Paterson, C. J. Marshall, *Cell* **63**, 133 (1990).
17. K. Balasubramanian, B. Mirnikjoo, A. J. Schroit, *J. Biol. Chem.* **282**, 18357 (2007).
18. T. G. Bivona *et al.*, *Mol. Cell* **21**, 481 (2006).
19. S. McLaughlin, A. Aderem, *Trends Biochem. Sci.* **20**, 272 (1995).
20. We thank V. A. Novakovic for excellent technical assistance. Supported by the Heart and Stroke Foundation of Canada, Canadian Institutes of Health Research, and NIH. S.G. holds the Pitblado Chair in Cell Biology.

Supporting Online Material
www.sciencemag.org/cgi/content/full/319/5860/210/DC1
Materials and Methods
Figs. S1 to S9
References

23 October 2007; accepted 30 November 2007
10.1126/science.1152066

The Limits of Counting: Numerical Cognition Between Evolution and Culture

Sieghard Beller and Andrea Bender*

Number words that, in principle, allow all kinds of objects to be counted ad infinitum are one basic requirement for complex numerical cognition. Accordingly, short or object-specific counting sequences in a language are often regarded as earlier steps in the evolution from premathematical conceptions to greater abstraction. We present some instances from Melanesia and Polynesia, whose short or object-specific sequences originated from the same extensive and abstract sequence. Furthermore, the object-specific sequences can be shown to be cognitively advantageous for calculations without notation because they use larger counting units, thereby abbreviating higher numbers, enhancing the counting process, and extending the limits of counting. These results expand our knowledge both regarding numerical cognition and regarding the evolution of numeration systems.

The discovery of the largely restricted (*1*) or probably even nonexistent (*2*) numeration system of the Pirahã in the Amazonian Basin contributed to the discussion of how numerical cognition depends on language. Numeration systems are cognitive tools for numerical cognition (*3*–*6*), and the experimental evidence gathered among the Pirahã provided a sound basis for an analysis of how such tools interact with the cognitive processing of numbers. Cognitive tools, like tools in general, may be more or less efficient, and respective differences in efficiency have been demonstrated both for notational (*7*, *8*) and for purely linguistic numeration systems (*9*–*12*). It should be noted, however, that the assessment of whether a feature is efficient always depends on the nature of the task and on the context of usage and that the efficiency of a specific numeration system does not say anything about the cognitive abilities of its users.

Apart from their efficiency, cognitive tools can also be ordered according to their presumed evolution. Because tools are typically developed in order to improve their efficiency, it is reasonable to assume that numeration systems evolve from being simpler to more sophisticated (*6*, *13*–*15*). But can one also conclude that the simpler a numeration system, the older it is? Although the authors of the recent studies on the Amazonian cases were careful not to draw this conclusion, the evolutionary status of the Pirahã system has become a matter of lively debate, both inside (*2*) and outside of academia. We propose that drawing conclusions on the cognitive and evolutionary status of specific numeration systems requires both diachronic and synchronic data. We set out to highlight the cognitive efficiency of some allegedly primitive systems in another part of the world and to show how they may have evolved from abstract to more specific as a result of cultural adaptation.

Among the properties commonly taken as indices for the simplicity of a numeration system are its extent and its degree of abstractness. The two are largely independent of each other, both on theoretical grounds as well as in practice, and they differ in terms of the attention they have attracted: Whereas the extent of numeration systems has been extensively addressed recently (*1*, *2*, *12*), the degree of abstractness has largely been neglected so far. We will illustrate these properties with two instances for each but will focus on the second feature.

One region where systems with limited extent abound is Papua New Guinea (*16*). Takia, a language in Madang Province, contains five numerals—*kaik*, *uraru*, *utol*, *iwaiwo*, and *kafe-n* (also denoting "his/her thumb"). Higher numbers may be composed by adding or multiplying numerals to the word for 5, but this seems to have been done rarely and for low numbers only (*17*). Adzera, a related language in the Markham River valley in Morobe Province, contains an even more restricted system. Its number words for 1 to 5 are composed of numerals for 1 and 2 only: *bits*, *iru*$^{?}$, *iru*$^{?}$ *da bits* (= 2 + 1), *iru*$^{?}$ *da iru*$^{?}$ (= 2 + 2), and *iru*$^{?}$ *da iru*$^{?}$ *da bits* (= 2 + 2 + 1). Although because of its recursive character this system is in principle infinite, the inevitable difficulties in tallying the terms in higher-number words render it cumbersome. In such cases, people nowadays prefer to use loan words from Tok Pisin instead, a creole language based on English and used as lingua franca in New Guinea (*18*).

These two numeration systems are admittedly not as simple as the case of the Pirahã system, but their low bases and the lack of higher powers of their base restrict both of them. Although numerical cognition among the two Melanesian groups has not been studied experimentally, it can be inferred by analogy that, with such restricted systems, precise numerical operations should be laborious, if not impossible, for larger numbers (*1*, *12*, *19*).

The second property that is readily taken as evidence for restricted efficiency of a numeration system is its object specificity. Menninger inferred that the more object-specific counting sequences a language contains, the more antiquated the numeration system is (*14*). One of the languages referred to as having such object-specific counting sequences is Old High Fijian, a language in the eastern part of Fiji: Whereas it denotes 100 as *bola* when canoes are counted, for coconuts *koro* is used (*20*). Similar object-specific counting sequences can be found in the related Polynesian languages. On Mangareva, for instance, a volcanic island group in French Polynesia, tools, sugar cane, pandanus, breadfruit, and

Table 1. Numerals in traditional Mangarevan (abstract sequence).

Single numerals				Power numerals (quantities)			
1	tahi	6	ono	10^1	rogo'uru	$2 \cdot 10^5$	makiukiu
2	rua	7	hitu	$2 \cdot 10^1$	takau	$2 \cdot 10^6$	makore
3	toru	8	varu	$2 \cdot 10^2$	rau	$2 \cdot 10^7$	makorekore
4	hā	9	iva	$2 \cdot 10^3$	mano	$2 \cdot 10^8$	tini
5	rima			$2 \cdot 10^4$	makiu	$2 \cdot 10^9$	maeaea

Department of Psychology, University of Freiburg, D-79085 Freiburg, Germany.

*To whom correspondence should be addressed. E-mail: bender@psychologie.uni-freiburg.de

octopus were counted with different sequences (*21*). From an evolutionary point of view, it appears reasonable to regard such specific counting systems as predecessors of an abstract mathematical comprehension. But surprisingly, these same systems often also contained numerals for large powers—as far as 10^9 in Mangarevan—thus defining an extent not compatible with the conception of "primitive" numerical tools.

Why did we pick these particular instances? All four languages belong to the same linguistic cluster, namely, to the Oceanic subgroup of the Austronesian language family, and all inherited a regular and abstract decimal numeration system with (at least) two powers of base 10 from their common ancestor, Proto-Oceanic (*17*, *22*, *23*). Both the relative limitation of the two numeration systems in Papua New Guinea and the specific counting sequences in Fiji and Polynesia therefore constitute subsequent developments. Although the former might count as a case of regression in evolutionist terminology, the Polynesian cases are more complex and therefore require an elaborate analysis.

Traditional Mangarevan contained an abstract numeration system (Table 1) and three additional counting sequences for specific objects (*21*). As can be seen from Table 2, each of these sequences contained quantity terms different from the abstract power numerals and appears to have proceeded in diverging steps. However, this apparent divergence disappears when the value of the counting unit to which these sequences refer is extracted. For the first group of objects, the smallest unit *tauga* equals 2, for the second it equals 4, and for the third it equals 8 (for the polynomial composition and the sequence patterns, see Fig. 1C) (*24*).

Specific counting sequences were adopted in nearly every language in Polynesia and even beyond, and they all operated with counting units other than 1 (*25*–*27*). However, despite being based on the same construction principles, each of them was idiosyncratic with regard to the value of counting units, the objects of reference, and even to the numeration principles themselves. This indicates that each culture adapted its inherited system individually, in response to cultural needs. With only a few exceptions, the specific sequences regularly accompanied a general sequence that was purely decimal and abstract (*28*). Because this general sequence is constructed according to simple and coherent rules (Fig. 1A), it fulfills—unlike the English or German sequences (*4*, *5*, *9*–*11*)—all of the requirements of a well-designed and efficient numeration system. Why, then, the object-specific counting sequences?

One of the remarkable facts about numeration systems in Polynesian languages is their large extent. Clearly, Polynesians were interested in high numbers and had a need to operate with them (*25*). For instance, in precolonial times, Mangareva was home to a highly stratified society and was a junction for the long-distance exchange of goods. Accordingly, tributes and large shares for trade were regularly due (*29*–*31*). However, without notation, dealing with large numbers is difficult. In this context, specific counting sequences served practical reasons.

Their main effect was to abbreviate numbers by extracting from the absolute amount the factor inherent in the counting unit. This extraction has implications for critical factors for mental arithmetic: It directly affects the problem size effect in that it reduces calculation time (*3*), and it indirectly affects base size (*8*). Although large bases are more efficient for encoding large numbers and may, by virtue of compact internal representations, facilitate mental operations, they also require the memorization of larger addition and multiplication tables. Small bases, on the other hand, are cumbersome for the representation of large numbers but advantageous when it comes to simple calculations. This holds particularly for the binary system, as is well known since the work of Leibniz.

In Mangarevan, a preoccupation with 2 is apparent. Not only do the three specific sequences differ with regard to the value of their counting unit *tauga* by factor 2, but their general decimal pattern is also modulated with elements of a binary system. Because of its irregularities, the Mangarevan system gave rise to disadvantages not faced by other Polynesian languages with more-regular specific systems, but the disadvantages were compensated by a range of facilitation effects.

One of these effects was that counting specific objects was enhanced by counting them

Table 2. Different counting sequences in Mangarevan, ordered by number of single objects counted. Group 1 consisted of tools, pandanus, sugar cane, and breadfruit; group 2 of ripe breadfruits and octopus; and group 3 of the first breadfruits and octopus of a season. Ellipses indicate that parts of the counting sequence were omitted for reasons of space; dash entries indicate that a regular number word is lacking for this number in the respective sequence.

Objects	1…	2…	4…	8…	10…	20…	40…	80…	160…	200…	320…	640…
general	tahi	rua	hā …	varu	rogo'uru	takau				rau		
group 1	–	tauga	rua tauga	hā tauga		paua	tataua	varu	rua varu		hā varu	varu varu
group 2	–	–	tauga	rua tauga	–		paua	tataua	varu		rua varu	hā varu
group 3	–	–	–	tauga	–	–		paua	tataua		varu	rua varu

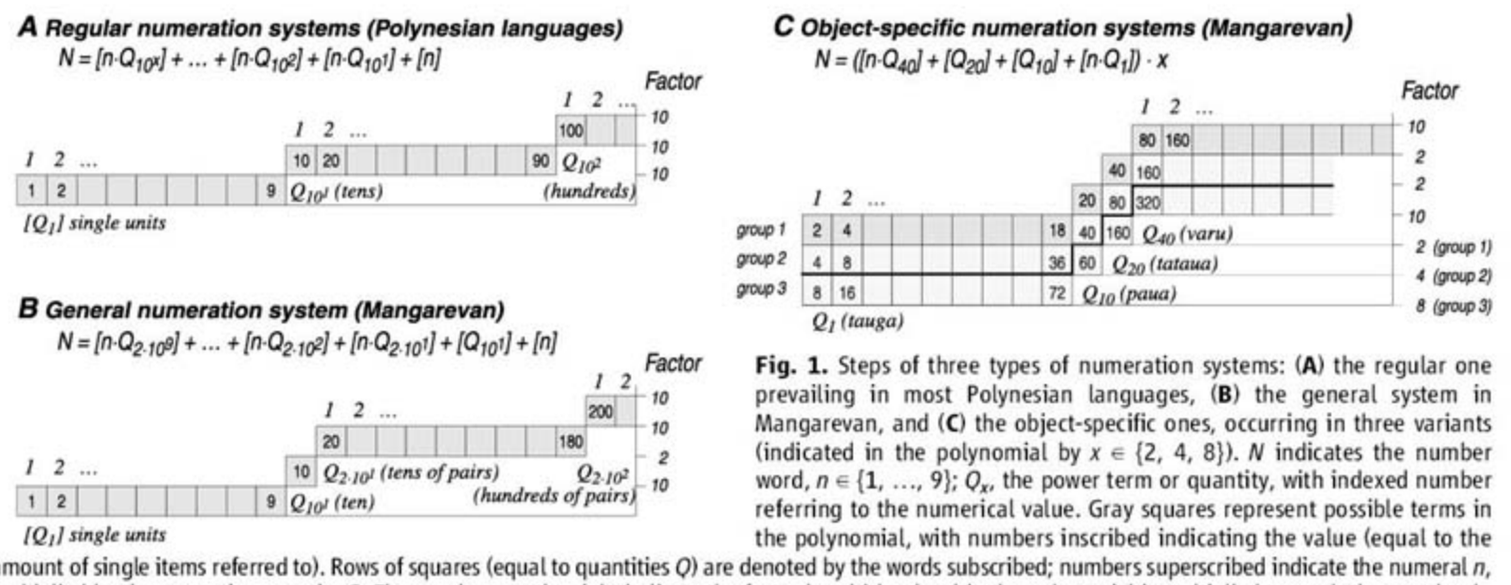

Fig. 1. Steps of three types of numeration systems: (**A**) the regular one prevailing in most Polynesian languages, (**B**) the general system in Mangarevan, and (**C**) the object-specific ones, occurring in three variants (indicated in the polynomial by $x \in \{2, 4, 8\}$). N indicates the number word, $n \in \{1, \ldots, 9\}$; Q_x, the power term or quantity, with indexed number referring to the numerical value. Gray squares represent possible terms in the polynomial, with numbers inscribed indicating the value (equal to the amount of single items referred to). Rows of squares (equal to quantities Q) are denoted by the words subscribed; numbers superscribed indicate the numeral n, multiplied by the respective quantity Q. The numbers on the right indicate the factor by which a level in the polynomial is multiplied to reach the next level.

in larger units (of pairs, quadruples, or eights). In addition, extracting the respective factor extended the limits of the counting sequence, but more importantly it also abbreviated higher numbers and consequently combined effects of large and small base sizes: Encoding produced compact number representations (e.g., 48 ripe breadfruits could be represented as 12 units = 1 *paua* + 2 *tauga*) as in a base 40 system; at the same time, calculating ensued with the addition and multiplication tables of the decimal base, supported by two binary steps.

To sum up, the linguistic analysis reveals that the specific counting systems in Mangareva did not precede an abstract system but were rather derived from it, despite their nonabstract nature (*32*). And the cognitive analysis suggests that this was done deliberately and for rational purposes. This justifies the conclusion that a feature of apparently little efficiency, once taken as indicator for an earlier evolutionary step in numerical cognition, can be used to overcome another such feature.

Not all cultures value numbers in the same way, even if they are concerned with mathematical topics (*33*). In some cultures in Papua New Guinea, for instance, large power numerals were given up together with decimal systems and replaced by quinary or body-counting sequences. In other cultures, the reverse of this took place: Not satisfied with the restrictions posed by their inherited numeration system, many Polynesian cultures not only extended its limits of counting but also designed efficient strategies to cope with the cognitive difficulties of mental arithmetic. Both lines of development started from the same regularly decimal and abstract numeration system inherited from Proto-Oceanic and therefore speak against a linear evolution of numerical cognition. Numeration systems do not always evolve from simple to more complex and from specific to abstract systems.

There may be no other domain in the field of cognitive sciences where it is so obvious that language (i.e., the verbal numeration system) affects cognition (i.e., mental arithmetic). One of the two core systems of number hinges on language (*6*, *34*). If one's language does not contain numerals beyond 1 and 2, calculating larger amounts is difficult, if not impossible. However, people are also very creative in adapting their cognitive and linguistic tools to cultural needs, and cases like those presented here add to our knowledge of how they achieve this.

References and Notes

1. P. Gordon, *Science* **306**, 496 (2004); published online 19 August 2004 (10.1126/science.1094492).
2. D. L. Everett, *Curr. Anthropol.* **46**, 621 (2005).
3. S. Dehaene, *Cognition* **44**, 1 (1992).
4. S. Dehaene, *The Number Sense: How the Mind Creates Mathematics* (Oxford Univ. Press, Oxford, 1997).
5. H. Wiese, *Numbers, Language, and the Human Mind* (Cambridge Univ. Press, Cambridge, 2003).
6. H. Wiese, *Lingua* **117**, 758 (2007).
7. R. S. Nickerson, *Hum. Factors* **30**, 181 (1988).
8. J. Zhang, D. A. Norman, *Cognition* **57**, 271 (1995).
9. K. C. Fuson, Y. Kwon, in *Language in Mathematical Education: Research and Practice*, K. Durkin, B. Shire, Eds. (Open Univ. Press, Milton Keynes, PA, 1991), pp. 211–226.
10. D. C. Geary, C. C. Bow-Thomas, F. Liu, R. S. Siegler, *Child Dev.* **67**, 2022 (1996).
11. K. Miller, C. M. Smith, J. Zhu, H. Zhang, *Psychol. Sci.* **6**, 56 (1995).
12. P. Pica, C. Lemer, V. Izard, S. Dehaene, *Science* **306**, 499 (2004).
13. G. Ifrah, *From One to Zero: A Universal History of Numbers* (Viking, New York, 1985).
14. K. Menninger, *Number Words and Number Symbols* (MIT Press, Cambridge, MA, 1969).
15. F. Klix, *Erwachendes Denken: Geistige Leistungen aus evolutionspsychologischer Sicht* (Spektrum Akademischer Verlag, Heidelberg, Germany, 1993).
16. G. A. Lean, *Counting Systems of Papua New Guinea* (Department of Mathematics and Computer Science, Papua New Guinea University of Technology, Lae, 1992).
17. J. Lynch, M. Ross, T. Crowley, *The Oceanic Languages* (Curzon, Richmond, 2002).
18. S. Holzknecht, *Pac. Linguist.* **A-70**, 77 (1986).
19. J. Wassmann, P. R. Dasen, *J. Cross-Cult. Psychol.* **25**, 78 (1994).
20. C. M. Churchward, *A New Fijian Grammar* (Australasian Medical, Sydney, Australia, 1941).
21. Les Missionaires catholiques de cet Archipel, membres de la Congrégation des Sacrés-Coeurs de Picpus, *Essai de Grammaire de la Langue des Isles Gambier ou Mangaréva* (Imprimerie Zech et Fils, Braine-le-Comte, Belgium, 1908).
22. D. T. Tryon, Ed., *Comparative Austronesian Dictionary: An Introduction to Austronesian Studies* (Mouton de Gruyter, Berlin, 1995).
23. The common ancestor for a group of related languages, if not documented, is reconstructed by way of a systematic comparison of these languages. This method is inductive, but—because of the extensive database and the high convergence—the reconstructed number words for Proto-Oceanic can be regarded as firmly established. They are further supported by a comparison with other Austronesian languages ranging from Madagascar in the West to Easter Island in the East (*22*). This comparison shows that the development in parts of Melanesia must have taken place early on but still was an exception in the larger Austronesian cluster.
24. If *varu* was the principal counting unit of the specific sequences as indicated by cultural preferences, even the unusual steps (i.e., *paua* and *tataua*) could be explained, namely as short cuts to facilitate the representation of the incomplete units. The specific sequence would then be a modulo 40 system, in which units of 40 *tauga* were counted, and the remainder (if any occurred at all) was decomposed in 20 + 10 + *n*. This may not be the most efficient method of decomposition, but—given the generally decimal nature of the system—it was surely the most preferable. The next possible decomposition (20 + 10 + 5 + *n*) would have arbitrarily restricted the single numerals to $n \in \{1, 2, 3, 4\}$.
25. A. Bender, S. Beller, *J. Polynesian Soc.* **115**, 7 (2006).
26. A. Bender, S. Beller, *Ocean. Linguist.* **45**, 380 (2006).
27. A. Bender, S. Beller, *J. Cognit. Cult.* **7**, 213 (2007).
28. The switch from 10 to 20 in the general sequence in Mangarevan is atypical in this regard. However, because many of the traditional numeration systems were replaced in colonial times before they were documented, information on a regular system may simply have been lost.
29. P. Bellwood, *The Polynesians: Prehistory of an Island People* (Thames and Hudson, London, 1987).
30. R. C. Green, M. Weisler, *Asian Perspect.* **41**, 213 (2002).
31. P. V. Kirch, *The Evolution of the Polynesian Chiefdoms* (Cambridge Univ. Press, Cambridge, 1984).
32. These conclusions can be further corroborated by an analysis of the composition principles for the object-specific counting sequences. It shows that these specific counting sequences are derived from abstract counting sequences with the aid of residuals of numeral classifiers [which, in several languages, are obligatory in counting to specify and classify the counted objects, such as words like "sheet" in "two sheets of paper"; for more details see (*26*)].
33. M. Ascher, *Ethnomathematics: A Multicultural View of Mathematical Ideas* (Brooks/Cole, Pacific Grove, CA, 1991).
34. L. Feigenson, S. Dehaene, E. Spelke, *Trends Cogn. Sci.* **8**, 307 (2004).

35. We are grateful to H. Spada for institutional support, to A. Rothe for assistance with the material, and to S. Mannion as well as two anonymous reviewers for discussion and valuable comments on earlier versions of this paper.

25 July 2007; accepted 29 November 2007
10.1126/science.1148345

Recognition of a Ubiquitous Self Antigen by Prostate Cancer–Infiltrating CD8$^+$ T Lymphocytes

Peter A. Savage,[1] Keith Vosseller,[2] Chulho Kang,[3] Kevin Larimore,[4] Elyn Riedel,[5] Kathleen Wojnoonski,[1] Achim A. Jungbluth,[6] James P. Allison[1]*

Substantial evidence exists that many tumors can be specifically recognized by CD8$^+$ T lymphocytes. The definition of antigens targeted by these cells is paramount for the development of effective immunotherapeutic strategies for treating human cancers. In a screen for endogenous tumor-associated T cell responses in a primary mouse model of prostatic adenocarcinoma, we identified a naturally arising CD8$^+$ T cell response that is reactive to a peptide derived from histone H4. Despite the ubiquitous nature of histones, T cell recognition of histone H4 peptide was specifically associated with the presence of prostate cancer in these mice. Thus, the repertoire of antigens recognized by tumor-infiltrating T cells is broader than previously thought and includes peptides derived from ubiquitous self antigens that are normally sequestered from immune detection.

T lymphocytes that are reactive to antigens expressed by tumor cells have been shown to modulate cancer development in animal models and human cancer patients (*1*, *2*). Thus, much effort has been devoted to the development of immunotherapeutic strategies aimed at

inducing cancer regression by enhancing antitumor T cell responses (*3*). The identification of T cell tumor antigens typically relies on the in vitro culture of T cell lines reactive to clonal tumor cell lines or to candidate peptide antigens (*4*). However, antigens defined in this manner may not provide a complete picture of the range of antigenic peptides in primary, heterogeneous tumors comprising a variety of cell types at different stages of differentiation. In this study, we set out to define a naturally arising T cell response to a tumor-associated antigen in an autochthonous mouse model of cancer.

Our approach was based on the direct detection of T cell populations that infiltrate primary tumors in vivo, thereby bypassing the need for in vitro T cell manipulation. To do this, we used a model in which male transgenic adenocarcinoma of mouse prostate (TRAMP) mice express simian virus 40 T antigen (Tag) under the control of a prostate-specific promoter, resulting in the development of spontaneous adenocarcinoma in the prostate by 14 to 20 weeks of age (*5*, *6*). In a screen to identify endogenous T cell responses in the TRAMP model, we analyzed T cell receptor (TCR) repertoire diversity within the prostate infiltrate of late-stage tumor-bearing TRAMP$^{+/+}$ mice (≥27 weeks of age, B6 genetic background) in order to identify reproducible T cell clonal expansions expressing conserved TCRs. We analyzed repertoire diversity using TCR CDR3 size spectratyping (*7*), in which the length distribution of the hypervariable complementarity-determining region 3 (CDR3) of a TCR chain is analyzed via a polymerase chain reaction (PCR)–based approach (*8*). Spectratyping analysis of the TCRβ chain variable region (Vβ) families 1 through 20 revealed the consistent overrepresentation of Vβ8.3 TCR transcripts with a conserved CDR3 length in the prostates of tumor-bearing TRAMP$^{+/+}$ mice but not in the prostates of control B6 mice (Fig. 1A and fig. S1A). Sequencing of the prominent Vβ8.3 transcripts from several TRAMP$^{+/+}$ mice identified conserved transcripts that preferentially encoded a CDR3 of 10 amino acids in length and a conserved amino acid sequence (fig. S2). Spectratyping analysis of prostate-infiltrating CD4$^+$ and CD8$^+$ T cells from tumor-bearing TRAMP$^{+/+}$ mice revealed that T cells expressing the conserved Vβ8.3 TCRβ chain fall within the CD8$^+$ T cell subset (Fig. 1B and fig. S1B), suggesting that these cells are major histocompatibility complex (MHC) class I–restricted. In an analogous manner, we used CDR3 size spectratyping and sequence analysis to identify restricted Vα2 and Vα18 TCRα chains that preferentially pair with the conserved TCRβ chain to form a functional TCRαβ heterodimer (fig. S3 and tables S2 and S3). Overall, the finding that CD8$^+$ T cells infiltrating TRAMP$^{+/+}$ prostate tumors express highly conserved TCRs suggested that a T cell response reactive to the same antigen was arising spontaneously in most tumor-bearing TRAMP$^{+/+}$ mice.

Having identified a conserved TCRαβ receptor expressed by T cells infiltrating TRAMP$^{+/+}$ prostate tumors, we generated transgenic mice expressing the conserved Vα2$^+$ TCRα and Vβ8.3$^+$ TCRβ chains (Fig. 1C and fig. S4). When a TCRαβ transgenic line was crossed to the *Rag1*$^{-/-}$ (recombination activating gene 1) background, in which rearrangement of endogenous TCRs is precluded, mature peripheral T cells were selected to the CD8$^+$ lineage (Fig. 1C). In addition, T cells in *Rag1*$^{-/-}$ TCRαβ transgenic mice exhibited no evidence of clonal deletion or coreceptor downregulation in the thymus or activation in the periphery (Fig. 1C and fig. S4),

[1]Department of Immunology, Howard Hughes Medical Institute, and Ludwig Center for Cancer Immunotherapy, Memorial Sloan-Kettering Cancer Center (MSKCC), New York, NY 10021, USA. [2]Department of Biochemistry and Molecular Biology, Drexel University College of Medicine, Philadelphia, PA 19102, USA. [3]Cancer Research Laboratory, University of California, Berkeley, CA 94720, USA. [4]Department of Molecular and Cell Biology, University of California, Berkeley, CA 94720, USA. [5]Department of Epidemiology and Biostatistics, MSKCC, New York, NY 10065, USA. [6]New York Branch, Ludwig Institute for Cancer Research, New York, NY 10021, USA.

*To whom correspondence should be addressed. E-mail: allisonj@mskcc.org

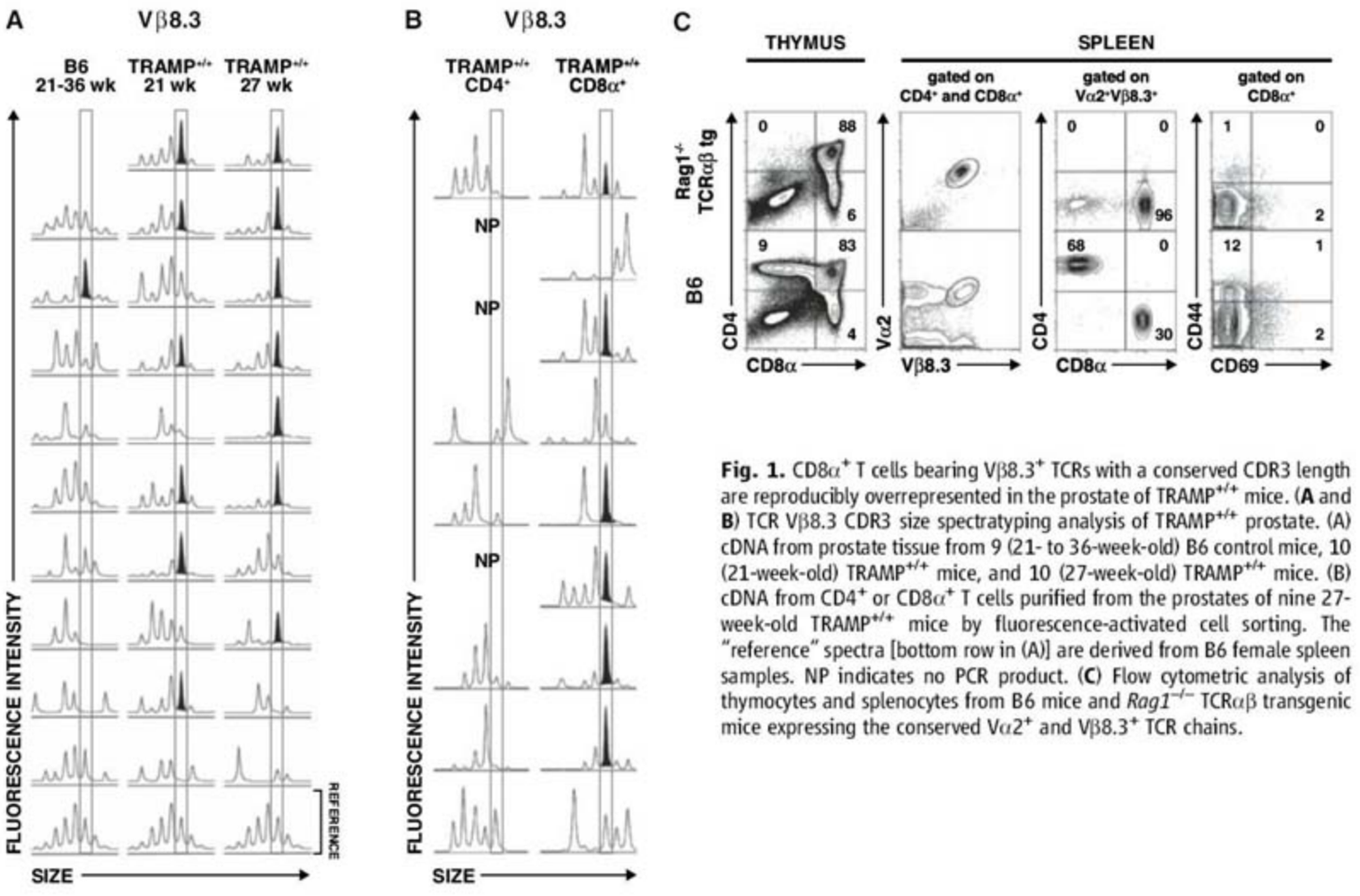

Fig. 1. CD8α$^+$ T cells bearing Vβ8.3$^+$ TCRs with a conserved CDR3 length are reproducibly overrepresented in the prostate of TRAMP$^{+/+}$ mice. (**A** and **B**) TCR Vβ8.3 CDR3 size spectratyping analysis of TRAMP$^{+/+}$ prostate. (A) cDNA from prostate tissue from 9 (21- to 36-week-old) B6 control mice, 10 (21-week-old) TRAMP$^{+/+}$ mice, and 10 (27-week-old) TRAMP$^{+/+}$ mice. (B) cDNA from CD4$^+$ or CD8α$^+$ T cells purified from the prostates of nine 27-week-old TRAMP$^{+/+}$ mice by fluorescence-activated cell sorting. The "reference" spectra [bottom row in (A)] are derived from B6 female spleen samples. NP indicates no PCR product. (**C**) Flow cytometric analysis of thymocytes and splenocytes from B6 mice and *Rag1*$^{-/-}$ TCRαβ transgenic mice expressing the conserved Vα2$^+$ and Vβ8.3$^+$ TCR chains.

suggesting that there was no overt immunological self-reactivity in tumor-free TCRαβ transgenic mice.

To facilitate the characterization and identification of the antigen driving the observed T cell response, we generated an immortalized T cell hybridoma expressing the conserved TCRαβ (hereafter referred to as the "clonotypic hybridoma," clone 6B1-6) from T cells from TCRαβ transgenic mice. In vitro, stimulation of the clonotypic hybridoma was not observed after direct culture of the hybridoma with a variety of tumor cell lines [including the TRAMP-C2 prostate cell line (*9*)] and primary immune cell types. Instead, stimulation was only observed when the clonotypic hybridoma was cultured with high-performance liquid chromatography (HPLC) fractions of crude cellular acid extracts together with MHC-expressing antigen-presenting cells (APCs). When crude extracts from the prostate of tumor-bearing TRAMP$^{+/+}$ males were assayed in this manner for stimulation of the clonotypic hybridoma, a single peak of stimulatory activity was observed (Fig. 2A). Additionally, stimulatory activity was found in extracts from other organs (including liver, lung, spleen, and thymus) and bone marrow from TRAMP$^{+/+}$ mice, as well as in organs from male and female B6 mice (Fig. 2A and fig. S5). T cell stimulation was only observed when APCs expressed the K^b class I MHC molecule, and was blocked by culture with antibodies to K^b (Fig. 2A), indicating that antigen recognition is K^b-restricted. Taken together, experiments that used crude extracts from mouse tissue indicate that the antigen recognized by clonotypic prostate-infiltrating T cells is derived from a self molecule that is present in many organs of both tumor-bearing and tumor-free mice.

In addition to the crude extracts from primary mouse tissue, the stimulatory activity was present in crude extracts from all mouse cell lines assayed. Biochemical fractionation of cellular extracts from a tumor cell line revealed that the stimulatory activity is preferentially associated with the chromatin-enriched nuclear fraction (Fig. 2B). We therefore assayed the highly conserved histone proteins, an abundant constituent of chromatin, and found that preparations from a histone mixture and from purified histone H4 stimulated the clonotypic hybridoma (Fig. 2C). To identify the potential antigenic histone H4–derived peptides, we acid-treated, purified, and sequenced histone H4 using liquid chromatography–tandem mass spectrometry (LC-MS/MS) (*7*). A single 17-mer peptide (i.e., 17–amino acid peptide) of sequence VVYALKRQGRTLYGFGG (*10*) (identical to the C terminus of histone H4, residues 86 to 102) was identified (fig. S6). LC-MS/MS analysis of peptides present in the stimulatory fractions obtained from crude extracts (Fig. 2A) revealed the presence of the histone H4(86–102) 17-mer. Analysis of clonotypic T cell stimulation after culture with histone H4(86–102) or smaller truncated peptides in the presence of APCs confirmed that clonotypic T cells recognize histone H4(86–102) and revealed that the minimal core epitope for recognition is the heptamer H4(86–92): VVYALKR

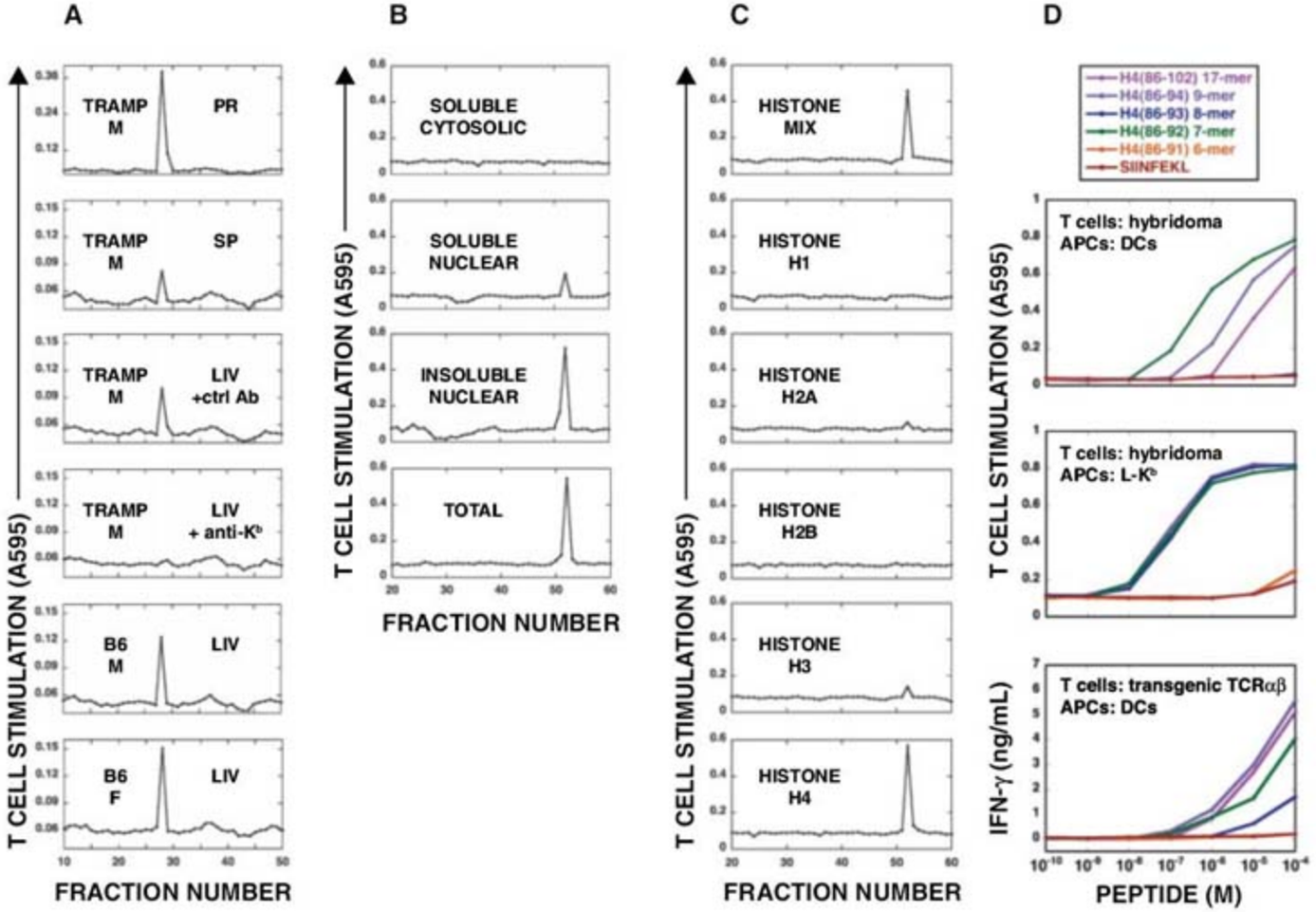

Fig. 2. T cells expressing the conserved TCRαβ recognize a histone H4–derived peptide. (**A** to **C**) Reactivity of the clonotypic T cell hybridoma 6B1-6. Extracts or proteins were boiled in 10% acetic acid and resolved by reversed-phase HPLC. Fractions were then dried and cultured with 6B1-6 and K^b-expressing APCs, and 6B1-6 stimulation was assayed. (A) Reactivity of 6B1-6 to crude extracts from prostate (PR), spleen (SP), and liver (LIV) from 27-week-old male TRAMP$^{+/+}$ mice and liver from male (M) and female (F) B6 mice. Where indicated, a cocktail of antibodies to K^b (anti-K^b) or control antibodies (ctrl Ab) was added to the culture. (B) Reactivity of 6B1-6 to extracts of subcellular fractions. B16 melanoma cells were fractionated according to Wysocka *et al.* (*16*). The indicated subcellular fractions were isolated, acid-treated, processed, and assayed. (C) Reactivity of 6B1-6 to histone H4. A mixture of histone proteins or the indicated individual histones were acid-treated, processed, and assayed. (**D**) Stimulation of clonotypic T cells with histone H4–derived peptides. T cells expressing the conserved TCRαβ (either 6B1-6 or TCRαβ transgenic T cells) were cultured with peptide and APCs [either primary dendritic cells (DCs) or L-K^b cells]. The histone H4–derived peptides assayed and the control SIINFEKL peptide are indicated.

(Fig. 2D). The finding that clonotypic T cells recognize histone H4(86–92) presented by K^b is unexpected, given the preference of K^b for peptides that are eight amino acids in length and that contain a phenylalanine or tyrosine in the fifth residue (*11*). Consistent with this idea, histone H4 peptide binding to K^b, as measured by stabilization of K^b on the surface of RMA-S cells, was barely detectable (fig. S7), suggesting that H4 peptides bind K^b with low affinity. Having determined that clonotypic T cells are reactive to histone H4(86–92)–related peptides, we designated TCRαβ transgenic mice as "HRC" (histone H4–reactive TCR transgenic, complete expression).

In order to directly identify endogenous histone H4–reactive T cells in tumor-bearing $TRAMP^{+/+}$ mice, we used fluorescent peptide/MHC tetramers in conjunction with flow cytometry. Because the low affinity of wild-type histone H4(86–92) VVYALKR binding to K^b precluded the generation of stable tetramers, we produced K^b tetramers bearing the analog peptide VVYAFKR, in which the leucine lying in the dominant K^b-binding anchor position is mutated to a phenylalanine. The VVYAFKR peptide exhibited increased affinity for K^b and was recognized by clonotypic T cells in vitro (fig. S8), and VVYAFKR/K^b tetramers (hereafter referred to as "H4/K^b tetramers") stained HRC T cells efficiently (fig. S4). With the use of H4/K^b tetramers, histone H4–reactive T cells were not observed in the prostates of tumor-free B6 mice (n = 9 mice, Fig. 3A). In contrast, antigen-experienced $CD44^{high}$ $CD8^+$ H4/K^b $tetramer^+$ T cells were detected in the prostate infiltrate of most tumor-bearing $TRAMP^{+/+}$ mice (Fig. 3A, with a median frequency of 0.15% of $CD8^+$ T cells), with prominent H4/K^b $tetramer^+$ populations in 3 out of 13 mice that were analyzed (≥0.2% of $CD8^+$ T cells and ≥20 $tetramer^+$ cells were recovered from the prostate). The frequency of histone H4–reactive cells in $TRAMP^{+/+}$ prostate is comparable to that reported for T cells specific for tumor-associated antigens found commonly in the tumor infiltrate and metastatic lymph nodes of human melanoma patients (*12*). In addition to those identified in the prostate, antigen-experienced H4/K^b $tetramer^+$ cells were also identified at detectable frequencies in the prostate-draining periaortic lymph nodes (7 out of 13 mice, with median frequency 0.029%) and the spleen (4 out of 13 mice, with median frequency 0.023%) of some $TRAMP^{+/+}$ mice (Fig. 3A), including the 3 mice with prominent H4/K^b $tetramer^+$ populations in the prostate.

To evaluate antigen recognition by histone H4–reactive T cells in late-stage prostate cancer, we analyzed the proliferation of HRC T cells after adoptive transfer into $TRAMP^{+/+}$ mice. HRC T cells labeled with the dye carboxyfluorescein diacetate succinimidyl ester (CFSE) were transferred into tumor-bearing $TRAMP^{+/+}$ mice and B6 control mice and were analyzed 5 or 30 days after transfer. At both time points, HRC T cells that had undergone division (i.e., with diluted CFSE) were observed in $TRAMP^{+/+}$ mice but not in B6 controls (Fig. 3B). CFSE-diluted HRC T cells were predominantly found in

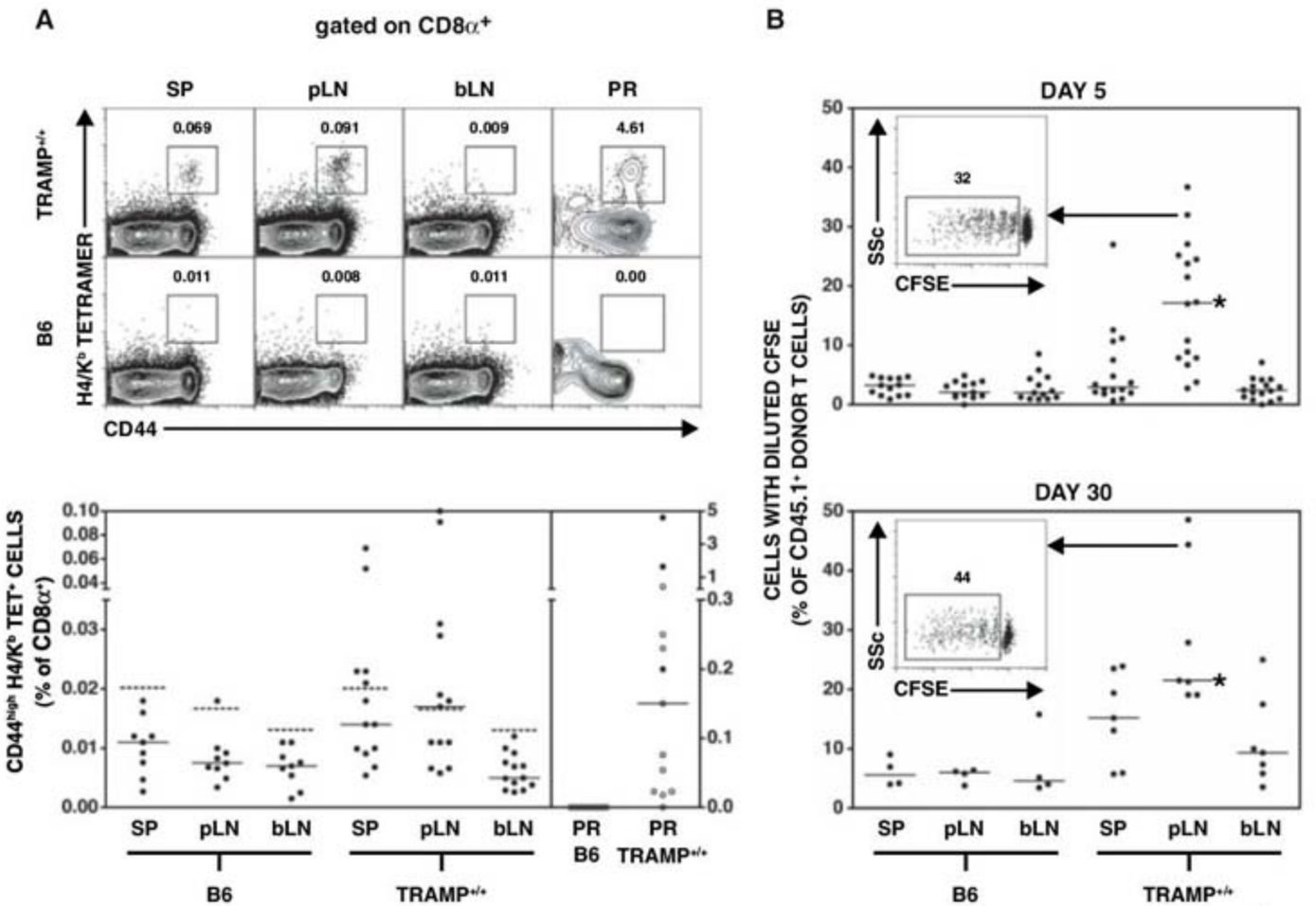

Fig. 3. T cell recognition of histone H4 in vivo. (**A**) Identification of endogenous histone H4–reactive T cells with peptide/MHC tetramers. T cells from ≥24-week-old $TRAMP^{+/+}$ and B6 mice were stained with H4/K^b tetramer and antibodies to cell-surface markers. (Top) Representative samples from SP, periaortic lymph nodes (pLN), brachial lymph nodes (bLN), and PR. (Bottom) Summary of tetramer staining results, pooled from five experiments. To determine which TRAMP samples were "$tetramer^+$," we used data from B6 samples to establish a limit of detection (dashed horizontal bars), defined as the mean plus two SDs. For PR samples, solid and open circles denote samples in which ≥20 or ≤20 H4/K^b $tetramer^+$ cells, respectively, were identified. (**B**) Division of HRC T cells transferred into $TRAMP^{+/+}$ mice. $CD45.1^+$ HRC T cells were labeled with CFSE, transferred into $TRAMP^{+/+}$ and B6 mice, and analyzed 5 days (top) or 30 days (bottom) after transfer. Asterisks indicate statistically significant differences between $TRAMP^{+/+}$ and B6 pLN values ($P \leq 0.0001$ for day 5, $P \leq 0.006$ for day 30). For 5 and 30 days after transfer, data are pooled from four and two experiments, respectively. Solid horizontal bars in (A) and (B) indicate median values.

the tumor-draining periaortic lymph nodes (Fig. 3B), indicating that T cell antigen recognition in the lymphoid organs is mainly restricted to the lymph nodes draining the tumor site.

Together, tetramer analysis of endogenous T cells and adoptive T cell transfer studies indicate that, despite the ubiquitous nature of histone H4, MHC class I–restricted T cell recognition of histone H4 peptide is specifically associated with the presence of prostate cancer in TRAMP$^{+/+}$ mice (*13*).

Next, we performed a series of experiments to analyze the ability of HRC T cells to traffic to the prostate and develop effector function after antigen recognition in tumor-bearing TRAMP$^{+/+}$ mice. First, when analyzed 4 to 8 weeks after transfer, prostate infiltration of HRC T cells was observed in a proportion (10 out of 31 mice, ~32%, with ≥20 HRC T cells recovered) of TRAMP$^{+/+}$ recipients, with a median frequency of 0.27% of prostate-infiltrating CD8$^+$ T cells (Fig. 4A). Second, when analyzed either 5 or 30 days after transfer, HRC T cells that had undergone division exhibited increased expression of the activation marker CD44 but generally produced little or no interferon-γ (IFN-γ) (Fig. 4B). Third, HRC T cells transferred into tumor-bearing TRAMP$^{+/+}$ mice did not exhibit detectable cytolytic activity (Fig. 4C) and did not express the cytotoxic effector molecules granzyme B or perforin (fig. S11). Thus, after transfer into tumor-bearing TRAMP$^{+/+}$ mice, HRC T cells proliferate and traffic to the prostate in a proportion of mice but typically fail to develop measurable effector function. These functional characteristics are analogous to those of tumor-reactive T cells found in tumor lesions of melanoma patients (*12*, *14*, *15*).

To gain insight into the contribution of histone H4–reactive T cells to antitumor immunity or to tolerance, we crossed TRAMP$^{+/+}$ mice to a TCR transgenic line exhibiting variegated expression of the histone H4–reactive TCR (designated "HRV"), resulting in expression of the complete TCRαβ heterodimer on 10 to 20% of mature T cells (fig. S4). The resulting male offspring, either TRAMP$^{+/-}$ or TRAMP$^{+/-}$ HRV, were euthanized between 26 and 28 weeks of age, and the mass of the genitourinary tract and prostate was determined. Although there was no difference in survival to the 26- to 28-week end point (fig. S12), analysis revealed a slight, statistically significant reduction (~10%) in prostate and genitourinary tract mass in TRAMP$^{+/-}$ HRV mice relative to that in TRAMP$^{+/-}$ controls. This finding suggests that, on average, a high precursor frequency of histone H4–reactive T cells results in decreased tumor burden in TRAMP mice. Despite this effect, the animals eventually die of prostate cancer, indicating that histone H4–reactive T cells are not by themselves protective in the absence of immune intervention. We are currently performing histological analyses of TRAMP prostate tumor pathology and immune infiltration in an effort to elucidate the mechanisms underlying the observed reduction in tumor burden in TRAMP$^{+/-}$ HRV mice.

On account of its abundant, ubiquitous nature, the histone H4 antigen described here does not fit into the major classes of tumor-associated antigens (*4*) and may represent a previously undefined type of antigen. Hypothetically, antigens of this type would be derived from ubiquitously expressed proteins that, under normal circumstances, are not efficiently processed in the MHC class I presentation pathway because of sequestration within the cell, either by compartmentalization within the nucleus or mitochondria or by segregation within supermolecular complexes. The CD8$^+$ T cell repertoire would be largely ignorant of such antigens. However, as a result of distinct conditions within the tumor microenvironment, changes in antigen processing and presentation would induce MHC class I–restricted presentation of the antigen, allowing recognition

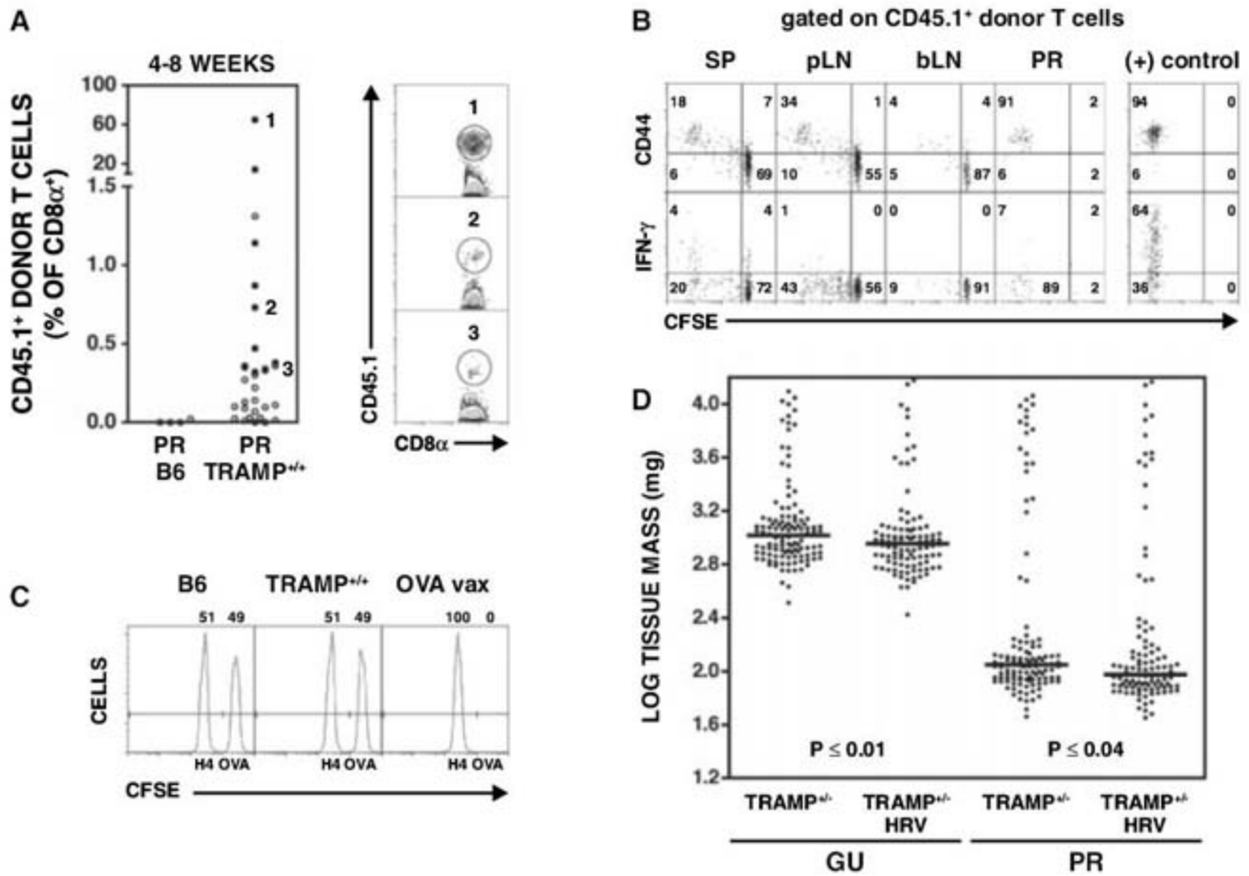

Fig. 4. Trafficking and effector function of histone H4–reactive T cells. (**A**) Trafficking of HRC T cells to TRAMP$^{+/+}$ prostate. CD45.1$^+$ HRC T cells were transferred into ≥23-week-old TRAMP$^{+/+}$ or B6 mice and analyzed 4 to 8 weeks after transfer. Solid and open circles denote samples in which ≥20 or ≤20 CD45.1$^+$ cells, respectively, were identified. For three representative mice, flow plots are shown. (**B**) CD44 expression and IFN-γ production by HRC T cells. CFSE-labeled CD45.1$^+$ HRC T cells that had been transferred 30 days earlier into 23-week-old TRAMP$^{+/+}$ mice were re-stimulated in vitro and analyzed. The positive control indicates cells from B6 mice that had previously received in vitro–activated CD45.1$^+$ HRC cells. (**C**) Lack of detectable cytolytic activity of HRC T cells. CD45.1$^+$ HRC cells were injected into ≥24-week-old TRAMP$^{+/+}$ or B6 mice. Fourteen days later, mixtures of target cells labeled with either VVYAFKR (H4) or control SIINFEKL [ovalbumin (OVA)] peptide were injected, and the recovery of targets was quantified. The positive control (OVA vax) indicates B6 mice that had been vaccinated against OVA peptide. (**D**) Slight reduction in PR mass and in genitourinary tract (GU) mass in TRAMP$^{+/-}$ HRV mice. Organ masses were determined for 26- to 28-week-old TRAMP$^{+/-}$ HRV (n = 106 mice) and TRAMP$^{+/-}$ (n = 119 mice) animals. Mice that died before the analysis point (n = 9 for TRAMP$^{+/-}$ HRV and n = 10 for TRAMP$^{+/-}$) were not included in the analysis. Median masses were 902 mg (GU) and 95 mg (PR) for TRAMP$^{+/-}$ HRV mice and 1042 mg (GU) and 112 mg (PR) for TRAMP$^{+/-}$ mice. Horizontal bars indicate median values.

Molecular Biology Liquid Handling

Three products have been released in the CyBi-GeneRobots line that combine reliable nucleic acid purification processes with precise low-volume pipetting capacity. The CyBi-DiluSpro is an eight-channel pipettor suited for many molecular biology applications. Because it offers high precision over the pipetting range of 0.5 ml to 250 ml, it is a suitable choice for polymerase chain reaction set-up and clean-up, as well as sequencing reaction set-up and clean-up. The CyBi-Well vario is a multi-channel pipettor suited for nucleic acid transfer applications in the 96-well, 384-well, and 1536-well format, such as high-throughput small-interfering RNA screenings. Exchangeable pipetting heads cover a volume from 25 nl to 250 ml to provide flexibility from the downscaling of reaction volumes to throughput increases. Sterile and polymerase chain reaction-certified disposable tips provide reliable results without cross-contamination. The pipetting technology enables gentle cell handling as well as rapid nucleic acid transfer protocols on the same instrument. The CyBi-RoboSpense is an all-purpose pipetting robot with four or eight individually addressable channels, suitable for nucleic acid purification, processing, and analysis applications. The system works with tubes and plates both in the 96-well and 384-well format. It is designed for fully automated sample purification and reaction set-up and clean-up tasks.

CyBio
For information +49 36 41 351 0
www.cybio-ag.com

Mobile Ductless Fume Hoods

The EDU Mobile Ductless Fume Hoods are a low-cost solution for clean air requirements, providing operator protection when using hazardous substances. These economical and efficient units feature high-quality pre-filters and carbon filters with efficiencies greater than 99.6%, all-around visibility, mobility from laboratory to laboratory, and easy installation. They include alarms that monitor filter, airflow, and filter lifetime.

Air Science USA
For information 800-306-0656
www.air-science.com

Trypsin Removal

Mag-Trypsin provides a method for magnetically immobilizing trypsin that allows it to be removed easily from a protein digestion mixture using a magnetic separator after the reaction is complete. Treatment with trypsin immobilized on magnetic beads prior to immobilization inhibits chymotrypsin activity without any effect on trypsin. Unlike agarose-linked immobilized trypsin, Mag-Trypsin does not require any centrifugation or use of columns. It provides a simple method for eliminating trypsin contamination after digesting protein samples to their peptide constituents in preparation for such techniques as mass spectroscopy or peptide enrichment.

Clontech Laboratories
For information 650-919-7382
www.clontech.com

Protein Expression Media

The ProNSO Chemically Defined (CD) Serum-free Media support maximal production of recombinant protein in NSO cells. The NSO cell line is widely used for recombinant mammalian protein expression in research and biotherapeutic applications. Two formulas are available to cover a broad range of nutritional needs, with a companion ProNSO Lipid CD Supplement also available.

Lonza
For information 800-521-0390
www.lonza.com

T Cell Isolation

The flow-compatible Dynal Dynabeads Regulatory CD4+CD25+ T Cell Kit is used for positive isolation of human regulatory T cells (Treg cells). The tube-based technology provides highly functional Treg cells with up to 97% purity. In the three-step isolation procedure, cells are left both bead-free and antibody-free after isolation, and can be used in any downstream experiment.

Invitrogen
For information 800-955-6288
www.invitrogen.com

Diamond Knife

A new diamond knife for the sectioning of frozen hydrated specimens features a 25° angle for the least possible compression and the best structural preservation. Its cutting range is from 25—200 nm and it is available in a 3.0-mm diamond width. The triangular holder, suitable for dry sectioning, as well as the trough, for sectioning using fluids, are both made from a special copper-nickel alloy, for the best possible heat/cold conduction. A cold-resistant epoxy resin is used for the seal.

Diatome
For information 215-412-8390
www.emsdiasum.com

Electronically submit your new product description or product literature information! Go to **www.sciencemag.org/products/newproducts.dtl** for more information.

Newly offered instrumentation, apparatus, and laboratory materials of interest to researchers in all disciplines in academic, industrial, and governmental organizations are featured in this space. Emphasis is given to purpose, chief characteristics, and availabilty of products and materials. Endorsement by *Science* or AAAS of any products or materials mentioned is not implied. Additional information may be obtained from the manufacturer or supplier.

We've got **Careers** down to a **Science.**

For full advertising details, go to **www.sciencecareers.org** and click on **For Advertisers,** or call one of our representatives.

United States & Canada

E-mail: advertise@sciencecareers.org
Fax: 202-289-6742

IAN KING
Recruitment Sales Manager/
Industry – US & Canada
Phone: 202-326-6528

ALEXIS FLEMING
Northeast Academic
Phone: 202-326-6578

TINA BURKS
Southeast Academic
Phone: 202-326-6577

DARYL ANDERSON
Midwest/Canada Academic
Phone: 202-326-6543

NICHOLAS HINTIBIDZE
West Academic
Phone: 202-326-6533

Europe & International

E-mail: ads@science-int.co.uk
Fax: +44 (0) 1223 326532

TRACY HOLMES Sales Manager
Phone: +44 (0) 1223 326525

ALEX PALMER
Phone: +44 (0) 1223 326527

ALESSANDRA SORGENTE
Phone: +44 (0) 1223 326529

MARIUM HUDDA
Phone: +44 (0) 1223 326517

LOUISE MOORE
Phone: +44 (0) 1223 326528

To subscribe to *Science*:
In US/Canada call 202-326-6417 or 1-800-731-4939
In the rest of the world call +44 (0) 1223-326-515

Science makes every effort to screen its ads for offensive and/or discriminatory language in accordance with US and non-US law. Since we are an international journal, you may see ads from non-US countries that request applications from specific demographic groups. Since US law does not apply to other countries we try to accommodate recruiting practices of other countries. However, we encourage our readers to alert us to any ads that they feel are discriminatory or offensive.

Science Careers
From the journal *Science* AAAS

POSITIONS OPEN

Material Intelligence has the following positions open.

(1) **SENIOR SCIENTIST.** Requires Ph.D. in physics or closely related field and working knowledge of scalar diffraction and inverse scattering in nonuniform media. Duties will include both theory and experiments. Software, electronic design, or mechanical skills are desirable.

(2) **PROGRAM MANAGER.** Requires degree in engineering or physical science, experience in similar job function, and competency in office and project management software. Duties include administering a government contract; preparing and submitting reports and data items; and coordinating meetings, program reviews, and field tests.

(3) **ELECTRICAL ENGINEER/DESIGNER.** Requires degree plus five years of experience in electrical engineering, analog circuit design for instrumentation, digital design with field-programmable gate array, layout, and test. Degree in a physical science with relevant experience may be accepted. Also desirable are ultrasound, microwave, and video experience.

(4) **SOFTWARE ENGINEER.** Requires degree in engineering, or physical science, plus five years of experience designing and programming real time systems, device drivers, signal processing, data acquisition, graphics, and video.

(5) **MECHANICAL ENGINEERING TECHNICIAN.** Requires degree in mechanical engineering, or physical science, and relevant experience. Duties include light mechanical design, machining and assembly, and assisting in experiments. Experience in environmental testing is desirable.

(6) **TECHNICAL ASSISTANT/COMPUTER SUPPORT.** Requires degree in engineering or physical science, experience in system management, and software programming skills. Mechanical and electrical skills are desirable. Duties include maintaining computer systems and assisting the senior technical staff.

All positions are located near Morristown, New Jersey.

Please send resumes to **e-mail: jobs@mi-llc.com.**

ASSISTANT PROFESSOR POSITION
Dalhousie University
Cardiovascular Physiology

The Department of Physiology and Biophysics invites applications for a position at the Assistant Professor level available for the 2008 academic year. Qualified candidates will have demonstrated research expertise in cardiovascular physiology, with an emphasis on molecular or cellular research in cardiovascular physiology/pathophysiology. Applicants must have a Ph.D. and/or M.D. degree, several years of postdoctoral training, excellent communication skills, and a strong record of peer-reviewed publications. The successful candidate will be expected to develop active and synergistic research collaborations with other cardiovascular researchers in both the basic science and clinical departments of the Faculty of Medicine. The candidate is expected to develop an extramurally funded research program and to participate in the teaching mission of the Department. This is a salaried, probationary tenure-track appointment; however, the candidate will be expected to apply for external salary support from appropriate granting agencies.

Interested applicants should submit curriculum vitae along with a brief description of research experience and interests, teaching experience and interests, and arrange to have three letters of reference sent directly to: **Dr. Paul R. Murphy, Head, Department of Physiology and Biophysics, Faculty of Medicine, Dalhousie University, Sir Charles Tupper Medical Building, 5850 College Street, Halifax, Nova Scotia B3H 1X5, Canada.**

Review of applications will begin March 31, 2008, and will continue until the position is filled.

All qualified candidates are encouraged to apply; however, Canadians and permanent residents will be given priority. Dalhousie University is an Employment Equity/Affirmative Action Employer. The University encourages applications from qualified Aboriginal people, persons with a disability, racially visible persons and women.

POSITIONS OPEN

BIOLOGY FACULTY POSITION in HUMAN ANATOMY

The Department of Biology at the University of Alabama at Birmingham (UAB) seeks highly qualified candidates for a full-time nontenure-track teaching position at the rank of **ASSISTANT PROFESSOR.** This full-time position is renewable subject to performance. The primary responsibility of the successful candidate will be to teach human anatomy and either genetics or introductory biology courses. Candidates must have a Ph.D. in biology or related fields, a commitment to undergraduate education and outreach, and preferably a record of excellence in teaching. Applicants should submit curriculum vitae, a statement of teaching interests, and copies of recent teaching evaluations, and have three letters of reference sent to: **Dr. Ken Marion, Chair, Department of Biology, University of Alabama at Birmingham, 1300 University Boulevard, Birmingham, AL 35294-1170.** The anticipated start date is August 1, 2008. Review of materials will begin March 1, 2008, and will continue until the position is filled. *The Department of Biology and UAB are committed to building a culturally diverse workforce and strongly encourage applications from women and individuals from underrepresented groups. UAB has an active National Science Foundation-supported ADVANCE Program and a Spouse Relocation Program to assist in the needs of dual-career couples. UAB is an Affirmative Action/Equal Employment Opportunity Employer.*

NEUROANATOMIST

The Section of Anatomy at the Southern Illinois University (SIUE) School of Dental Medicine is seeking applicants for a full-time (12-month) tenure-track appointment for a Neuroanatomist at the **ASSISTANT/ASSOCIATE PROFESSOR** level. Applicants must have a Ph.D. or equivalent, teaching experience in neuroanatomy, and the background to assist in teaching in the gross anatomy laboratory. Experience in teaching histology, oral biology, and/or pain mechanisms is preferred but not required. Postdoctoral fellowship is desirable. The candidate is expected to be active in dentally related research, particularly the pathways and mechanisms of dental pain. Academic rank and salary are commensurate with experience and qualifications. The school is located on a historic campus, 15 minutes from the campus of Southern Illinois University Edwardsville and 30 minutes from St. Louis. Review of applications will begin in February 2008, and continue until the position is filled. Send a letter of interest, curriculum vitae, and three letters of reference to: **Dr. Ann Boyle, Dean, School of Dental Medicine, Southern Illinois University, 2800 College Avenue, Alton, IL 62002-4900.** *SIUE is an Equal Employment Opportunity/Affirmative Action Employer committed to diversity in education and employment. SIUE is a state university; benefits under state-sponsored plans may not be available to holders of F-1 or J-1 visas.*

The Section of Nephrology at the University of Chicago is seeking a **MOLECULAR BIOLOGIST** for a **RESEARCH ASSOCIATE** position; academic rank will be commensurate with previous experience and accomplishments. Cultured renal cells as well as whole animal studies will be used to answer complex scientific questions. Microscopic, biochemical, molecular biologic, and genomic approaches will be utilized. At least five years of experience in the study of cultured cells, including with imaging, signal transduction, and transfection is required. Experience with transgenic mice is preferred, but not required. Our ongoing work is in the physiology of ion transport, although experience in this area is not essential. Substantial resources are in place for this work. Send curriculum vitae and names of three references to: **Dr. Robert Hoover, Assistant Professor, Section of Nephrology, e-mail: rhoover@medicine.bsd.uchicago.edu.**

UMDNJ
NEW JERSEY MEDICAL SCHOOL
UNIVERSITY HOSPITAL
CANCER CENTER
UNIVERSITY OF MEDICINE & DENTISTRY OF NEW JERSEY

Faculty Positions in a New Cancer Center

The New Jersey Medical School (NJMS) – University Hospital (UH) Cancer Center, a new 220,000 square foot state-of-the-art facility on the Newark Campus of UMDNJ, is looking to continue its major expansion through aggressive recruitment of outstanding scientists in basic and translational cancer research, at both the junior and senior levels. The NJMS-UH Cancer Center is located within the New York Metropolitan area and contains three research floors, a 20,000 sq. ft. mouse barrier facility, and three clinical floors for outpatient cancer services. There are twelve cancer researchers already housed in the building, and a broad cancer research community on campus. Areas of excellence include: breast cancer research, signal transduction, oncogenes and tumor suppressors, tumor virology, immunology, and cancer stem cells. Core facilities located in the building include those for confocal microscopy, digital imaging and histology, biostatistics, a proteomics facility and a tissue culture core. Additional core facilities are conveniently situated in adjacent buildings. Successful candidates must have an M.D. and/or Ph.D. degree together with outstanding credentials and will be expected to maintain a vigorous, independent extramurally funded research program. Generous start-up funds, competitive salary, and ultra-modern laboratory space are available for both tenured and tenure track positions.

Electronic applications, including *curriculum vitae*, a brief summary of accomplishments and future research directions, should be sent to **muhammdi@umdnj.edu**. Applicants should also arrange to have three letters of reference sent to:

Harvey L. Ozer, M.D.,
Professor and Director, NJMS-UH Cancer Center
UMDNJ-New Jersey Medical School
Rm H1202, 205 South Orange Ave., Newark, N.J. 07101

Senior investigators need not provide letters of reference at this time and their applications will be treated with confidentiality if requested. For more information about the NJMS-UH Cancer Center visit: **http://njmsuhcc.umdnj.edu/research**.

UMDNJ is an AA/EOE, M/F/D/V Employer. The Cancer Center is an Affiliate of the UMDNJ Cancer Institute of New Jersey. Women, minority applicants, and dual career couples are encouraged to apply.

DEPARTMENT OF HEALTH AND HUMAN SERVICES
NATIONAL INSTITUTES OF HEALTH
OFFICE OF THE DIRECTOR
OFFICE OF PORTFOLIO ANALYSIS AND STRATEGIC INITIATIVES
DIVISION OF RESOURCE DEVELOPMENT AND ANALYSIS

The Office of the Director, National Institutes of Health (NIH) in Bethesda, Maryland, is seeking a Director of the Division of Resource Development and Analysis (DRDA) within the Office of Portfolio Analysis and Strategic Initiatives (OPASI). If you are an exceptional candidate with an M.D. and/or Ph.D., we encourage your application.

The OPASI's primary objective is to develop: a transparent process of planning and priority-setting characterized by a defined scope of review with broad input from the scientific community and the public; valid and reliable information resources and tools, including uniform disease coding and accurate, current and comprehensive information on burden of disease; an institutionalized process of regularly scheduled evaluations based on current best practices; the ability to weigh scientific opportunity against public health urgency; a method of assessing outcomes to enhance accountability; and a system for identifying areas of scientific and health improvement opportunities and supporting regular trans-NIH scientific planning and initiatives.

As the DRDA Director, you will be responsible for employing resources (databases, analytic tools, and methodologies) and developing specifications for new resources, when needed, in order to conduct assessments based on NIH-owned and other databases in support of portfolio analyses and priority setting in scientific areas of interest across NIH.

Salary is commensurate with experience and includes a full benefits package. A detailed vacancy announcement with the mandatory qualifications and application procedures can be obtained on **USAJOBS at www.usajobs.gov** (announcement number **OD-08-236976-T42**) and the NIH Web Site at **http://www.jobs.nih.gov**. Questions on the application procedures may be addressed to Brian Harper on 301-594-5332. Applications must be received by midnight eastern standard time on **February 14, 2008**.

This position is subject to a background investigation.

DHHS and NIH are Equal Opportunity Employers

THE UNIVERSITY OF CALIFORNIA, BERKELEY
Department of Integrative Biology
Faculty Position in Plant Paleobiology and Evolution
Position ID #714

The Department of Integrative Biology at the University of California, Berkeley, is soliciting applications for a tenure-track position (Assistant Professor) in **Plant Paleobiology and Evolution**. We seek a colleague to join a department with a strong interdisciplinary emphasis who will develop a vigorous, independent research and teaching program in the area of plant paleobiology. Applicants should have a Ph.D. or equivalent advanced degree and an exceptional research record in: the evolution and ecology of past plant communities or ecosystems, the evolution of vascular plant lineages in deep time, and/or long-term plant response to environmental change using paleontological and neontological data. The position entails teaching both lower and upper level courses in plant evolution/paleobotany, with an emphasis on structure and function, phylogeny, paleoecology, and/or historical biogeography. An academic curatorship in the UC Museum of Paleontology is associated with this appointment; the successful candidate will be encouraged to promote the use of the museums' extensive holdings, supervise student research, work with museum staff to pursue opportunities for collection improvement and growth, and participate in UCMP and the Berkeley Natural History Museums activities and events. For more information, see: **http://ib.berkeley.edu**.

Application packages should include a CV with a bibliography of published work, a description of research accomplishments and objectives, a statement of teaching interests, and selected reprints. Three letters of reference should be sent separately by the recommender.

Both applications and letters of reference should be submitted electronically via: **http://ib.berkeley.edu/admin/jobs/paleobiojob.php** or via email to: **PlantPaleobiology@gmail.com**. If electronic submission is not possible, materials may be sent by regular mail to:

Plant-Paleobiology Search Committee
Department of Integrative Biology
3060 Valley Life Sciences Building
University of California
Berkeley, CA 94720-3140 USA

Applications and supporting letters must be received electronically or postmarked by **February 29, 2008**. Review of application will begin **March 10, 2008**. Applicants should refer their reviewers to the UC Berkeley Statement of Confidentiality at **http://apo.chance.berkeley.edu/evalltr.html**.

The University of California is an Equal Opportunity/Affirmative Action Employer.

UNIVERSITY of NEW HAMPSHIRE
Associate Dean of Undergraduate Studies

The University of New Hampshire, **College of Life Sciences and Agriculture**, seeks an **Associate Dean for Undergraduate Studies**. Reporting to the Dean, the ideal candidate will have a record of distinguished research and education achievement and a commitment to undergraduate education that warrants appointment as a tenured faculty member, demonstrated administrative skills, excellent communication and interpersonal skills, a commitment to the principles of diversity, the ability to enhance the college's role within the University and the broader academic community, and the commitment to a college leadership team focused on academic excellence.

Applicants should submit Curriculum Vitae, 1-2 page vision statement on research and education, and names and contact information of four references to: **Gale B. Carey, Search Committee Chair, 403 Kendall Hall, 129 Main Street, University of New Hampshire, Durham, NH 03824.** Review of applications will begin Feb. 1, 2008 and continue until the position is filled. For more information go to: **http://www.colsa.unh.edu/employment/index.html**

The University is committed to excellence in its faculty and staff and strongly encourages women and minorities to apply.

U.S. MILITARY HIV RESEARCH PROGRAM

Clinical Program Manager
HIV/AIDS Prevention, Care and Treatment

The U.S. Military HIV Research Program (USMHRP), supported by the Henry M. Jackson Foundation for the Advancement of Military Medicine, is a key contributor the President's Emergency Plan for AIDS Relief (PEPFAR/Emergency Plan) in Kenya, Nigeria, Tanzania, and Uganda. This internationally recognized program is seeking a dynamic physician to manage USMHRP's clinical programs supporting the Emergency Plan. Ensure quality clinical services are supported overseas (OCONUS) by the Walter Reed Army Institute of Research (WRAIR), as well as plan, implement and monitor clinical activities supporting the prevention, care and treatment initiatives. Must have demonstrated knowledge and ability related to HIV pathogenesis and treatment (initial infection to end stage disease palliative care); HIV transmission and prevention; Medical Education program development and management experience; Program monitoring and evaluation; Budget development, management and reporting; Excellent communication skills; troubleshooting and supervisory skills.

Must have a Medical (MD) degree with post medical graduate education in Internal Medicine and fellowship in Infectious Disease or related. A minimum of 2 years of managing hospital based Infectious Disease service; field or clinical research experience is desired; 3 to 5 years of international work experience is preferred. Incumbent will be located at Rockville, Maryland offices and travel to research/field as required on at least a semiannual basis, sponsored by the USMHRP to assist program personnel and liaise with on the ground U.S. government agencies.

Please e-mail resumes to **careers@hjf.org** or fax to **240-314-7334** with **Job No. 203001** in subject line. The Henry M. Jackson Foundation for the Advancement of Military Medicine offers a competitive salary and generous benefits package.

AA/EEO

VE RI TAS

Harvard University
Associate Dean for the Sciences Division

This search seeks an implementing partner for the Dean for the Sciences of the Faculty of Arts and Sciences of Harvard University as he builds the new sciences division, improves its administrative systems, and undertakes a series of science initiatives. The division is expected to pursue objectives within existing departments and centers as well as themes that bring together scientists from across the University. This recently created position will manage administrative activities spanning eleven science departments plus several research centers.

The Associate Dean position offers a significant opportunity to build an administrative career at the University. It reports to the Dean for the Sciences with a dotted line report to the Executive Dean of the Faculty of Arts and Sciences. The search is currently scheduled to conclude in the coming winter with a starting date as soon thereafter as possible.

Inquiries, referrals, and resumes should be sent (electronic submission to 3482@imsearch.com encouraged), in confidence, with a cover letter to: Liz Vago, Internal Box 3483, Isaacson, Miller, 334 Boylston Street, Suite 500, Boston, MA 02116.

For further information: 3482@imsearch.com and www.harvard.edu

Harvard University is an equal opportunity/affirmative action employer. Candidates from all backgrounds are encouraged to apply.

POSITIONS OPEN

TWO FACULTY POSITIONS

Searches are underway in the Department of Plant Sciences at the University of Tennessee Knoxville (UT). Both positions are **ASSISTANT/ASSOCIATE** level, tenure track, 100 percent research appointments in the Tennessee Agricultural Experiment Station. Full position descriptions can be found at **website: http://plantsciences.utk.edu/positions.htm.**

The first search is for a **COMPUTATIONAL/SYSTEMS BIOLOGIST** in plant science who uses bioinformatic, statistical, in silico, and/or experimental approaches. The second search is for a **POSITION in BIOFUEL CROPS BREEDING** of grasses for cellulosic ethanol production. The selected individual will conduct applied and basic plant breeding research to identify and incorporate key plant traits for optimum bioenergy production.

Successful candidates will be expected to create and sustain nationally recognized, vigorous research programs that will be competitive for substantial external funding. The successful candidates will have excellent communication skills, mentor graduate students and other scientists, and publish results in peer-reviewed journals. Collaborative opportunities at UT abound, including those at the nearby Oak Ridge National Laboratory, which has extraordinary computing capabilities, with opportunities for adjunct status.

Application procedure: Each applicant should send curriculum vitae and a statement of research interest, along with the names and contact information (including e–mail) of at least three references to: **Janice Crockett (e-mail: janice@tennessee.edu), Department of Plant Sciences, 252 Ellington Plant Science Building, 2431 Joe Johnson Drive, Knoxville, TN 37996-4561.**

Inquiries for positions should be made to **Search Chairs:** Computational/Systems Biologist: **Neal Stewart (e-mail: nealstewart@utk.edu, telephone: 865-974-6487),** Biofuel Crops Breeder: **Vince Pantalone (e-mail: vpantalo@utk.edu, telephone: 865-974-8801)** Review of applications will begin on March 15, 2008, and continue until the position is filled.

The University of Tennessee is an Equal Employment Opportunity/Affirmative Action/Title VI/Title IX/Section 504/ ADA/ADEA Institution in the provision of its education and employment programs and services.

The DEPARTMENT of PSYCHIATRY
University of Pennsylvania's
School of Medicine

The Department of Psychiatry seeks candidates for an **ASSISTANT or ASSOCIATE PROFESSOR** position in either the nontenure clinician-educator track or the tenure track. Track and rank will be commensurate with experience. The successful applicant will have experience in the field of neuroscience with a focus on behavioral neuroscience, functional magnetic resonance imaging, or electrophysiology. Responsibilities include participation in a multidisciplinary team of basic and clinical neuroscientists with opportunities to contribute to study of schizophrenia and other brain disorders while pursuing independent research. Applicants must have an M.D. or Ph.D degree and have demonstrated excellent qualifications in education and research. Individuals with training in developmental neuroscience are especially encouraged to apply. Opportunities for clinical and teaching activities are available. Please submit curriculum vitae, a cover letter, three reference names, and a statement of research interests to: **Dwight L. Evans, M.D., Professor and Chair; Raquel E. Gur, M.D., Ph.D., Director of Neuropsychiatry; Reference #75-2, c/o A. Plotnick, Department of Psychiatry, 305 Blockley Hall, 423 Guardian Drive, Philadelphia, PA 19104-6021; e-mail: plotnick@mail.med.upenn.edu.**

The University of Pennsylvania is an Equal Opportunity, Affirmative Action Employer. Women and minority candidates are strongly encouraged to apply.

POSITIONS OPEN

The Cell and Molecular Biology (CMB) Program at Grand Valley State University (Michigan) is seeking candidates with experience in biotechnology and molecular biology for a **TENURE-TRACK POSITION** to begin in the fall 2008. A Ph.D. in molecular biology or related field and excellent communication skills are required; biotechnology, teaching, and postdoctoral experience are desired. Teaching responsibilities will include an advanced undergraduate nucleic acids laboratory, courses in the professional sciences Master's biotechnology curriculum, and other CMB offerings. The successful candidate will be expected to maintain active scholarship; research involving undergraduate and/or Master's students is desired. Grand Valley State University is a primarily undergraduate institution whose faculty members are expected to advise students and participate in the academic governance of the Department, College, and University. Apply online at **website: http://www.gvsujobs.org/.** Include a cover letter, curriculum vitae, statements of teaching philosophy and research interests, and scanned copies of your transcripts. Arrange to have three letters of reference sent to: **Mark Staves, Cell and Molecular Biology Search Committee Chair, Biology Department, Grand Valley State University, Allendale, MI 49401-9403 (e-mail: stavesm@gvsu.edu).** If you have questions or need assistance, call **Human Resources** at **telephone: 616-331-2215.** Review of applications begins February 18, 2008. *Grand Valley State University is an Affirmative Action/Equal Opportunity Employer.*

BIOLOGICAL OCEANOGRAPHER
TENURE-TRACK FACULTY POSITION
Florida State University
Department of Oceanography

The Department of Oceanography is seeking to fill a tenure-track faculty position in biological oceanography. We are looking for excellent candidates who are expected to become leaders in their respective fields. The Department actively collaborates with the Department of Biological Sciences **(website: http://www.bio.fsu.edu/),** the Geophysical Fluid Dynamics Institute **(website: http://www.gfdi.fsu.edu),** and supports the Florida State University Coastal and Marine Laboratory **(website: http://www.marinelab.fsu.edu/),** a facility with coastal vessels and laboratories, focusing on research in the pristine ecosystems of the northeastern Gulf of Mexico. The search will continue until the position is filled, but applications received by March 1, 2008, are guaranteed full consideration. Applicants are asked to send separate PDF files containing curriculum vitae, a statement of research/teaching interests, and the names of three references via e-mail to **Dr. Joel Kostka (e-mail: jkostka@ocean.fsu.edu), Department of Oceanography, Florida State University, 117 N. Woodward Avenue, P.O. Box 3064320, Tallahassee, FL 32306-4320. Telephone: 850-644-6700; fax: 850-644-2581.** *FSU is an Equal Opportunity Employer; applications from underrepresented groups are encouraged.*

PHARMACOLOGY TENURE-TRACK
FACULTY POSITION
University of Wisconsin, Madison

A tenure-track faculty position as an **ASSISTANT PROFESSOR** is available in the Department of Comparative Biosciences, School of Veterinary Medicine. Qualifications include Ph.D., postdoctoral experience, and potential to develop an outstanding, extramurally funded research program in pharmacology that complements existing departmental strengths. Teaching responsibilities include instruction in fundamentals of pharmacology. To apply, send curriculum vitae, brief statements of research interests and teaching philosophy, and three reference letters to: **Gordon S. Mitchell, Chair, Department of Comparative Biosciences, University of Wisconsin, 2015 Linden Drive, Madison, WI 53706.** Apply by March 1, 2008. For additional information, see **website: http://www.vetmed.wisc.edu/jobs.html.** *Equal Opportunity/Affirmative Action Employer.*

POSITIONS OPEN

USDA Agricultural Research Service

The U.S. Department of Agriculture, Agricultural Research Service (ARS), Vegetable Crops Research Unit, located on the University of Wisconsin campus in Madison, Wisconsin, is accepting applications for a permanent, full-time position. Interdisciplinary: **RESEARCH PLANT MOLECULAR BIOLOGIST/RESEARCH GENETICIST PLANTS,** GS-12/13 to lead research on a project developing tools for evaluating and improving cucumber germplasm, identifying traits useful for cucumber breeders, determining their inheritance, developing enhanced germplasm for use by geneticists and breeders, and broadening the molecular knowledge base of cucurbits. This position presents rich opportunities to work in an interdisciplinary environment and to collaborate with faculty, staff, and industry. Salary is commensurate with experience ($63,417 to $98,041 per annum), plus benefits. *Candidates must be U.S. citizens.* Candidates must request a copy of the vacancy announcement (ARS-X8W-0091) by calling **telephone: 301-504-1583,** via the ARS homepage at **website: http://www.ars.usda.gov** or by contacting **Jean Weinbrenner** at **telephone: 608-890-0044, e-mail: jean.weinbrenner@ars.usda.gov.** Candidates must submit specific information as outlined in the vacancy announcement. Applications must be postmarked by the closing date of February 13, 2008. For information on the Research Program contact **Philipp Simon** at **telephone: 608-262-1248** or **e-mail: psimon@wisc.edu.** *USDA is an Equal Opportunity Provider and Employer. Women and minorities are encouraged to apply.*

FEINBERG SCHOOL of MEDICINE
Department of Medicine
Division of Hematology/Oncology

The Division of Hematology/Oncology of Northwestern University's Feinberg School of Medicine is seeking accomplished investigators for full-time, tenure-track positions in basic or translational research. The Division consists of a faculty of over 35 **(website: http://www.medicine.northwestern.edu/divisions/hematology_oncology/),** all members of the National Cancer Institute-Designated Robert H. Lurie Comprehensive Cancer Center **(website: http://www.lurie.northwestern.edu).**

Candidates should have an M.D., Ph.D., or M.D./Ph.D. degree and an established publication record. Faculty rank and salary are negotiable based upon experience. The proposed start date is summer 2008. Interested candidates should submit curriculum vitae by March 1, 2008, to:

Jonathan D. Licht, M.D.
Chief, Division of Hematology/Oncology
Northwestern University Feinberg
School of Medicine
Lurie 5-123
303 East Chicago Avenue
Chicago, IL 60611
E-mail: hemonc@northwestern.edu

The Feinberg School of Medicine is an Affirmative Action/Equal Opportunity Employer. Women and minorities are encouraged to apply. Hiring is contingent upon eligibility to work in the United States.

POSTDOCTORAL POSITION available to work in a confocal Raman/atomic force microscopy imaging facility to investigate the molecular mechanisms of eye diseases. Applicants with either Raman/Fourier transform infrared-spectroscopy/microscopy, or protein-nuclear magnetic resonance experience will be preferred. Please send complete curriculum vitae and contact information of three references, electronically to: **Dr. J. Pande, e-mail: jpande@albany.edu**

POSITIONS OPEN

USDA ARS Agricultural Research Service
www.ars.usda.gov

RESEARCH LEADER. Agricultural Research Service (ARS) is seeking applications for a permanent, full-time, Research Leader. This position is interdisciplinary (**SUPERVISORY RESEARCH GENETICIST/ ENTOMOLOGIST/BIOLOGIST/ PLANT PATHOLOGIST,** GS-440/414/401/434-14/15) and is located at the Wheat, Peanut, and Other Field Crops Research Unit, in Stillwater, Oklahoma. As Research Leader (RL), the incumbent will be responsible for overall management and development of programs in a premier unit that conducts research on pest-resistant germplasm and the associated pests. The RL is also responsible for developing a highly visible and effective personal research program fundamental to plant protection of wheat, barley, sorghum, or peanut through approaches including developing single and multiple pest-resistant germplasm, elucidating biological, ecological, or genetic mechanisms leading to improved management of pests, and/or developing improved pest management methods or technologies. Salary is commensurate with experience ($91,562 to $140,020 per annum) plus benefits. *U.S. citizenship is required.* The full-text announcement (ARS-X8S-0059) is available at the ARS careers website **(website: http://www.ars.usda.gov/careers)** or by calling **telephone: 301-504-1482.** Location contact: **Diana Wehr, telephone: 405-624-4141, extension 247,** or **e-mail: diana.wehr@ars.usda.gov.** Applicants must address specific education and experience requirements. Ph.D desirable. Applications must be postmarked by February 29, 2008. *USDA/ARS is an Equal Opportunity Employer and Provider.*

ASSISTANT PROFESSOR in ECOLOGICAL ECONOMICS or BIOECONOMICS

The School of Life Sciences at Arizona State University (ASU) invites applications for a tenure-track faculty position in ecological economics or bioeconomics at the Assistant Professor level. The appointment supports an initiative to strengthen capacity in the field within the School of Life Sciences, **e-mail: ecoservices@asu.edu,** and to promote collaboration with other academic units in ASU.

To apply, send curriculum vitae, three research papers, and a statement of research plans, plus names and contact information for three references to: **Chair, Ecological Economics Search Committee, School of Life Sciences, P.O. Box 874501, Arizona State University, Tempe, AZ 85287-4501.** Inquiries and e-mailed applications may be sent to **e-mail: nclesko@asu.edu.** The initial deadline for receipt of applications is February 15, 2008, with applications reviewed weekly thereafter until the search is closed. *A background check is required for employment. Arizona State University is an Affirmative Action, Equal Opportunity Employer committed to excellence through diversity.*

POSTDOCTORAL POSITIONS in molecular endocrinology and cancer therapeutics. Seeking recent Ph.D. graduates for funded openings on two projects: (1) growth hormone action and JAK-STAT, using Chromatin Immunoprecipitation/microarray technologies combined with computational analysis and traditional molecular approaches to elucidate sexually dimorphic liver gene expression (*Molecular Endocrinology* **20:**2613-29, 2006); (2) cytochrome P450 prodrug-based gene therapy for cancer (*Molecular Cancer Therapeutics* **5:**541-5, 2006; **6:**2879-90, 2007). Expertise in cell and molecular biology, genomics and computational biology, gene therapy and/or pharmacology, and animal models highly desirable. Flexible start date. Send curriculum vitae, summary of research experience and interests, and three references to: **Dr. David J. Waxman, Department of Biology, Boston University, 5 Cummington Street, Boston, MA 02215. E-mail: djw5@bu.edu.**

POSITIONS OPEN

FULL-TIME ENDOCRINOLOGY

ASSISTANT PROFESSOR, Department of Medicine, Division of Endocrinology, University of Pittsburgh School of Medicine. M.D. or M.D., Ph.D. candidates are welcome. The successful applicant will be an M.D. with exceptional skills and experience in clinical and basic research aspects of diabetes and obesity, including but not limited to rodent insulin and glucose clamps, mathematical modeling of clamp-derived datasets, liver, fat, beta cell, and/or human skeletal muscle biopsy with biochemical and histological evaluation, intermediary carbohydrate and fat metabolism, signaling and enzymatic assays, and large dataset management skills. He/she must also have excellent collaborative skills as well as current or anticipated academic independence with respect to manuscript preparation and grant preparation. Full training and Board certification in clinical endocrinology are also required.

Please send curriculum vitae to:

Dr. Andrew Stewart, Chief
Division of Endocrinology
c/o Nancy Penney
Endocrinology Division Administrator
University of Pittsburgh
E1140 BST, 200 Lothrop Street
Pittsburgh, PA 15261

The University of Pittsburgh is an Affirmative Action, Equal Opportunity Employer.

AVIAN RESEARCH ECOLOGIST
U.S. Geological Survey's Patuxent Wildlife Research Center

The U.S. Geological Survey's Patuxent Wildlife Research Center in Laurel, Maryland **(website: http://www.pwrc.usgs.gov/)** seeks a Research Ecologist with experience conducting research in avian biology, ecology, and conservation. The candidates' research interests may be broad but special consideration will be given to those with research interests that bridge population ecology, monitoring, and conservation biology. As lead investigator the Ecologist conducts original research that responds to regional and national conservation goals, primarily in support of Department of Interior agencies missions. Applications must be completed online at **website: http://www.usgs.gov/ohr/oars/.** Announcement ER-2008-0042 is open to *all qualified U.S. citizens;* announcement ER-2008-0043 is open to current and former Federal employees. Announcements will open on January 7, 2008, and close at midnight eastern standard time on February 19, 2008. Applications must be filled out completely and all supplemental materials, such as proof of education, must be submitted to be considered. Additional details regarding position and application are provided on the website. *The U.S. Geological Survey is an Equal Opportunity Employer.*

RESEARCH ASSOCIATE (ASSISTANT PROFESSOR)

The University of Chicago, the Ben May Institute for Cancer Research is seeking a full-time Research Associate (Assistant Professor) to examine the structural interactions and biological functions of cellular signaling molecules involved in growth control using a range of molecular, cellular, genetic, and/or biophysical approaches. Applicants should have Ph.D. degree, and at least five years of research experience in signal transduction.

Qualified applicants should provide current curriculum vitae, bibliography, and statement of research interest and goals, along with full names, addresses, telephone/fax numbers, and e-mail addresses of at least three scholars who can provide academic references. Application materials should be sent to: **Azisti Dembowski, Executive Administrator, The University of Chicago, The Ben May Institute for Cancer Research, 929 E. 57th Street, CIS, W-421B Chicago, IL 60637.**

The University of Chicago is an Affirmative Action/Equal Opportunity Employer.

POSITIONS OPEN

UAB

INSTRUCTOR of MEDICINE POSITION
School of Medicine
Department of Medicine
Division of Cardiovascular Disease

The University of Alabama at Birmingham, Division of Cardiovascular Disease is seeking applicants with a Ph.D. or M.D. for the position of Instructor. This is a nontenure-earning faculty position. Candidates must be capable of independently designing and conducting experiments and preparing and submitting data for publication. It is expected that the successful candidate will be able to secure independent, extramural funding to support ongoing research. Individuals interested in this position should have experience in small animal surgery and be able to work in both in vitro and in vivo. Interested candidates should send curriculum vitae, three letters of reference, and a brief statement of your interest to: **Robert C. Bourge, M.D., Director, 1900 University Boulevard, University of Alabama at Birmingham Station, Birmingham, AL 35294.**

UAB is an Equal Opportunity/Affirmative Action Employer.

POSTDOCTORAL RESEARCH FELLOW in ATMOSPHERIC SCIENCES

The Energy Biosciences Institute at the University of Illinois at Urbana-Champaign is seeking a Postdoctoral Researcher to conduct innovative research examining the biophysical implications of large-scale biofuel production as part of an interdisciplinary research program. The specific duties include the integration of an existing biogeochemical cycle model with an agriculture crop model to explore our understanding of how biogeochemical systems interact with land cover and land use and agriculture crops. This research will also investigate the implications of large-scale production of biofuels in the United States and other countries for agricultural land use, soil carbon sequestration, and greenhouse gas emissions.

A Ph.D. in atmospheric sciences or another related field in the sciences or engineering is required. The applicant should have working experience with high-speed, super fast computers, numerical simulation models and ability to analyze satellite data for land use changes and dynamics of the agro-ecosystems. Key factors in our hiring decision will be intelligence, thoughtfulness, creativity, motivation, productivity, and a record of successful scientific publication.

Applicants should send the following materials by e-mail to **Prof. Atul Jain (e-mail: jain1@uiuc.edu)**: (1) curriculum vitae, (2) a letter describing research interests and experience, and (3) names and contact information for three references. Review of completed applications will begin January 15, 2008, and continue until position is filled.

Science Careers
From the Journal Science AAAS

Make your faculty, scientist, or postdoc line ad
STAND OUT ON THE PAGE.
Call 202-326-6543
to find out more about line ad upgrades.

MARKETPLACE

Widely Recognized Original & Guaranteed
KlenTaq1
8¢/u Truncated Taq DNA Polymerase Withstand 99°C
US Pat #5,436,149
Call: **Ab Peptides**
Fax: 314•968•8988
e-mail: abpeps@msn.com
1•800•383•3362
www.abpeps.com